Monotonic and Fatigue Flexural Performance of RC Beams Strengthened with Externally Post-Tensioned CFRP Tendons

by

Ahmed Mokhtar El Refai

A thesis
presented to the University of Waterloo
in fulfillment of the
thesis requirement for the degree of
Doctor of Philosophy
in
Civil Engineering

Waterloo, Ontario, Canada, 2007

AUTHOR'S DECLARATION

I hereby declare that I am the sole author of this thesis. This is a true copy of the thesis, including any required final revisions, as accepted by my examiners.

I understand that my thesis may be made electronically available to the public.

Abstract

External post-tensioning is an attractive technique for strengthening reinforced concrete structures because of its ability to actively control stresses and deflections, speed of installation, minimum interruption for the existing structure, and ease of inspection under service conditions. However, external prestressing implies exposing the tendons to the environment outside the concrete section, which may lead to corrosion in steel tendons. Therefore, the interest in using fiber reinforced polymer (FRP) tendons, which are corrosion resistant, has increased.

The present work investigated, experimentally and analytically, the flexural performance of reinforced concrete beams strengthened with externally post-tensioned Carbon FRP (CFRP) tendons, under monotonic and fatigue loadings. Initially, tensile fatigue tests were carried out on CFRP tendon-anchor assemblies to assess their response under repeated cyclic loads, before implementing them in the beam tests. New wedge-type anchors (Waterloo anchors) were used in gripping the CFRP specimens. The assemblies exhibited excellent fatigue performance with no premature failure occurring at the anchorage zone. The fatigue tests suggested a fatigue limit of a stress range of 10% of the tendon ultimate capacity (approximately 216 MPa). Monotonic and fatigue experiments on twenty-eight beams (152x254x3500 mm) were then undertaken. Test parameters included the tendon profile (straight and double draped), the initial loading condition of the beam prior to post-tensioning (in-service and overloading), the partial prestressing ratio (0.36 and 0.46), and the load ranges applied to the beam during the fatigue life (39% to 76% of the yield load). The CFRP tendons were post-tensioned at 40% of their ultimate capacity.

The monotonic tests of the post-tensioned beams suggested that overloading the beam prior to post-tensioning increased the beam deflections and the strains developed in the steel reinforcing bars at any stage of loading. However, overloading had no significant effect on the yield load of the strengthened beam and the mode of failure at ultimate. It also had no discernable effect on the increase in the tendon stress at yielding. The maximum increase in the CFRP stress at yield load was approximately 20% of the initial post-tensioning stress, for the in-service and overloaded beams.

A very good performance of the strengthened beams was observed under fatigue loading. The fatigue life of the beams was mainly governed by the fatigue fracture of the internal steel reinforcing bars at a flexural crack location. Fracture of the bars occurred at the root of a rib where high stress concentration was likely to occur. No evidence of wear or stress concentration were observed at the deviated points of the CFRP tendons due to fatigue. The enhancement in the fatigue life of the strengthened beams was noticeable at all load ranges applied. Post-tensioning considerably decreased the stresses in the steel reinforcing bars and, consequently, increased the fatigue life of the beams. The increase in the fatigue life was slightly affected by the loading history of the beams. At the same load range applied to the beam, increasing the amount of the steel reinforcing bars for the same post-tensioning level decreased the stress range in the bars and significantly increased the fatigue life of the strengthened beams.

In the analytical study, a monotonic model that predicts the non-linear flexural response of the CFRP post-tensioned beams was developed and implemented into a computer program. The model takes into account the loading history of the strengthened beams prior to post-tensioning (in-service and overloading). Good agreement was obtained between the measured and the predicted monotonic results. A strain-life based fatigue model was proposed to predict the fatigue life of the CFRP post-tensioned beams. The model takes into consideration the stress-strain history at the stress raisers in the steel bars. It accounts for the inelastic deformation occurring at the ribs during cycling and the resulting changes in the local mean stresses induced. Good agreement between the experimental and predicted fatigue results was observed. A step-by-step fatigue design approach is proposed for the CFRP externally post-tensioned beams. General conclusions of the study and recommendations of future work are given.

Acknowledgements

I would like to express my sincere thanks and gratitude to my parents and to my family who encouraged and supported me during the completion of this work. I doubt that I will ever be able to convey my appreciation fully, but I owe them my endless gratitude.

I would also like to express my appreciation and gratitude to my supervisors, Professors Khaled Soudki and Jeff West from Civil Engineering at the University of Waterloo, for their guidance during the research program. They provided me with direction, technical support, and encouragement and became more of friends than professors. It was their persistence, understanding, and kindness that I was encouraged to complete this work.

Special thanks go out to Professor Tim Topper, whose expertise, understanding, and patience added considerably to my graduate experience. I am very grateful to him for the time, effort, and patience he dedicated to me.

I would also like to acknowledge and thank Ken Bowman, from the Civil Engineering Laboratories at the University of Waterloo, for his assistance during the experimental phase of this program. I would also like to thank Doug from the Civil Engineering Laboratories, Andy from the Mechanical Engineering Laboratories, and all the technicians from the Engineering Machine Shop, especially Fred Bakker and John Boldt, whose expertise and skills added a lot to my work. Their assistance during the experimental phase of this program is greatly appreciated.

I would also like to thank all my colleagues in the Civil Engineering Research Group for their support and useful discussion. I would also like to express my gratitude to the Natural Sciences and Engineering Research Council of Canada (NSERC) for their financial support. Material donation by Hughes Brothers, Inc. is greatly appreciated.

To my mother, my father, my wife, and my kids

Table of Contents

Chapter 1 Introduction **1**

1.1 General 1

1.2 Organization of the present work 2

Chapter 2 Literature Review and Research Objectives **5**

2.1 General 5

2.2 Background 5

2.3 External post-tensioning with steel tendons 7

2.3.1 Deviators and tendon profile 9

2.3.2 Non-prestressed bonded reinforcement 10

2.3.3 Post-tensioning force 11

2.3.4 Beam span-to-depth ratio 12

2.4 External post-tensioning with FRP tendons 13

2.4.1 General 13

2.4.2 Harping of FRP tendons 17

2.4.3 FRP anchoring systems 19

2.4.4 Previous studies on FRP externally post-tensioned beams 26

2.5 Monotonic analysis of FRP externally post-tensioned beams 32

2.6 Fatigue loading 37

2.6.1 General 37

2.6.2 Fatigue of plain concrete 38

2.6.3 Fatigue of steel reinforcing bars 39

2.6.4 Fatigue of FRP strengthened reinforced concrete beams 41

2.7 Conclusions based on previous research 42

2.8 Research objectives 45

Chapter 3 Fatigue of CFRP Tendon-Anchor Assembly 47

3.1 Introduction 47

3.2 The Waterloo anchor system 47

3.3 CFRP tendon-anchor assembly: Test program 49

3.3.1 Group (1): Proof tests 51

3.3.2 Groups (2) and (3) 51

3.4 Test specimen 52

3.5 Test setup and test procedure 54

3.6 Cyclic test observations 54

3.7 PTI proof tests 60

3.8 Fatigue life 63

3.9 Use of the anchor test results in concrete beam design 65

Chapter 4 Beam Experimental Program 67

4.1 Introduction 67

4.2 Beam test program 69

4.2.1 Group-A: Unstrengthened control beams 69

4.2.2 Group-B: Initially-in-service strengthened beams – SL15 70

4.2.3 Group-C: Initially-in-service strengthened beams – SL20 75

4.2.4 Group-D: Initially-overloaded strengthened beams - OL15 76

4.3 Test specimen 77

4.4 Specimen fabrication 79

4.5 Post-tensioning setup 84

4.5.1 Deviating system 84

4.5.2 End-bearing systems 86

4.6 Post-tensioning procedure 90

4.6.1 Beam-ends preparation 91

4.6.2 CFRP tendons preparation 92

4.6.3 Installation and post-tensioning of CFRP tendons 92

4.7 Loading test setup 93

4.7.1 Strain measurements 94
4.7.2 Beam deflection measurements 96
4.8 Loading test procedure 99

Chapter 5 Beam Experimental Results and Discussion 101

5.1 Introduction 101
5.2 Monotonic test results 101
5.2.1 In-service strengthened beams 103
5.2.2 Overloaded strengthened beam (OL15-M) 111
5.2.3 Modes of failure 119
5.3 Fatigue test results 119
5.3.1 Cyclic deflection response 122
5.3.2 Cyclic strain response 130
5.3.3 Changes in the CFRP tendon stresses 138
5.3.4 Cyclic strain investigation 144
5.3.5 Fatigue strength 151
5.4 Summary and conclusions 166
5.4.1 Monotonic tests 166
5.4.2 Fatigue tests 167

Chapter 6 Modeling the Monotonic Flexural Response of Externally Post-Tensioned Beams 169

6.1 Introduction 169
6.2 Analysis approach 169
6.3 Materials modeling 173
6.3.1 Concrete 173
6.3.2 Steel reinforcement 177
6.3.3 CFRP tendon 177
6.4 Modeling the monotonic behaviour of the in-service beams 179
6.4.1 The initial loading stage: in-service beam 179
6.4.2 The unloading stage: in-service beam 182

6.4.3 The post-tensioning stage: in-service beam 182
6.4.4 The reloading stage: in-service beam 186
6.5 Proposed model for the overloaded beam 191
6.5.1 The initial loading stage: overloaded beam 191
6.5.2 The unloading stage: overloaded beam 191
6.5.3 The post-tensioning stage: overloaded beam 194
6.5.4 The reloading stage: overloaded beam 194
6.6 Computer program 197
6.7 Analysis results 203

Chapter 7 Fatigue Life Prediction for Beams 209

7.1 General 209
7.2 Fatigue model for strengthened beams 210
7.2.1 Stress increase in the steel at crack locations 210
7.2.2 Strain-life analysis for the reinforcing steel 212
7.3 Fatigue analysis results 223
7.3.1 Estimation of the fatigue notch factor, K_f 223
7.3.2 Local stresses and strains 225
7.3.3 Fatigue life of beams 231
7.4 Example of fatigue life calculation 234
7.5 Existing fatigue design provisions 234
7.5.1 Canadian Highway Bridge Design Code (CHBDC, 2000) 234
7.5.2 American Concrete Institute (ACI-215 Committee, 1997) 236
7.5.3 AASHTO LRFD specifications (2004) 237
7.5.4 Proposed design methodology 238

Chapter 8 Conclusions and Recommendations 241

8.1 Introduction 241
8.2 Tendon-anchor fatigue tests 242
8.3 Monotonic beam tests 243

8.4 Fatigue beam tests 245
8.5 Modeling of the monotonic response 247
8.6 Modeling of the fatigue response 249
8.7 Recommendations for future studies 250

Appendix A: Prediction Equations for the Unbonded Tendon Stress at Ultimate 251

Appendix B : Load-Deflection Relationships 260

Appendix C: Mean Stress Equations 273

Appendix D: Strengthening Applications 276

References 279

List of Figures

Figure 2.1: Common profiles for external tendons: (a) straight, (b) straight with guides, (c) single draped, and (d) double draped 8
Figure 2.2: Depth and eccentricity variations of a straight tendon 8
Figure 2.3: Samples of FRP tendons (El Refai et al., 2003) 16
Figure 2.4: Typical stress-strain relationship of different tendon materials (adapted from CPCI Design Manual, 1996 and ISIS Canada Educational Modules, 2004) 16
Figure 2.5: Anchors for FRP tendons: (a) clamp, (b) plug and cone, (c) resin sleeve, (d) resin potted, (e) metal overlay, and (f) split wedge anchors (adapted from ACI 440.4R, 2004) 22
Figure 2.6: Fatigue strength of plain concrete (adapted from ACI 215, 1997) 40
Figure 2.7: Effect of repeated load on concrete strains (adapted from ACI-215, 1997) 40
Figure 3.1: (a) Parts of the Waterloo anchor; (b) The assembled Waterloo anchor 48
Figure 3.2: CFRP tendon-anchor test specimen 53
Figure 3.3: Pre-seating rig for CFRP tendon-anchor assembly 53
Figure 3.4: Test rig attached to the actuator 56
Figure 3.5: (a) Catastrophic broom-shaped failure (b) Longitudinal split in specimen No. 11 56
Figure 3.6: Stress versus strain for specimen No. 11 of stress range 260 MPa (total life = 363,600) 57
Figure 3.7: Stress versus strain for specimen No. 12 of stress range 288 MPa (total life = 572,700) 57
Figure 3.8: Stress versus strain for specimen No. 13 of stress range 324 MPa (total life = 18,400) . 58
Figure 3.9: Stress versus strain for specimen No. 14 of stress range 360 MPa (total life = 9,100) ... 58
Figure 3.10: Measured maximum strain versus the number of cycles (Test No. 11) 61
Figure 3.11: Measured maximum strain versus the number of cycles (Test No. 12) 61
Figure 3.12: Measured maximum strain versus the number of cycles (Test No. 13) 62
Figure 3.13: Measured maximum strain versus the number of cycles (Test No. 14) 62
Figure 3.14: Effect of the minimum stress on the fatigue life of the specimens 64
Figure 3.15: Applied stress range versus the life of the tendon-anchor assembly (all tests) 64

Figure 3.16: Applied stress range versus the life of the tendon-anchor assembly (excluding proof tests) 65
Figure 4.1: A schematic view of the straight and double draped tendon profiles 72
Figure 4.2: Idealization of the stages of monotonic loading of the (a) in-service beam and (b) overloaded beams (D: cracking load, E: yield load, and F: ultimate load)..... 75
Figure 4.3: Typical dimensions and reinforcement details of the virgin beam specimen 80
Figure 4.4: Cross section of the post-tensioned beams in the constant moment zone 80
Figure 4.5: General view of a strengthened beam with straight tendon profile 81
Figure 4.6: General view of a strengthened beam with draped tendon profile 81
Figure 4.7: Strain gages covered with wax (left) and steel bars inside the timber forms (right) 82
Figure 4.8: (a) Slump test, (b) casting cylinders, (c) finishing surfaces, and (d) curing 83
Figure 4.9: A schematic view of the deviating system 85
Figure 4.10: Photos of the deviating system (left) showing the curved saddle used (right)..... 85
Figure 4.11: General view of the jacking end (left) and the dead end (right) of the end-bearing system..... 87
Figure 4.12: Post-tensioning system: (a) straight bearing plate, (b) tapered bearing plate, (c) grooves in the bearing plates, and (d) locking-assembly..... 88
Figure 4.13: Post-tensioning system: close-up of the (a) screw adjusters, (b) thrust bearing, (c) jacks, and (d) hydraulic pumps 89
Figure 4.14: Post-tensioning system: (a) load cell between pocketed plates at the jacking end, (b) load cell seated on spherical seat at the dead end..... 90
Figure 4.15: Finished surface of the beam ends 91
Figure 4.16: (a) The pre-seating rig, (b) the hydraulic jack, and (c) the prestressing fixtures 92
Figure 4.17: A schematic view of the beam loading test set-up..... 95
Figure 4.18: A photo of the test setup of a post-tensioned beam..... 95
Figure 4.19: (a) Steel angles located at the beam edges and (b) the restraint system for spreader beam 96
Figure 4.20: Location of strain gages on the steel bars 97
Figure 4.21: Location of strain gages on the concrete surface 97

Figure 4.22: A schematic view of the LVDTs locations 98
Figure 4.23: Locations of LVDTs at the midspan section of the beam 98
Figure 4.24: A general view of the data acquisition system 99
Figure 5.1: Load-deflection response of the unstrengthened and in-service beams..... 102
Figure 5.2: Applied load versus the measured steel strains at midspan of the in-service strengthened beams and the control beam 106
Figure 5.3: Applied load versus the measured concrete strains at midspan of the in-service strengthened beams and the control beam 106
Figure 5.4: Variation of the tendon stress with the applied load in the in-service strengthened beams..... 108
Figure 5.5: Variation in the depth of the CFRP tendon with applied loads for the in-service beams 111
Figure 5.6: Load-deflection response of the overloaded (OL15-M) and in-service (SL15-MDD) strengthened beams..... 112
Figure 5.7: Yield crack in the overloaded beam compared to the adjacent cracks 112
Figure 5.8: Applied load versus the measured steel strains at midspan of the overloaded and the in-service strengthened beams 115
Figure 5.9: Applied load versus the measured concrete strains at midspan of the overloaded and the in-service strengthened beams..... 116
Figure 5.10: Variation of the tendon stress with the applied load for the overloaded (OL15-M) and the in-service (SL15-MDD) beams 117
Figure 5.11: Variation of depth of the CFRP tendon with the applied load for the in-service (SL15-MDD) and the overloaded (OL15-M) beams 118
Figure 5.12: Unstrengthened and strengthened beams at failure 121
Figure 5.13: Cyclic load-deflection behaviour for the(a) UN15-F52 beam, (b) SL15-F72 beam, (c) SL20-F87 beam, and (d) OL15-F82 beam..... 123
Figure 5.14: Variation of midspan deflection over the beam fatigue life for (a) UN15 beams , (b) SL15 beams, (c) SL20 beams, and (d) OL15 beams 127
Figure 5.15: Schematic view of the crack height in the (a) in-service and (b) overloaded beams 129

Figure 5.16: Regression analysis of midspan deflection under fatigue loading for (a) UN15 beams, (b) SL15 beams, (c) SL20 beams, and (d) OL15 beams 131
Figure 5.17: Variation in the concrete strain ranges over the beam fatigue life for (a) UN15 beams, (b) SL15 beams, (c) SL20 beams, and (d) OL15 beams 135
Figure 5.18: Load versus strain at S_{400} for the OL15-F82 beam 137
Figure 5.19: Load versus steel strain for the OL15-F76 beam 137
Figure 5.20: Variation in the steel strain ranges over the beam fatigue life for (a) UN15 beams, (b) SL15 beams, (c) SL20 beams, and (d) OL15 beams 139
Figure 5.21: CFRP tendon stress variation over the beam fatigue life for (a) SL15 beams, (b) SL20 beams, and (c) OL15 beams 141
Figure 5.22: (a) Deformed rebar and (b) standard machined fatigue specimen 145
Figure 5.23: Fatigue testing machine for steel specimens 146
Figure 5.24: Cyclic simulation tests: steel strain response at maximum stress applied 147
Figure 5.25: Cyclic simulation tests: steel strain range response 147
Figure 5.26: Test setup for concrete cylinder cyclic simulation tests 148
Figure 5.27: Variation of the concrete stress-strain relationships with number of cycles (a) Low stress range, (b) medium stress range, and (c) high stress range 149
Figure 5.28: Typical failure of the unstrengthened beams (a) UN15-F50 and (b) UN15-F53 154
Figure 5.29: Unstrengthened beam UN15-F59: steel strains versus the applied loads 154
Figure 5.30: Unstrengthened beam UN15-F59: concrete strains versus the applied loads 155
Figure 5.31: Failure of the in-service SL15 beams near the stirrup and at location of lugs 156
Figure 5.32: Beam SL15-F92-a: (a) local cracking extending from the loading point and (b) failure due to concrete crushing 156
Figure 5.33: Typical failure of the SL20-group of beams: (a) fatigue fracture of both reinforcing steel bars, (b) failure occurring at the crack location in the vicinity of a stirrup 158
Figure 5.34: Typical failure of the OL15-group of beams: fatigue fracture at the location of yield crack for the beams (a) OL15-F76, and (b) OL15-F88 158
Figure 5.35: Failure of the beam OL15-F72 by concrete crushing 159
Figure 5.36: Load range versus number of cycles to failure from experimental data 162

Figure 5.37: Normalized load range for the UN15, SL15, and the OL15 versus number of cycles to failure from experimental data 162
Figure 5.38: Stress range in reinforcing steel versus number of cycles to failure from experimental data: UN15 and SL15 beams 164
Figure 5.39: Stress range in reinforcing steel versus number of cycles to failure from experimental data: SL15 and SL20 beams 165
Figure 5.40: Stress range in reinforcing steel versus number of cycles to failure from experimental data: SL15 and OL15 beams 165
Figure 6.1: Idealization of the stages of monotonic loading of the (a) in-service beam and (b) overloaded beams (D: cracking load, E: yield load, and F: ultimate load) 171
Figure 6.2: Modeling of beam using longitudinal elements 172
Figure 6.3: Layer-by-layer concrete section analysis 172
Figure 6.4: Assumed stress-strain relationship of concrete 174
Figure 6.5: Average tensile stress in concrete 175
Figure 6.6: Average stress and average strain in concrete beyond cracking (adapted from Collins and Mitchell, 1991) 176
Figure 6.7: Effective embedment zone in cracked section (CEB Model Code, 1990) 176
Figure 6.8: Idealized stress-strain relationship of (a) steel reinforcement and (b) CFRP tendon . 178
Figure 6.9: Unloading lines of (a) initially compressed and (b) initially cracked concrete layers 183
Figure 6.10: Variation of the tendon eccentricity and depth in the shear span 185
Figure 6.11: Post-tensioning path of the initially compressed upper concrete layers 186
Figure 6.12: Behaviour of the initially compressed upper layers during the reloading stage 189
Figure 6.13: Behaviour of the initially cracked lower layers during the reloading stage 190
Figure 6.14: Steel response during unloading, post-tensioning, and reloading stages of the overloaded beam 193
Figure 6.15: Flow chart for the loading procedure (prior to strengthening) 198
Figure 6.16: Flow chart for the unloading procedure 199
Figure 6.17: Flow chart for the post-tensioning procedure 200
Figure 6.18: Flow chart for the reloading procedure 201

Figure 6.19: Flow chart of the calculation of the cracked strain-reduction coefficient, Ω_{cr}, for overloaded beams 202
Figure 6.20: Predicted versus experimental midspan deflection for the (a) in-service strengthened beam and the (b) overloaded beam strengthened beam 204
Figure 6.21: Predicted versus experimental force in the CFRP external tendon for the (a) in-service strengthened beam and the (b) overloaded strengthened beam 205
Figure 6.22: Predicted versus experimental steel strain for the (a) in-service strengthened beam and the (b) overloaded strengthened beam 206
Figure 6.23: Predicted versus experimental top concrete strain for the (a) in-service strengthened beam and the (b) overloaded strengthened beam 207
Figure 7.1: Cyclic stress-strain curve obtained by connecting tips of stabilized hysteresis loops (Bannantine et al., 1990) 213
Figure 7.2: True cyclic stress versus true cyclic plastic strain (Bannantine et al., 1990) 214
Figure 7.3: True cyclic stress versus true cyclic plastic strain for steel (Al-Hammoud, 2006) 214
Figure 7.4: Strain-life relationship (adapted from Bannantine et al., 1990) 215
Figure 7.5: Hysteresis loop (adapted from Bannantine et al., 1990) 216
Figure 7.6: Strain-life data for steel as reported by Al-Hammoud (2006) 217
Figure 7.7: Intersection of cyclic stress-strain curve and Neuber's hyperbola (adapted from Bannantine et al. 1990) 220
Figure 7.8: Intersection of the hysteresis loop and Neuber's hyperbola (adapted from Bannantine et al., 1990) 221
Figure 7.9: Experimental and predicted fatigue life of the unstrengthened beams using K_f= 2.0 224
Figure 7.10: Hysteresis loops of the steel of the unstrengthened beams UN15 227
Figure 7.11: Hysteresis loops of the steel of the in-service strengthened beams SL15 228
Figure 7.12: Hysteresis loops of the steel of the in-service strengthened beams SL20 229
Figure 7.13: Hysteresis loops of the steel of the overloaded strengthened beams OL15 230
Figure 7.14: Experimental and predicted fatigue life of the in-service SL15 beams versus the load range (K_f= 2.0) 232

Figure 7.15: Experimental and predicted fatigue life of the in-service SL20 beams versus the load range (K_f= 2.0) 232
Figure 7.16: Experimental and predicted fatigue life of the in-service OL15 beams versus the load range (K_f= 2.0) 233
Figure 7.17: Local stress distribution at a notch root (adapted from Masoud, 2002) 233

List of Tables

Table 2.1: Mechanical properties of FRP tendons (data compiled from different references) 14
Table 2.2: Effect of harping and cushioning on CFC cables (after Grace and Abdel-Sayed, 1998) 18
Table 2.3: Test results of the Aslan200™ CFRP tendons of 9.5 mm diameter (adapted from Quayle, 2005) 20
Table 2.4: Values of strain reduction coefficient, Ω, in uncracked state (adapted from Naaman, 2005) 34
Table 3.1: Properties of CFRP tendon Aslan200™ 49
Table 3.2: Test matrix for CFRP tendon-anchor assembly 50
Table 3.3: Change of modulus of elasticity, E_f, with number of cycles for specimens of Group (2) 59
Table 4.1: Test matrix for the reinforced concrete beams 71
Table 4.2: Concrete compressive strength results 83
Table 5.1: Change in tendon stress, Δf_f, for straight-with-guides and double draped tendons 108
Table 5.2: Midspan deflections of the in-service and overloaded beams (in mm) 113
Table 5.3: Variation of beam midspan deflections over beam life 126
Table 5.4: Variation of maximum concrete and steel strains at midspan over beam life 134
Table 5.5: Variation of CFRP stresses over the beam fatigue life 143
Table 5.6: Summary of beam fatigue parameters and failure modes 153
Table 6.1: Predicted versus experimental yield and ultimate loads of the in-service (SL) and overloaded (OL) beams 208
Table 7.1: Reinforcing steel fatigue properties (Al-Hammoud, 2006) 217
Table 7.2: Analytical nominal stress and local strains and stress values (K_f = 2.0) 226
Table 7.3: Fatigue provisions (adapted from CHBDC, 2000) 235

Notations

Δe	the nominal strain range
ΔM	the change in bending moment
ΔS	the nominal stress range
$\Delta \varepsilon$	the local strain range
$\Delta \varepsilon_{cp}$	the strain change in the concrete fibre at the level of the unbonded tendon
$\Delta \varepsilon_e$	the local elastic strain range
$\Delta \varepsilon_f$	the variation in the tendon strain due to load application
$\Delta \varepsilon_p$	the local plastic strain range
$\Delta \sigma$	the local stress range
$\Delta \sigma_e$	the local elastic stress range
a	the depth of the equivalent rectangular stress block in the concrete compression zone
a/d_p	the span-to-depth ratio
A_f	the area of the unbonded FRP tendons at the critical section
A_s	the area of the non-prestressed steel bars at the critical section
b	the width of the beam
	the fatigue strength exponent
c	the depth of the neutral axis
	the fatigue ductility exponent
$C_{(j,i)}$	the concrete compressive force at element j in the middle of layer i
$c_{(j)}$	the depth of the neutral axis at element j
C_i	the concrete force in layer i at the critical section
c_{ps}	the depth of the neutral axis at the end of post-tensioning stage
D	the midspan deflection of the beam after a certain number of cycles
d_f	the depth of the FRP tendons at the critical section
$d_{f(j)}$	the depth of the FRP tendon at element j
d_{fi}	the depth of the FRP tendon at any load level at the critical section
d_{fo}	the depth of the FRP tendon at the end of post-tensioning at the critical section
d_s	the depth of the steel bars at the critical section
E_c	the modulus of elasticity of concrete
E_f	the modulus of elasticity of the FRP tendon material
e_f	the eccentricity of the FRP tendon at the critical section
$e_{f(j)}$	the eccentricity of the FRP tendon at element j
e_m	the eccentricity of the unbonded steel tendons at midspan
e_{max}	the maximum nominal strain in the steel bar
e_{min}	the minimum nominal strain in the steel bar
E_{ps}	the elastic modulus of the unbonded steel tendons
$E_{rel(low)}$	the modulus of elasticity of concrete for the lower layers during the reloading stage
$E_{rel(up)}$	the modulus of elasticity of concrete for the upper layers during the reloading stage
E_s	the modulus of elasticity of the steel reinforcing bars
e_s	the eccentricity of the unbonded steel tendons at the support
E_{un}	the modulus of elasticity of concrete during the unloading stage
f'_c	the concrete compressive strength
f_c	the stress in the concrete top fibre at the critical section
$f_{c(j,i)}$	the stress in concrete at element j in the middle of layer i
$f_{c(avg)}$	the average tensile stress in concrete beyond its tensile rupture strength

f_{ci}	the stress in the concrete layer i at the critical section
f_f	the stress in the FRP unbonded tendon
f_{fe}	the effective prestressing force in the FRP unbonded tendon
f_{fh}	the additional local stress in FRP tendon due to harping
f_{fu}	the ultimate stress of the FRP tendon
f_{min}	the minimum stress level in the steel bar.
f_r	the rupture strength of concrete (tensile strength)
$f_{r(red)}$	the reduced concrete tensile strength due to fatigue
f_s	the steel stress for a given loading condition
f_{sr}	the permissible stress range in the steel bar.
f_{sunl}	the steel stress at the onset of the unloading stage
f_{sy}	the yield stress of the steel reinforcing bar
h	the total height of the beam
h_i	the height of the concrete layer i
I_{cr}	the cracked moment of inertia of the beam section
I_g	the gross moment of inertia of the beam section
I_{ps}	the moment of inertia of the beam section at the end of post-tensioning
k'	the strength coefficient of steel
K_f	the fatigue notch factor
$K_{f(exp)}$	the experimental fatigue notch factor
K_t	the stress concentration factor
L	the length of the beam
	the percentage of the fatigue life of the beam.
L_c	the width of the concrete crack
$l_{el(j)}$	the longitudinal length of element j
M_{ext}	the moment due to external loads at the critical section
$M_{ext(j)}$	the moment due to external loads at element j
M_{int}	the moment due to internal forces at the critical section
$M_{int(j)}$	the moment due to internal forces at element j
N	the number of cycles to failure
n	the number of concrete elements within half of the beam span
n'	the strain-hardening exponent of steel
n_f	the modular ratio for FRP
n_s	the modular ratio for steel
P	the external loads applied on the beam
P_{max}	the maximum fatigue peak load applied on the beam
P_{min}	the minimum fatigue peak load applied on the beam
P_y	the yield load of the beam
R	the fatigue load range applied on the beam
r/h	the ratio of base radius to height of rolled-on transverse deformation in the steel bar
R_f	the radius of the FRP tendon
R_h	the radius of curvature of the FRP tendon at the harped point
S	the nominal stress
S_{max}	the maximum nominal stress
S_{min}	the minimum nominal stress
T_f	The post-tensioning force in the FRP tendon at any loading stage
T_s	the steel tensile force at the critical section
$T_{s(j)}$	the steel tensile force at element j
$x_{(j)}$	the distance from the support to the center of the longitudinal beam element j

α_1	the tension stiffening factor accounting for bond characteristics of reinforcement
α_2	the tension stiffening factor accounting for type of loading
β	the tension stiffening bond factor
Δ	the deflection of the beam at the critical section
Δ_{ci}	the deflection of the concrete beam at any stage of the monotonic loading i
Δ_{co}	the deflection of the concrete beam at the end of post-tensioning
Δd_f	the variation in depth of the FRP unbonded tendon
Δf_f	the stress change in the FRP unbonded tendon
Δ_{fi}	the deflection of the FRP tendon at any stage of the monotonic loading
Δ_{fo}	the deflection of the FRP tendon at the end of post-tensioning
Δf_s	the change in steel stress during the unloading and reloading stages
$\Delta\varepsilon_s$	the change in steel strain during the unloading and reloading stages
ε	the local strain in steel
ε_c	the strain in the concrete top fibre at the critical section
$\varepsilon_{c\,(j)}$	the strain in the concrete top fibre at element j
$\varepsilon_{c\,(j,i)}$	the strain in concrete at element j in the middle of layer i
$\varepsilon_{c(avg)}$	the average tensile strain in concrete corresponding to the average tensile stress
ε_{ce}	the strain in concrete at the tendon level due to effective prestress
ε_{cf}	the strain in the concrete at the tendon level
ε_{ci}	the strain in concrete at the middle of layer i
ε_{co}	the strain in concrete corresponding to f'_c
ε_{cu}	the concrete strain at crushing
ε_f	the strain in the FRP tendon
ε'_f	the fatigue ductility coefficient
ε_{fe}	the effective strain in the FRP tendon due to the initial prestress
ε_{fu}	the strain of the FRP tendon at rupture
ε_{max}	the maximum local strain in steel
ε_{min}	the minimum local strain in steel
ε_p	the cyclic plastic strain in steel
ε_r	the tensile strain in concrete corresponding to f_r
ε_s	the steel strain
$\varepsilon_{s\,(j)}$	the steel strain at element j
ε_{su}	the steel strain at rupture
ε_{sunl}	the steel strain at the onset of the unloading stage
ε_{sy}	the steel yield strain
ρ_f	the FRP reinforcement ratio
σ	the local stress in steel
ΣC	the resultant internal compressive force in the beam section
ΣF	the resultant force at the beam section
σ_f'	the fatigue strength coefficient
σ_{max}	the maximum local stress in steel
σ_{mean}	the mean local stress in steel
σ_{min}	the minimum local stress in steel
ΣT	the resultant internal tensile force in the beam section
φ	the curvature of the beam at the critical section
$\varphi_{(j)}$	the curvature of element j
Ω	the strain reduction coefficient for unbonded tendon
Ω_{cr}	the strain reduction coefficient for unbonded tendon at cracking stage

Chapter 1

Introduction

1.1 General

Strengthening of reinforced concrete structures is a growing concern worldwide. A significant number of existing structures are now facing deterioration in the form of steel corrosion, concrete spalling, or excessive deflections. In addition, some of these structures were designed to carry loads that are significantly less than the current applied loads. This necessitates an immediate upgrading of these structures in order to improve their performance under the actual existing loads.

Strengthening of concrete structures can be achieved by various techniques, usually governed by the type of the structure and its functionality. External post-tensioning is a promising technique that is characterized by its ability to actively control stresses and deflections, its speed of installation, minimum interruption for the existing structure, and ease of inspection under service conditions. External post-tensioning implies exposing the tendons to the environment outside the concrete section. If steel tendons are used, they are placed inside ducts filled with grease or cement grout to minimize the corrosion of the external tendons. With the introduction of the fibre-reinforced polymer (FRP) materials in civil engineering applications, FRP tendons, with their excellent mechanical properties and high corrosion resistance, are a potential alternative to steel tendons for external post-tensioned applications.

External post-tensioning may be used to strengthen concrete structures having substantial spans, such as bridges. These types of structures are typically expected to resist repeated cyclic loading during their service lifetime, which might lead to a fatigue failure even at load ranges considerably less than the ultimate capacity of the structure. Fatigue is usually a concern in these strengthened elements owing to the existence of initial flexural cracks that fluctuate with the application of the peak cyclic loads.

To date, there have been few investigations on the performance of concrete structures strengthened with external post-tensioned FRP tendons under repeated cyclic loads, and experimental data on the behaviour of such members is limited. Most previous studies on externally post-tensioned elements have focused on investigating the monotonic response at the ultimate loading stage.

In the present research work, the monotonic and fatigue flexural behaviour of reinforced concrete beams strengthened with external post-tensioned Carbon FRP (CFRP) tendons are investigated. The potential for external post-tensioning as a strengthening technique to restore the monotonic capacity and the fatigue life of the strengthened beams is investigated, taking into consideration the loading history of the strengthened member prior to post-tensioning. In the following section, the organization of the present work is described.

1.2 Organization of the present work

The present research work investigates, experimentally and analytically, the flexural performance of reinforced concrete beams strengthened with externally post-tensioned CFRP tendons under monotonic and fatigue loading.

A literature review on the behaviour of externally post-tensioned beams using steel and FRP tendons is presented in Chapter 2. The main concerns on the use of FRP external tendons are discussed. A brief review of commercially available anchor systems for FRP tendons and their use

in post-tensioning construction, with a focus on their fatigue performance, is given. The effect of fatigue loading on the constituents of reinforced concrete and on reinforced and post-tensioned concrete beams is presented. The chapter concludes with the research needs and the main objectives of the current work.

Chapter 3 provides information on the FRP tendon-anchor system, known as the Waterloo anchor, used in post-tensioning the reinforced concrete test specimens of this study. The experimental test program developed to investigate the fatigue performance of the Waterloo anchor is described. Cyclic test observations and the fatigue results are discussed. The use of these results in designing the beam test specimens is presented.

Chapter 4 describes the main experimental program, consisting of twenty-eight unstrengthened and strengthened reinforced concrete beams. The methods adopted in the experimental phase of the study, along with a description of the material properties, the specimen geometry and fabrication, the post-tensioning setup, and the strengthening methodology are reported. A full description of the test setup, instrumentation, and monotonic and fatigue loading procedures is also presented.

In Chapter 5, the main results and observations of the monotonic and fatigue beam tests are discussed. The structural performance of the externally post-tensioned beams is described in terms of the measured beam deflections, the measured strains in the steel bars and concrete, and the observed changes in the stresses in the external CFRP tendons. The effects of different parameters on the fatigue life of the strengthened beams are also discussed.

In Chapter 6, a model that predicts the monotonic non-linear flexural response of the reinforced concrete beams strengthened with external post-tensioned FRP tendons is presented. The model incorporates the effect of the beam loading history on its structural performance until failure. The analytical predictions by the model are compared to the obtained experimental results.

Chapter 7 presents a strain-life based model to predict the fatigue life of the FRP externally post-tensioned beams. The methodology adopted in developing the model and current approaches for the fatigue life design are presented. Recommendations for design of FRP externally post-tensioned beams subjected to fatigue are provided.

Chapter 8 gives a summary of the current study, along with the conclusions and the recommendations for future work.

Chapter 2

Literature Review and Research Objectives

2.1 General

In this chapter, a review of the published experimental and analytical studies carried out on externally post-tensioned beams is provided. The main parameters affecting the behaviour of such beams are presented. The review focuses on the use of FRP tendons in external post-tensioning applications. Also presented in this chapter is the effect of the fatigue loading on the constituent materials of reinforced concrete structures. The chapter concludes with the research needs and the main objectives of the current work.

2.2 Background

Post-tensioned unbonded members are concrete members where no bond exists between the concrete and the post-tensioned tendons along the tendon length. Two categories of such members are defined according to the location of the unbonded tendons relative to the concrete section: internal unbonded and external unbonded members.

Internal unbonded tendons are placed inside the concrete element within ducts or sheaths extending along the post-tensioned member and are connected to the concrete element only at the anchored ends. Relative movement between the tendon and the concrete occurs along the tendon length during post-tensioning and under loading of the structure. This type of tendon has

been widely used in post-tensioned concrete structures, such as one-way and two-way slab systems. Since no grouting of ducts is required, the unbonded construction can be cost and labor effective in comparison to grouted or bonded tendon systems.

The unbonded tendons for external post-tensioning systems are placed completely outside of the concrete section. Similar to the unbonded internal tendons, the external tendons are attached to the concrete structure by anchors, usually placed at the ends of the element. External post-tensioning is used in the construction of new structures and the strengthening of the existing ones. The tendons may be straight or draped at one or more points. Deviators (or guides) are placed at specific locations along the concrete element to create different profiles of the external tendons. Figure 2.1 shows the most commonly used profiles of external tendons; the straight profile (with or without in-span guides), the single draped profile, and the double draped profile.

The analysis of internally and externally unbonded post-tensioned elements is conceptually similar, as no bond exists between the tendons and the concrete. The main difference in behaviour between the two types of unbonded construction lies in the change in depth of the external tendons (and consequently the change in their eccentricity) with respect to the axis of the beam, as the loads progressively increase to ultimate conditions. The depth and eccentricity variations in external tendons (known as second-order effects) are caused by the tendons remaining rectilinear between the deviators (or the end anchorages) while the beam deformation is curvilinear (Figure 2.2).

When used in new structures, the unbonded tendons constitute the main reinforcement of the member. The member may be “fully prestressed,” where the tendons constitute the only flexural reinforcement, or “partially prestressed,” where bonded non-prestressed flexural reinforcement exists in addition to the unbonded tendons (ACI-423.5R, 1999). When used for strengthening, the external tendons represent only a portion of the total reinforcement of the element. Reinforced

concrete elements strengthened with external post-tensioned tendons are thus considered "partially prestressed" elements.

The design engineer decides on a number of factors when strengthening an existing concrete element: the tendon profile, the location and the number of deviators, the number of tendons, and the magnitude of the post-tensioning force to be applied to the tendons. At this stage, the structural condition of the element and the existing constraints that surround the element are also taken into consideration. If steel tendons are used, they are placed inside ducts filled with grease or cement grout to minimize the corrosion of the external tendons. With the introduction of the fibre-reinforced polymer (FRP) materials in civil engineering applications, FRP tendons, with their excellent mechanical properties and high corrosion resistance, are a potential alternative to steel tendons for external post-tensioned applications. In the following sections, a literature review on external post-tensioning with steel and FRP tendons is presented.

2.3 External post-tensioning with steel tendons

Numerous studies have been devoted to investigate the flexural response of externally post-tensioned concrete beams. Of these studies, a considerable amount of research has dealt with beams externally post-tensioned with steel tendons. The flexural response of such elements is influenced by different parameters such as the number of deviators used, the external tendon profile, the geometry of the external loads applied, the amount of the non-prestressed bonded reinforcement, the level of external post-tensioning force, the member span-to-depth ratio, and the concrete strength of the element. The effects of the most commonly investigated parameters on the structural performance of the externally post-tensioned beams are briefly discussed in the following sections.

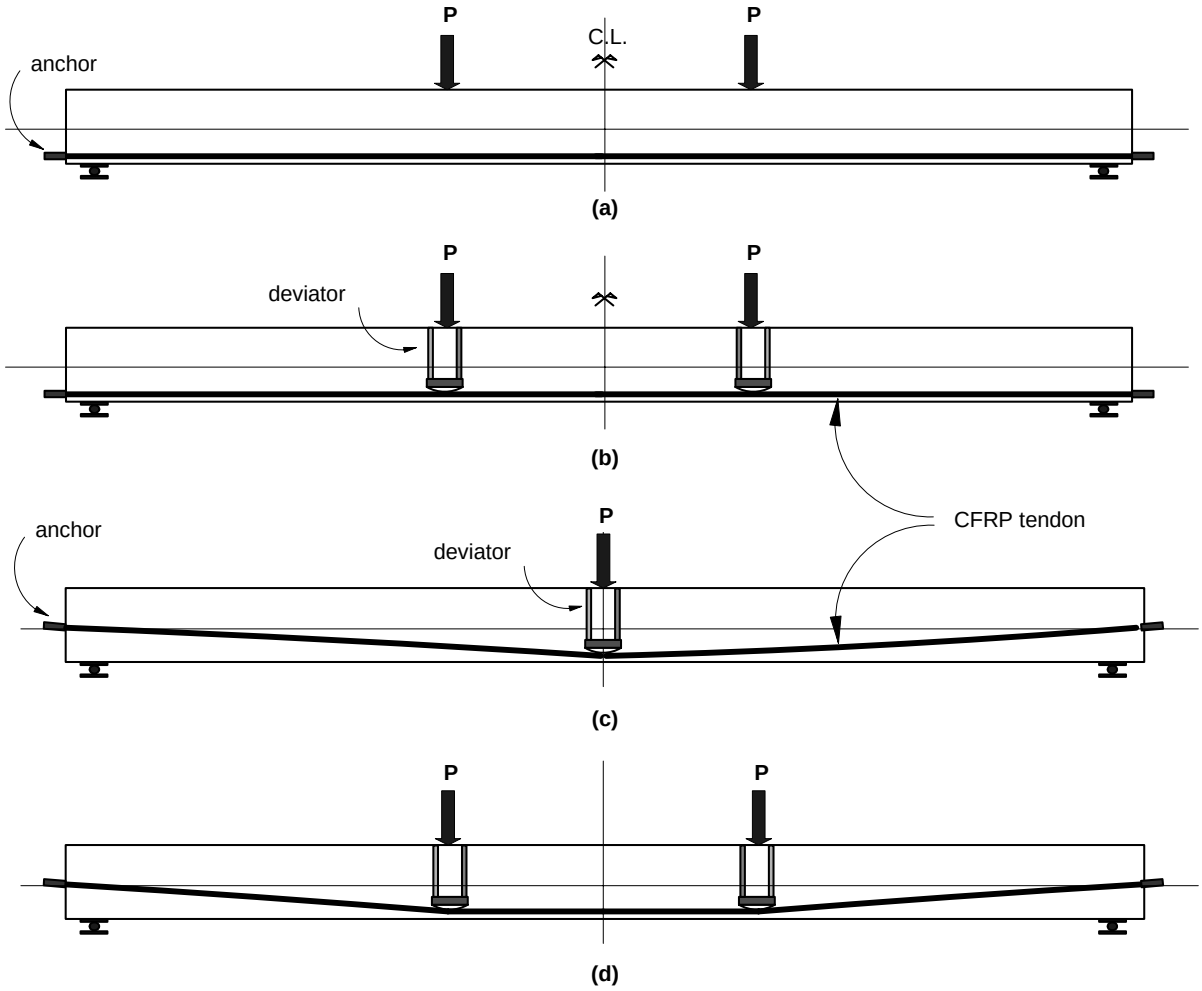

Figure 2.1: Common profiles for external tendons: (a) straight, (b) straight with guides, (c) single draped, and (d) double draped

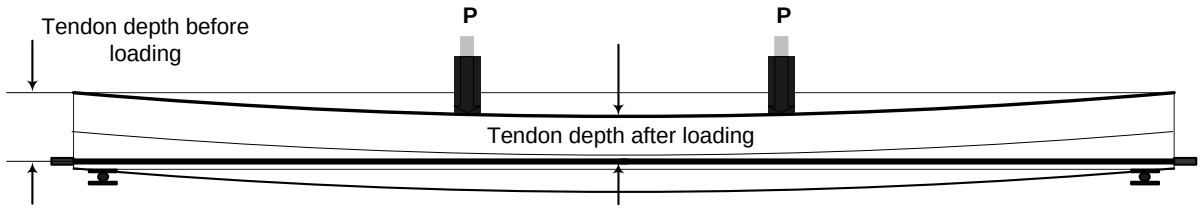

Figure 2.2: Depth and eccentricity variations of a straight tendon

2.3.1 Deviators and tendon profile

External tendons may have different profiles as they are placed outside the concrete section (Figure 2.1). Straight tendons and tendons that are draped at one or two points are the most commonly used profiles. A draped profile is achieved by means of deviators (or guides). Straight tendons may also be guided by deviators in order to minimize the second-order effects during the beam loading (Figure 2.2).

Providing one or two deviators at mid-span considerably reduces the change in the tendon eccentricity and hence, enhances the ultimate capacity and the ductility of the beams, as reported by many authors (e.g., Rao and Mathew, 1996; Ariyawardina et al., 2000; Wu et al., 2003). This effect is more substantial in beams with a large span-to-depth ratio. Campos et al. (2001) reported that the effect of the variation of the tendon eccentricity is significant for beams with span-to-depth ratio higher than 21, leading to up to a 70% reduction in the initial tendon eccentricity.

Tan and Ng (1997) tested six identical reinforced concrete beams externally post-tensioned with steel tendons. As part of the study, the effect of the presence of deviators on the flexural response of the beams was investigated. Straight tendons (with and without deviators) and singly draped tendons (using one deviator at midspan) were investigated. Similar load-deflection relationships were reported up to the cracking load for all beams. Beyond cracking, the beam with straight tendons and deviators registered smaller deflections at any particular load level than those without deviators. Negligible change in the eccentricity of the singly draped tendons was encountered. A reduced stiffness and wider spread of cracks at midspan were reported for the beam with singly draped tendons. This was attributed to the gradual change in the tendons depth in the constant moment region, as imposed by the deviated profile of the tendon. The beam also exhibited a greater tendon stress increase, and a more ductile behaviour compared to the beam with straight tendons.

Harajli et al. (1999) conducted a parametric investigation to study the effect of deviators on the behaviour of beams strengthened with external straight steel tendons. Beam models with and without deviators located at mid-span were studied. In the presence of deviators, the influence of the second-order effects on the flexural response of the beams was minimal. For the beams without deviators, the progressive reduction in the tendons eccentricity with the increasing load led to a lower nominal flexural strength and lower inelastic deformations of the beams, as compared to beams with deviators. The study showed that the ultimate strength of the beams can be increased by providing one or two deviators at mid-span. It was also reported that the nominal moment capacity increased with increasing the distance between the deviators up to one-fourth of the span length and then decreased depending on the extent of the second-order effects.

2.3.2 Non-prestressed bonded reinforcement

Unbonded post-tensioned beams are characterized by fewer cracks developed in the region of the maximum moment in comparison to the bonded post-tensioned beams. After cracking, the unbonded element behaves as a shallow tied arch rather than a flexural member due to the absence of bonded reinforcement in the cross section of the element (Mattock, 1971). As the load increases progressively, the cracks become wider and the deflection increases significantly before additional cracks will form. These cracks open more rapidly than cracks in bonded prestressed concrete members.

Adding bonded non-prestressed reinforcement to the section results in crack widths and spacing similar to those found in bonded prestressed concrete beams. It also decreases the deflection of the beams compared to those with unbonded tendons only (Burns and Pierce, 1967; Eibl, 1990; Campbell et al., 1991; Chakrabarti et al., 1994; Ariyawardina, 2000; Ghallab and Beeby, 2005).

Tao and Du (1985) tested 26 prestressed beams with different amounts of unbonded and bonded steel. The bonded steel was selected on the basis that the beams at failure would fall into three categories, with the non-prestressed steel carrying 30%, 50%, and 70% of the total ultimate load. It was reported that the tendon stress increment at failure increased with the decrease of the total reinforcement amount (bonded and unbonded reinforcement). Beams with low total reinforcement amount were more ductile than those beams with high reinforcement amount. The same conclusion was reported by Chakrabarti (1995), who concluded that the change in stress in the unbonded steel tendons at ultimate was smaller when the total reinforcement amount increased.

2.3.3 Post-tensioning force

Increasing the magnitude of the post-tensioning force in the external steel tendons generally leads to a decrease in the stress change at ultimate. It also causes a significant increase in the nominal flexural strength of the concrete members (Chakrabarti, 1995). However, the gain in the nominal flexural strength is accompanied by a reduction in the ductility of the flexural failure, as reported by Harajli et al. (1999). That is, the deflection of the concrete element at failure tends to decrease as the magnitude of the external post-tensioning force increases.

The increase in the external post-tensioning force also affects the stiffness of the post-tensioned beams. This is of great significance in strengthening applications where external post-tensioning is used to restore the stiffness and deflection of cracked concrete elements. Harajli et al. (1999) reported that, if the external post-tensioning force is large, the slope of the load-deflection response after post-tensioning becomes equal to that of the non-post-tensioned beam before cracking. This would lead to enhancing the service load behaviour of the beam, as the deflection induced by the applied live load is reduced due to stiffness improvement. This agreed with the

findings of Tan and Ng (1997) who reported that the use of smaller effective post-tensioning force led to larger crack widths and larger service load deflections.

2.3.4 Beam span-to-depth ratio

The effect of the span-to-depth ratio, a/d_p, on the flexural behaviour of concrete beams post-tensioned with internally unbonded and external steel tendons has been widely investigated in the literature. Mojtahedi and Gamble (1978) investigated data from tests carried out on internally unbonded specimens with various span-to-depth ratios. It was reported that increasing the a/d_p ratio would result in a significant reduction in the stress increase of the unbonded tendons at ultimate. A similar conclusion was reported by Harajli (1990) in his parametric study on externally post-tensioned beams.

Harajli and Hijazi (1991) carried out an analytical investigation on the behaviour of the unbonded post-tensioned beams. It was reported that increasing the span-to-depth ratio, a/d_p, decreased the predicted stress increase in the unbonded tendons at ultimate. The effect of the span-to-depth ratio diminished with the increase in the length of the constant moment region (e.g. in case of one-third span loading with two-point loads) or, equivalently, the length of the plastic hinge zone developed in the member at failure. The reduction in the change in the tendon stress at ultimate with increasing a/d_p was most significant for members loaded with single concentrated load.

Harajli and Kanj (1992) tested twenty-six beams with different span-to-depth ratios (ranging from 8 to 20), different internal bonded non-prestressed reinforcement, and different unbonded prestressed tensile reinforcement. The obtained results confirmed that increasing the span-to-depth ratio, a/d_p, decreased the predicted stress increase in the unbonded tendons at ultimate. In contradiction with the analytical observations reported by Harajli and Hijazi (1991), the type of

load application did not show significant influence on the stress increase in the unbonded tendons at ultimate.

From a parametric study carried out on simple beams post-tensioned with external tendons deviated at third points, Alkhairi (1991) concluded that, when the span-to-depth ratio of the beams changed from 8 to 57, the tendons eccentricity at mid-span reduced from 5% to as much as 50%, which in turn decreased the change in the tendon stress at ultimate.

Ng (2003) demonstrated analytically that the average strain in the external tendons at all stages of loading is independent of the span-to-depth ratio of the beam. An experimental study was conducted on seven externally post-tensioned beams having the same internal amount of reinforcement but with different span-to-depth ratios ranging from 7.5 to 30. The obtained results confirmed the analytical findings that the span-to-depth ratio had no effect on the stress increase in the tendons at ultimate.

2.4 External post-tensioning with FRP tendons

2.4.1 General

FRPs are composite materials consisting of high strength fibres impregnated in a resin matrix. The fibres are the reinforcement medium of the FRP composite that provides the strength and the stiffness of the composite. The volume of the fibres may vary relative to the matrix, thus obtaining a wide range of the composite mechanical properties, such as ultimate strength, modulus of elasticity, and strain to rupture (Table 2.1). The FRP composites used for construction are classified according to the type of fibre into three categories: Aramid FRP (AFRP), Carbon FRP (CFRP), and Glass FRP (GFRP), as follows:

Aramid FRP (AFRP) — AFRP are manufactured in various shapes such as braided, spiral wound and flat rods. They are available commercially in four main types: Arapree (Italy), Fibra

(Japan), Technora (Japan), and Parafil (UK). AFRPs are characterized by their good fatigue resistance; however, they are susceptible to damage by ultraviolet radiation.

Carbon FRP (CFRP) — CFRPs are available in the form of bars, multi wire strands, ropes, and cables. They are available commercially as Leadline (CFRP) and Carbon Fibre Composite Cable (CFCC), both of Japan, and Aslan200™ tendons of USA. Carbon fibres are characterized by their high longitudinal tensile strength and their high modulus of elasticity.

Glass FRP (GFRP) — two types of glass fibres are commonly used in construction: E-glass and S-glass, with the later having a higher tensile strength. GFRP tendons are commercially available as Isorod (Canada), Aslan100 (USA), and Plalloy (Japan). GFRPs are characterized by their low modulus of elasticity and their low transverse shear resistance. GFRP tendons are not recommended as prestressing tendons (ACI 440.4R, 2004), but are commonly used in non-prestressed applications. Figure 2.3 shows FRP tendons available commercially for general prestressing applications.

Table 2.1: Mechanical properties of FRP tendons (data compiled from different references)

Property	AFRP				CFRP		
	Arapree	Fibra	Technora	Parafil	Leadline	CFCC	Aslan 200
Longitudinal Tensile Strength, GPa	1.2-1.5	1.25-1.4	1.7-2.1	1.2-1.9	2.25-2.55	1.8-2.1	2.06-2.4
Transverse Tensile Strength, MPa	-	30	-	nil	57	-	-
Transverse Tensile Modulus, GPa	-	5.5	-	nil	10.3	-	7-8
Longitudinal Tensile Modulus, GPa	62-64	65-70	54	120-130	142-150	137	120
Ultimate tendon Elongation, %	2.4	2.0-3.7	3.7-3.8	1.5-1.7	1.3-1.5	1.57	1.89
Coefficient of thermal expansion	$-2x10^{-6}$	$-2x10^{-6}$	$-3x10^{-6}$	-	$-0.9x10^{-6}$	$0.5x10^{-6}$	-
Poisson's Ratio	0.38	0.34-0.6	0.35	-	0.27	-	-

The use of FRP in external post-tensioning industry has grown significantly in the last decades. The interest in composite technology in concrete construction is primarily to avoid the problem of steel reinforcement corrosion. In comparison to steel cables, FRP tendons are non-corroding with good fatigue properties and low relaxation losses. They also possess smaller diameters and require only small and simple deviation devices (Keller, 2003). The high strength-to-weight ratio of FRPs allows the application of large prestressing forces with minimal weight added to the structure. Thus, they present strong alternatives to steel as external tendons in repairing and strengthening damaged concrete structures.

On the other hand, FRPs are brittle materials that do not show plastic behaviour or yielding. Figure 2.4 shows typical stress-strain relationship of FRP material. If bonded to concrete, the FRP tendons will experience high local strains at the crack locations in the concrete beam (Burgoyne, 1993). If the strength of the tendon is exceeded, the tendon will rupture, leading to a brittle failure. This is not the case in unbonded tendon where, due to the lack of bond between the tendon and the surrounding concrete, no local stress will develop in the tendon at the crack locations. The stress in an unbonded tendon is constant along its entire length between the end anchorages (neglecting prestress losses and friction between the tendons and the deviators). As the beam deforms under loading, the tendon elongates causing the stress in the tendon to increase. Since the tendon is unbonded, the elongation is uniform along the tendon length, and hence, the stress increase is also constant along the tendon. The consequence of this behaviour is that, for the same support and loading conditions, the stress increases at a slower rate in an unbonded tendon in comparison to a bonded tendon, and the stress in the unbonded tendon will generally be less than its rupture stress when the beam reaches its ultimate capacity. This avoids a sudden brittle failure of the FRP tendon, and results in an increase in the ductility of the unbonded concrete element (Mutsuyoshi et al.,1990; Alkhairi, 1991; Kato and Hayashida, 1993).

Figure 2.3: Samples of FRP tendons (El Refai et al., 2003)

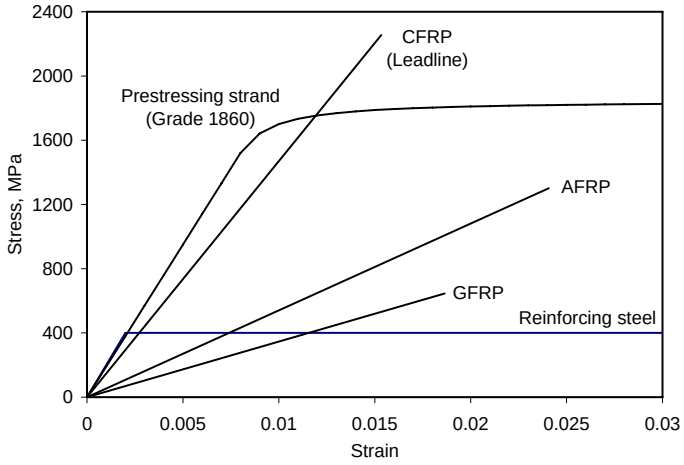

Figure 2.4: Typical stress-strain relationship of different tendon materials (adapted from CPCI Design Manual, 1996 and ISIS Canada Educational Modules, 2004)

2.4.2 Harping of FRP tendons

Draped tendon profile imposes the tendons to be harped at one or more points at the deviator locations. When FRP tendon is harped, localized curvature stress in the tendon is developed leading to a high stress concentration in the tendon. Due to the elastic behaviour of FRP up to failure, the increase in stress at the curved points may lead to premature failure at the harped locations. This amount of stress must be accounted for in determining the tendon strength. The deviator curvature, the tendon size, and the harped angle are the most common factors affecting the increase in the tendon stress.

Few investigations have focused on the effect of harping on the tensile capacity of FRP tendons. As part of their study on externally post-tensioned beams, Mutsuyoshi and Machida (1993) found that CFRP tendons ruptured at 77% to 80% of their breaking load when deviated at angles of 7.1^{o} and 11.3^{o} using steel deviators of 400 mm diameter. Adachi et al. (1997) carried out static tensile tests on AFRP and CFRP tendons deviated at 10 degrees over a radius of curvature of 3000 mm and reported a 10% reduction of the tendons tensile capacity.

Grace and Abdel-Sayed (1998) reported that increasing the deviator diameter and decreasing the draping angle, combined with the use of cushioning material between the FRP tendons and the deviators, significantly minimized the reduction in the breaking force of CFC cables and Leadline CFRP tendons. These findings are summarized in Table 2.2. For the same draping angle (5^{o}), only 12% reduction of the tendon breaking force was observed for a deviator diameter of 508 mm (20 in.), compared to a 34% reduction when a deviator diameter of 50.8 mm (2 in.) was used. A draping angle as large as 10 degrees was used without an appreciable reduction in the strength of the tendons providing that cushioning material is used.

Table 2.2: Effect of harping and cushioning on CFC cables (after Grace and Abdel-Sayed, 1998)

Harping angle (Degrees)	Deviator diameter (mm)	Cushioning	Avg. breaking load (kN)	Reduction in breaking load
0	0	NO	163.8	0%
3	50.8	NO	132.2	19%
5	50.8	NO	106.5	34%
5	508	NO	143.3	12%
10	508	NO	121.8	26%
5	508	YES	161.5	1%
10	508	YES	149.1	9%

Dolan et al. (2001) conducted twelve tests on Leadline and Strawman CFRP tendons using saddle of radii ranging from 28.5 to 914 mm. The following equation was suggested to estimate the localized additional stress due to bending at the deviator, f_{fh}:

$$f_{fh} = \frac{E_f R_f}{R_h} \tag{2.1}$$

where R_f is the radius of the FRP tendon, R_h is the radius of curvature at the harp point, and E_f is the modulus of the tendon material.

Santoh (1993) depicted the relationship between the tensile strength of the CFC cables and the angle of curvature when the cables were bent while subjected to tension. A slight reduction in the cable strength was observed when the angle of curvature is 10 degrees or less. According to the Tokyo Rope manufacturer, a cushion material such as low-density polyethylene or Teflon sheaths must be used at the saddle point when the angle of bent at the saddle is larger than 5 degrees (Santoh, 1993).

Quayle (2005) carried out a comprehensive experimental investigation on the effect of harping of CFRP tendons on their tensile capacity, using the same tendons used in the current study

(Aslan200™ CFRP tendons). Three main parameters were investigated: the tendon diameter (6.3 mm and 9.5 mm), the deviator radius (50 mm, 100 mm, 250 mm, 500 mm, and 1000 mm), and the harping angle (2, 3, 5, 6, 9, 10, and 15 degrees). Twenty-four combinations were investigated under tensile loading. Three modes of failure were observed: bending-tension, bending-compression, and bending-shear failure, with the last two modes occurring at relatively low load levels. Table 2.3 shows the experimental results of the tested specimens of 9.5 mm diameter that failed in tension. The reduction in the tensile strength of the CFRP tendons ranged between 13% and 50% of the tendon ultimate capacity. Increasing the harping angle or decreasing the deviator radius decreased the tensile capacity of the harped tendons.

It is worth mentioning that the discrepancy of the reported results on the reduction in the tensile capacity of the FRP tendons due to harping is attributed to the wide range of the tendon materials used and on the various methods of testing adopted in these investigations. It is also related to the inconsistency in the characteristics of the FRP tendons made of the same material. This indicates that each type of tendon should be assessed individually before using the tendon in practical applications. However, most of these investigations confirmed the fact that reducing the deviated angle of the FRP tendons and increasing the deviator curvature would limit the reduction of tendon capacity at the harped locations.

2.4.3 FRP anchoring systems

As previously mentioned, the fibres are the reinforcement medium of the FRP composite. Most of the FRP tendons have uni-directional fibres linearly oriented along the tendon. Despite their high tensile strength in the direction of the fibres, FRP tendons are weak in the transverse direction. They are highly vulnerable to premature failure at the anchor zones if notching occurs in the tendon during the post-tensioning process or during service. This makes the conventional anchors used for steel tendons not suitable for FRP.

Table 2.3: Test results of the Aslan200™ CFRP tendons of 9.5 mm diameter (adapted from Quayle, 2005)

Specimen	Deviator radius	Harp angle	Reduction in breaking load compared to straight tendon
1	50	2	23.4%
2	50	3	39.3%
3	100	3	44.0%
4	250	2	15.0%
5	250	3	27.0%
6	250	5	49.0%
7	500	2	13.0%
8	500	3	26.0%
9	500	5	34.0%
10	500	6	43.0%
11	500	9	36.0%
12	500	10	50.0%
13	1000	5	21.0%

Various anchor systems for FRP tendons have been developed over the last two decades. Anchor systems are often recommended by the manufacturer of the FRP tendon, and are usually classified based on their gripping mechanism. Since each type of FRP tendon has its unique characteristics, none of the existing anchor systems ensures full transfer of the ultimate capacity for all of them. Figure 2.5 shows a schematic of commercially available anchors, which are briefly described as follows:

Clamp anchor — clamp anchor consists of grooved steel plates held together, clamping the FRP tendon by prestressed bolts and springs (Figure 2.5-a). The tensile force of the tendon is transferred to the anchor by a shear-friction mechanism. Sleeves encasing the tendon are used to protect it from the compressive clamping force. The sleeves smoothly redistribute pressure on the tendon thus, preventing high stress concentration. These anchors perform best on glass tendons and are less effective with high strength carbon tendons.

Plug and cone anchor — the plug and cone anchor consists of a socket housing and conical spike (Figure 2.5-b). The system is used to anchor Parafil ropes where the fibres are not encased in resin media but are, alternatively, held only by an outer protection sheath. The rope is held by a compressive force, generated by inserting the spike into the barrel, together with friction forces developed between the rope and the socket. The spike generates friction stresses that resist the slipping of the rope out of the socket.

Resin sleeve anchor — in this anchor system (Figure 2.5-c), the FRP tendon is embedded in resin filling a metallic housing (steel or copper). The tendon is gripped by bond between the tendon and the filling material. Sand may be added to the resin to ensure load transfer between the resin and the housing socket. A drawback of this anchor is the curing time required by the expansive cementitious materials used as resin filling.

Resin potted anchor — this system is similar to the resin sleeve anchor (Figure 2.5-d). It has the same components except that the profile of the inner surface of the socket is not straight. Load is transferred from the tendon to the sleeve by interfacial shear stresses that vary with the variation of the normal stress produced by the potting material profile. A conical profile with a constant taper angle is the most commonly used resin potted anchor.

Metal overlay anchor — a metal overlay is attached to the ends of FRP tendon during the manufacturing process by means of die molding (Figure 2.5-e). The tendon and the molded metal are compressed by a typical wedge anchor. Load is transferred by friction between the tendon and the anchor. The use of this system is limited since it requires a predefined length of the tendon to cast the metal tube at a specific location on the tendon during fabrication.

Split wedge anchor — the wedge anchor (Figure 2.5-f) consists of a number of wedges fitted into a barrel or socket. The number of wedges varies from two to six. Increasing the number of wedges helps to ensure a smooth distribution of radial stresses on the tendon surface. A soft metal sleeve encasing the tendon is usually used to protect it from notching.

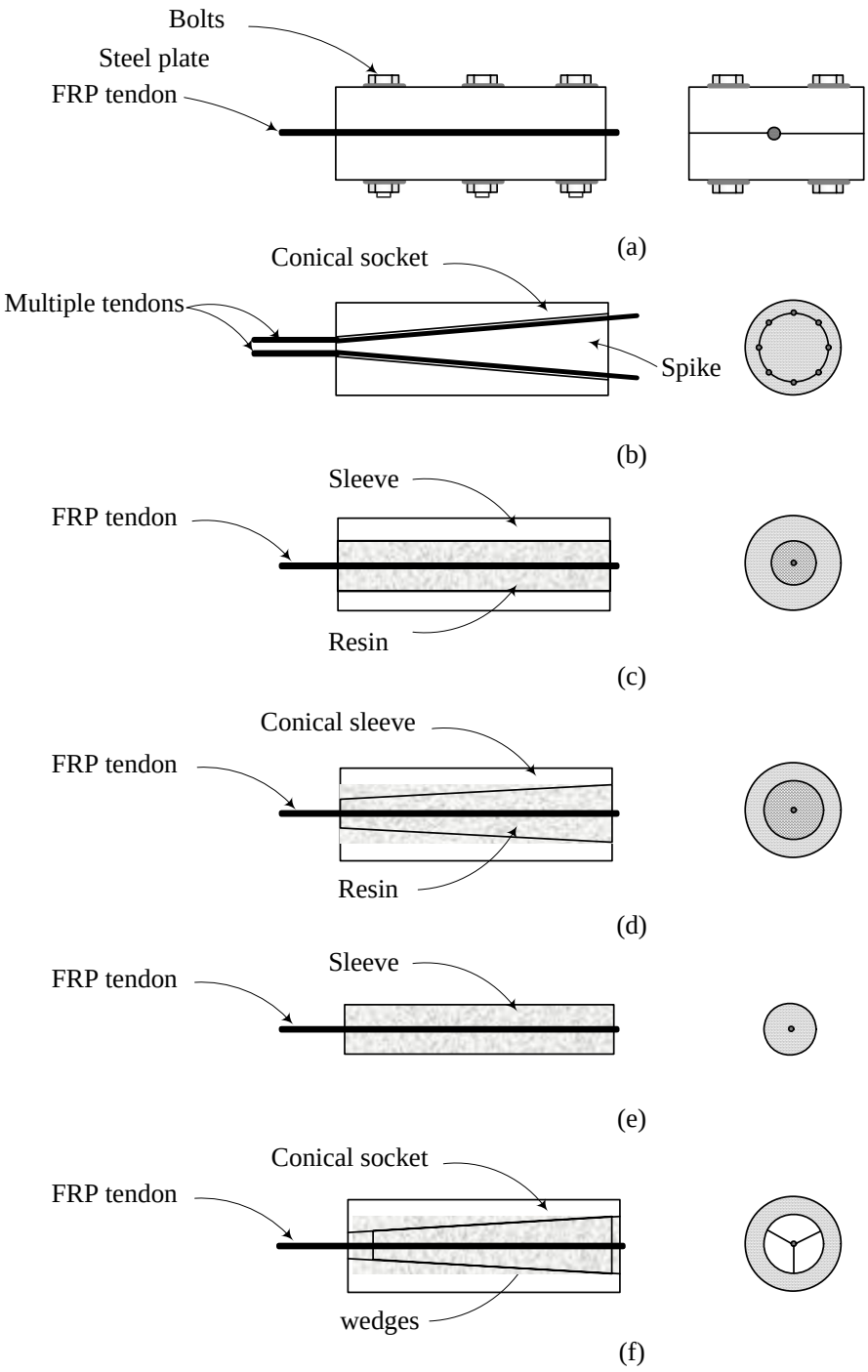

Figure 2.5: Anchors for FRP tendons: (a) clamp, (b) plug and cone, (c) resin sleeve, (d) resin potted, (e) metal overlay, and (f) split wedge anchors (adapted from ACI 440.4R, 2004)

Several investigations have been conducted on various FRP tendon-anchor systems to evaluate their efficiency under static loading (Walton and Yeung, 1986; Schmidt et al., 1994; Nanni et al., 1996; Benmokrane et al., 2000; Al-Mayah, 2001; Taha and Shrive, 2003; ACI-440.4R, 2004). In most cases, the anchor, rather than the tendon itself, controlled the ultimate capacity of the tendon with varying degrees of success in maintaining the applied load.

Nanni et al. (1996) conducted a comprehensive short-term evaluation of some commercially available FRP tendon-anchor systems. Wedge anchors with steel, plastic, and aluminum wedges as well as potted anchors with cylindrical, conical, and parabolic steel chucks were investigated under sustained loading. For wedge-type anchors, high localized stresses were reported depending on the wedge materials, with the damage more pronounced when steel wedges were used. Sudden slip was reported when plastic or aluminum wedges were used. Potted anchors performed well, and showed less local damage in the vicinity of the anchors.

Repeated or cyclic loading on the structural element adds another dimension to the anchoring problem for FRP tendons. Structures such as bridges are expected to sustain millions of load cycles during their service life, which could cause fatigue damage to the tendon-anchor system. Due to the absence of a reliable universal anchor for FRP tendons, data on the fatigue performance of the FRP tendon-anchor systems are few.

Uomoto et al. (1995) investigated the tensile strength and the fatigue life of aramid, glass, and carbon FRP tendons using split wedge anchors. Twenty-one tendons 6 mm diameter and 400 mm long, were tested. In the fatigue tests, the applied upper stress varied between 20% and 100% of the static tensile strength of the specimens. Five load ranges varying between 7% and 72% of the tendon strength were considered under frequency of loading varying from 1 to 10 Hz. The fatigue strength of the carbon tendons was superior over that of the aramid and glass tendons. The CFRP tendons withstood more than 4 million cycles when the maximum stress was less than 87.5% of the tensile strength. It was reported that the fatigue strength of the tendons was governed by

creep failure at higher applied stress levels. No data was reported on the type and the performance of the anchor system used in these tests.

Saadatmanesh and Tannous (1999) tested 190 samples of Leadline and CFC cables in tension-tension fatigue to investigate the variation in their mechanical properties with the applied fatigue loading. The specimens were 400 mm long and were instrumented with strain gages to monitor strain values while loading. Wedge-type anchors specified by the manufacturer were used in anchoring the Leadline specimens. Three different stress ranges and seven minimum stress levels were considered. It was reported that limited changes in the modulus of elasticity and Poisson's ratio had occurred when the tendons were subjected to a stress range of 5% of the ultimate strength of the tendon. When the stress range increased to 10% of the ultimate capacity of the tendon, an increase in the modulus of elasticity and Poisson's ratio of the tendon material was observed, indicating brittleness with increasing fatigue cycles. The performance of the anchor under fatigue loading and its influence on the failure or fatigue life of the tendon was not reported.

The results reported by Saadatmanesh and Tannous (1999) were consistent with the findings of Dolan (1993) that under fatigue loading, the stiffness (elastic modulus) of glass FRP tendons was reduced as the number of cycles increased, while the aramid and carbon FRP tendons gained stiffness. The gain in stiffness was attributed to the tendency of the fibres to straighten out during cyclic loading.

Walton and Yeung (1986) tested FRP tendons made of E-Glass, aramid (Kevlar 49) and carbon FRP of 5.0 mm diameter under fatigue loading. The tendons, anchored with potted conical sockets at both ends, were subjected to load steps of two-million cycles each, and of increasing applied load ranges. It was reported that failure of all specimens had initiated at the neck of the conical sockets due to the high local stress concentration in the anchor zone.

Budelmann et al. (1990) conducted fatigue tests on E-glass FRP tendons of diameter of 7.5 mm anchored with a bond-type anchor consisting of a cylindrical steel tube filled with quartz sand and polyester resin mortar. Two maximum stresses varying between 50% and 60% of the tendon ultimate strength (1600 MPa) were considered. Stress amplitudes between 30 and 100 MPa were applied. The typical fracture mode reported for all specimens was the fracture of the fibres near the anchor. Failure started inside the tube due to the loss of bond between the tendon and the grout mortar. Fatigue damage was due to the superficial wear between the bar and the anchorage mortar.

Odagiri et al. (1997) conducted fatigue tests on aramid FRP tendons (6 mm and 7.4 mm in diameter) of 200 and 300 mm long. A bond type anchor consisting of a steel tube filled with a non-shrink grout mortar was used for the specimens. The anchor had a bond length varying between 300 and 500 mm for the 6 mm and 7.4 mm diameter, respectively. The maximum stresses applied varied between 54% and 73% of the ultimate tensile stress of the specimen (550 MPa). The loading frequency was set between 4 and 6 Hz and testing continued up to the failure of the specimen or 2 million cycles. It was reported that the strength of the AFRP tendon was governed, without exception, by the failure at the end of the anchor system.

Sayed-Ahmed and Shrive (1998) tested a stainless steel wedge-type anchor (known as the Calgary anchor) for CFRP tendons. The anchor consisted of a stainless steel barrel having a conical shape, four steel wedges and a copper sleeve placed between the wedges and the tendon. Five fatigue tests were performed on the CFRP tendon-anchor system by applying sequential load ranges each lasting for a specified number of cycles. Four rates of loading ranging from 1 to 10 Hz were considered. It was reported that the anchor system successfully passed all the tests without premature failure at the anchored ends. The stress range, rather than the mean stress, had the most significant effect on the life of the specimens. The PTI fatigue requirements (1997) were also met by the anchor. However, data on the fatigue life of the specimens were not reported.

Fatigue versus slip behaviour of a stainless steel wedge-type anchor was also investigated by Al-Mayah et al. (2001). Cyclic load tests were conducted on CFRP Leadline gripped at both ends by the anchor, using aluminum sleeve inserted between the tendon and the wedges. Different stress ratios (0.65, 0.86, and 0.9), defined as the ratio of the minimum to the maximum stress, were adopted to the anchored specimens. The fatigue life of the specimens decreased with the increase of the applied stress ratio. The anchor withstood two million cycles with little effect on the relative movement of the sleeve along the tendon.

Taha and Shrive (2003) tested a concrete wedge-type anchor for CFRP tendons. The anchor consisted of a conical-shaped barrel and four wedges all made of ultra-high-performance concrete (UHPC) of more than 200 MPa compressive strength. The barrel was wrapped with CFRP sheets to increase the load carrying capacity of the anchor. Six CFRP tendon-anchor assemblies of 1500 mm length each were tested under cyclic load in conformance with the Post-Tensioning Institute (PTI) standards. Two tendons were reported to have failed in the anchor zones due to fatigue.

2.4.4 Previous studies on FRP externally post-tensioned beams

A survey of the research studies conducted on concrete members post-tensioned with unbonded FRP tendons was conducted. The available studies are categorized and summarized in the following points:

Steel versus FRP unbonded tendons — experimental and analytical studies were conducted in order to compare the monotonic behaviour of concrete beams post-tensioned with steel and FRP unbonded tendons. Various types of FRP tendons were used in these studies. Manabe et al. (1997) tested three T-girders (1:2.5 scale) post-tensioned externally with steel, AFRP, and CFRP tendons. The beams were loaded statically up to failure. All beams failed by concrete crushing at the loading points. It was reported that there were no significant differences in the cracking load and

the ultimate capacity between the FRP and the steel prestressed beams. All beams showed similar relationships between the load and deflection at all stages of loading.

Mutsuyoshi et al. (1993) tested six beams externally post-tensioned with three types of tendons: steel, AFRP, and CFRP tendons. The beams were three metres long each, with a T-cross section of 100x300x400 mm. Steel deviators were used to create two angles of deviations of 7.1 and 11.3 degrees. The external tendons were draped at two deviated points and prestressed with a force less than 50% of the nominal tensile strength of the tendon. Similar behaviour was reported for both steel and FRP beams in terms of the load-deflection characteristics.

Ariyawardina et al. (2000) studied analytically the behaviour of steel and CFRP externally prestressed simply-supported and continuous beams, of span-to-depth ratio more than 15. It was concluded that externally prestressed beams with at least two deviators had relatively high ultimate strength and improved ductility, regardless of the type of the external tendons used (steel or CFRP).

Campos et al. (2001) carried a numerical parametric study on the flexural resistance of concrete beams prestressed with external steel and AFRP tendons. The main variables considered were the span-to-depth ratio, total reinforcement index, concrete strength, initial prestressing stress, modulus of elasticity of the prestressing tendon, cross sectional shape, and type of loading. No significant difference in behaviour of the beams having different moduli of elasticity was encountered.

Tjandra and Tan (2001) investigated strengthening of reinforced concrete continuous beams with external CFRP tendons at intra-span locations. Three two-span continuous T-beams, each of 6-metre long with an overall depth of 300 mm, were tested. The first beam was strengthened over the positive moment regions while the second beam was strengthened only over the negative moment region at the interior support. The third beam was strengthened at both positive and negative moment regions. Three other beams prestressed externally with conventional steel

tendons were strengthened at the same locations as the CFRP strengthened beams. It was concluded that, despite the lower modulus of elasticity of the CFRP tendons, the behaviour of the beams strengthened with steel and CFRP was similar.

Parameters affecting the response of FRP post-tensioned beams — some researchers carried out experimental investigations on FRP post-tensioned beams by studying different parameters commonly known to influence the behaviour of the steel post-tensioned members. Jerrett et al. (1996) tested six steel prestressed beams externally post-tensioned with Leadline CFRP tendons, harped at 4.8 degrees at two points. The beams were 5490 mm long, and had a rectangular cross section of 203x406 mm. Two main parameters were studied: the internal prestressing bonded reinforcement (one and two 13-mm, 7-wire steel strands) and the initial post-tensioning force in the external tendons (between 60% and 73% of the tendon capacity). It was reported that the amount of internal reinforcement significantly affected the capacity of the beams post-tensioned with CFRP tendons. An increase of 215 % was measured in the capacity of the beams internally prestressed with a single steel strand and 146 % in those prestressed with double steel strands. A reduction of 60% and 85% in the midspan deflections was observed at ultimate for both beams, respectively. All beams failed by crushing in concrete.

Taniguchu et al. (1997) conducted static loading tests on prestressed concrete T-beams (400x100x100 mm) using external AFRP and CFRP tendons. CFRP transverse reinforcement was used in all specimens to increase the ductility of the beams. The prestressing force introduced was approximately 40% and 22% of the nominal breaking load of the AFRP and CFRP tendons, respectively. All specimens failed by crushing of concrete. It was reported that the transverse reinforcement increased the ductility of the beams. The beams continued to deflect even after the concrete cover in the compression zone came off until rupture of the tendons occurred. At this point, the CFRP bars ruptured at 72% of the nominal breaking load while AFRP tendons ruptured at 90% of their nominal capacity. In all cases, rupture of the tendons occurred either in

the vicinity of the deviators or at the anchors. Specimens with larger amount of internal reinforcement exhibited more flexural strength than those with less reinforcement.

El-Hacha et al. (1997) tested twelve reinforced and internally prestressed concrete rectangular beams to study the effect of the span-to-depth ratio and the partial prestressing ratio on the behaviour of the beams externally prestressed with Carbon Fibre Cables (CFC). Three span-to-depth ratios (10.7, 17.9, and 25) with three partial prestressing ratios (0, 0.53, and 0.7) were used in the investigation. The external cables were singly draped at midspan by means of a steel deviator. The cables were stressed up to 55% of their guaranteed breaking load. All beams were tested under third point loading and were subjected to a load large enough to produce a deflection at mid span equal to 1/460 of the span. Beams were externally post-tensioned under load and then tested up to failure. It was reported that for the same partial prestressing ratio, increasing the span-to-depth ratio of the beam increased the stress in the external cables and the flexural resistance of the beam. It was also found that for the same span-to-depth ratio, decreasing the partial prestressing ratio increased the stress in the external cables. Beams with smaller span-to-depth ratio failed in shear while beams with larger span-to-depth ration failed by crushing of the compressed concrete. Two beams with high partially prestressing ratio failed by the rupture of the cables.

Bakis et al. (2001) tested four rectangular beams post-tensioned with unbonded 8-mm CFRP tendons under static load to failure. The beams were post-tensioned by Leadline and Strawman CFRP tendons at 38-42% and 62-68% of ultimate, respectively. All beams failed by compression in concrete at a load approximately equal two times the cracking load. The total increase of the tendon strain was between 6-13% of the ultimate strain of the tendons.

Ghallab and Beeby (2003) reported on the deflection of prestressed concrete beams externally post-tensioned with Parafil ropes draped at two points along the beams by means of steel deviators. Eleven I-section beams were tested statically up to failure. Five parameters were taken

into consideration: the external prestressing force, the number of deviators, the effective depth of the external tendons, the concrete strength, and the span-to-depth ratio of the beam. It was reported that the amount of deflection at any stage of loading was reduced by increasing the external prestressing force and increasing the eccentricity of the external ropes. However, increasing the external prestressing level decreased the ductility of the beams. The higher strength concrete led to a larger ductility in the beams at ultimate. It was also reported that the cracks completely closed and the full cross section can be used in deflection calculations whenever the bottom concrete stress is still in compression due to the prestressing force. All beams failed by yielding of steel reinforcement followed by crushing of concrete.

Use of FRP in strengthening applications — the use of external FRP tendons in strengthening applications has been studied by Shahrooz et al. (2002). The flexural strengthening of four 76-year-old T-beams was investigated using various FRP strengthening techniques to retrofit the four damaged beams: external post-tensioning with CFRP tendons, bonded CFRP plates, bonded CFRP fabrics, and bonded CFRP plates gripped with mechanical anchors. For the externally post-tensioned strengthened beam, four external CFRP tendons, two on each side of the beam, were used. Each tendon was post-tensioned to 45% of its nominal ultimate capacity. The initial seating and relaxation loss was estimated to be 10.5% of the prestressing force. The external post-tensioning enhanced the stiffness and the capacity of the beam by 9% and 14%, respectively. The ductility of the retrofitted beam with external tendons was evident by the large deflection of the beam at ultimate. It was reported that this method of retrofitting offered the best option, particularly for members with extensive deterioration, because it did not rely on the quality of bond between the poor concrete and the FRP material.

The effect of the load history of the concrete beams prior to strengthening with external post-tensioned tendons was studied, among other parameters, by Ghallab and Beeby (2003). Two concrete beams were subjected to 36% and 60% of their ultimate strength before being strengthened with externally post-tensioned double draped Parafil ropes. It was reported that the

ultimate flexural capacity after external prestressing was independent of the load history prior to strengthening, but depended mainly on the concrete strength and the external prestressing level.

Fatigue of FRP post-tensioned beams — a limited number of studies conducted on the fatigue performance of FRP externally post-tensioned beams was found in the literature. Saeki et al. (1993) studied the behaviour of reinforced and prestressed concrete beams strengthened by external prestressed AFRP tendons under fatigue loading. Twelve, 3-metre long, reinforced and prestressed concrete beams with rectangular cross sections were tested. The external tendons were prestressed at 34% of their tensile strength. One concentrated load was applied at mid-span of the beams. It was reported that the fatigue loading applied for two million cycles at 33% of the ultimate load (with a constant lower limit for all beams) had an insignificant effect on the rigidity of the tested beams.

Taniguchu et al. (1997) tested three prestressed T-beams (100x100x400 mm) post-tensioned with external AFRP tendons under fatigue loading for two million cycles. The beams were internally prestressed with CFRP tendons. CFRP transverse reinforcement was used in the specimens to increase the ductility of the beams. The cracking load and the load at which the maximum crack width became 0.5 mm were selected as lower and upper limits for the fatigue load ranges applied to the beams, respectively. Two prestressing levels were investigated: 40% and 53% of the ultimate capacity of the AFRP tendons. All of the beam specimens survived two millions cycles without failure. A decrease between 12% and 15% in the prestressing forces was recorded in the AFRP external tendons. This was attributed to either the relaxation of the tendons or the slippage of the tendons within the anchors used. The beams were then tested statically to failure. No reduction in the ultimate capacity of the beams was reported due to fatigue.

Grace and Abdel-Sayed (1998) used a combination of bonded internal CFRP tendons with unbonded external double draped CFC cables in the construction of four bridge models having a

Double-Tee cross section. The post-tensioning forces in the external tendons varied between 57% and 78% of their ultimate capacity. The four models of the bridges were tested under fatigue loading at different load ranges within the working load limit (less than the cracking loads). The bridge models were able to withstand millions of repeated cycles without failure and an infinite fatigue life was reported. Insignificant losses in the prestressing forces were encountered in the externally draped tendons (about 3% of the initial force). The four models were then loaded statically up to failure. Failure of the tested models was governed by concrete crushing with no premature rupture occurring in the tendons.

An experimental fatigue program was conducted by Braimah et al. (2006) to investigate the fatigue performance of concrete beams post-tensioned with internally unbonded Leadline CFRP tendons. The beams were 4000 mm long with a T-cross section of flange width of 500 mm and a total depth of 300 mm. The test program included five fully post-tensioned beams subjected to a sinusoidal fatigue load at a frequency of 1 Hz. Three beams were post-tensioned with CFRP tendons and two with conventional steel strands. The CFRP tendons were post-tensioned to 60% of their ultimate capacity using the Calgary and the Mitsubishi anchors. It was reported that the CFRP post-tensioned beams exhibit higher mid-span deflection than steel post-tensioned beams at the same load level after cracking. Only one CFRP post-tensioned beam survived two million cycles of fatigue loading. Failure of other post-tensioned beams was caused by fracture of the tendons at the tendon-anchor junction after surviving a few number of cycles. For one beam where the Calgary anchor was used, failure at the anchor occurred during the initial static loading.

2.5 Monotonic analysis of FRP externally post-tensioned beams

Due to the lack of bond between the tendons and the surrounding concrete, the conventional strain compatibility approach used to analyze a section with bonded reinforcement is not

applicable in the case of unbonded tendons. Strains in the unbonded tendon at any load level depend on the total change in the tendon length between the anchorages (or deviators). This makes the strain in the tendon member dependent rather than section dependent.

Most analytical approaches found in the literature have focused on predicting the increase in stress in the unbonded tendons at ultimate stages (Tao and Du, 1985; Naaman and Alkhairi, 1991; Harajli and Hijazi, 1991; Harajli and Kanj, 1991; Chakrabarti, 1995; Aravinthan et al., 1997; Lee et al., 1999; Ghallab and Beeby, 2004; among others). These approaches were mainly developed based on experimental or numerical studies dealing with unbonded *steel* tendons. Harajli (2006) conducted a comprehensive review on these approaches. A brief review on some of these approaches of analysis is given in Appendix A.

On the other hand, a relatively few analytical approaches have been devoted to study the serviceability of externally post-tensioned elements. Naaman (1990, 2005) suggested a simplified method in order to reduce the analysis of the section with unbonded tendons to that of a section with bonded tendons by applying a reduction coefficient, Ω, to the strain values. The coefficient related the change in strain of the unbonded tendon to the change in strain of an equivalent bonded tendon and, consequently, to the change in strain in the concrete at the level of the tendon, as follows:

$$\Omega = \frac{(\Delta\varepsilon_{tendon})_{unbonded-\max}}{(\Delta\varepsilon_{tendon})_{bonded-\max}} = \frac{(\Delta\varepsilon_{tendon})_{unbonded-average}}{(\Delta\varepsilon_{tendon})_{bonded-\max}} = \frac{(\Delta\varepsilon_{cp})_{unbonded-average}}{(\Delta\varepsilon_{cp})_{bonded-\max}} \qquad (2.2)$$

where $\Delta\varepsilon_{tendon}$ is the variation in strain in the tendon, The subscript "*max*" implies the section of maximum moment and the subscript "*cp*" refers to the concrete fibre at the level of the unbonded tendon. The factor Ω was then determined analytically for many tendon profiles and loading conditions. For simply supported beams, with symmetrical loading and tendon profile, Naaman (1990, 2005) showed that Ω could be calculated as follows:

$$\Omega = \frac{2}{L\,\Delta M_{\max}\,e_{\max}} \int_0^{L/2} \Delta M(x)\, e(x)\, dx \tag{2.3}$$

where L is the span length of the beam, ΔM_{max} and $\Delta M\,(x)$ are the change in bending moment at the critical section and at any section x along the span, respectively, and e_{max} and $e(x)$ are the corresponding eccentricities of the tendons at these sections. Exact values derived by Naaman (2005) for beams with different tendon profiles and different types of load applications are summarized in Table 2.4.

Table 2.4: Values of strain reduction coefficient, Ω, in uncracked state (adapted from Naaman, 2005)

Loading type	Tendon profile	Strain reduction coefficient, Ω
Uniform load	Straight	Ω = 2/3
Uniform load	Single draping at midspan	Ω = 5/12+1/4 e_s/e_m
Uniform load	Parabolic	Ω = 8/15+2/15 e_s/e_m
Third-point loads	Straight	Ω = 2/3
Third-point loads	Single draping at midspan	Ω = 23/54+13/54 e_s/e_m
Third-point loads	Parabolic	Ω = 44/81+10/81 e_s/e_m
Single midspan load	Straight	Ω = 1/2
Single midspan load	Single draping at midspan	Ω = 1/3+1/6 e_s/e_m
Single midspan load	Parabolic	Ω = 5/12+1/4 e_s/e_m

Note: e_s is the eccentricity of the tendons at supports and e_m is the eccentricity of the tendons at midspan

Using the same concept, Naaman (2005) derived a strain reduction factor, Ω_{cr}, after cracking occurs, assuming that the beam is divided into two parts: an uncracked portion with a gross moment of inertia, I_g, and a cracked portion with a cracked moment of inertia, I_{cr}, as follows:

$$\Omega_{cr} = \Omega \frac{I_{cr}}{I_g} + \frac{2}{L}\left(1 - \frac{I_{cr}}{I_g}\right) \int_0^{L_c/2} \frac{\Delta M(x)\, e(x)}{\Delta M_{\max}\, e_{\max}}\, dx \tag{2.4}$$

where L_c is the width of the crack. Since the crack width is relatively small in comparison to the length of the beam, it was shown that:

$$\Omega_{cr} \approx \Omega \frac{I_{cr}}{I_g} \tag{2.5}$$

Once the strain reduction coefficient is determined, the analysis of the unbonded tendons is reduced to that of the bonded tendons by satisfying the equilibrium and strain compatibility conditions.

Harajli and Kanj (1992) reported that the strain reduction coefficient, Ω_{cr}, did not differ significantly from its value before cracking, Ω. For two-point loading, the maximum drop in the strain reduction coefficient after cracking did not exceed 10% of its value before cracking when I_{cr}/I_g = 0.5. Harajli and Kanj (1992) proposed that the strain reduction coefficient could be considered unchanged after cracking. Good agreement between the analytical and experimental results verified the validity of this approximation.

Bakis et al. (2001) carried out an analytical investigation using the strain reduction coefficient approach to model the behaviour of beams prestressed with CFRP unbonded tendons up to failure. It was observed that at the onset of cracking, the theory was in good accord with the load deflection data obtained. At ultimate, the theory over predicted the deflections by about 200% and the loads by about 25%. It was reported that the predicted values of the tendon strains at failure were 30-40% higher than the actual values. The discrepancy in the predicted tendon strains from the experimental values was attributed to the overestimated cracked region used in the analysis, which increased the cracked strain reduction coefficient and, consequently, overpredicted the strains in the tendons. However, this did not justify the increase in the predicted deflections of the beams. It was recommended that the non-linear stress-strain behaviour of concrete should be incorporated in the analysis.

Naaman et al. (2002) suggested that the strain reduction approach could be applied for the use of FRP tendons by modifying the upper limit stress to account for the fact that FRP tendons behave linearly up to failure. Naaman et al. (2002) suggested a tentative upper limit of $0.80\, f_{fu}$ that

could be further calibrated for FRP materials, where f_{fu} is the ultimate stress of the FRP tendon. No experimental results were carried out for verification.

An et al. (2003) compared the experimental results of two groups of specimens post-tensioned with external FRP tendons (those of Mutsuyoshi and Machida, 1993 and El-Hacha, 2001) to predicted values obtained using the equations developed for steel tendons by Naaman and Alkhairi (1991) , Harajli and Hijazi (1991), and Aravinthan et al. (1997). See Appendix A for more information about these models. It was concluded that the proposed equations could not be used effectively for external FRP tendons before the limitation conditions in the models were modified. Since FRP tendons do not yield, and the assessed models were mainly developed for unbonded steel tendons, the limitations set by the equations were not suitable for FRP use. It was found that all the predicted ultimate stresses exceeded the limitation values given in the steel models (a value of 70% f_{fu} was considered for safety reasons). On the other hand, An et al. (2003) reported contradictory results between the analytical data and the experimental results obtained by El-Hacha (2001). El-Hacha (2001) reported that the stress increase in the external FRP tendons increased as the span-to-depth ratio of the post-tensioned beams increased. This contradicted the analytical results obtained using the three models under investigation. An et al. (2003) attributed this contradiction to the variation of the tendon eccentricity (the second order effects) during the beam loading. As reported by El-Hacha (2001), some beams under study failed in a shear mode rather than a flexural mode, which resulted in a small stress increase in the FRP tendons.

Tjandra and Tan (2003) incorporated the elastic modulus of FRP tendons in the ACI-318 equation (2005) used to predict the stress in the unbonded tendons at ultimate. Previous experimental results of simply supported and continuous span beams with internally unbonded and external FRP tendons (those of Bakis et al., 2001; Mutsuyoshi and Machida, 1993; Tan et al., 2001; Tjandra and Tan, 2001) were used in the analysis. The beams had span-to-depth ratios varying from 7 to 22, and were strengthened with FRP tendons having elastic moduli between 82

and 161 GPa. The beams were subjected to a four-point loading pattern. Using a regression analysis, the following equation was proposed to predict the stress in the FRP tendons at ultimate:

$$f_f = f_{fe} + 71.2 + 0.01\frac{f_c' E_f}{\rho_f E_{ps}} \quad (2.6)$$

where f_{fe} is the effective prestressing force in the FRP tendons, f_c is the concrete compressive strength, ρ_f is the FRP reinforcement ratio, and E_f and E_{ps} are the elastic moduli of FRP and steel tendons, respectively. As noticed from the above equation, the effect of the internal reinforcement (non-prestressed reinforcement or internal bonded tendons), and the type of loading were not incorporated. This limitation was attributed to the absence of enough test results of FRP externally post-tensioned beams in the available literature.

2.6 Fatigue loading

In the following sections, a background on the fatigue performance of the concrete and steel is presented. Previous studies conducted on FRP strengthened concrete beams are summarized.

2.6.1 General

Concrete elements such as bridges and marine structures are subjected to repeated loading during their life. This type of loading may considerably reduce the capacity of the structure. Significant deformations usually occur due to fatigue even if the loading peaks applied on the structure are less than its ultimate capacity. This must be accounted for in the design of concrete members subjected to fatigue.

The most common approach to relate the applied stress to the fatigue life of a material is the stress-life (S-N) approach, in which the number of cycles to failure is plotted against the applied

stress range. Most S-N plots are based on testing a considerable number of samples made of the same material under fatigue loading. The endurance limit of the material is defined as the stress range below which no failure due to fatigue is likely to occur.

In order to assess the capability of the structure in resisting cyclic loading, the fatigue behaviour of its constituents should first be addressed. For externally post-tensioned beams, the effect of fatigue on the concrete, steel, and external tendon materials should be considered and analyzed. The fatigue life of the beam is usually governed by the shortest fatigue life of its component materials. If one component fails to withstand the applied fatigue loading, the concrete element would fail.

2.6.2 Fatigue of plain concrete

Concrete fails under fatigue loading at stress values well below its ultimate compressive capacity. Many researchers have investigated the fatigue behaviour of concrete under fatigue loading. ACI Committee 215 (1997) provides a comprehensive review on the fatigue performance of plain concrete. The committee defines the fatigue strength of concrete as a fraction of the static strength that it can support repeatedly for a given number of cycles.

The stress range applied on concrete is the main factor affecting the fatigue strength of concrete. Other factors such as the cement content, water cement ratio, stress gradient, and the rate of loading also affect the fatigue concrete strength. A loading frequency between 1 to 15 Hz was reported to have an insignificant effect on the strength provided that the maximum stress level is less than 75% of the static strength (ACI 215, 1997).

ACI 215 (1997) recommended the use of the modified Goodman chart shown in Figure 2.6 to estimate the limiting stress range in concrete. The chart shows a relationship between the minimum and maximum stresses applied to concrete for a fatigue life of one million cycles. Stresses are shown as fraction of the static compressive strength of concrete. For a zero minimum

stress, the concrete can withstand one million cycles without failure, providing that a maximum stress of 50% of the concrete static strength is not exceeded. For a given minimum stress, the chart can be used to get the corresponding maximum stress for concrete to withstand one million cycles.

Under repeated loads, the stress-strain curve of concrete shows cyclic creep, as indicated by the increase in the strain values at the same stress applied (Neville and Brooks,1990; ACI 215, 1997). Softening in concrete also occurs (Figure 2.7), where the slope of the stress-strain curve varies with an increasing number of cycles (ACI 215, 1997).

2.6.3 Fatigue of steel reinforcing bars

The fatigue of reinforcing bars became a key component in design since the use of the ultimate strength design procedures and the use of higher yield strength reinforcement (ACI 215, 1997). Deformations on the bar in the form of ribs, manufacture markings, or any other form of raised features, induce stress concentrations and thus decrease its fatigue life (MacGregor et al., 1971; Bannantine et al., 1990; Dowling, 1998; among others). The width, height, angle of rise, and base radius of the ribs affect the magnitude of the induced stress concentration (Tilly, 1979). Decreasing the angle of inclination of the sides of the deformations with respect to the longitudinal axis increases the fatigue strength of the deformed bars. In most deformed bars, ACI 215 (1997) recommends the use of a stress concentration factor between 1.5 and 2.0 in fatigue analysis. As reported by Tilly (1979), the increase in the stress range considerably decreases the fatigue strength of the bar. For the same stress range, the increase in the tensile mean stress also decreases the fatigue life of the bar. ACI Committee 215 (1997) provides a comprehensive review on the fatigue performance of steel bars including the effect of other parameters on its fatigue life, such as the minimum stress applied, the bar size, and its yield strength.

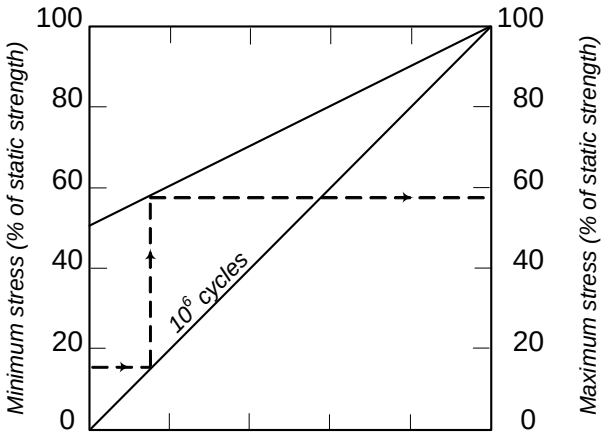

Figure 2.6: Fatigue strength of plain concrete (adapted from ACI 215, 1997)

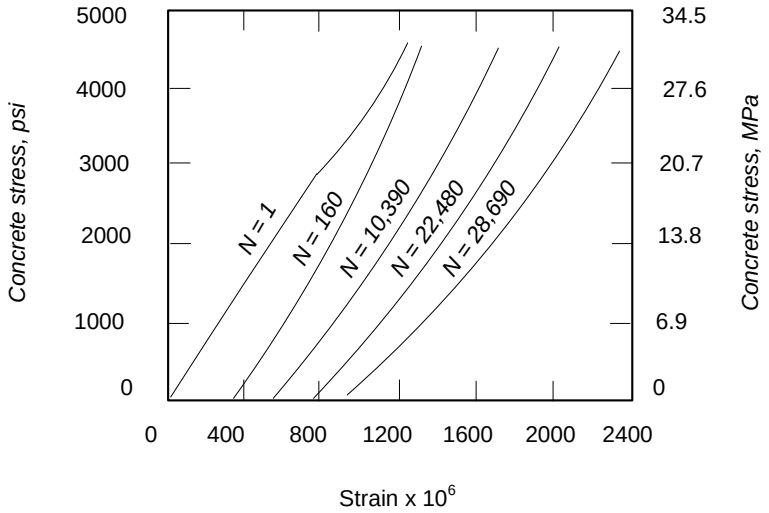

Figure 2.7: Effect of repeated load on concrete strains (adapted from ACI-215, 1997)

2.6.4 Fatigue of FRP strengthened reinforced concrete beams

The fatigue behaviour of reinforced concrete members is primarily dominated by the reinforcing steel performance (ACI 215, 1997). Tilly (1979) conducted fatigue tests on reinforcing bars subjected to uniaxial loads in air, and on reinforcing bars subjected to flexural loads when embedded in concrete. It was reported that the difference in fatigue life results between the two types of tests was small. Heffernan (1997) reported that softening of concrete due to cyclic loading increased the tensile stress in the reinforcing bars by approximately 2 to 6%. It was recommended that this amount should be considered in calculating the stress in the reinforcing bars. Bishara (1982) reported that cyclic loading of reinforced concrete beams increased the measured steel stress at crack locations by approximately 7%. A slight reduction in the flexural rigidity of the beams was observed, as indicated by the increase in midspan deflections of the beams.

In investigating the fatigue behaviour of CFRP strengthened reinforced concrete elements, two categories are identified based on the bond between the composite material and the surrounding concrete as follows:

Use of fully bonded FRP composites — this category includes the use of non-prestressed or prestressed FRP sheets and FRP plates bonded to the surface of the concrete element. It also includes the use of the near-surface mounted technique (NSM) in which the FRP bars are epoxy-bonded to concrete inside grooves made on the surface of the element. Using these methods, full strain compatibility exists between the FRP and the surrounding concrete. A considerable research on the fatigue performance of such elements has been reported in the literature (Heffernan, 1997; Barnes and Mays, 1999; El-Tawil et al., 2001; Wight and Erki, 2003; Brena et al., 2005; Masoud et al., 2005; Rosenboom and Rizkalla, 2006; among many others). In most cases,

the fatigue life of the beams was controlled by the fatigue rupture of the steel reinforcing bars or by debonding of the FRP composite.

Use of unbonded FRP composites — this category includes the use of externally post-tensioned FRP tendons in strengthening the concrete elements. Tendons are located outside the concrete section and no strain compatibility exists between the composite and the surrounding concrete. As reported in Section 2.4.4, a limited number of studies dealing with FRP externally post-tensioned elements under fatigue were reported in the literature (Saeki et al., 1993; Taniguchu et al., 1997; and Grace and Abdel-Sayed, 1998).

2.7 Conclusions based on previous research

A survey of the previous studies carried out on externally post-tensioned concrete elements was conducted. The most significant parameters recognized to affect the behaviour of these elements were presented. The studies were categorized based on the type of the external tendons used in post-tensioning application (steel or FRP tendons). A general review on the FRP tendon characteristics was also presented with a focus on the various features that make them different from the steel tendons (such as the harping effect on their tensile strength and their anchoring systems). From the presented literature survey, the following points can be concluded:

- A number of studies were carried out to investigate the effect of different parameters on the monotonic behaviour of externally *steel* post-tensioned members. The presence and number of deviators, the amount of bonded reinforcement, the level of prestressing in the external tendons, and the span-to-depth ratio of the post-tensioned element were among the most commonly investigated parameters that affect the behaviour of these elements. Other parameters such as the loading history of the beams prior to post-tensioning and fatigue loading have received little interest.

- A large number of investigators focused on predicting the stress in the unbonded steel tendons at ultimate stages. A brief review on the models used is presented in Appendix A.
- Comparative studies were conducted on steel and FRP post-tensioned beams to investigate the effect of different parameters, known to affect the behaviour of the steel post-tensioned elements, when FRP tendons were used. The outcome of these studies confirmed the fact that similar monotonic behaviour regardless of the tendon material is likely to take place under similar testing conditions.
- The wide variety in the mechanical properties of FRP tendons was a source of inconsistency in the obtained experimental results. This was obvious in many aspects, such as the wide range in the reported reduction in the tensile capacity of the deviated tendons. Lack of homogeneous properties in all FRP tendons necessitates dealing with each tendon type on a distinct basis.
- The absence of a reliable anchor system capable to withstand the post-tensioning force in the external FRP tendons represented a major obstacle in previous studies. The premature failure of the tendon in the vicinity of the anchorage zone was reported by many researchers.
- Most previous studies have dealt with the external tendons (steel or FRP) as the main reinforcement of the post-tensioned element. As such, a major part of the experimental tests was conducted on newly constructed, virgin, and uncracked beams. Few studies considered the potential of external post-tensioning as a strengthening technique where flexural members undergo cracking at various levels before being strengthened with external tendons.
- Limited research has been devoted to model the effect of loading history of the beam prior to being post-tensioned with external tendons on its monotonic response after being post-tensioned.

- The efficiency of external post-tensioned tendons in restoring the flexural capacity of severely damaged and overloaded members has received little attention in the literature. The deformations induced by overloading a concrete element are unlikely to be restored with conventional methods of repair, such as steel plating or bonded FRP sheets. The possibility of upgrading such elements with external post-tensioning technique needs to be investigated.
- The research conducted to date on concrete beams post-tensioned with external FRP tendons has focused on quantifying the increase in the monotonic load-carrying capacity of the beams with little consideration of their serviceability. The analysis approaches developed for the steel post-tensioned members has seldom been assessed for applicability for FRP tendons.
- A noticeable shortage in studies on the long-term response of externally post-tensioned concrete elements is realized from the available literature. Fatigue tests on such elements received little attention in the following aspects:
    - Most of the reported fatigue tests have focused on the fatigue response of the post-tensioned beams when subjected to load ranges below the cracking loads of the beams. As a result, the tested specimens generally survived an infinite fatigue life, which prevented the researchers from distinguishing the impact of each parameter on the fatigue life of the post-tensioned beam.
    - Most of the fatigue studies conducted on externally post-tensioned beams were reported on virgin beams. The effect of the loading history of the externally post-tensioned concrete elements prior being strengthened on their fatigue behaviour has not been carefully investigated. This is attributed to the fact that little effort has been devoted to strengthening applications using external post-tensioning technique in general, and under fatigue loading in particular.

- The fatigue studies conducted on externally post-tensioned beams did not report on extending the fatigue life of the post-tensioned elements. As a result, there is no rational assessment of the efficiency of the external post-tensioning technique to restore the fatigue life of the beams.
- Limited number of studies reported on the structural performance of externally post-tensioned elements during their fatigue life in terms of deflection variation, stiffness degradation, and stresses redistribution between the constituent materials.
- Up to date, there is no rational analytical or design approach capable to model the behaviour of externally post-tensioned elements subjected to cyclic fatigue or to predict the life of such members.

2.8 Research objectives

The overall objective of the current study is to investigate the monotonic and fatigue response of reinforced concrete beams strengthened externally with post-tensioned FRP tendons. The detailed objectives of the current research study are initiated to fill the gap in the state-of-the-art as follows:

- To investigate the monotonic behaviour of reinforced concrete beams strengthened with external post-tensioned FRP tendons. This includes:
  - The assessment of the monotonic behaviour using two tendons profiles commonly used in practical applications;
  - The assessment of the effect of the initial load level applied on the beam before being strengthened on the monotonic behaviour of the strengthened beam;

- The development of an analytical monotonic model that takes into account the loading history of the beam prior to and after being strengthened with FRP external tendons.

- To investigate the fatigue response of reinforced concrete beams strengthened with external post-tensioned FRP tendons. This includes:
  - The assessment of the fatigue behaviour of the anchor system used in gripping the FRP tendons;
  - The investigation of the structural performance of the strengthened beams during their fatigue life in terms of deflection variation, tendon stress variation, and stress redistribution within the section of the strengthened beams;
  - The assessment of the efficiency of the external FRP post-tensioning technique to extend the fatigue life of the strengthened beams;
  - The evaluation of the effect of different loading histories of the beam on its fatigue performance after being strengthened with FRP external post-tensioned tendons;
  - The development of a rational analytical model that predicts the fatigue life of the strengthened beams taking into consideration its loading history prior to post-tensioning application;
  - The development of a fatigue design approach for beams externally post-tensioned with FRP tendons.

Chapter 3

Fatigue of CFRP Tendon-Anchor Assembly

3.1 Introduction

The anchor system used to grip the CFRP tendons used in this study is known as the Waterloo anchor. Fatigue tests were carried out on the tendon-anchor assemblies before using the anchors to post-tension the concrete beams. In this chapter, the results of these tests are presented and discussed. These results are considered in the design of the strengthened beams, as will be illustrated at the end of this chapter.

3.2 The Waterloo anchor system

Research conducted at University of Waterloo led to the development of a new wedge-type steel anchor for CFRP tendons (Al-Mayah et al., 2003). The Waterloo anchor consists of three main parts, as shown in Figure 3.1:

- A steel cylinder (barrel) of 70 mm length and 45 mm diameter, with an inner conical opening having a smooth surface.
- An annealed copper sleeve with a small wall thickness of 0.64 mm. The soft material of the sleeve prevents the wedges from notching the CFRP tendon, thus avoiding premature failure of the tendon due to stress concentration.

- Four steel wedges with an inner diameter matching the outer diameter of the copper sleeve. The wedges slide inside the barrel and grip the tendon by wedge action. The wedges ensure the smooth distribution of radial stresses on the tendon surface, thus preventing the failure of the tendon.

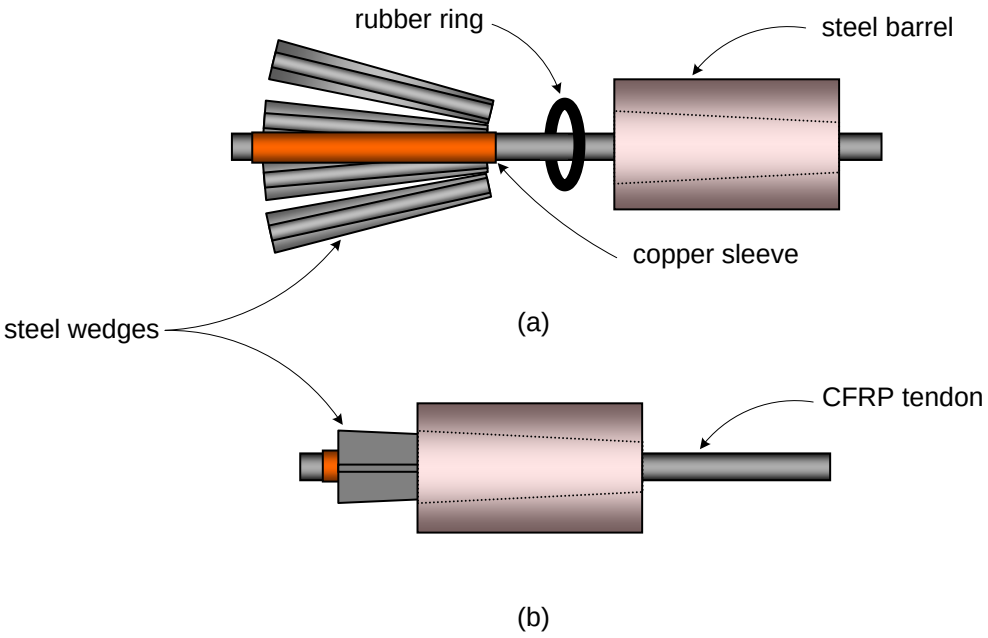

Figure 3.1: (a) Parts of the Waterloo anchor; (b) The assembled Waterloo anchor

The Waterloo anchor is characterized by its ability to sustain the full tensile capacity of CFRP tendons (Aslan200™ tendons, used in this study) under static loading without premature failure at the anchorage zone (Al-Mayah, 2004). These tendons have a rough surface pattern with single spiral indentations. They are made of Toray fibres having a tensile strength of 4800 MPa. Fibre content is about 60% by volume, impregnated in a vinyl-ester matrix. The nominal ultimate strength of the tendon material is 2162 MPa with a modulus of elasticity of about 144 GPa. The properties of the Aslan200™ tendon are given in Table 3.1.

Table 3.1: Properties of CFRP tendon Aslan200™

	Diameter (mm)	Area (mm^2)	Tensile strength (MPa)	Modulus of Elasticity (GPa)	Ultimate strain (%)
Guaranteed [a]	9.53	71.25	2068	124	0.017
Measured [b]	9.40	69.39	2162	144	0.015

[a] *Reported by the manufacturer*
[b] *Tested at University of Waterloo*

3.3 CFRP tendon-anchor assembly: Test program

As mentioned previously in Chapter 2, the absence of a reliable anchor that could withstand the ultimate capacity of FRP tendons has limited the number of fatigue tests performed on FRP tendon-anchor assemblies. Most of the available results reported on the effect of the fatigue loading on the tendon material rather than the anchorage system itself (Budelmann et al., 1990; Uomoto et al., 1995; Odagiri et al., 1997; Saadatmanesh and Tannous, 1999).

In this study, the use of the newly developed Waterloo anchors necessitated a careful assessment of their fatigue performance before their use in the beam tests. An experimental fatigue program was developed in order to achieve the following objectives:

- To evaluate the fatigue performance of the CFRP tendon-anchor assembly under various stress ranges;
- To investigate the ability of the CFRP tendon-anchor assembly to meet the Post-Tensioning Institute acceptance criteria (PTI, 1997);
- To study the effect of different parameters on the mechanical properties of the CFRP tendon material subjected to cyclic loading;
- To use the results of the fatigue tests carried out on the tendon-anchor assemblies in the design of the post-tensioned beams under study.

A total of 14 uniaxial tensile fatigue tests were conducted on tendon-anchor assemblies. The test matrix is given in Table 3.2. The tendon-anchor specimens were subjected to fatigue loading until failure occurred or a limiting number of two million cycles was reached. The specimen was considered to have failed when one of its components (the tendon or the anchor) ceased to sustain the applied load.

Table 3.2: Test matrix for CFRP tendon-anchor assembly

Test No.	Min Stress, MPa (% of ultimate) [a]	Max Stress, MPa (% of ultimate) [a]	Stress range, MPa (% of ultimate) [a]	Fatigue Life, N_{anc}
Group-1: Proof Tests				
1	1297 (60%)	1427 (66%)	130 (6%)	>500,000
2	865 (40%)	1729 (80%)	865 (40%)	181
3	720 (33%)	1873 (87%)	1153 (53%)	20
Group-2				
4	865 (40%)	1081 (50%)	216 (10%)	> 2,000,000
5		1124 (52%)	260 (12%)	378,000
6		1153 (53%)	288 (13%)	250,000
7		1189 (55%)	324 (15%)	48,000
8		1225 (57%)	360 (17%)	10,000
Group-3				
9	1009 (47%)	1153 (53%)	144 (7%)	> 2,000,000
10		1225 (57%)	216 (10%)	> 2,000,000
11-a		1268 (59%)	260 (12%)	363,600
11-b				124,000 [b]
12-a		1297 (60%)	288 (13%)	478,100
12-b				572,700
13		1333 (62%)	324 (15%)	18,400
14		1369 (63%)	360 (17%)	9100

[a] *Based on ultimate strength of 2162 MPa*

[b] *This result was neglected in the analysis*

3.3.1 Group (1): Proof tests

Due to the absence of a definite acceptance criterion for the FRP tendon-anchor assembly, the Post-Tensioning Institute (PTI, 1997) acceptance criteria for post-tensioning anchors for steel tendons were used. Under static loading, the tendon-anchor assembly for steel tendons is required to sustain at least 95% of the tendon ultimate capacity. The assembly should also sustain 500,000 cycles when loaded between 60% and 66% of the minimum specified tendon strength and 50 cycles when loaded from 40% to 80% of the steel tendon strength. Specimens 1 and 2 of Table 3.2 simulated the PTI (1997) fatigue conditions. Specimen 3 was tested to represent an extreme condition where the assembly was loaded between 33% and 87% of its ultimate capacity.

3.3.2 Groups (2) and (3)

The tests of groups (2) and (3) served to investigate the effect of different parameters on the fatigue life of the tendon-anchor assembly, namely, the minimum stress and the stress range applied. The applied minimum stresses were selected according to the recommendations of the ISIS Canada (2003) and the ACI 440 Committee (2004). According to these recommendations, the permissible stress in the post-tensioned CFRP tendons is 60% of the tendon ultimate capacity at transfer stage, and 85% of its capacity at ultimate stage. Thus, minimum stress levels representing 40% and 47% of the ultimate strength of the tendon, combined with stress ranges varying between 7% and 17% of the ultimate strength of the tendon were considered to simulate moderate and severe conditions.

3.4 Test specimen

The test specimen consisted of a CFRP Aslan200™ tendon of 1000 mm length, gripped at both ends with the Waterloo anchors. Prior to anchoring, the surface of the CFRP tendon in the anchorage zone was cleaned using acetone. The copper sleeves were then placed onto the tendons. The steel wedges were assembled around the sleeve before lubricating their outer surface with a thin layer of lubricant (G-n Metal Assembly Paste) to facilitate the movement of the wedges inside the barrel. The tendon-sleeve-wedges assembly was then inserted inside the barrel, as shown in Figure 3.1-b, by hammering the top of the wedges. The barrel was then inserted in steel-pocketed bearing plates, as shown in Figure 3.2. This procedure was repeated at both ends of the specimen.

The Waterloo anchor is a self-seating anchor. However, pre-seating of the wedges into the cylindrical barrel was done in order to minimize the slippage of the tendon relative to the anchor during the load application. A pre-seating load of 90 kN (approximately 60% of the tensile strength of the tendon) was applied using a hydraulic jack of 120 kN capacity and a pre-seating rig fabricated for this purpose at University of Waterloo, as shown in Figure 3.3.

It is worth mentioning that the steel barrel and the wedges were reusable. Only the copper sleeves were discarded at the end of each test, and new sleeves were used for the next specimen. When the test was completed, the same pre-seating rig was used to release the anchor from the broken tendon.

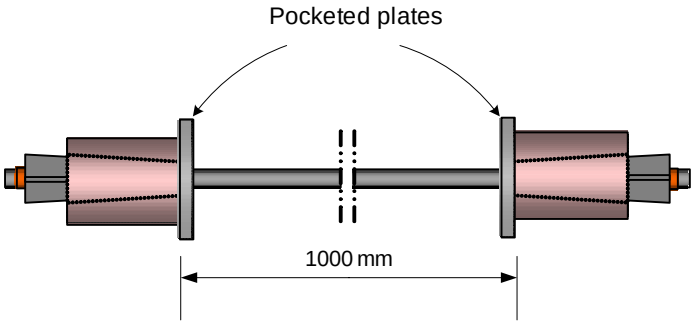

Figure 3.2: CFRP tendon-anchor test specimen

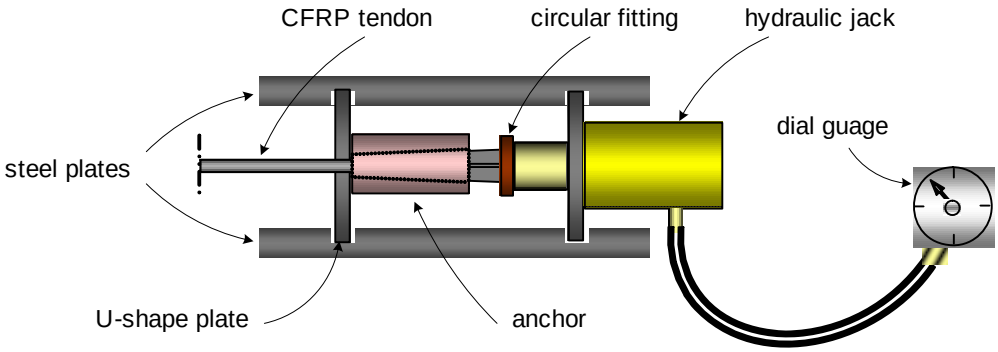

Figure 3.3: Pre-seating rig for CFRP tendon-anchor assembly

3.5 Test setup and test procedure

The tendon-anchor assembly was tested vertically in a MTS loading frame having a capacity of 250 kN. A test rig consisting of two steel plates (25 mm thick) separated by four steel bars (250 mm long) was attached to the actuator, as shown in Figure 3.4. The lower steel plate of the rig was grooved to facilitate the insertion and removal of the specimen. One anchored end was placed on the lower plate of the test rig while the other end was placed below the lower crosshead of the loading frame. The applied load was measured by a load cell attached to the hydraulic actuator of the system. The specimens were instrumented with 5 mm strain gages placed longitudinally at the mid point between the two anchored ends. Load cell measurements and strain gage readings were recorded by a National Instrument SCXI data acquisition system. Readings were taken at intervals of approximately 10-20 minutes depending on the life of the specimen.

To ensure the alignment of the test specimen, the upper end of the specimen was first mounted in place and the specimen was left hanging under its own weight before applying the load. The specimen was then loaded to the required mean load and cycled under constant load amplitude at a frequency of 3 to 4 Hz until failure. A limit of two million cycles was chosen; specimens exceeding this number of cycles were intentionally halted and considered as run-out specimens.

3.6 Cyclic test observations

The tendon-anchor specimens were subjected to cyclic loading until fatigue failure occurred or the limiting number of cycles ($2x10^6$) was reached with the exception of proof test No. 1 (Table 3.2) that was stopped after 500,000 cycles, as recommended by PTI (1997). All specimen failures occurred due to the fracture of the CFRP tendon within the tendon free-length with no indication of a premature failure occurring in the anchorage zone. Catastrophic failure took place

in a "broom-shape" manner as shown in Figure 3.5 (a). A longitudinal split along the tendon was observed in test No. 11 after completing 172,800 cycles, which represented approximately half-life of the specimen (Figure 3.5-b). The test was continued and the specimen withstood a life of 363,600 cycles.

Figures 3.6 through 3.9 show the relationship between the applied stress versus strain for specimens of Group 2 (minimum cyclic stress of 1009 MPa) at different stress ranges. The stress-strain curves were plotted at different numbers of cycles throughout the fatigue life of the specimens. All specimens showed a perfect elastic relationship between the stress and the measured strain until failure occurred.

Table 3.3 gives the variation in the modulus of elasticity, E_f, of the CFRP tendon calculated based on the obtained slope of the curves at three stages of the tendon's life, namely, at the onset of the cycling loading, at half-life, and close to failure. It is noticed that the fatigue loading had a limited effect on the modulus of elasticity of the CFRP tendon, as the values of E_f did not change significantly over the life of the specimen. The constant slope of the curves indicated that no stiffness degradation occurred in the tendons due to fatigue. The decrease in E_f before failure varied between 0% and 4%, excluding the results of the test No. 11 where the higher decrease in E_f was attributed to the unexpected longitudinal split, as explained earlier. Note that specimen No. 14 came from a different batch of CFRP tendons that have a higher modulus of elasticity, E_f (Table 3.3).

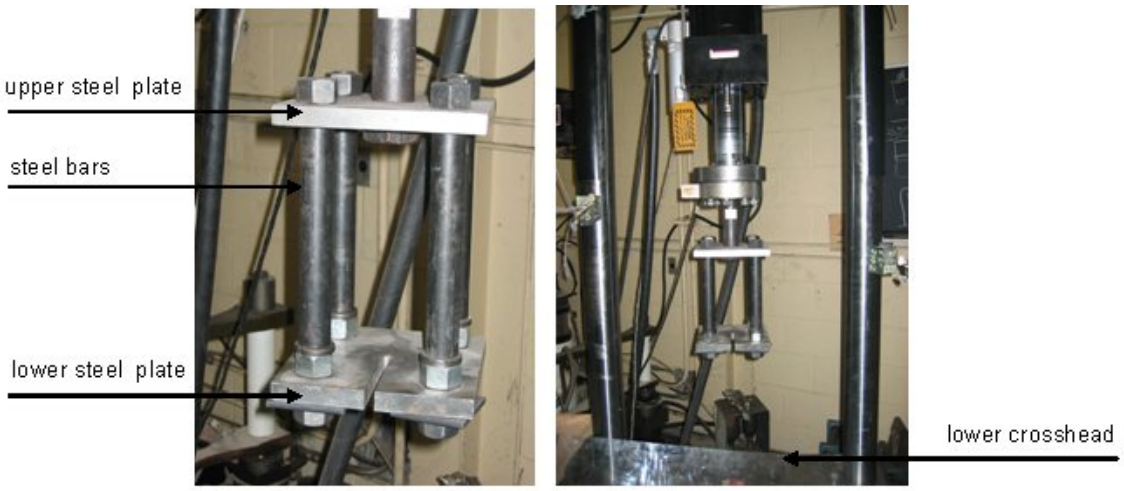

Figure 3.4: Test rig attached to the actuator

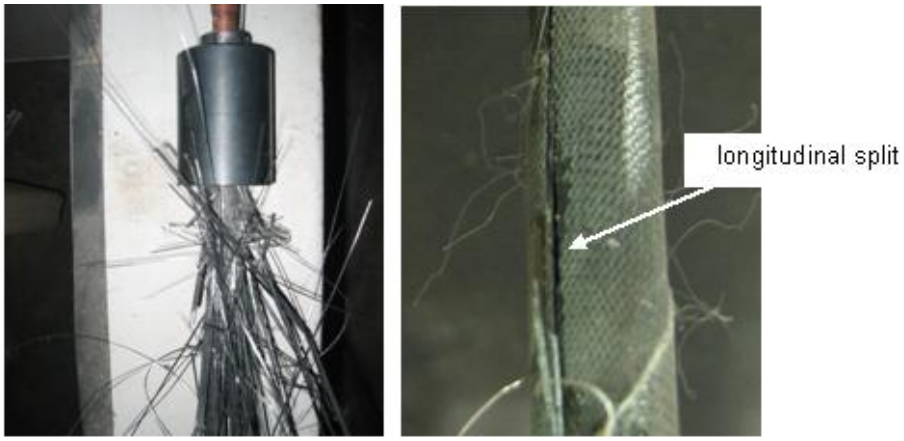

Figure 3.5: (a) Catastrophic broom-shaped failure (b) Longitudinal split in specimen No. 11

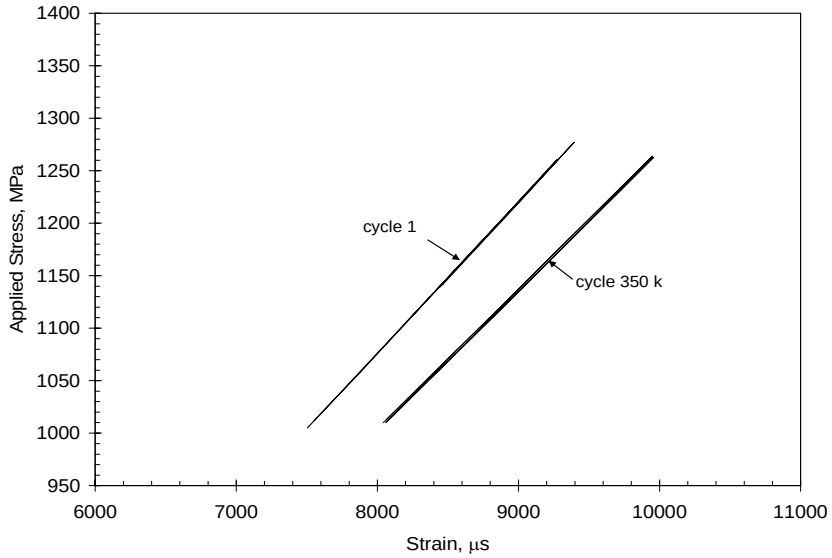

Figure 3.6: Stress versus strain for specimen No. 11 of stress range 260 MPa (total life = 363,600)

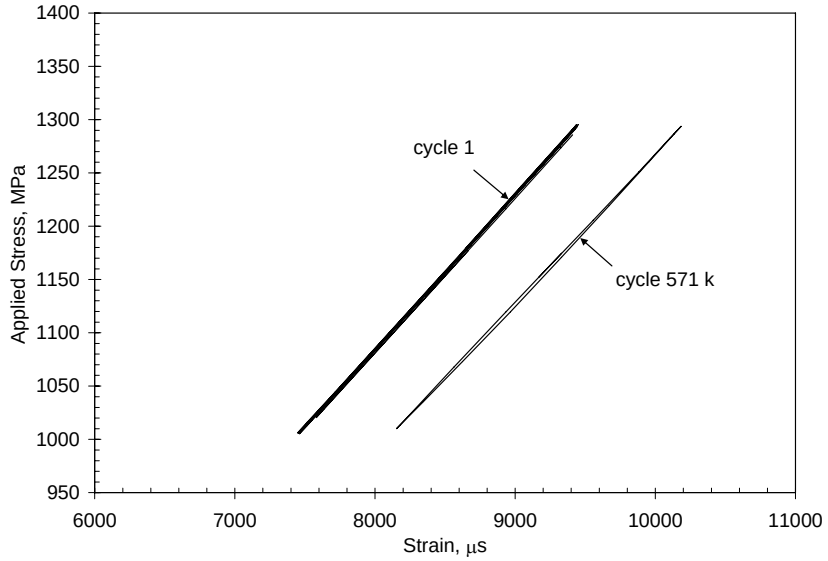

Figure 3.7: Stress versus strain for specimen No. 12 of stress range 288 MPa (total life = 572,700)

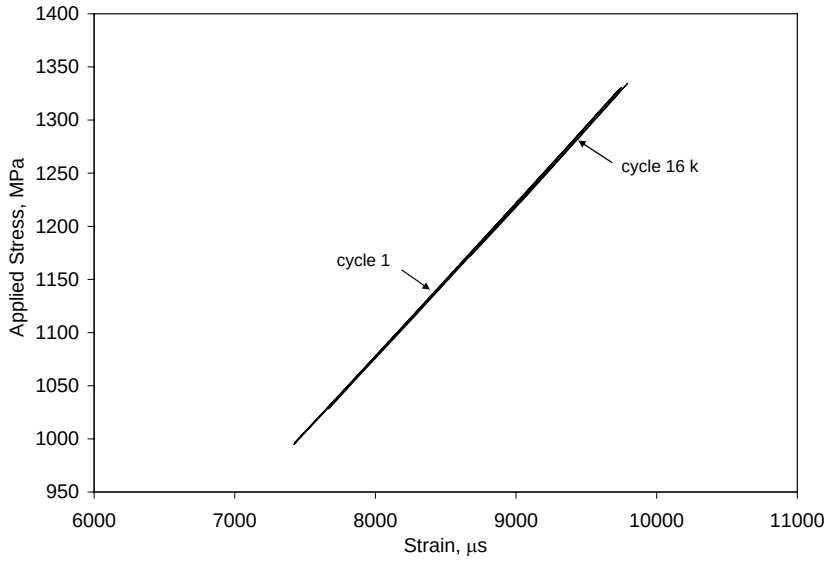

Figure 3.8: Stress versus strain for specimen No. 13 of stress range 324 MPa (total life = 18,400)

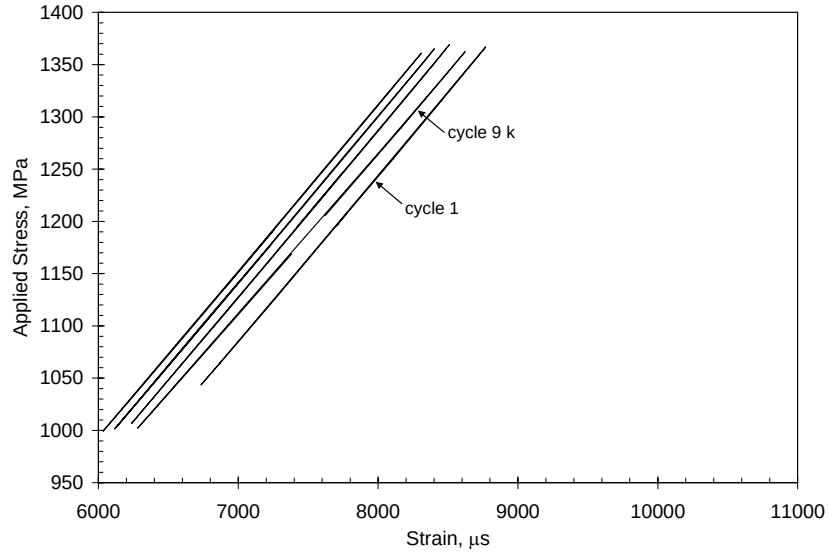

Figure 3.9: Stress versus strain for specimen No. 14 of stress range 360 MPa (total life = 9,100)

Table 3.3: Change of modulus of elasticity, E_f, with number of cycles for specimens of Group (2)

Test No.	Stress range (MPa)	Cycles to failure	At Onset of cycling (GPa)	At Half-life (GPa)	Before failure (GPa)	% of decrease in E_f before failure
11	260	363,600	144.37	144.11	133.27	8%
12	288	572,700	144.90	145.39	139.70	4%
13	324	18,400	144.19	144.42	144.41	0%
14	360	9,100	159.37	159.33	153.21	4%

The recorded maximum strain values were plotted against the corresponding number of cycles for the same specimens at different stress ranges (Figure 3.10 to Figure 3.13). Figure 3.10 and Figure 3.11 represent the results of tests No. 11 and 12 where the specimens exhibited relatively longer fatigue life. Specimens with short fatigue life are shown in Figure 3.12 and Figure 3.13 (tests No. 13 and 14). The variation in strain with the applied number of cycles was characterized by three stages. In the early life of the cyclic loading, the initial strain dropped from its original value recorded at the onset of the loading before it stabilized. The drop in strain values ranged between 0.7% and 5% of the initial recorded strain at the onset of the cyclic loading. After a period of stabilized strains, a third stage was noted where the strain values tended to increase while approaching the end of the tendon's life. This trend was clearly noticeable in specimens sustaining long life (Figure 3.10 and Figure 3.11), where the stabilization period represented most of the fatigue life of the specimen. This was not the case for short life specimens where the stabilization period disappeared after few thousand cycles (Figure 3.12 and Figure 3.13).

The decrease in measured strain in the early life of the specimen could be attributed to the tendency of the fibres to harden when subjected to cyclic loading (Dolan 1993). As the fibres hardened, the elongation of the tendon tended to decrease, thus affecting the measured strain values. When the tendon approached the end of its life, the individual fibres tended to break in a progressive manner. This was accompanied by a loud noise that occurred at tendon failure. The fibres, which constitute the main load-carrying element of the tendon, failed consecutively under

the effect of cyclic loading. This progressive mode of failure was previously reported by Walton et al. (1986). Since the applied stress range was kept constant during the cyclic tests, this continuous loss in fibres caused the increase in the measured strain until failure.

3.7 PTI proof tests

The PTI proof tests were successfully met by the tendon-anchor assembly. In all cases, the required number of cycles was achieved prior to stopping the tests or specimen failure. All failures occurred due to the breakage of the tendon, rather than failure of the anchor. No strain data were collected during these tests. Test specimen No. 1 was able to withstand more than 500,000 cycles at a stress range of 130 MPa (6% of the tendon tensile strength) and the test was stopped intentionally before the specimen failed. In the second test, the specimen survived 181 cycles at a stress range of 865 MPa (40% of the tendon strength) exceeding the PTI requirements (50 cycles). In the third test, representing an overload, the specimen survived 20 cycles when subjected to a high stress range of 1153 MPa (53% of the tendon strength). This demonstrated the ability of the tendon-anchor assembly to resist severe cyclic loading conditions.

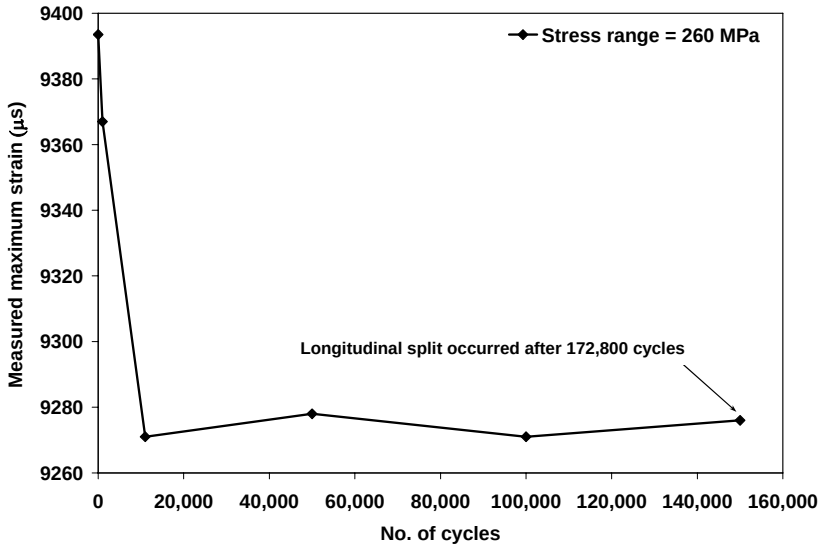

Figure 3.10: Measured maximum strain versus the number of cycles (Test No. 11)

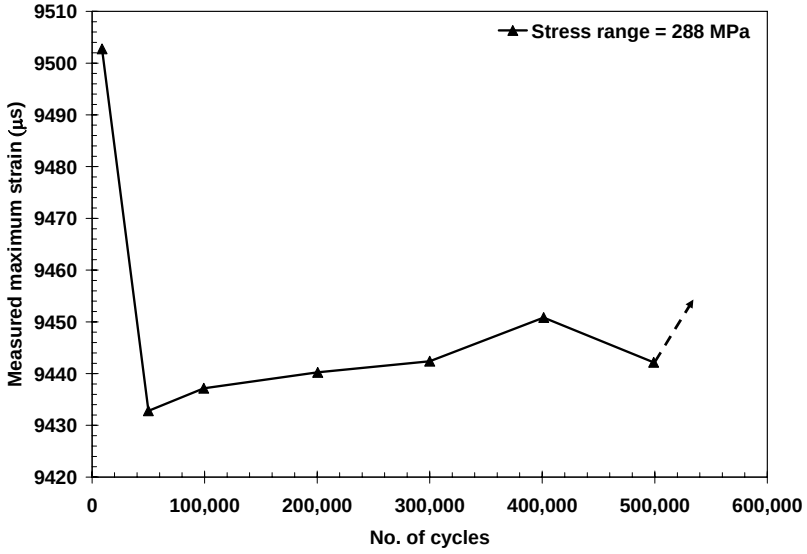

Figure 3.11: Measured maximum strain versus the number of cycles (Test No. 12)

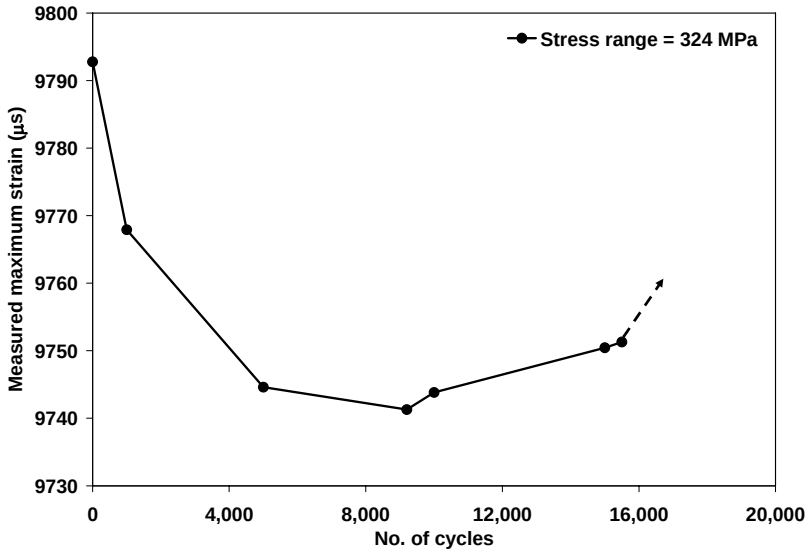

Figure 3.12: Measured maximum strain versus the number of cycles (Test No. 13)

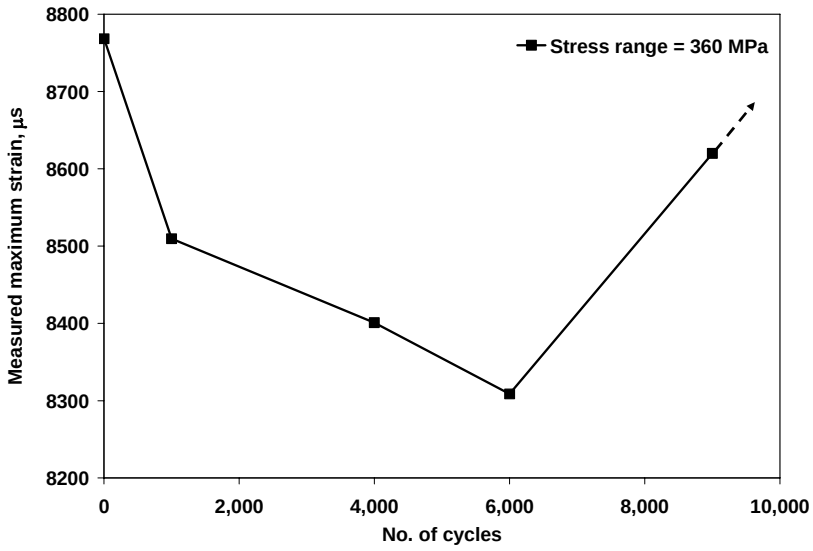

Figure 3.13: Measured maximum strain versus the number of cycles (Test No. 14)

3.8 Fatigue life

As given in Table 3.2, the tendon-anchor assembly exceeded the set limiting life (2 million cycles) when the applied stress range was less than or equal to 216 MPa, regardless of the minimum stress level applied (tests No. 4, 9, and 10). Hence, this stress range could be safely considered as the fatigue endurance limit of the tendon-anchor assembly. The lowest stress range that caused fatigue failure of the assembly was 260 MPa or 12% of the ultimate capacity of the tendon (tests 5 and 11). Figure 3.14 compares the fatigue life of the tendon-anchor assembly at different stress ranges for the two series tested (minimum stress of 865 MPa and 1009 MPa). At stress ranges of 260 MPa, 324 MPa, and 360 MPa, the fatigue life was approximately similar for both minimum stress values. The exception was at a stress range of 288 MPa, which could be attributed to the scatter usually encountered in fatigue data.

The applied stress range had a significant effect on the fatigue life of the specimen. The fatigue life dropped significantly as the applied stress range increased. A best-fit relationship between the fatigue life of the tendon-anchor assembly, N_{anc}, and the applied stress range, f_{fr}, for different minimum stress levels is shown in Figure 3.15.

In practical applications, the tendon-anchor assembly is not subjected to the extremely high stress range represented by proof tests 2 and 3. Thus, another graph relating the fatigue life of the tendon-anchor assembly, N_{anc}, and the applied stress range, f_{fr}, is plotted for design purposes excluding proof tests 2 and 3 (Figure 3.16). A log-linear best-fit trend line representing the obtained data can be expressed in mathematical form as follows:

$$f_{fr} = 541 - 20.5 \log (N_{anc}) \qquad 216 < f_{fr} < 360 \text{ (in MPa)} \tag{3.1}$$

The proposed relationship between the stress range applied and the fatigue life of the assembly could be used to predict the fatigue life of the assembly.

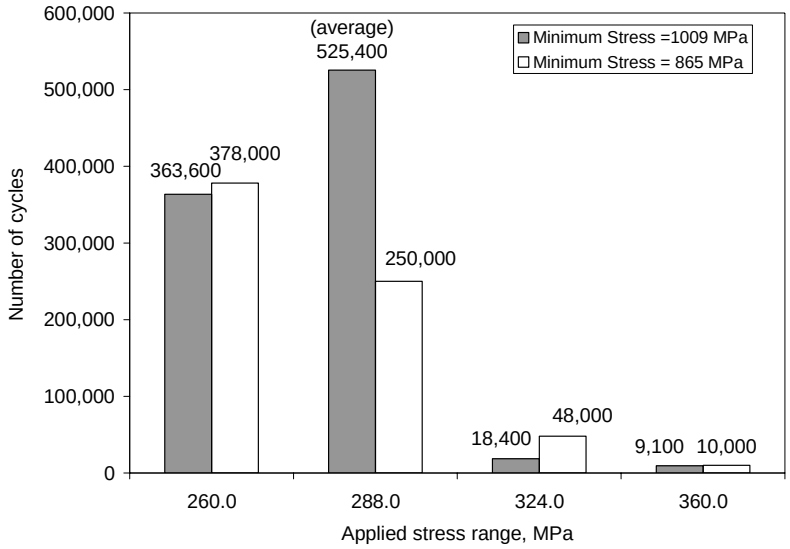

Figure 3.14: Effect of the minimum stress on the fatigue life of the specimens

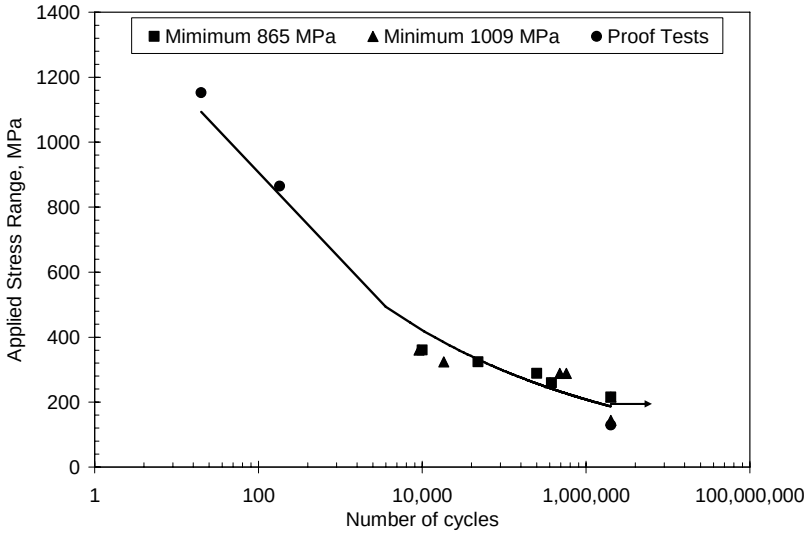

Figure 3.15: Applied stress range versus the life of the tendon-anchor assembly (all tests)

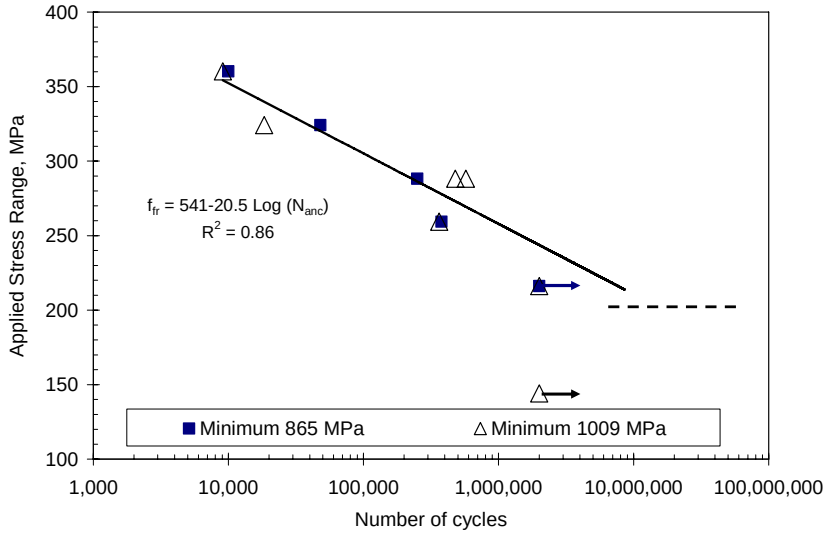

Figure 3.16: Applied stress range versus the life of the tendon-anchor assembly (excluding proof tests)

3.9 Use of the anchor test results in concrete beam design

The CFRP tendon-anchor assembly used in this study exhibited excellent performance when subjected to fatigue loading, indicating a promising potential for its use in post-tensioning of the concrete beams. The results of the fatigue tests were analyzed in two main aspects, namely, the effect of the fatigue loading on the material properties of the CFRP tendon and the effect of the fatigue loading on the performance of the anchor system itself.

Cyclic loading had a minimal effect on the mechanical properties of the CFRP tendon material. A maximum decrease of about 4% in the modulus of elasticity of the tendon was observed. This indicates that softening phenomenon, usually encountered with cyclic loading, can be neglected safely in design, within the stress range applied in this study. Therefore, the modulus of elasticity of the tendon material will be considered unchanged due to fatigue.

On the other hand, the anchor system withstood fatigue loading applied at different stress ranges. The fatigue life of the tendon-anchor assembly exceeded the PTI requirements specified for steel tendon anchors. Failure of all test specimens occurred in the CFRP tendon and no premature failure took place in the anchor. Based on the test results, an endurance limit of a stress range of 216 MPa was specified for the tendon-anchor assembly. Below this stress range, the tendon is expected to have an infinite fatigue life. These results were considered in the design of the strengthened beams to prevent the failure of the anchor system when fatigue loads are applied. The post-tensioning force applied to the tendons of the strengthened beams, along with other beam design parameters, were selected to ensure an infinite fatigue life of the anchor system. Details about the beam test specimens will be given later in Chapter 4.

Chapter 4

Beam Experimental Program

4.1 Introduction

The beam experimental program was developed to examine the monotonic and fatigue flexural response of reinforced concrete beams strengthened with externally post-tensioned CFRP tendons. The program was carried out on two levels:

- the component level: where the fatigue response of the CFRP tendon-anchor assembly was investigated (as reported in chapter 3), along with the fatigue response of the steel and the concrete (as will be illustrated in Chapter 5); and
- the member level: where monotonic and fatigue tests were carried out on reinforced concrete beams strengthened with externally post-tensioned CFRP tendons.

On the component level, the CFRP tendon-anchor assembly demonstrated excellent fatigue performance. The endurance limit of the assembly was determined as a tendon stress range of 216 MPa. This suggested that the fatigue life of the anchor system would not limit the fatigue life of the beam providing that the stress in the tendons was maintained less than its fatigue limit.

Cyclic simulation tests were also conducted on standard steel specimens and concrete cylinders in order to interpret the fatigue response of the beam constituent materials. The details and the results of these tests will be described later in Chapter 5.

On the member level, reinforced concrete beams were subjected to monotonic and fatigue loading. The beams were either unstrengthened or strengthened by CFRP external post-tensioned tendons. The main test parameters included the CFRP tendon profile (for monotonic response comparison), the initial loading conditions of the beams prior to being strengthened (service loading or overloading conditions), the amount of the non-prestressed reinforcement (two values corresponding to two partial prestressing ratios, PPR, of 0.36 and 0.46), and the fatigue load ranges applied to the beam (39% to 76% of the yield load).

The beam specimens were designed as flexural-critical reinforced concrete beams and were tested under a four-point loading pattern. Practical considerations were applied during the beam fabrication and the strengthening procedures. A special configuration was used in post-tensioning the concrete beams with external CFRP tendons, as will be illustrated later in this chapter.

The beams were designated by their conditions prior to strengthening, the internal reinforcing steel bar size, and the type of the applied loading. The label UN refers to the UNstrengthened beams used as controls. For strengthened beam specimens, the label SL refers to a Service-Level initial condition, and the label OL refers to an OverLoading initial condition. The numbers 15 and 20 in the beam designation refer to the bar size of the internal non-prestressed steel reinforcement. The letters M and F refer to the type of loading applied: Monotonic or Fatigue. The beams tested under fatigue were then ordered in an ascending order based on the maximum load applied. For example, beam SL15-F66 refers to a beam that was subjected to an in-service loading condition prior to being strengthened (SL). The beam was reinforced internally with 15M deformed bars (15) and was tested under fatigue loading (F) having a maximum peak load of 66 kN (66).

In this chapter, the details of the experimental program are given. A description of the test specimen, the fabrication process, the material properties, the post-tensioning technique, the test setup, and the test procedure are provided. The methodology used in monitoring the deflections

of the beam specimens, the strains in steel and concrete, and the stresses induced in the external tendons at various stages of loading are presented.

4.2 Beam test program

The beam experimental program consisted of testing twenty-eight unstrengthened and strengthened reinforced concrete beams under monotonic and fatigue loading. The main objectives of the program can be summarized as follows:

- to investigate the efficiency of the external post-tensioning technique to restore/enhance the structural performance of the reinforced concrete beams;
- to evaluate experimentally the fatigue behaviour and fatigue life of the reinforced concrete beams strengthened with external post-tensioned CFRP tendons with different partial prestressing ratios; and
- to investigate the effect of the initial load level applied to the beam before strengthening on its monotonic and fatigue response.

The test matrix is given in Table 4.1. The beams were divided into four groups: A, B, C, and D. Each group was designed to achieve one or more objectives of the experimental program. Details of the groups are described in the following sections.

4.2.1 Group-A: Unstrengthened control beams

Six unstrengthened beams were tested either monotonically or under fatigue as given in Table 4.1. One beam was tested monotonically up to failure in order to characterize experimentally the specimen flexural response at different stages of loading. The other five beams were tested under fatigue loading at different load amplitudes. Each fatigued beam was cycled between two loads, P_{min} and P_{max}. The minimum load, P_{min}, was maintained constant for all load ranges at 25% of the

yield load of the beam in order to simulate the sustained load for a typical beam in service. Based on a measured yield load of 60 kN, P_{min} was taken as 15 kN.

Five load ranges were generated by varying the maximum load applied, P_{max}. The load ranges varied between 58% and 73% of the yield load of the beam (between 35 kN and 44 kN). These load ranges were selected in order to provide reasonable fatigue lives before failure. The corresponding maximum loads, P_{max}, ranged between 83% and 98% of the yield load (between 50 kN and 59 kN). Although these values were higher than the loads expected to act on a typical beam in service, applying high load ranges was necessary in the experimental investigations to ensure fatigue failure of the beams for comparison purposes. Lower ranges, if applied, would lead to an infinite fatigue life and no comparison of failure modes would be possible.

4.2.2 Group-B: Initially-in-service strengthened beams – SL15

Group-B consisted of two strengthened beams tested monotonically up to failure and eight other beams tested under fatigue at different load ranges. Draped and straight CFRP tendons profile were used in strengthening the beams SL15-MDD and SL15-MST, respectively. Figure 4.1 shows a schematic view of the two tendon profiles used in strengthening the beams. Steel deviators were installed at the load points for both tendon profiles. The use of two tendon profiles in the monotonic tests of this group aimed to:

- investigate experimentally the possibility of harping the CFRP tendons with the required configuration;
- compare the structural response of the strengthened beams post-tensioned with straight and draped profiles when steel deviators are used; and
- decide on a tendon profile to be used in strengthening the beam specimens tested under fatigue loading.

Table 4.1: Test matrix for the reinforced concrete beams

No.	Specimen	Type of Load	Condition prior to strengthening	P_{max}, kN	*Range*, *R,* kN	R/P_{y}[a], %
Group-A: Unstrengthened specimens						
1	UN15-M	Monotonic		-		
2	UN15-F50	Fatigue	-	50	35	58%
3	UN15-F52	Fatigue	-	51.5	37	62%
4	UN15-F53	Fatigue	-	53	38	63%
5	UN15-F57	Fatigue	-	57	42	70%
6	UN15-F59	Fatigue	-	59	44	73%
Group-B: In-service Strengthened specimens PPR= 0.46						
7	SL15-MST[b]	Monotonic		-		
8	SL15-MDD[c]	Monotonic		-		
9	SL15-F61	Fatigue	Service	61	46	43%
10	SL15-F66	Fatigue	Service	66	51	47%
11	SL15-F68	Fatigue	Service	68	53	49%
12	SL15-F72	Fatigue	Service	72	57	53%
13	SL15-F82	Fatigue	Service	82	67	62%
14	SL15-F88	Fatigue	Service	88	73	68%
15	SL15-F92	Fatigue	Service	92	77	71%
16	SL15-F97	Fatigue	Service	97	82	76%
Group-C: In-service Strengthened specimens PPR= 0.36						
17	SL20-F79	Fatigue	Service	79	58	47%
18	SL20-F83	Fatigue	Service	83	62	50%
19	SL20-F87	Fatigue	Service	87	66	53%
20	SL20-F100	Fatigue	Service	100	79	64%
21	SL20-F110	Fatigue	Service	110	89	72%
Group-D: Overloaded Strengthened specimens						
22	OL15-M	Monotonic		-		
23	OL15-F57	Fatigue	Over-load	57	42	39%
24	OL15-F67	Fatigue	Over-load	67	52	48%
25	OL15-F72	Fatigue	Over-load	72	57	53%
26	OL15-F76	Fatigue	Over-load	76	61	56%
27	OL15-F82	Fatigue	Over-load	82	67	62%
28	OL15-F88	Fatigue	Over-load	88	73	68%

[a] *P_{y} refers to the yield load of the corresponding beam*

[b] *ST refers to straight tendon profile*

[c] *DD refers to double draped tendon profile*

A straight tendon profile is characterized by its ease of application, the simplicity of installing the prestressing fixtures, and, most significantly, a minor risk of harming the tendons at the harped points. Unlike the draped profile, no stress concentration will occur at the locations of contact between the tendons and the deviators. On the other hand, double draped tendons are commonly used in strengthening applications because of their efficiency in counteracting the effect of the uniformly distributed loads usually applied to concrete elements. They also minimize the stresses at the beam-ends where the tendons have no eccentricity from the neutral axis of the beam. They represent the most critical shape for FRP tendons in terms of strength, as FRP are known to weaken at the harped locations (refer to section 2.4.2).

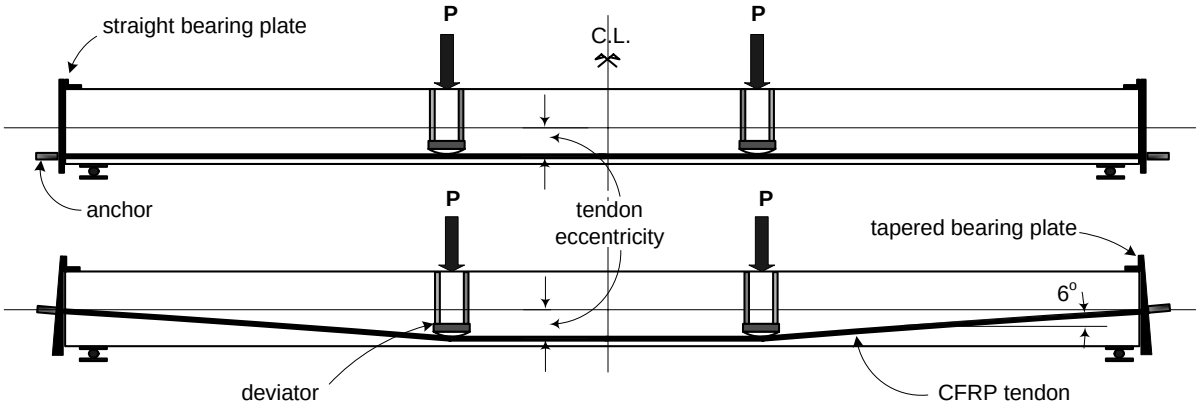

Figure 4.1: A schematic view of the straight and double draped tendon profiles

The specimens tested under monotonic loading also served as control specimens for the specimens tested under fatigue. All specimens of this group simulated typical under-reinforced beams that needed strengthening. The beams were reinforced with two 15M deformed bars and strengthened with two CFRP external tendons post-tensioned at 40% of their ultimate capacity (60 kN in each tendon). This percentage was selected within the values recommended by the ISIS Canada (2003) and ACI-440 (2004) Committees for FRP post-tensioned tendons. It also conforms to the results of the fatigue tests carried out on the tendon-anchor specimens (refer to Chapter 3)

to prevent premature fatigue failure at the anchorage zones. The beams had a partial prestressing ratio, *PPR*, of 0.46. The partial prestressing ratio is defined as the ratio between the nominal moment resistance due to the prestressing reinforcement to the nominal total moment resistance of the section (i.e., due to prestressed and non-prestressed reinforcement) (Naaman and Siriaksorn, 1979; ACI-423.5R, 1999). This is given in the following expression:

$$PPR = \frac{A_f f_f \left(d_f - \frac{a}{2} \right)}{A_f f_f \left(d_f - \frac{a}{2} \right) + A_s f_{sy} \left(d_s - \frac{a}{2} \right)} \tag{4.1}$$

where:

A_f = area of the prestressed CFRP tendons at the critical section;

A_s = area of the non-prestressed steel bars at the critical section;

f_f = stress in the CFRP tendon at ultimate;

f_{sy} = yield strength of the steel reinforcing bars;

d_f = depth of the CFRP tendons at the critical section;

d_s = depth of the steel bars at the critical section; and

a = depth of the equivalent rectangular stress block in the concrete compression zone.

The load ranges varied between 43% and 76% of the measured yield load of the strengthened beam (approximately 108 kN). The corresponding maximum peak loads ranged between 56% and 90% of the yield load. These load ranges reproduced moderate to severe fatigue loading conditions for the beams.

The load ranges applied to the strengthened beams had the same minimum load value applied to the unstrengthened beams. This simulated the actual conditions of a beam in-service where the sustained loads acting on the beam might remain constant during and after post-tensioning.

As mentioned in Chapter 2, most of the previously reported tests have been carried out on virgin beams. In addition, most of these tests neglected the effect of the sustained loads that might exist during post-tensioning application. These two drawbacks were avoided in the current investigation by carrying out the tests in four stages as follows (Figure 4.2-a):

- *The initial loading stage* — in this stage, the virgin beam was initially precracked by loading to 50% of its yield strength (point A). This represented a moderate level of applied live load that simulated the conditions of a cracked, in-service beam that needed strengthening.
- *The unloading stage* — in this stage, the beam was unloaded to 25% of its yield load after being cracked (point B, load = 15 kN). Unloading the beam represented the removal of the applied live load prior to strengthening. This load level represented the sustained load that would act on an in-service beam during strengthening. This load was maintained during the post-tensioning process.
- *The post-tensioning stage* — in this stage, an initial post-tensioning force of 40% of the ultimate tendon capacity was applied gradually in each tendon. The force was applied in each tendon separately as will be explained later in Section 4.6. During this stage, the beam was subjected to a sustained load of 15 kN, representing 25% of its yield load. When the force in each tendon reached 60 kN, the jacking process was stopped (point C).
- *The reloading stage* — after being post-tensioned, the beam was re-loaded until failure occurred under monotonic loading (points D, E, and F) or under fatigue.

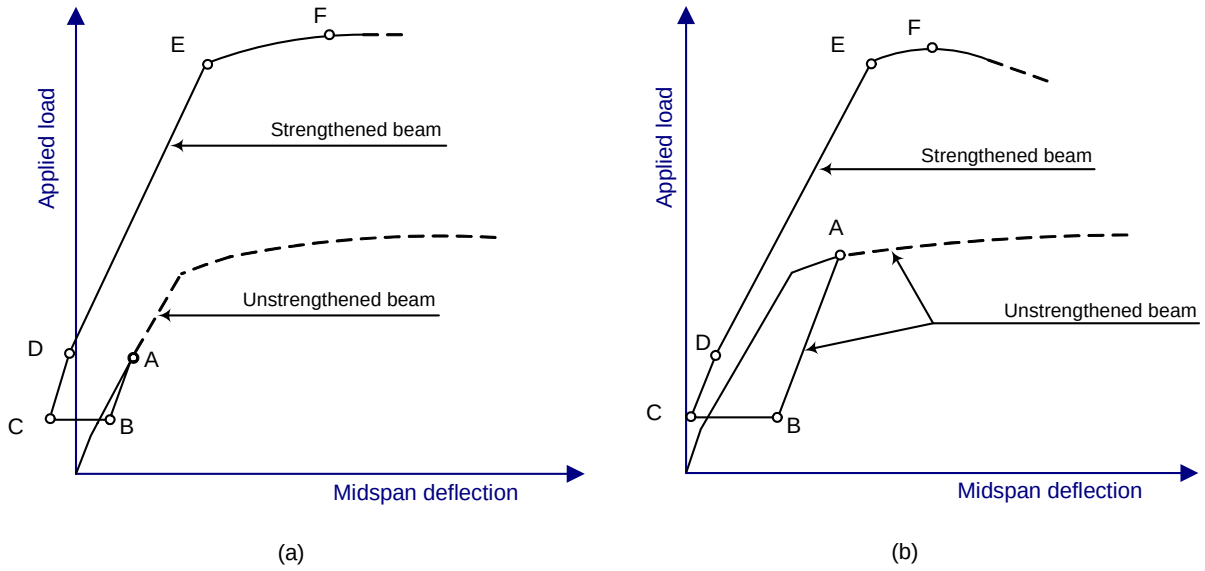

Figure 4.2: Idealization of the stages of monotonic loading of the (a) in-service beam and (b) overloaded beams (D: cracking load, E: yield load, and F: ultimate load)

4.2.3 Group-C: Initially-in-service strengthened beams – SL20

Group-C consisted of five beams tested under fatigue at load ranges varying from 47% to 72% of the estimated yield load of the strengthened beam (124 kN). The beams were reinforced with two 20M deformed bars and strengthened with two CFRP external tendons post-tensioned to 40% of their capacity (60 kN in each tendon). Post-tensioning occurred while the beam was subjected to a sustained load of 21 kN, representing 25% of its yield load. The beams had a partial prestressing ratio, *PPR*, of 0.36.

This series of beams, along with the beams of group-B, represented two partial prestressing ratios. They aimed to compare experimentally the efficiency of the post-tensioning technique to increase the capacity and reduce the deflection of beams with different amounts of reinforcement when the same post-tensioning force was applied. The results of fatigue tests of both groups will

be used to examine the applicability of the proposed fatigue model. The test procedure for group-C was similar to that described for group-B.

4.2.4 Group-D: Initially-overloaded strengthened beams - OL15

The beams of this group were reinforced with two 15M deformed bars and strengthened with two external CFRP tendons post-tensioned to 40% of their capacity (60 kN in each tendon). All beams were first overloaded before being strengthened. This condition represented situations where a beam was severely overloaded and it was necessary to simultaneously recover permanent deflections and strengthen the beam.

One overloaded-strengthened beam was tested monotonically up to failure to serve as control for the other beams. The four remaining beams were tested under fatigue at load ranges varying between 39% and 68% of the measured yield load of the strengthened beam. The corresponding maximum load ranged between 53% and 81% of the yield load.

The results for this group were used to study and to model the fatigue behaviour of the overloaded beams after being strengthened with CFRP externally post-tensioned tendons. These results were compared to those of group-B in order to evaluate the effect of the loading history of the beam on its monotonic and fatigue performance after being post-tensioned with CFRP tendons.

The tests on these beams were carried out in four stages.

- *The overloading stage* — in this stage, the beams were overloaded beyond the yield strain of the steel bars to simulate severe overloading conditions. A load producing a steel strain between 1.5 to 2 times its yield value was applied (approximately 4000 microstrain – point A in Figure 4.2-b).

- *The unloading stage* — in this stage, the beam was unloaded to 25% of its yield load after being overloaded (point B, load = 15 kN). This load level represented a sustained load that would be present in a beam in service during strengthening. This load was maintained during the post tensioning process.
- *The post-tensioning stage* — in this stage, an initial post-tensioning force of 40% of the ultimate tendon capacity was applied gradually in each tendon (point C). During post-tensioning, the beam was subjected to a sustained load of 15 kN, representing 25% of the yield load of the virgin beam. The post-tensioning force was kept equal to that applied to the beams of groups B and C for comparison purpose. As such, the effect of overloading would be the only variable that affected the beams response.
- *The reloading stage* — after being post-tensioned, the beam was re-loaded up to failure under monotonic (points D, E, and F) or fatigue loading.

4.3 Test specimen

The test specimen is shown in Figure 4.3. The beam was 3500 mm (11.48 feet) long with a depth of 254 mm (10 in.) and a width of 152 mm (6 in.). The specimen had a span-to-depth ratio of 15.40. The flexural tension reinforcement consisted of two 15M or two 20M Grade 400 deformed bars, with nominal diameters of 16 mm and 19.5 mm, respectively. Two 8 mm diameter plain steel bars were used in the compression zone, representing about 8% and 12% of the main tensile reinforcement, respectively. The shear reinforcement consisted of 8 mm diameter mild steel stirrups spaced at 75 mm (3 in.) over the length of the beam. This arrangement was designed to prevent any shear deficiency in the post-tensioned beams and to ensure that all beams developed their full flexural capacity. The yield and the ultimate strengths of the steel reinforcing bars were 440 MPa and 585 MPa, respectively. The yield strength and the ultimate strength for the 8 mm

smooth bars used for top reinforcement and stirrups were 340 MPa and 500 MPa, respectively (Masoud, 2002 and El Maadawy, 2004)[1].

Strengthening of the beam specimens was achieved by two external CFRP tendons post-tensioned at 40% of their ultimate capacity (approximately 120 kN). Draped tendons had an eccentricity, e_f, of 87 mm from the longitudinal axis of the beam, in the constant moment region, with no eccentricity at the beam-ends. This configuration kept the tendons at a depth, d_f, of 214 mm from the top concrete fibre at midspan, as shown in Figure 4.4. Double draped profile was achieved by means of two steel curved deviators located at the third points of the beam. The inclined portions of the draped tendons in the shear spans made an angle of approximately 6 degrees with the horizontal axis of the beam. Details of the deviating system and the post-tensioning setup are illustrated in the following sections.

Steel deviators were also placed at the third points of the beam post-tensioned with straight tendons (beam No. 8 in Table 4.1). For comparison purposes, the tendons had the same eccentricity, e_f, and depth, d_f, as the double draped tendons (87 and 214 mm, respectively) along the beam length. The steel deviators served as guides for the straight tendons when the deflection of the beam increased, in order to minimize the second order effects. Figure 4.5 and Figure 4.6 show general views of the strengthened beams with straight and double draped tendon profiles, respectively.

It is worth mentioning that the tendon eccentricities at midspan section and at the beam-ends, along with other design parameters (such as the beam dimensions, the loading pattern, and the post-tensioning forces) were selected to satisfy the following conditions:

---

[1] Tested at University of Waterloo on similar deformed steel bars

1. To develop a reasonable strengthening ratio between the ultimate capacity of the strengthened beam to that of the unstrengthened beam;
2. To minimize the stress concentration on the CFRP tendons at the harped locations. Stress concentration is likely to reduce the tensile strength of the harped CFRP tendons, which might lead to catastrophic results, if exceeded (see Section 2.4.2); and
3. To prevent any premature failure in the tendon-anchor zone during the fatigue load application.

4.4 Specimen fabrication

Reinforcement cages were prepared in accordance with typical construction practice. The steel reinforcement was instrumented using three strain gages prior concrete casting. Prior to installing the strain gages, the bar surface was sanded by grinding and cleaned with Ethanol and acidic conditioner. The surface was then cleansed with a neutralizer solution. The strain gages were attached to the bars using a special cement recommended by the manufacturer. Electrical wires were soldered to the ends of the strain gages and attached to electrical terminators placed along the steel bar. The wires were then projected outside the steel cage at different locations. The strain gages and the terminators were covered with wax to protect the gages from damage during the concrete casting (Figure 4.7).

Three sets of formwork were used in casting the test specimens. Each formwork accommodated five specimens (Figure 4.7). Precautions were taken to ensure the vertical alignment of the form end plates in order to facilitate the placing of the bearing plates while post-tensioning. The forms were coated with form oil prior to the installation of the steel cages. Plastic bar chairs were used to maintain the required clear cover between the steel cages and the bottom of the form.

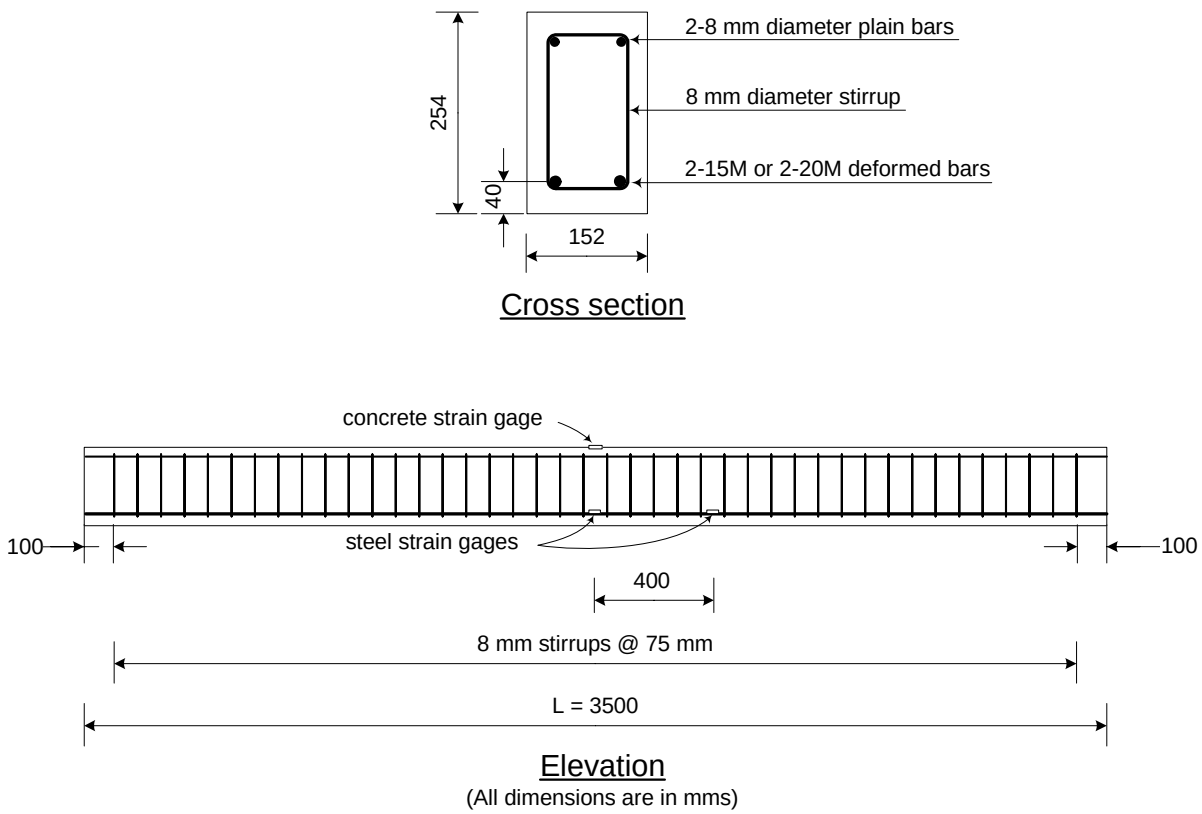

Figure 4.3: Typical dimensions and reinforcement details of the virgin beam specimen

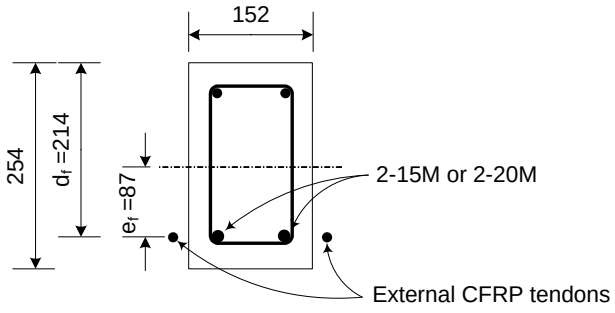

Figure 4.4: Cross section of the post-tensioned beams in the constant moment zone

Figure 4.5: General view of a strengthened beam with straight tendon profile

Figure 4.6: General view of a strengthened beam with draped tendon profile

Figure 4.8 shows the different stages of the casting procedure. Three ready mix concrete batches were used to construct the beam specimens on three separate dates. Before casting, slump tests on fresh concrete were conducted to ensure the workability of the provided mix. Slump of concrete ranged between 150 mm and 170 mm (6 to 7 in.). Standard concrete cylinders of 100 mm (4 in.) diameter and 254 mm (10 in.) height were cast for compressive strength tests. The 28-day compressive strengths of all batches are shown in Table 4.2. The average compressive strength of the concrete for all batches was 35 MPa.

Electric vibrators were used during casting of concrete specimens to minimize voids and honeycombing. The surface was then finished using steel flat trowels. After the completion of casting, the forms were covered by polyethylene sheets to minimize the moisture evaporation. The specimens were then left to cure for 15 days. During the curing process, the beams and the concrete cylinders were covered by wet burlap and polyethylene sheets as shown in Figure 4.8.

Figure 4.7: Strain gages covered with wax (left) and steel bars inside the timber forms (right)

(a)

(b)

(c)

(d)

Figure 4.8: (a) Slump test, (b) casting cylinders, (c) finishing surfaces, and (d) curing

Table 4.2: Concrete compressive strength results

Batch No.	Beams	Cylinder 1	Cylinder 2	Cylinder 3	f'_c
Batch 1	SL15, SL20	40	43	35	39
Batch 2	SL15, OL15	32	36	35	34
Batch 3	UN15, SL15, OL15	32	30	31	31

4.5 Post-tensioning setup

The post-tensioning setup consisted of two main systems positioned onto the beam namely, the deviating system and the end-bearing system. A description of both systems is presented in the following sub-sections.

4.5.1 Deviating system

Reusable steel deviators were used to create the draped profile of the CFRP external tendons. The same deviators were used as guides for the straight tendons of beam SL15-MST of Table 4.1. As explained earlier in Chapter 2, the use of deviators or guides minimizes the change in the tendons eccentricity and depth with the application of loads on the tested beam.

A pair of steel deviators was fabricated at University of Waterloo. Figures 4.9 and 4.10 show schematic and photographic views of the deviating system, respectively. The system consisted of a steel channel of 50.8x127x305 mm (2x5x12 in.) clamped by two 10 mm diameter (3/8 in.) threaded rods to a steel plate of 230x100 mm (9x4 in.) placed at the top surface of the beam specimen. The channel was placed at the bottom of the beam at the loading points. Two vertical side plates spaced apart by 152 mm (6 in.) were bolted to the channel section and placed against the sides of the beam. A tolerance of 1 to 2 mm allowed the beam to fit in between the side plates. The channel, along with the top plate and the two vertical side plates, formed a closed frame to which the curved deviators (saddles) were attached.

The saddles had the same width as the vertical side plates, as shown in Figure 4.10. They were fastened to the side plates by means of three high strength steel bolts of 10 mm (3/8 in) diameter each. The saddles, with their upper flat and lower curved planes, were placed in position for the CFRP tendons to have an eccentricity of 87 mm.

Large saddles of 500 mm radius of curvature were used based on the findings of Grace and Abdel-Sayed (1998) and Quayle (2005). The purpose was to minimize any stress concentration at the harped point of the CFRP tendons in order to prevent any significant reduction in the tensile capacity of the tendons. Thin Teflon sheets were used as cushioning material to minimize the friction between the CFRP tendon and the saddles. Steel plates of 127 x 63.5 mm (5 x 2.5 in.) were attached to the saddles. The plates were used as shields in order to prevent the deviated tendons from moving out of the plane of the beams (Figure 4.10).

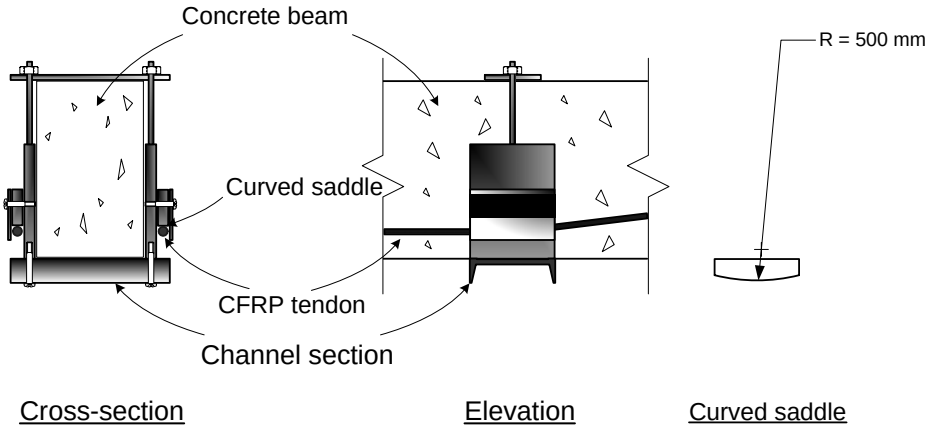

Figure 4.9: A schematic view of the deviating system

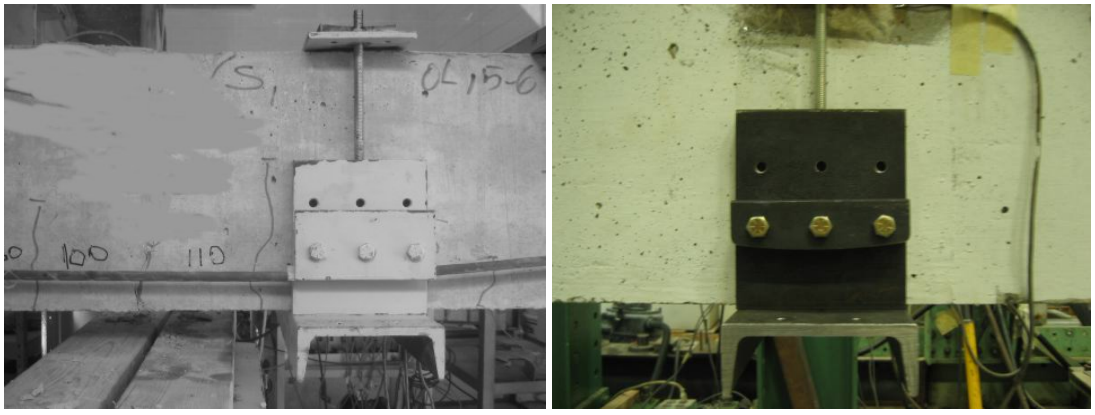

Figure 4.10: Photos of the deviating system (left) showing the curved saddle used (right)

4.5.2 End-bearing systems

The end-bearing systems consisted of two separate assemblies namely, the jacking end, where the jacking force was applied to the tendons, and the dead end, corresponding to the other gripped end of the tendon. A general view of both ends is shown in Figure 4.11.

The jacking end consisted of a structural steel stressing chair composed of an I-beam section of 406.5 mm (16 in.) long and 230 mm (9 in.) deep placed between a channel and a bearing plate. The bearing plate rested against the beam end. The web of the channel was bolted to the I-beam section by means of four 16 mm (5/8 in.) steel bolts. The dead end consisted of a similar bearing plate resting against the other end of the beam.

Straight and tapered steel bearing plates were used as necessary to match the required deviation angle of the external tendons (Figure 4.12). Straight plates of 380x280x25.4 mm (15x11x1 in.) were used to create straight tendon profile. Tapered plates, of thickness varying between 12.5 mm (1/2 in.) at the top and 35 mm (1.40 in.) at the bottom, made a vertical angle of 6 degrees. This ensured that the longitudinal axis of the tendons was orthogonally projected on the inclined plane of the tapered plates, and prevented the tendons from being bent during post-tensioning. The plates were grooved on both sides to facilitate the installation of the tendons from the sides of the beam as illustrated in Figure 4.12-c.

The bearing plates were held in place by means of a locking-assembly as shown in Figure 4.12-d. The assembly consisted of two angle sections of 50.8x50.8 mm (2x2 in.) attached together by two 10 mm diameter (3/8 in) threaded rods. The upper angle section rested on the top of the beam and the system was then "locked" by tightening the threaded rods to fit the height of the beam's cross section.

Prestressing fixtures — two hollow steel screw adjusters rotating on thrust bearings were aligned with the tendon's axis (Figure 4.13-a, b). The adjusters, when opened, served to maintain

the applied post-tensioning force in the tendons. They also allowed the tendons to be de-tensioned at the end of the test. Grooved steel shims of 10 mm thickness were used to fill the gap between the adjuster and the bearing plates when the tendons were post-tensioned. The thrust bearings were used to prevent any twisting of the tendon during the rotation of the screw adjusters.

The tendons were post-tensioned using two hollow hydraulic jacks of 120 kN (27 kips) capacity mounted on the stressing chair (Figure 4.13-c). Jacking was carried out separately in each tendon to ensure even forces applied to both tendons. Two manual hydraulic pumps were used in stressing the tendons (Figure 4.13-d). The jacking force was applied against a pair of anchors placed at the ends of each tendon (jacking anchors). The post-tensioning force in each tendon was monitored by two hollow load cells of capacity of 222.4 kN (50 kips) placed between the anchor and the thrust bearing. The load cells rested between a pair of pocketed plates as shown in Figure 4.14-a.

Figure 4.11: General view of the jacking end (left) and the dead end (right) of the end-bearing system

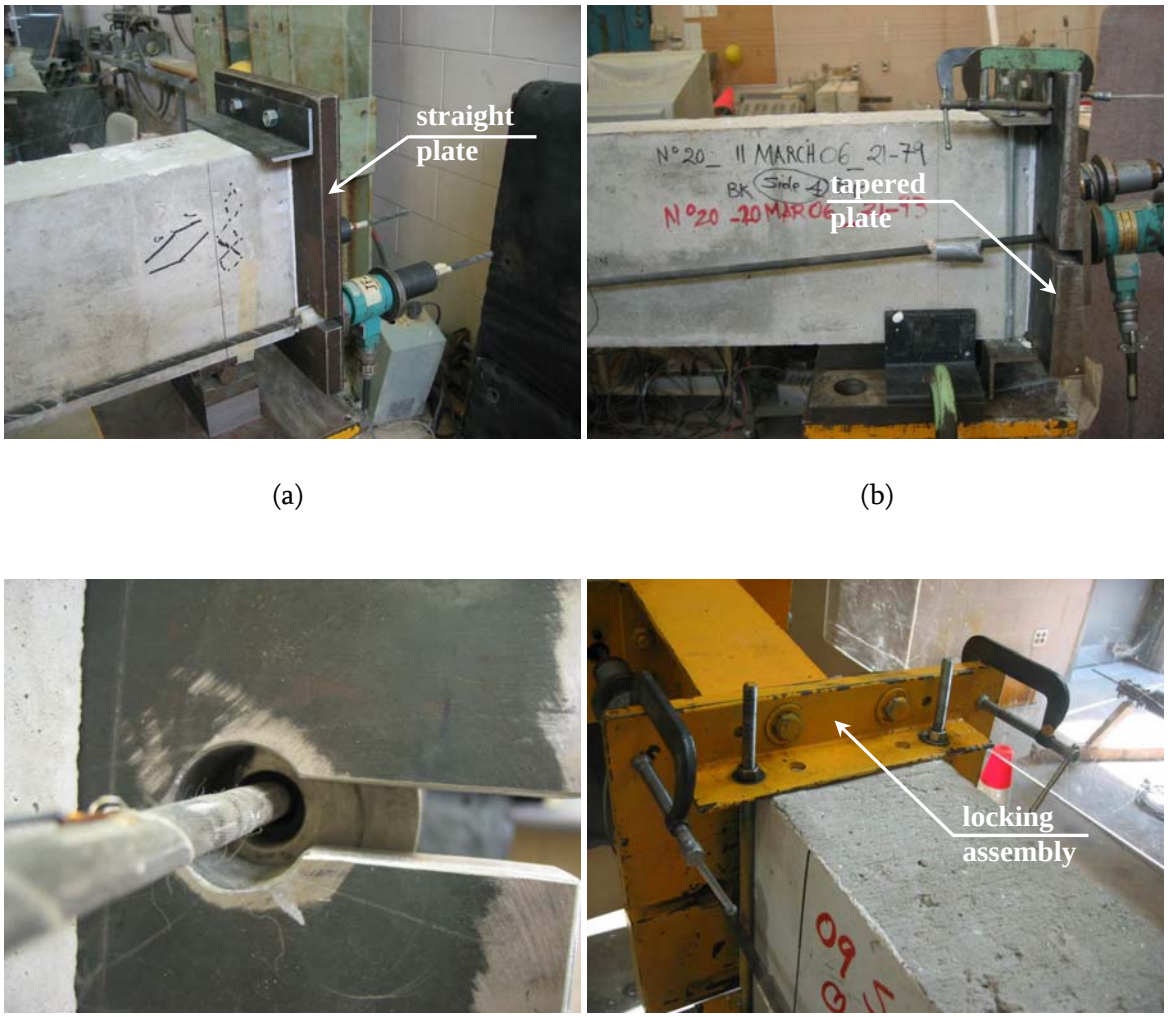

(a) (b)

(c) (d)

Figure 4.12: Post-tensioning system: (a) straight bearing plate, (b) tapered bearing plate, (c) grooves in the bearing plates, and (d) locking-assembly

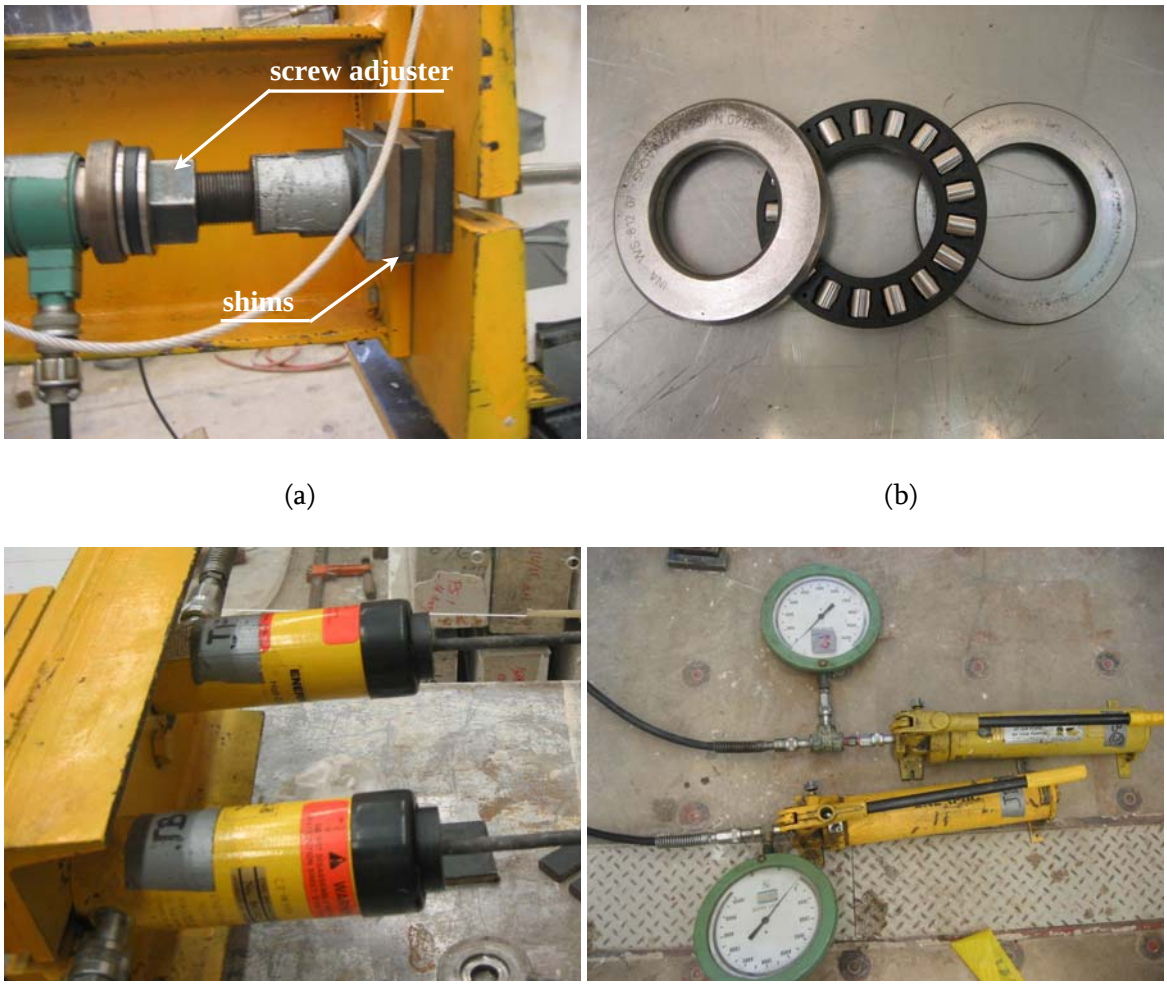

(a) (b)

(c) (d)

Figure 4.13: Post-tensioning system: close-up of the (a) screw adjusters, (b) thrust bearing, (c) jacks, and (d) hydraulic pumps

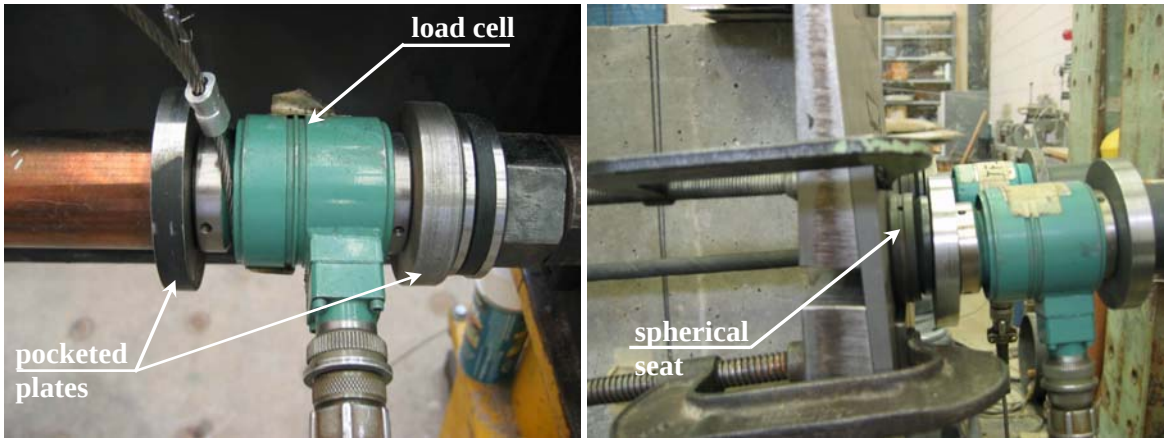

(a) (b)

Figure 4.14: Post-tensioning system: (a) load cell between pocketed plates at the jacking end, (b) load cell seated on spherical seat at the dead end

Tendons at the dead end were instrumented by another pair of hollow load cells as shown in Figure 4.14-b. The load cells were seated on spherical bearings to eliminate any tendon misalignment that might occur during post-tensioning. As in the jacking end, pocketed bearing plates were also used to maintain the load cells in place.

4.6 Post-tensioning procedure

Post-tensioning of the strengthened beams was carried out in three consecutive phases starting with the preparation of the beam-ends, through the fixation of all prestressing fixtures on to the tendons, and ending with positioning the tendons in their final locations on the sides of the beams before the post-tensioning force was applied.

4.6.1 Beam-ends preparation

As the CFRP tendons are weak in their transverse direction, a precise alignment between the tendons and the longitudinal axis of the beam was necessary to prevent twisting or bending of the tendons. The beam-ends were thus prepared in order to create a leveled plane orthogonal to the longitudinal axis of the beam. This precaution would prevent the rotation of the bearing plates when the post-tensioning force was applied.

Both beam-ends were leveled by adding a thin layer of hydrostone of 2-4 mm thick, depending on the conditions of the cast end. A small wooden form was used to cast the hydrostone mix. The form was then removed after 1-2 hours to ensure that the hydrostone was completely set and capable of bearing the compressive forces resulting from the post-tensioning application. Figure 4.15 shows the finished surfaces of the beam-ends after being leveled.

Figure 4.15: Finished surface of the beam ends

4.6.2 CFRP tendons preparation

The CFRP tendons were first cut to a length of 4500 mm (approximately 14.7 feet) and anchored at their anticipated jacking end with a pair of the Waterloo anchors (refer to section 3.2) after positioning the hydraulic jacks in place, as shown in Figure 4.16. Anchoring of the tendons was achieved using the pre-seating rig as explained in section 3.4. Prestressing fixtures, including the load cells, the pocketed plates, the thrust and spherical bearings, and the screw adjusters were then installed in place before the dead end was gripped by another anchor. Figure 4.16 shows the detailed tendon preparation steps.

(a) (b) (c)

Figure 4.16: (a) The pre-seating rig, (b) the hydraulic jack, and (c) the prestressing fixtures

4.6.3 Installation and post-tensioning of CFRP tendons

The end-bearing systems were installed on both ends of the beam before the CFRP tendons were positioned in place. The systems were securely tightened by the locking assembly described above. Alignment of both systems with the longitudinal axis of the beam was adjusted by eliminating any gap or tilting between the bearing plates and the leveled ends of the beams. The two deviators were then placed at the third points of the beam (location of the two applied point-loads).

The CFRP tendons were then installed on the sides of the beams through the grooved bearing plates. The jacks were tightened to the stressing chair by means of two steel bolts and were connected to the hydraulic pumps.

During post-tensioning, the force in the CFRP tendons was monitored by the two load cells placed at the dead ends of the beams. When the desired force was reached in each tendon, the screw adjusters were opened and the steel shims were installed between the bearing plates and the adjusters in order to maintain the force in the tendons. The jacking force was then released gradually and the readings of the four load cells were monitored until a complete release of pressure was achieved. A tolerance up to 5% in the load cells readings was acceptable. If the difference between the four readings exceeded this amount, the jacking force was released and the post-tensioning procedure was repeated until the required tolerance was achieved. The hydraulic pumps were then removed at the end of the post-tensioning procedure, and the beam was loaded either under monotonic or fatigue loading.

4.7 Loading test setup

Schematic and photographic views of the beam loading test setup are given in Figure 4.17 and Figure 4.18, respectively. All specimens were tested under four-point bending with a clear span of 3300 mm and a shear span of 1100 mm. The load was applied by means of a servo-hydraulic actuator with a maximum capacity of 155 kN reacting against a steel frame anchored to the laboratory strong floor. The load was transferred to the beam by means of a steel spreader beam through two supports, one roller and one hinged, placed at the third-points of the beam. The specimen was supported on a pair of roller and hinged supports resting on steel pedestals anchored to the strong floor.

Safety precautions were adopted while carrying out the beam loading tests. As the CFRP tendons were externally post-tensioned, they were vulnerable to notching during handling,

positioning, or stressing. If the prestressed tendons were to break, an enormous release of the prestressing force would occur, causing a dangerous situation.

Four Plexiglas™ sheets and two safety blankets were used as shields along the beam length and in front of the beam-ends, respectively, as shown in Figure 4.18. The shields were grooved at their top edges at two locations and were hanged freely by a pair of hooked steel bars. The shields and the blankets were anticipated to absorb any shock that might occur from the breakage of the tendons.

In order to prevent the lateral movement of the beam during fatigue tests, four steel angles covered with flexible rubber sheets were clamped to the pedestals at both beam-ends (Figure 4.19-a). In addition, the spreader beam was prevented from moving out of the test plane by fixing a steel restraint system as shown in Figure 4.19-b.

4.7.1 Strain measurements

Electrical resistance strain gages bonded to the surface of steel reinforcement and concrete were used to monitor the strain at two locations: at midspan and at a distance 400 mm from the midspan.

At the midspan section, the strain gages were placed on the bottom of the two reinforcing bars, on the concrete on one side of the beam (38 mm and at 63.5 mm below the concrete top surface), and on the top surface of the concrete beam. At the other section (400 mm from the midspan), strain gages were placed only on one of the two reinforcing bars and on the concrete top surface. Figures 4.20 and 4.21 show the locations of the strain gages installed on the surface of the steel and the concrete, respectively. Strain gages used on the steel bars had a 5 mm gage length, while those used on the concrete surface had a gage length of 70 mm. The strain gages had a gage resistance of 120.2 ± 0.2 ohms with a thermal expansion of 11.7 PPM/°C.

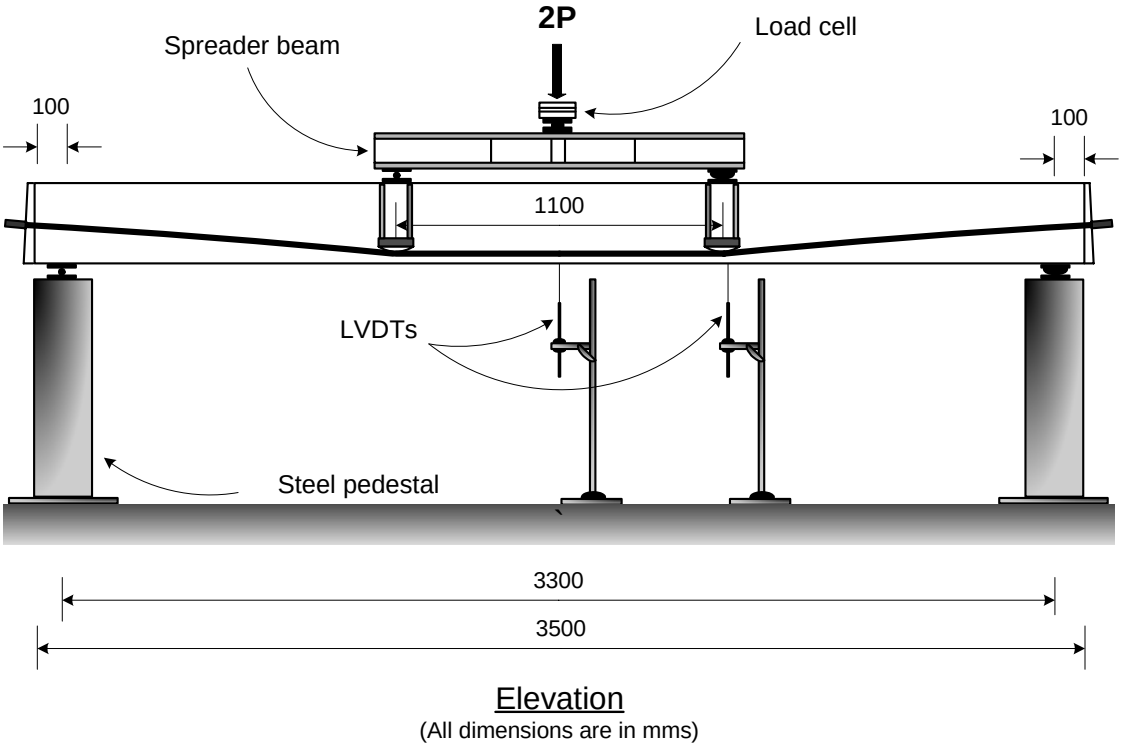

Figure 4.17: A schematic view of the beam loading test set-up

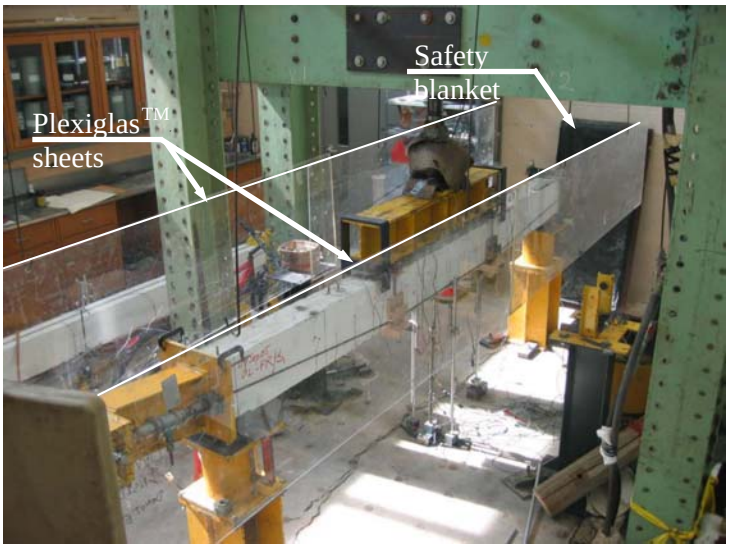

Figure 4.18: A photo of the test setup of a post-tensioned beam

Figure 4.19: (a) Steel angles located at the beam edges and (b) the restraint system for spreader beam

4.7.2 Beam deflection measurements

The beam deflection was recorded by means of two linear variable differential transducers (LVDTs). One LVDT was placed at mid section of the longitudinal span to record the maximum deflection in the constant moment zone. Another LVDT was placed under one of the point loading (550 mm away from the mid section).

At the same time, two other LVDTs were used to measure the deflection of the CFRP tendons at mid span. The recorded deflections of the beam and the CFRP tendons at midspan were compared and used to determine the change in the tendon eccentricity as the load increased to assess the second-order effects. Figure 4.22 and Figure 4.23 show schematic and photographic views of the LVDT locations. The LVDTs had a stroke of 100 mm and an accuracy of 0.01 mm, and their readings were recorded by a data acquisition system as shown in Figure 4.24.

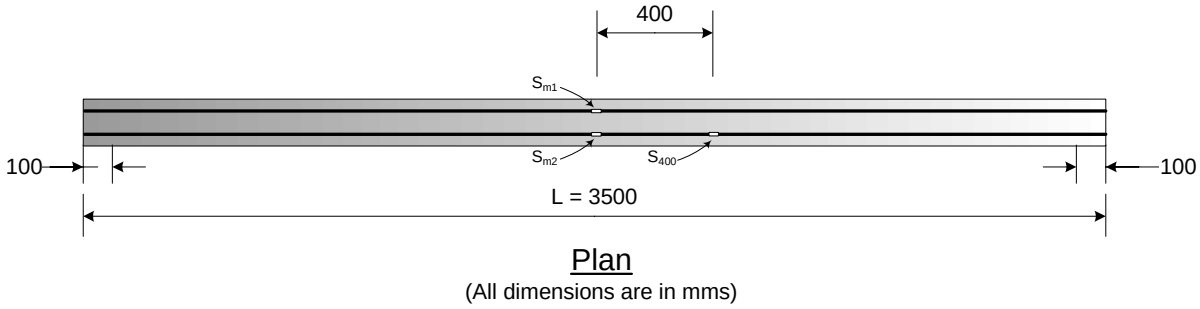

Figure 4.20: Location of strain gages on the steel bars

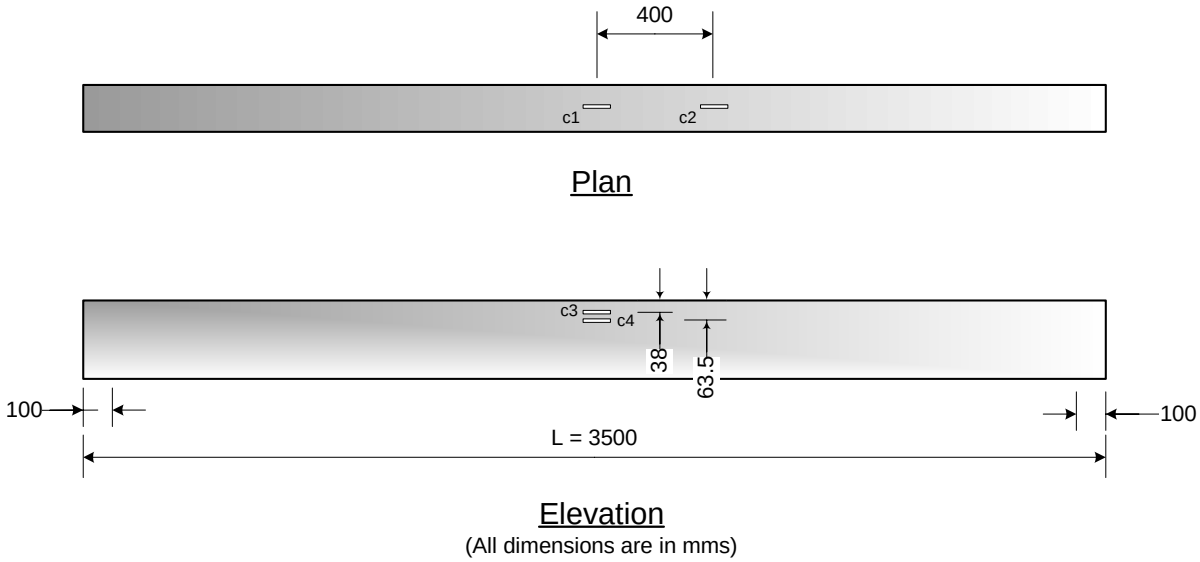

Figure 4.21: Location of strain gages on the concrete surface

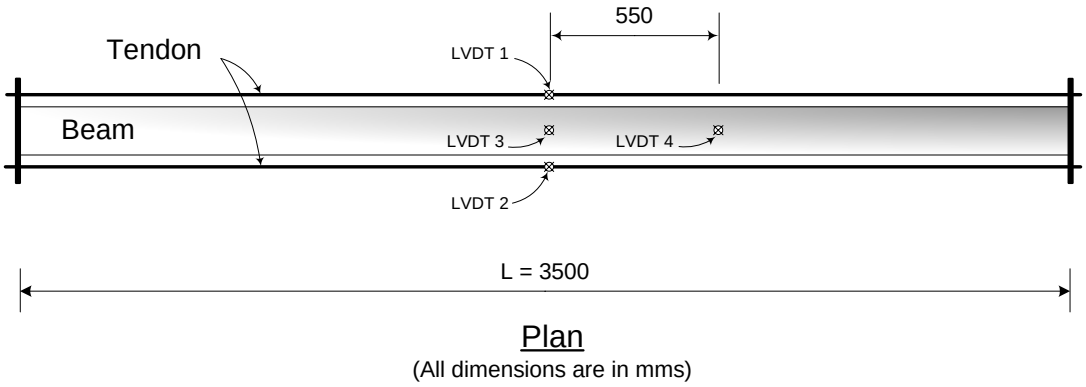

Figure 4.22: A schematic view of the LVDTs locations

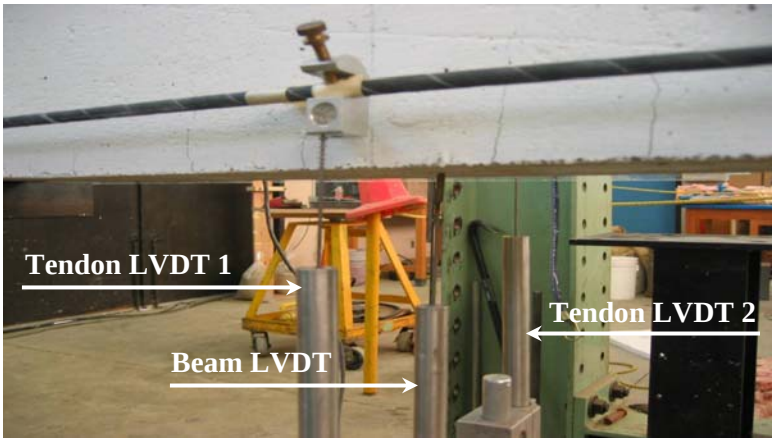

Figure 4.23: Locations of LVDTs at the midspan section of the beam

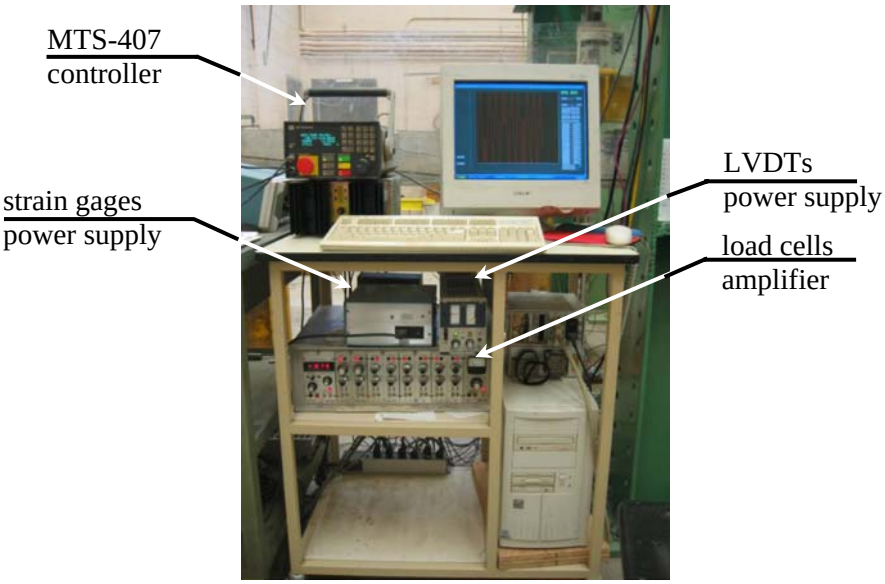

Figure 4.24: A general view of the data acquisition system

4.8 Loading test procedure

Testing of the specimens under monotonic and fatigue loading was preceded by the attachment of the various hardware and instrumentation. Monotonic tests were conducted on both unstrengthened and strengthened beams under stroke control at a stroke rate of 1.5 mm/min. Fatigue tests were conducted under load control by means of a MTS-407 function generator that produced sinusoidal variable load at a maximum frequency of 1.5 Hz. This is close to the typical frequency of vehicle loads on bridge decks, as reported by Mays and Tilly (1982).

Prior to applying cyclic loads, the beam was first loaded to its maximum peak load. The beam was then unloaded to the mean load level defined as the average value of the maximum and the minimum peaks. The mean load differed from one specimen to another based on the applied load range. The load was then cycled between the two peaks until failure occurred or the number of

the recorded cycles exceeded one million cycles. Tests of beams lasting for more than one million cycles were intentionally halted and were considered as run-outs. Data were recorded continuously for the first one-thousand cycles, and then in intervals of cycles specified based on the anticipated life of the beam.

Chapter 5

Beam Experimental Results and Discussion

5.1 Introduction

This chapter presents the results of the monotonic and fatigue tests carried out on the unstrengthened and strengthened reinforced concrete beams. As described in Chapter 4, the partial prestressing ratio, the loading type, and the loading conditions prior to strengthening were considered in this investigation. In this chapter, the effects of these parameters on the behaviour of both unstrengthened and strengthened beams are examined. Comparisons between various beam specimens in terms of their structural performance under monotonic and fatigue loads are presented.

5.2 Monotonic test results

One unstrengthened and three strengthened concrete beams were tested under monotonic loading to determine their structural response in terms of the cracking load, the yield load, the ultimate capacity, the load-deflection response, and the observed modes of failure (Beams No. 1, 7, 8, and 22 in Table 4.1). These beams also served as control beams to compare their response to the fatigue specimens.

All beams were reinforced with two 15M deformed steel bars and were tested under four-point loading until failure. Beam UN15-M was unstrengthened while the two beams SL15-MST and SL15-MDD (with straight and draped tendons profile, respectively) were post-tensioned with CFRP tendons at a sustained load of 15 kN after being subjected to an in-service load of 30 kN. The beam OL15-M (with draped tendons profile) was initially overloaded beyond its yield capacity prior to post-tensioning. All CFRP tendons were post-tensioned to 40% of the tendon ultimate capacity.

The response of the unstrengthened beam to failure under monotonic loading was typical for an under-reinforced concrete beam. The first crack occurred at a load of approximately 9 kN and a midspan deflection of about 1 mm. The internal reinforcement yielded at a load of 60 kN and a midspan deflection of 25 mm. The beam reached its ultimate capacity at 67 kN where the concrete started crushing at a deflection of approximately 85 mm (Figure 5.1).

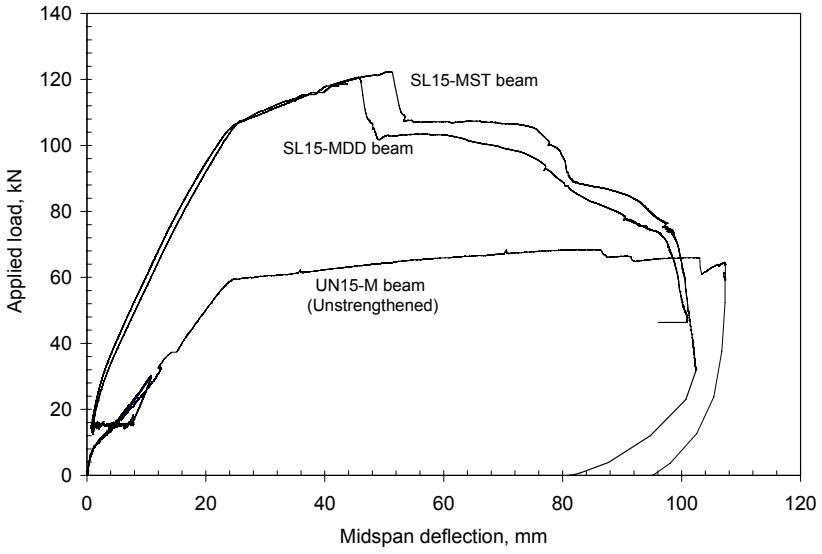

Figure 5.1: Load-deflection response of the unstrengthened and in-service beams

5.2.1 In-service strengthened beams

5.2.1.1 Deflection and stiffness response of the in-service beams

The load-deflection relationships of both in-service strengthened beams (SL15-MST and SL15-MDD) are shown in Figure 5.1. For comparison purposes, the load-deflection curve of the unstrengthened beam is also shown.

The beams were post-tensioned at a sustained load of 15 kN. At the end of post-tensioning, no upward camber was recorded for the beams; the measured downwards deflections were 0.85 mm and 1.01 mm for the SL15-MST and SL15-MDD beams, respectively. This is notably less than the 5 mm deflection of the control beam at the same load level. This reduction in deflection was attributed to the counteracting moment produced by the eccentric post-tensioning force applied by the external tendons.

As can be seen in Figure 5.1, the in-service post-tensioned beams behaved similarly at all stages of loading. The load-deflection relationship of the beams was characterized by three distinct stages defined by the level of the load applied as follows:

- *End of post-tensioning (15 kN up to 30 kN)* — in this stage, the stiffness of the strengthened beams was equal to the initial stiffness of the unstrengthened beam prior to cracking. This was indicated by the similar slopes of the portions of the load-deflection curves for the unstrengthened and the strengthened beams in the corresponding stages. This suggested that all flexural cracks developed earlier due to the initial loading were fully closed after post-tensioning. The cracks re-opened at about 30 kN and an approximately 3 mm deflection. This stage of loading (0-30 kN) is considered as the uncracked stage of the post-tensioned beams.

- *Between 30 kN and 108 kN* — this stage extended between the cracking load (30 kN) and the yield load (108 kN) of the post-tensioned beams, and represented the service-loading stage of the beams. A slight reduction in the beams stiffness was noticed as shown in Figure 5.1. However, the stiffness was still higher than that of the service-loading phase of the unstrengthened beam. This was attributed to the restrained crack opening and growth due to external post-tensioning, which resulted in an increase in the stiffness of the beam. As the load increased, existing cracks widened and new cracks initiated until the internal reinforcement yielded at a load of about 108 kN (compared to 60 kN for the unstrengthened beam). The deflection of the strengthened beams was about 24 mm at yield.
- *Post-yield stage* — this stage extended between the yield load and the failure of the beams. After yielding, a significant reduction in the stiffness of the beams was observed. The deflection of the beams increased until the upper layers of concrete began to crush at an applied load of approximately 120 kN (compared to 69 kN for the unstrengthened beam). At this point, the deflection was about 50 mm. The load dropped to approximately 102 kN due to spalling of the concrete cover in the compression zone. Note that this load was close to the yield load of the strengthened beams. The remaining concrete section, confined by the stirrups, was able to maintain the load until a deflection of 80 mm was attained. At that time, a substantial decrease in load occurred, and the stress in the CFRP tendons increased considerably until a complete failure by concrete crushing occurred at a deflection of about 95 mm.

5.2.1.2 Strain measurements of the in-service beams

Concrete and steel strains were measured at mid-span by means of electrical gages. Figure 5.2 and Figure 5.3 compare the measured steel and concrete strains at midspan, respectively, for the in-service strengthened beams and the control beam.

During post-tensioning, measured strain values in both the concrete and steel bars changed with the gradual increase of the post-tensioning force. As the strengthened beam was loaded, the observed trend in the steel strain values resembled to that observed in the deflection response. The strains developed in the steel reinforcement increased until the applied load reached 30 kN when flexural concrete cracks started to re-open. Beyond this cracking load, the tensile strains in the steel increased at a higher rate until failure occurred.

The steel strains in the post-tensioned beams were significantly less than those measured in the unstrengthened beams at all stages of loading. This was attributed to the effect of the post-tensioning force on the beams.

A similar trend was observed for the strain measurements at the top surface of concrete. The compressive strains in concrete resulting from the initial applied loads before post-tensioning were significantly reduced by post-tensioning. As the load applied to the strengthened beams increased, the compressive strains in the concrete increased until the concrete crushed. Cracking of the concrete at the top fibre was prevented during post-tensioning by limiting the post-tensioning force in the CFRP tendons to 40% of the tendon ultimate capacity.

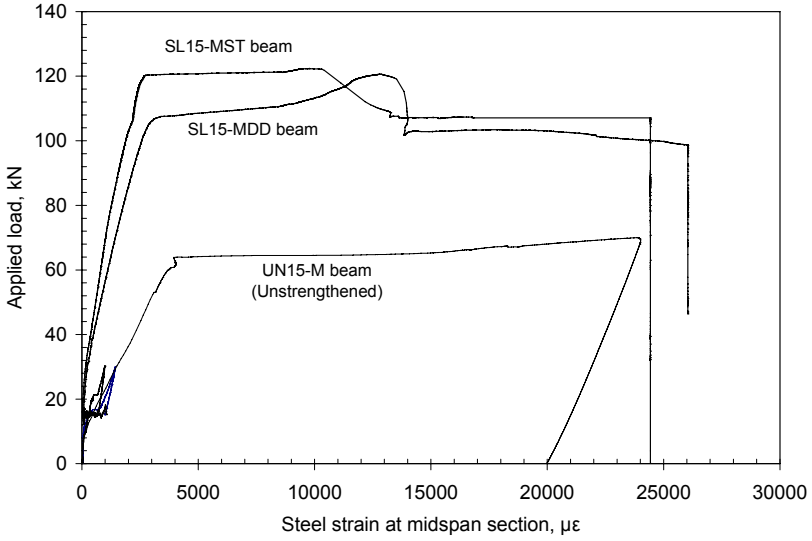

Figure 5.2: Applied load versus the measured steel strains at midspan of the in-service strengthened beams and the control beam

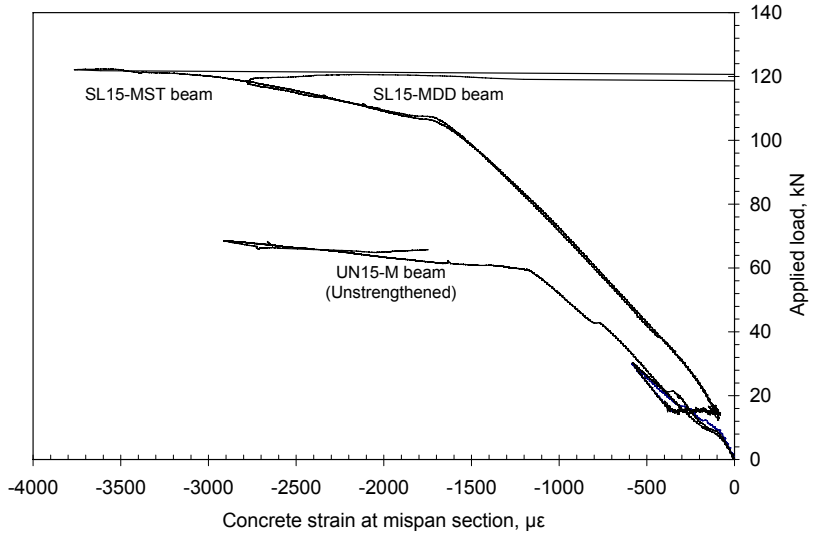

Figure 5.3: Applied load versus the measured concrete strains at midspan of the in-service strengthened beams and the control beam

5.2.1.3 Changes in the CFRP tendon stress of the in-service beams

The CFRP tendons were initially stressed to an average value of 831 MPa, representing about 40% of the tendon ultimate capacity. The stress in the CFRP tendons was calculated based on the readings from the load cells attached at the ends of each tendon. As the applied load on the strengthened beams increased, the stress in the tendons increased beyond the initial post-tensioning stress.

Due to the lack of bond between the tendons and the surrounding concrete, deformation compatibility, rather than strain compatibility, exists between the tendons and the concrete. As the applied load increased, the curvature of the beam increased. This produced a proportional increase in the tendon strain such that the tendon elongation at any stage of loading was equal to the total elongation of the adjacent concrete, at the same depth as the tendon. The variation of the tendon stress with the applied loads was similar to the load-deflection relationship, as shown in Figure 5.4.

The increase in the tendon stress was not significant until the cracks opened at an applied load of approximately 30 kN. Beyond this load, the stress in the tendon increased steadily until the internal steel reinforcement yielded. After yielding of steel, the stress in the tendon increased rapidly with the applied load. At maximum load, the maximum stress in the tendons never exceeded 1300 MPa, or about 60% of the tendon ultimate tensile capacity (2162 MPa). As such, the CFRP tendons did not rupture. Table 5.1 compares the stress increase, Δf_t, in the straight and double draped tendons at various stages of loading. As expected, the maximum increase in the CFRP tendon stress occurred when the beam reached its ultimate capacity. At this stage, the deformation of the beam was substantial.

The stress increase in the straight and double draped tendons was almost of same magnitude at all stages of loading. This was mainly attributed to the presence of deviators in both beams where

the variation of the tendons eccentricity at midspan was minimized. Note that the shift between the two curves shown in Figure 5.4 was attributed to the difference in the initial post-tensioning forces applied to the tendons (see Table 5.1).

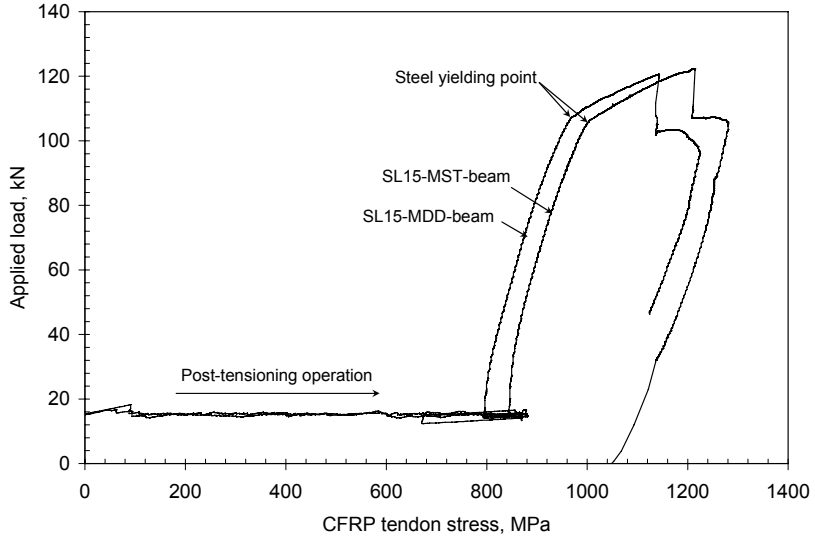

Figure 5.4: Variation of the tendon stress with the applied load in the in-service strengthened beams

Table 5.1: Change in tendon stress, Δf_f, for straight-with-guides and double draped tendons

Tendon Stress	Straight tendons (SL15-MST beam)	Draped tendons (SL15-MDD beam)	Draped tendons (OL15-M beam)
f_f initial, *MPa*	843	800	850
Δf_f at yield stage, *MPa*	160 (19%)*	168(21%)*	173(20%)*
Δf_f at ultimate stage, *MPa*	371 (44%)*	343 (43%)*	206(24%)*

** % of the initial (effective) post-tensioning stress*

5.2.1.4 Changes in the tendon depth of the in-service beams

The behaviour of an externally post-tensioned beam may be affected by the successive reduction in the tendon eccentricity with respect to the surrounding concrete, as beam deflections increase. With the absence of deviators, the tendons encounter a continuous loss of their depth and eccentricity. This is known as the second-order effect, and is caused by the tendon remaining rectilinear between the end anchorages while the beam deformation is curve-linear (see Figure 2.2). The presence of deviators has a significant effect on reducing the second-order effect and thus, on increasing the load-carrying capacity of the externally post-tensioned beams (Harajli, 1993; Taniguchi et al., 1997).

The deflections of the beams and the CFRP tendons were measured by means of LVDTs placed at the same section at midspan (see Figure 4.22). Based on the obtained readings, the variation in the tendon depth, Δd_f, at any stage of loading was calculated as the difference between the deflection of the beam and that of the tendon as follows:

$$\Delta d_f = (\Delta_{ci} - \Delta_{co}) - (\Delta_{fi} - \Delta_{fo}) \tag{5.1}$$

where

Δ_{ci} and Δ_{fi} = the deflections of the concrete beam and the CFRP tendon, respectively, at any stage of loading *i*, and;

Δ_{co} and Δ_{fo} = the deflections of the concrete beam and the CFRP tendon, respectively, at the conclusion of post-tensioning;

The depth of the CFRP tendon at any load level, d_{fi}, was thus calculated as the difference between the original depth, d_{fo}, and the variation that occurred in the depth, Δd_f, as follows:

$$d_{fi} = d_{fo} - \Delta d_f \tag{5.2}$$

The variation in the tendon depth was measured and plotted against the applied loads in Figure 5.5 for the straight and draped beams. Approximately similar results were obtained for both beams. The change in the tendon depth was linearly proportional to the load applied on the beam until the internal reinforcement yielded. The rate of change increased sharply until the ultimate load was reached. At yield, the loss in tendon depth was about 5.5 mm for the straight tendons and 4.5 mm for the draped tendons (approximately 2.5% and 2% of the initial depth, respectively). At the ultimate load, the reduction in the tendon depth was about 9 mm and 7 mm for the straight and draped tendons, respectively (about 4% and 3% of the initial depth, respectively).

These results suggested that, at service load levels, the reduction in the tendon depth was insignificant for both straight and draped beams. The in-span deviators had a considerable effect in maintaining the tendon eccentricity constant during the service life of the beam up to the yielding of the internal reinforcement. With the presence of the deviators, the use of straight and double draped tendons led to a very similar structural performance. The measured deflection data suggested that the flexural behaviour of the strengthened beams can be accurately predicted if the change in the tendon eccentricity is neglected. Based on these results, the variation in the depth of the tendons was not considered in the analysis presented in Chapter 6.

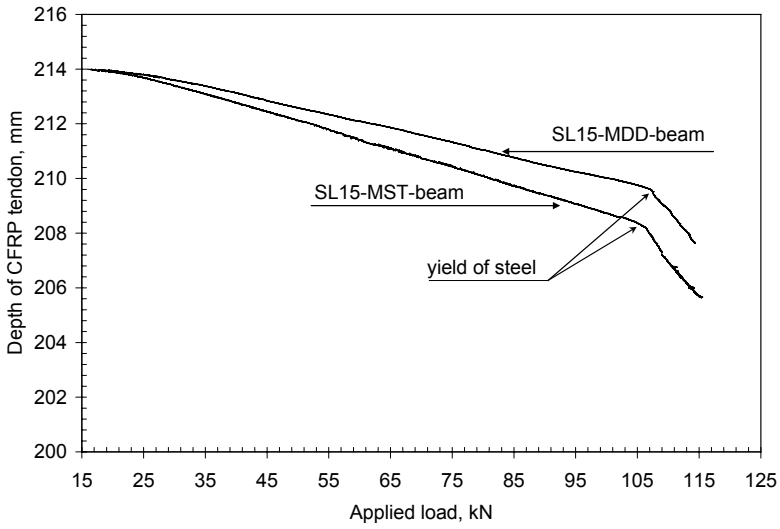

Figure 5.5: Variation in the depth of the CFRP tendon with applied loads for the in-service beams

5.2.2 Overloaded strengthened beam (OL15-M)

5.2.2.1 Deflection and stiffness response of the overloaded beam

Figure 5.6 shows the load-deflection curve of the over-loaded strengthened beam OL15-M. For the purpose of comparison, the load deflection curve of the in-service beam with draped profile (beam SL15-MDD) is also shown on the same plot. The beam OL15-M was first overloaded to a load of 61 kN with a deflection of 26.35 mm and a maximum steel strain of 4230 με. At this stage of loading, one flexural crack in the constant moment zone was noticeably wider and higher than the other cracks, as shown in Figure 5.7. It was assumed that this crack coincided with the location where the steel reinforcement had yielded locally (yield crack).

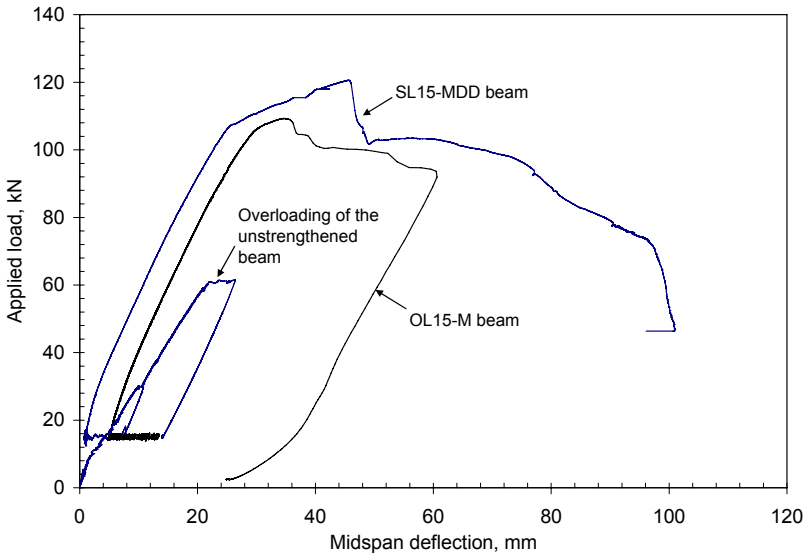

Figure 5.6: Load-deflection response of the overloaded (OL15-M) and in-service (SL15-MDD) strengthened beams

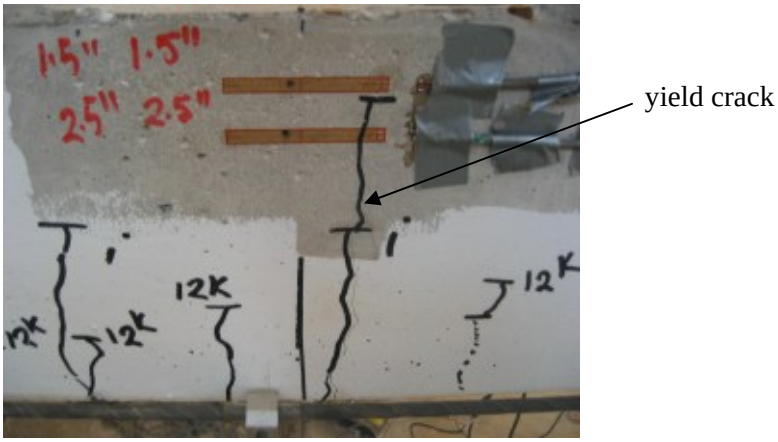

Figure 5.7: Yield crack in the overloaded beam compared to the adjacent cracks

After overloading, the beam was then unloaded to 15 kN, where the measured deflection was about 14 mm. The unloading stiffness of the beam was similar to the uncracked stiffness of the beam in the loading stage. When the beam was post-tensioned, approximately 9 mm of deflection was recovered, resulting in a net downward deflection of about 5 mm. The yield crack due to overloading appeared to be open at the end of the post-tensioning process. However, other flexural cracks in the constant moment region were completely closed.

Table 5.2 compares the midspan deflections of the in-service and overloaded post-tensioned beams at different stages of loading: at the end of the post-tensioning application, at 50% of the yielding capacity of the strengthened beam, and at the yield load. At any stage of loading, the midspan deflection of the overloaded beam was larger than the corresponding deflection of the in-service beam. This was attributed to the presence of permanent deformations in the beam due to the overloading and yielding of the reinforcement.

Table 5.2: Midspan deflections of the in-service and overloaded beams (in mm)

Stage of loading	SL15-MDD beam	OL15-M beam
at conclusion of post-tensioning	1.01	5.06
at 50% yield load	9.18	13.48
at yield load	26.84	32.19

The load deflection relationship of the overloaded beam was similar to that of the in-service beam. Due to the permanent deformations in the beam, the cracks started to re-open at a slightly lower load than that observed in the in-service beams. The three stages of the load-deflections were defined as follows:

- *End of post-tensioning (15 kN) up to cracking load (≈25 kN)* — in this stage, a major portion of the beam stiffness was restored due to post-tensioning until the cracks re-

opened at approximately 25 kN and 8 mm deflection. The yield crack was noticed wider than the adjacent cracks in the constant moment zone.

- *Between 25 kN and 108 kN* — this phase of loading represented most of the life of the strengthened beam. In this stage, the beam stiffness was similar to that of the in-service beam in its cracked stage, as indicated by the similar slopes of the load-deflection curves of both beams. At 108 kN, a kink in the load deflection curve was observed indicating the yield load of the beam. The deflection of the beam was about 32 mm at yield.
- *Yielding to concrete crushing (beyond 108 kN)* — this phase of loading extended between the yield load (108 kN) and the failure load of the beam. The overloaded beam encountered an ultimate deflection less than that of the in-service beam, as seen in Figure 5.6. Crushing of the concrete in compression started after the yield load was reached. At this point, the stiffness of the beam dropped significantly. The concrete completely crushed at 109 kN, followed by a rapid decrease in load to 92 kN, where the maximum deflection was 61 mm (compared to 95 mm in case of the in-service load).

The reduction in the ultimate strength and the corresponding maximum deflection as compared to the in-service beam can be explained as follows: due to overloading, tensile cracks were developed in the virgin beam rising up the neutral axis of the section. When the beam was post-tensioned, the force in the tendons was not sufficient to close all the cracks in the section due to the permanent deformation that had occurred. Due to the presence of the opened cracks, the neutral axis of the section was higher in the case of the overloaded beams than that in the in-service beam. The concrete compressive area needed to balance the tensile forces across the section was thus smaller. Therefore, at ultimate load, the compressed area was not enough to balance the increased tensile force in both internal and external reinforcement, and the concrete crushed abruptly.

5.2.2.2 Strain measurements of the overloaded beam

The responses of strains in the concrete and the steel of the overloaded beam, measured at midspan, were similar to its load-deflection response. Tensile steel strains and compressive concrete strains decreased significantly due to the post-tensioning operation. Figure 5.8 and Figure 5.9 compare the measured strains in steel and concrete, respectively, for the overloaded and in-service beams.

During reloading, the tensile steel strains increased until the concrete crushed. A similar trend was observed for the strain measurements at the top surface of the concrete. Due to overloading, the top concrete fibres encountered non-linear compressive strains before the beam was unloaded to 15 kN. Post-tensioning decreased the compressive strains in concrete, but no tensile strains were developed.

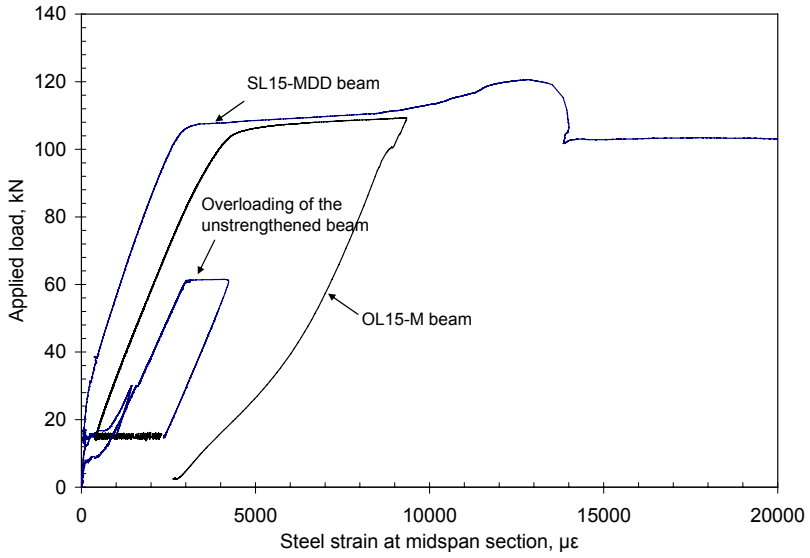

Figure 5.8: Applied load versus the measured steel strains at midspan of the overloaded and the in-service strengthened beams

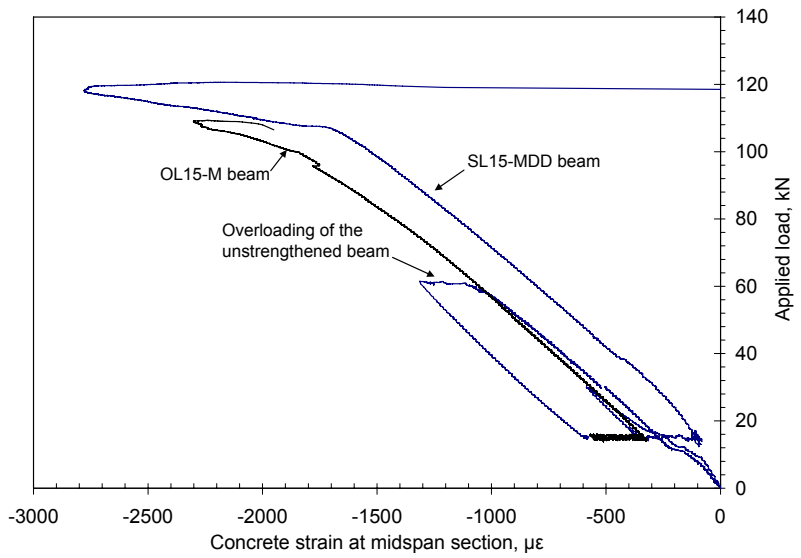

Figure 5.9: Applied load versus the measured concrete strains at midspan of the overloaded and the in-service strengthened beams

5.2.2.3 Changes in the tendon stress of the overloaded beam

Figure 5.10 shows the variation in the tendon stress with the loads applied on the overloaded beam. The in-service strengthened beam SL15-MDD is also included in the figure. For the overloaded beam, a curve similar to its load-deflection curve was noticed. The stress in the tendons increased steadily with the increase of the applied loads until yield occurred in the steel reinforcement.

Similar increase in both strengthened beams can be observed. This was attributed to the same initial post-tensioning system and similar forces applied to the tendons. An increase of approximately 20% of the initial stress applied in the tendons was encountered when yielding occurred, compared to 21% for the SL15-MDD beam (Table 5.1). As failure of the overloaded

beam occurred immediately after yielding, only a small further increase in the stress in the tendons was observed between yield and failure.

It is worth mentioning that the CFRP tendons in the overloaded beam did not show any degradation at the deviated points except for a minor wearing at the surface of the tendon due to friction occurring between the tendon and the Teflon sheets used. This shows that post-tensioning using CFRP tendons can restore the capacity and the deformation of a severely overloaded beam. Note that the post-tensioning force in the tendons had a significant effect in restoring the beam deformation when the tendons were stressed at 40% of their ultimate capacity. Increasing the post-tensioning force would increase the amount of the beam deformation restored. This was clear from the results obtained from both the in-service and the overloaded beams, where the gradual increase in the post-tensioning force during the strengthening application was always associated with a gradual reduction in the beams deflection.

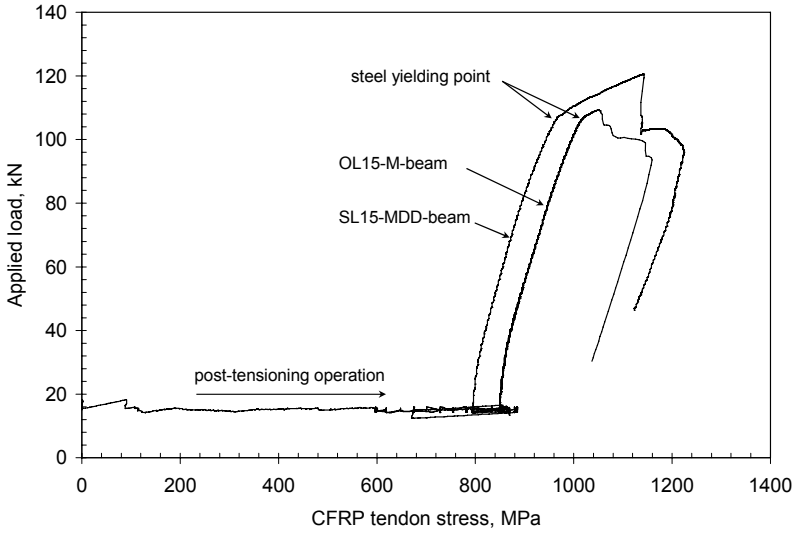

Figure 5.10: Variation of the tendon stress with the applied load for the overloaded (OL15-M) and the in-service (SL15-MDD) beams

5.2.2.4 Changes in the tendon depth of the overloaded beam

The change in the tendon depth in the overloaded beam was calculated using Equations 5.1 and 5.2. Figure 5.11 shows the variation in tendon depth with the applied load. The data for the in-service beam (SL15-MDD) is also shown for comparison purposes. The variation in tendon depth was similar for the two beams; the change in tendon depth was linearly proportional to the load applied to the beam until the internal reinforcement yielded. Similar to the results of the in-service beam (Section 5.2.1.4), the variation in the depth of the tendons of the overloaded beam was small and thus was not considered in the analysis presented in Chapter 6.

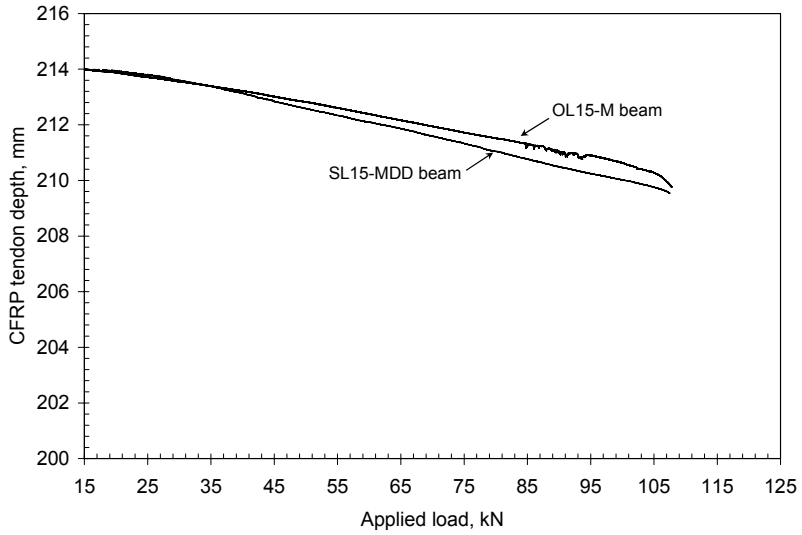

Figure 5.11: Variation of depth of the CFRP tendon with the applied load for the in-service (SL15-MDD) and the overloaded (OL15-M) beams

5.2.3 Modes of failure

Photographs of the unstrengthened and strengthened beams at failure are shown in Figure 5.12. As planned in the design, all beam specimens exhibited a pure flexural mode of failure. The control beam UN15-M failed in a typical mode of an under-reinforced concrete beam by concrete crushing after the steel reinforcement had yielded.

The in-service strengthened beams SL15-MST and SL15-MDD failed by concrete crushing after yielding of the internal reinforcement. The CFRP tendons exhibited high rotation capacity at failure by holding the beam in place after complete crushing of concrete.

The overloaded beam OL15-M also failed due to concrete crushing at the same location as the yield crack. This is shown in Figure 5.12-d where the yield crack extended to join the compressive crushed area. As in the case of the in-service beams, the CFRP tendons showed an excellent ability to maintain the beam in place after concrete crushing.

5.3 Fatigue test results

Twenty-four unstrengthened and strengthened beams were tested under fatigue loading. The beam specimens were categorized in four groups as described in Section 4.2 and summarized below:

Unstrengthened control beams (UN15-group) — five unstrengthened beams were tested under fatigue loading at different load ranges varying between 58% and 73% of the yield load of the beam (between 35 kN and 44 kN). The corresponding maximum loads, P_{max}, ranged between 83% and 98% of the yield load (between 50 kN and 59 kN). The minimum load, P_{min}, was maintained constant for all load ranges at 25% of the yield load of the beam (15 kN). This test group of beams

provided controls for the in-service (SL15-group) and the overloaded (OL15-group) strengthened beams when they were subjected to fatigue.

In-service strengthened beams (SL15-group) — eight specimens were reinforced with two 15M deformed bars and strengthened with two CFRP external tendons post-tensioned to 40% of their ultimate capacity (60 kN in each tendon). The beams had a partial prestressing ratio, *PPR*, of 0.46. The load ranges varied between 43% and 76% of the measured yield load of the strengthened beam (approximately 108 kN). The corresponding maximum peaks ranged between 56% and 90% of the yield load. The minimum load, P_{min}, was maintained constant for all load ranges at 25% of the yield load of the unstrengthened beam (15 kN).

In-service strengthened beams (SL20-group) — five beams having a partial prestressing ratio of 0.36, were tested under fatigue at load ranges varying from 47% to 72% of their estimated yield load (124 kN). The beams were reinforced with two 20M deformed bars and strengthened with two CFRP external tendons post-tensioned to 40% of their ultimate capacity (60 kN in each tendon). The minimum peak load of the fatigue loading was 21 kN, representing 25% of the yield load of the unstrengthened beam.

Overloaded strengthened beams (OL15-group) — six beams reinforced with two 15M deformed bars and strengthened with two external CFRP tendons were tested under fatigue loading. These beams were overloaded before being strengthened. Overloading was defined by subjecting the steel to strain values of 1.5 to 2 times the yield strain (approximately 4000 microstrain). The beams were then unloaded and post-tensioned with external CFRP tendons stressed at 40% of their ultimate capacity (60 kN in each tendon). Cyclic load ranges varying between 39% and 68% of the measured yield load of the strengthened beam were used. The corresponding maximum load peaks ranged between 53% and 81% of the yield load. The minimum load, P_{min}, was maintained constant for all load ranges at 25% of the yield load of the unstrengthened beam (15 kN).

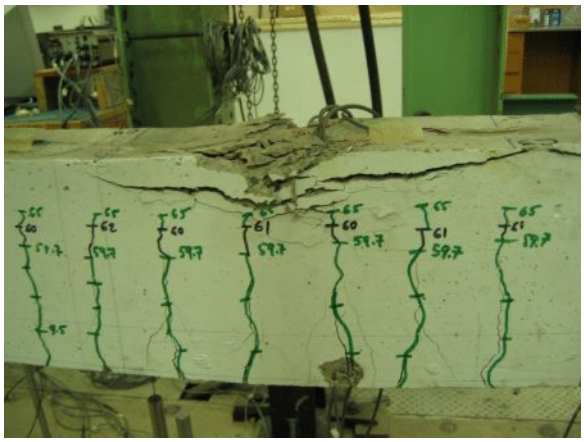

(a) The UN15-M beam

(b) The SL15-MST beam

(c) The SL15-MDD beam

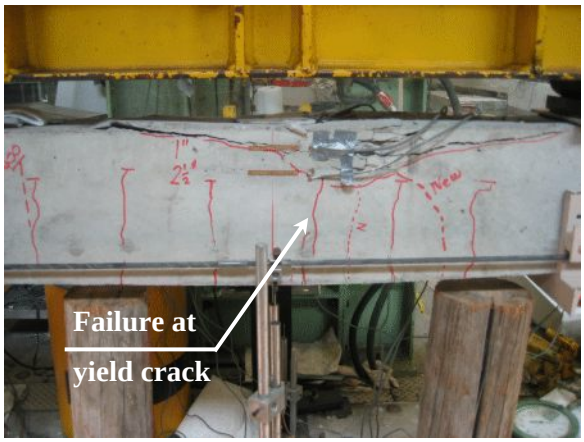

(d) The OL15-M beam

Figure 5.12: Unstrengthened and strengthened beams at failure

5.3.1 Cyclic deflection response

Figure 5.13 shows a typical cyclic load-midspan deflection plot of the unstrengthened (UN15 group), in-service strengthened (SL15 and SL20 groups), and overloaded strengthened (OL15 group) beam specimens at different load cycles throughout their fatigue-loading tests. Load-deflection curves for other beams are given in Appendix B. As seen in Figure 5.13, the unstrengthened and in-service strengthened beams were initially pre-cracked while loading to 50% of the yield load of the unstrengthened beams before being unloaded to 25% of the yield load. The in-service strengthened beams were then post-tensioned. The beams were then loaded gradually to their maximum peak load before being cycled within the assigned cyclic load ranges. The overloaded beams were subjected to a gradual increase of load until the steel yielded at a load of 61 kN. This load was maintained until the desired strain overload was reached. The beams were then unloaded to 25% of their yield capacity before being post-tensioned, followed by application of the cyclic load history.

The load-deflection response of all of the strengthened beams prior to post-tensioning was identical to the monotonic behaviour of the control beams in terms of crack patterns, deflection, and induced stresses in both concrete and steel bars. Note that the SL-20 group did not have a beam tested under monotonic load to failure. The response of the in-service and overloaded strengthened beams during post-tensioning and during the loading cycle to their maximum peak load replicated the monotonic response of their control beams tested under monotonic loading to failure (SL15-MDD and OL15-M), as described in Sections 5.2.1 and 5.2.2 for the in-service and overloaded groups, respectively.

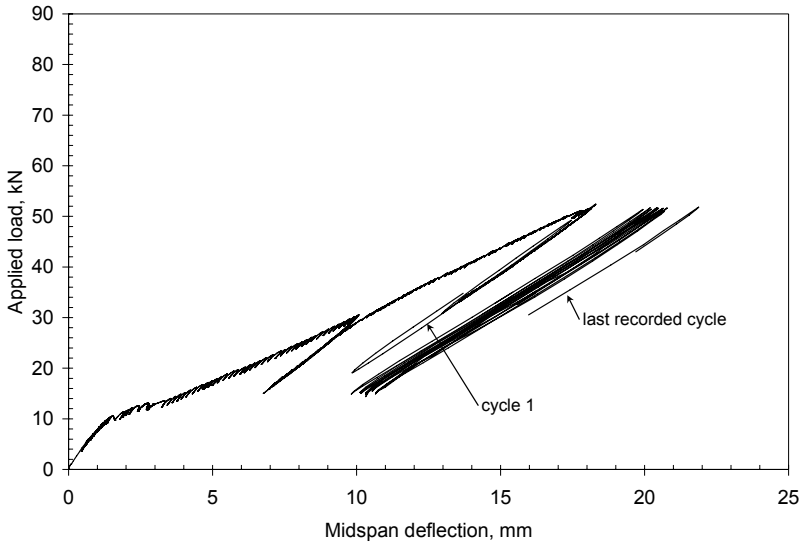

(a)

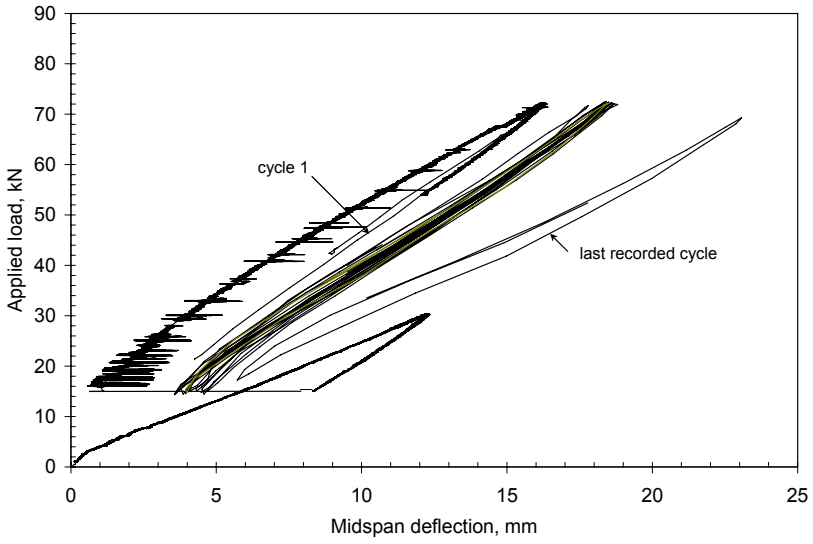

(b)

Figure 5.13: Cyclic load-deflection behaviour for the(a) UN15-F52 beam, (b) SL15-F72 beam, (c) SL20-F87 beam, and (d) OL15-F82 beam

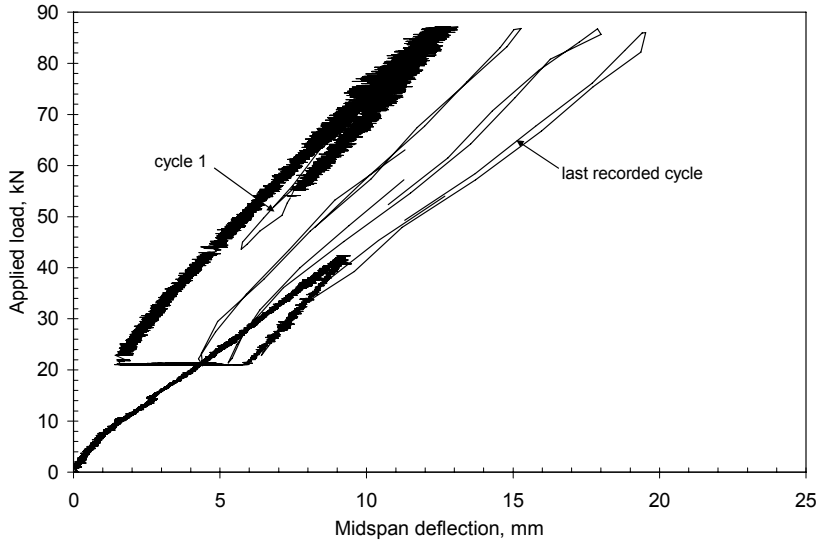

(c)

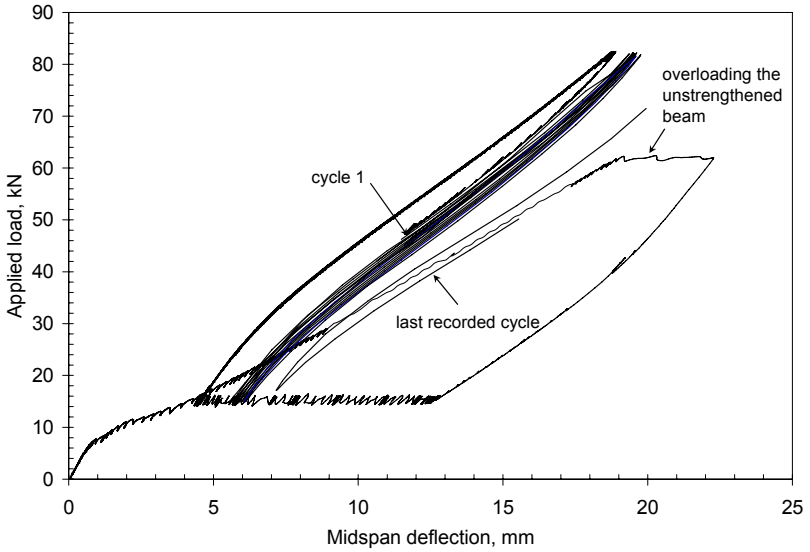

(d)

Figure 5-13 (cont): Cyclic load-deflection behaviour for the (a) UN15-F52 beam, (b) SL15-F72 beam, (c) SL20-F87 beam, and (d) OL15-F82 beam

The data in Figure 5.13 consistently show an increase in the midspan deflection for all of the beams as the number of cycles increased. Table 5.3 gives the midspan deflections for all tested specimens at the maximum peak loads at three stages of the life: at the onset of the cyclic loading, after surviving 50% of the life, and at the end (or close to end) of the fatigue life. Anomalous LVDT readings were omitted from the table, as in the case of the beams UN15-F57 and SL15-F68. Note that the results of the SL15-F61 and OL15-F57 beams are not reported as each of these two beams had an infinite fatigue life (see Section 5.3.5.1). Also, the results of the beam UN15-F59 were omitted because the concrete crushed after a small number of cycles (see Section 5.3.5.1). Figure 5.14 shows the changes of the midspan deflections of all the unstrengthened and strengthened beams with an increasing number of cycles during the beam life.

Under repeated loading, all beams demonstrated an increase in their midspan deflections in the early stages of their life (approximately during the first 10% of the life of the beam). The increase in deflections in the early stages of life was associated with the development of a few cracks between the initial cracks that had initiated during the monotonic loading, and a small expansion of the initial cracks. The cracks then stabilized and the deflection of the beam remained relatively constant with an increasing number of cycles until approximately 90% of the life of the beam was attained. The rate of deflection increased sharply during the last 10% of the beam life until failure occurred. The last stages of the life of all beams were characterized by the development of new cracks in the maximum moment and shear zones and the widening of the existing cracks.

The increase in the maximum midspan deflections of the overloaded beams was less than the other beams (Figure 5.14-d) during the early stages of their life (approximately 10% of the life of the beam). Due to overloading, permanent deformation occurred in the overloaded beam and large cracks were developed at the location where the internal reinforcement had yielded (yield cracks). When post-tensioning was applied, the permanent deformation was not completely restored and the yield cracks were not entirely closed. As the beam was cycled between the peak

loads, P_{min} and P_{max}, no further increase in the crack width and depth beyond the yield crack had occurred. This was in contrast to the SL-beam group where a noticeable increase in crack width and depth occurred during the first 10% of the beam life. This explains the reduced variation in the midspan deflections over the fatigue life of the overloaded beams. This is illustrated in Figure 5.15 where a schematic view of the crack height for the in-service and the overloaded beams is shown.

Table 5.3: Variation of beam midspan deflections over beam life

Specimen	Peak loads (kN)		Maximum deflection (mm)		
	Min	Max	Onset of cycling	Midlife	End or close to end of life
UN15-beams					
UN-F50	15	50	15.1	16.7	20.8
UN-F52	15	51.5	18.7	20.5	21.8
UN-F53	15	53	14.7	16.7	19.8
SL15-beams					
SL15-F66	15	66	11.6	12.6	12.9
SL15-F72	15	72	16.1	18.3	23.1
SL15-F82	15	82	15.9	19.0	19.7
SL15-F88*	15	88	11.8	12.9	15.0
SL15-F92	15	92	19.1	20.3	21.1
SL15-F97	15	97	18.2	21.3	22.5
SL20-beams					
SL20-F83	21	83	10.9	11.0	16.8
SL20-F87	21	87	12.7	15.3	19.5
SL20-F100	21	100	16.0	17.8	19.2
SL20-F110	21	110	18.5	20.5	21.7
OL15-beams					
OL15-F67	15	67	11.9	12.2	14.3
OL15-F72	15	72	17.1	18.4	23.5
OL15-F76	15	76	17.5	18.7	22.2
OL15-F82	15	82	19.2	19.5	19.8
OL15-F88	15	88	18.8	19.7	N.A.

** The beam was post-tensioned under zero-load maintained*

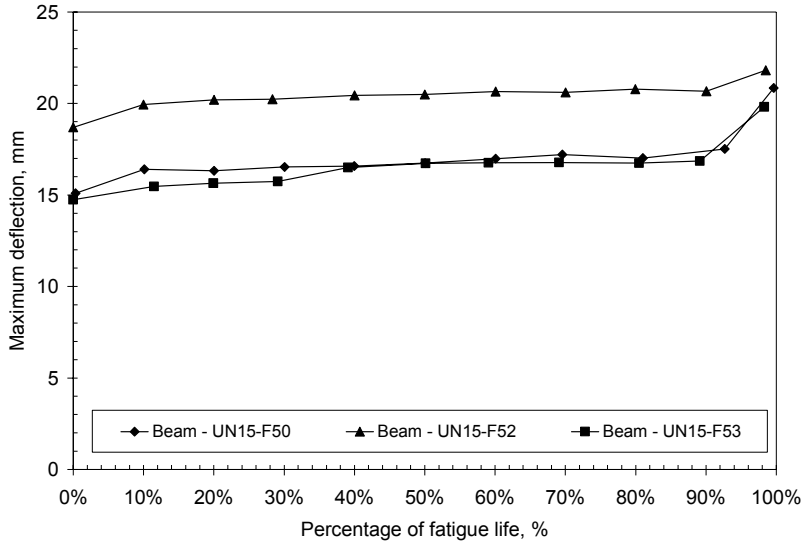

(a)

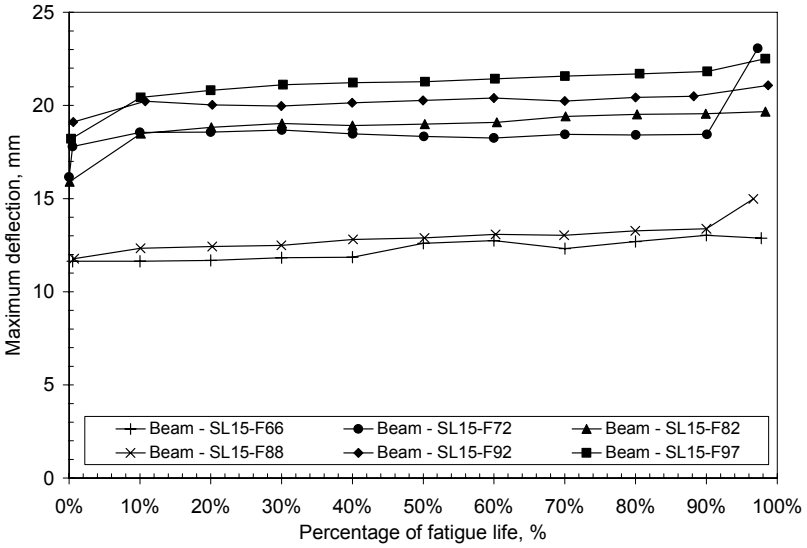

(b)

Figure 5.14: Variation of midspan deflection over the beam fatigue life for (a) UN15 beams , (b) SL15 beams, (c) SL20 beams, and (d) OL15 beams

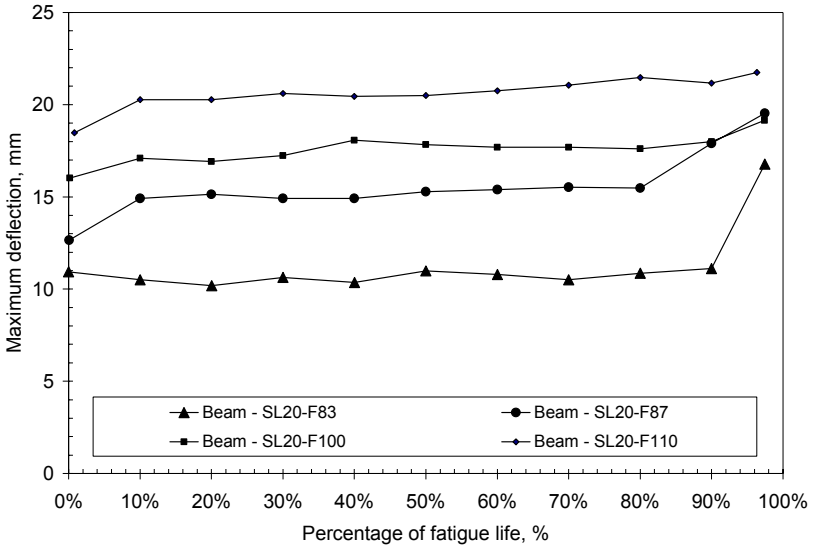

(c)

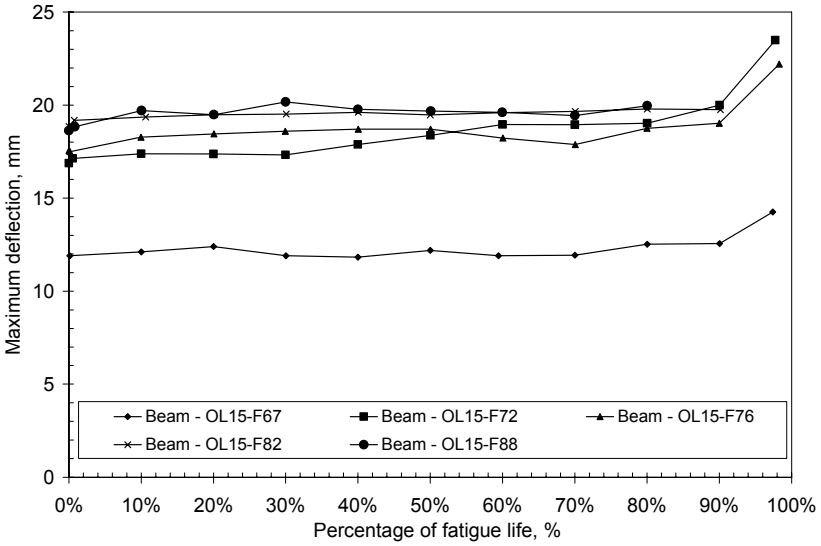

(d)

Figure 5.14 (cont.): Variation of midspan deflection over the beam fatigue life for (a) UN15 beams, b) SL15 beams, (c) SL20 beams, and (d) OL15 beams

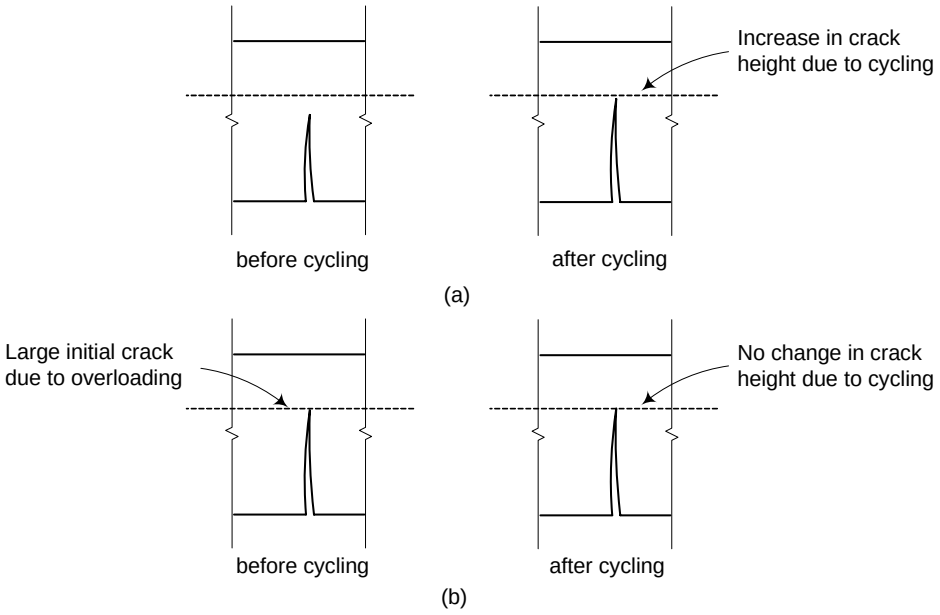

Figure 5.15: Schematic view of the crack height in the (a) in-service and (b) overloaded beams

A regression analysis was used to estimate the rate of increase in midspan deflection during the stabilization stage (approximately between 10% and 90% of the fatigue life, i.e., during 80% of the total life of the beam). The results are shown in Figure 5.16 for each set of beams, including the regression equation between the midspan deflection (referred to by the letter *D*) and the percentage of the fatigue life of the beam (referred to by the letter *L*).

The results showed that all beams exhibited a linear increase in their midspan deflections with an increasing number of cycles. The unstrengthened beams encountered a rate of increase in their midspan deflections of approximately 0.017 mm per 1% of the total number of cycles survived, representing an average increase in deflection of 1.38 mm during the stabilization period. The rate of increase in deflection was slightly reduced for the in-service strengthened beams (groups SL15 and SL20) to a value of 0.012 mm per 1% of the total number of cycles survived (an average increase of 1.00 mm during the stabilization period). The rate of increase of the midspan deflection further decreased in the case of the OL15-group of beams to 0.005 mm per 1% of the

total number of cycles, representing an average increase of 0.45 mm during the stabilization period of the cracks. This can be attributed to the presence of the pre-existing open cracks during the life of the overloaded beams, as explained previously.

5.3.2 Cyclic strain response

In the following subsections, the concrete and steel responses during the life of the unstrengthened and strengthened beams are presented.

5.3.2.1 Concrete strain response

The concrete strains in the compression zone exhibited a gradual increase in both the unstrengthened and strengthened beams due to fatigue loading. Values of the measured maximum concrete strains at midspan are given in Table 5.4 at three stages of the beam life: at the onset of fatigue cycling, after surviving 50% of the life, and at the end (or close to end) of the beam life. The increase in the recorded concrete strains at the maximum peak loads was accompanied by a similar increase in the strains at the minimum loads. Figure 5.17 shows the change in the range of the measured concrete strains with increasing number of cycles. The range of strains was determined as the difference between the maximum and the minimum strain readings at the peak loads applied to the beam under consideration. No significant changes in the strain ranges were encountered by any of the beams as indicated by the flat responses shown in Figure 5.17. This indicates that the similar increase in the strain readings at the maximum and minimum peak loads was a result of the cyclic creep of concrete. This will be discussed later in Section 5.3.4.

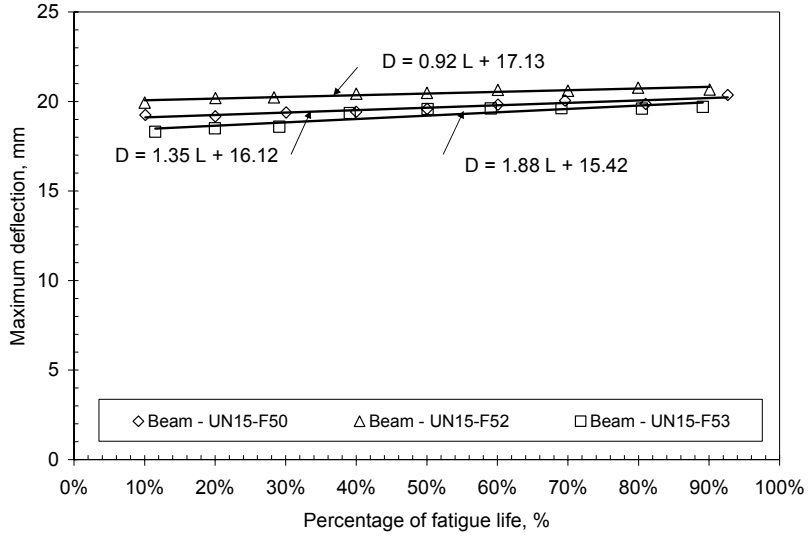

(a)

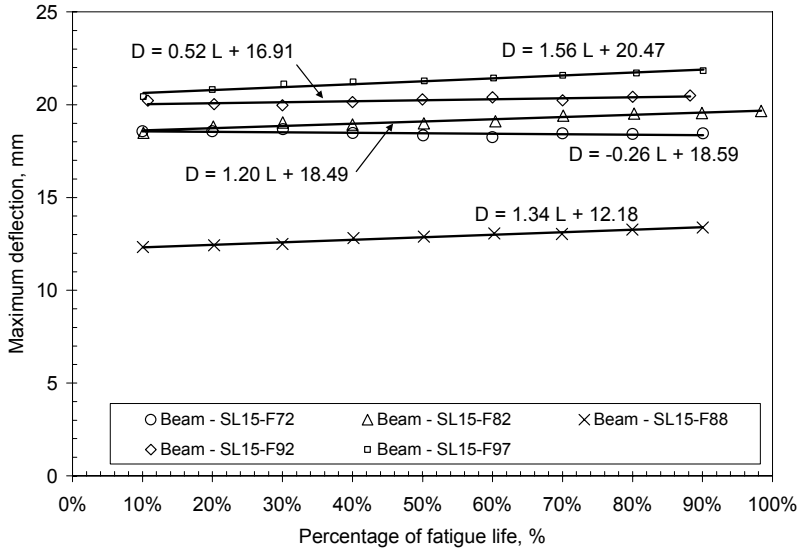

(b)

Figure 5.16: Regression analysis of midspan deflection under fatigue loading for (a) UN15 beams, (b) SL15 beams, (c) SL20 beams, and (d) OL15 beams

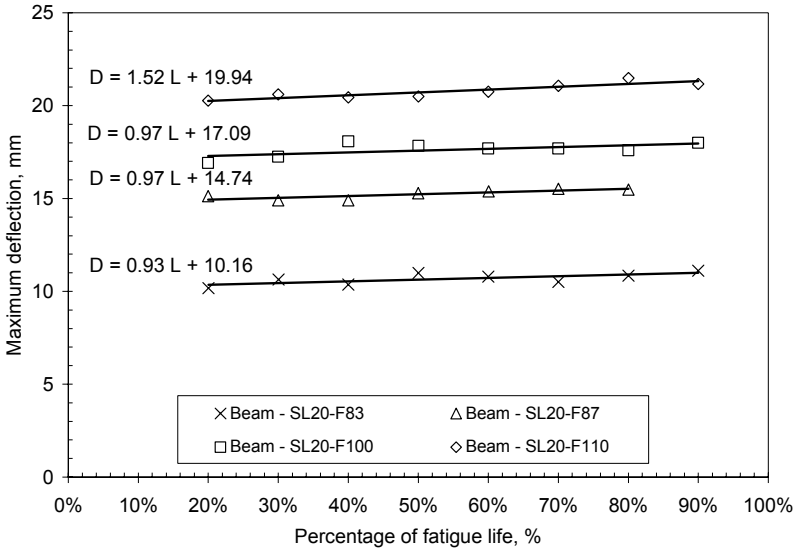

(c)

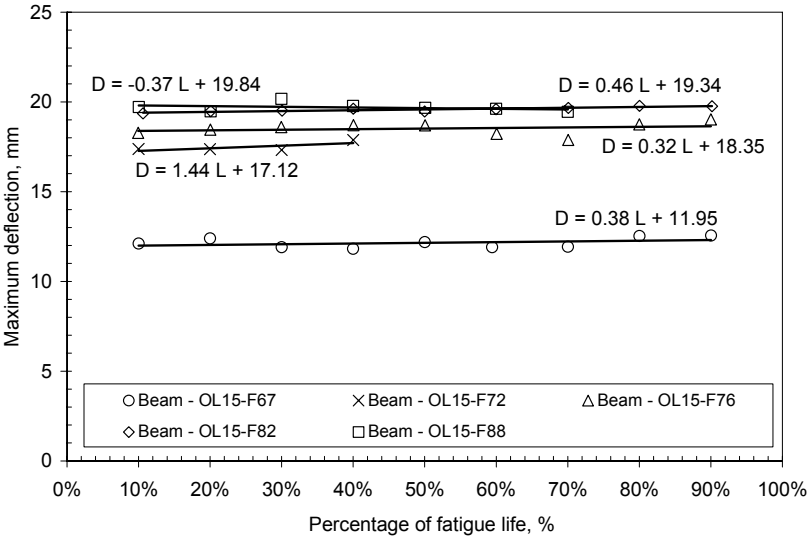

(d)

Figure 5.16 (cont.): Regression analysis of midspan deflection under fatigue loading for (a) UN15 beams , (b) SL15 beams, (c) SL20 beams, and (d) OL15 beams

5.3.2.2 Steel strain response

Steel strains were measured at the midspan of the two steel reinforcing bars (strain gages S_{m1} and S_{m2}) and at a distance of 400 mm from the midspan (strain gage S_{400}) for one of the reinforcing bars (refer to Figure 4.20). Discrepancies in the measured steel strain values were encountered, especially in the case of the overloaded beams. The strain readings were significantly affected by their location with respect to the flexural cracks. In some cases, compressive strains were developed in the steel bars at the end of the post-tensioning application, while in other cases the strains were tensile.

The magnitude of steel strains reached at the end of post-tensioning process for the overloaded beams depended on the amount of overloading applied (i.e., the strain reached at the end of overloading). This is explained by comparing the load-strain curve of the beam OL15-F82 loaded to 5750 με, as shown in Figure 5.18, and that of the beam OL15-F76 loaded to approximately 3000 με, as shown in Figure 5.19. In the former beam, the reinforcing bar had a tensile strain of approximately 1670 με after the full post-tensioning force was applied, while for the later beam, the post-tensioning force produced a compression strain of about -150 με on the bar. It is worth mentioning that the amount of steel strain recovered by post-tensioning was 1500 με, on average, for all of the overloaded beams.

In some overloaded beams, yielding of the steel occurred at a section beyond the midspan section in the constant moment region. In these cases, the readings of the strain gages nearest to the yield crack were considered. Some strain gages were damaged by flexural cracks. These readings were easily identified and were disregarded in the analysis of the test data.

Values of the maximum measured steel strains are given in Table 5.4 at three stages of the beam life: at the onset of fatigue cycling, after surviving 50% of the life, and at the end (or close

to end) of the beam life. The listed values correspond to the steel reinforcing bar that had broken at the end of the life of the beam (see Section 5.3.5.1).

Table 5.4: Variation of maximum concrete and steel strains at midspan over beam life

Specimen	Peak loads (kN)		Max. measured concrete strain (με)			Max. measured steel strain (με)		
	Min	Max	Onset of cycling	Midlife	End or close to end of life	Onset of cycling	Midlife	End or close to end of life
UN15-beams								
UN15-F50	15	50	-1056.6	-1215.1	-1604.2	1819.7	1866.4	3308.0
UN15-F52	15	51.5	-1226.0	-1195.9	-1229.2	2277.9	2277.9	2333.3
UN15-F53	15	53	-1495.1	-2052.1	-2148.8	2121.5	2294.6	2328.1
UN15-F57	15	57	-1301.2	-1634.4	-1757.5	2619.7	2905.0	2963.5
UN15-F59	15	59	-1699.4	-2395.7	-2566.2	N.A.	N.A.	N.A.
SL15-beams								
SL15-F66	15	66	-1194.0	-1251.5	-1590.2	1225.6	1268.1	1502.2
SL15-F68	15	68	-1377.2	-1365.8	-1934.9	1360.1	1494.9	N.A.
SL15-F72	15	72	-1606.0	-1666.6	-2862.7	1685.8	1689.3	24175.5
SL15-F82	15	82	-1655.0	-1980.0	-2069.3	1982.5	2110.5	1969.2
SL15-F88*	15	88	-1217.3	-1208.4	-1229.3	887.5	1046.2	1019.6
SL15-F92	15	92	-1815.3	-2262.6	N.A.	2252.4	2368.8	N.A.
SL15-F97	15	97	-1759.1	-2085.0	-2196.3	2050.1	2228.3	2197.9
SL20-beams								
SL20-F83	21	83	-1052.2	-1139.0	-1611.7	1158.4	1239.5	21643.6
SL20-F87	21	87	-1003.7	-1130.3	-1151.9	1396.6	1375.7	1481.5
SL20-F100	21	100	-1248.6	-1343.3	-1442.5	1753.0	1806.4	1692.1
SL20-F110	21	110	-1424.6	-1593.8	-1647.0	1931.2	1914.9	2327.9
OL15-beams								
OL15-F67	15	67	-1559.3	-1659.1	-1644.8	1159.5	1115.7	1030.5
OL15-F72	15	72	-1580.0	-1788.7	-1795.5	1706.1	1824.3	1876.1
OL15-F76	15	76	-1269.9	-1387.9	-1391.3	2202.0	2243.3	2143.7
OL15-F82	15	82	-1868.8	-2008.7	-2046.9	4116.6	4031.5	4077.2
OL15-F88	15	88	-1620.6	-1861.0	-1982.0	2156.8	2130.2	2169.8

** The beam was post-tensioned under zero-load maintained*

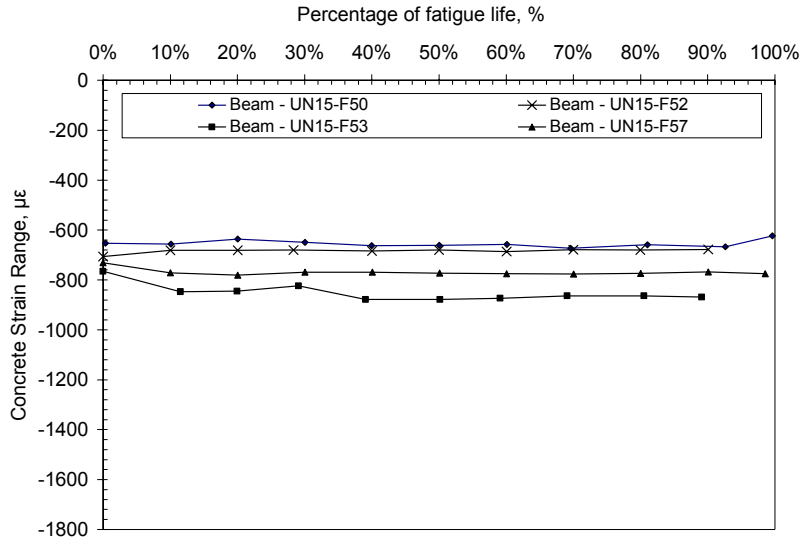

(a)

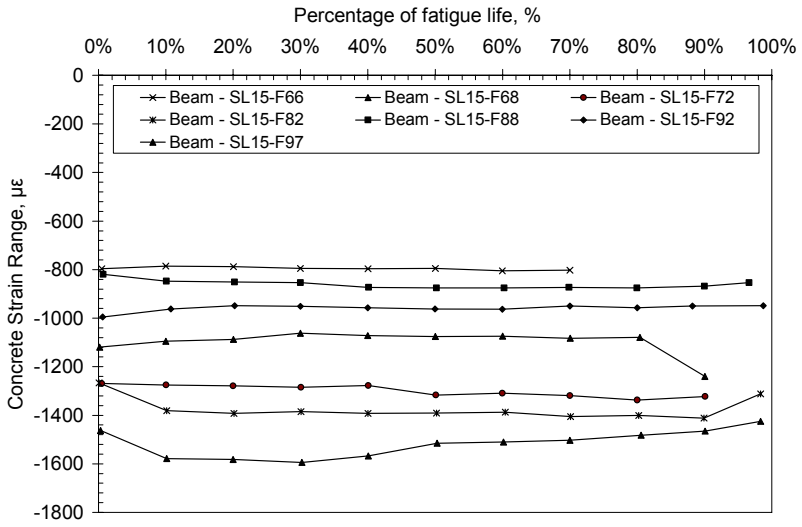

(b)

Figure 5.17: Variation in the concrete strain ranges over the beam fatigue life for (a) UN15 beams, (b) SL15 beams, (c) SL20 beams, and (d) OL15 beams

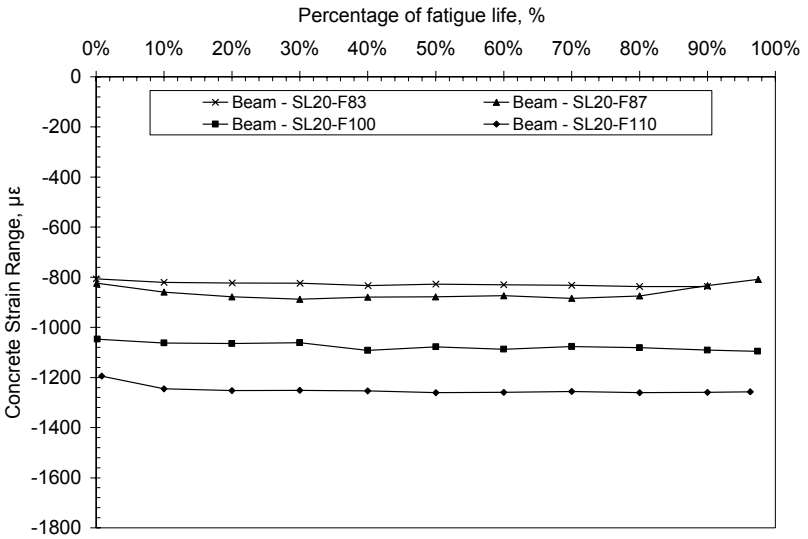

(c)

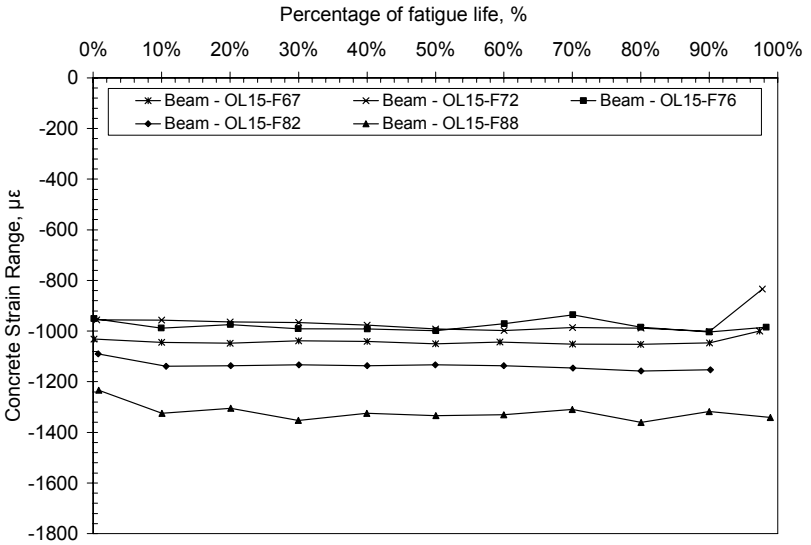

(d)

Figure 5.17 (cont.): Variation in the concrete strain ranges over the beam fatigue life for (a) UN15 beams, (b) SL15 beams, (c) SL20 beams, and (d) OL15 beams

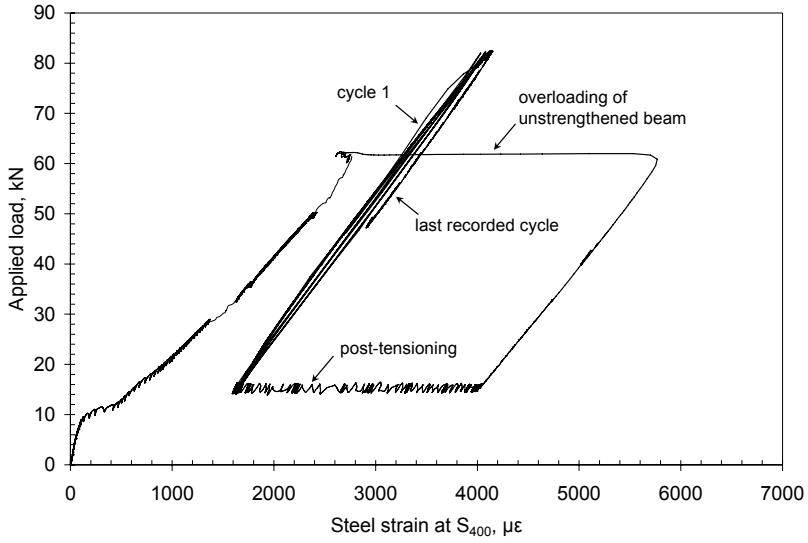

Figure 5.18: Load versus strain at S_{400} for the OL15-F82 beam

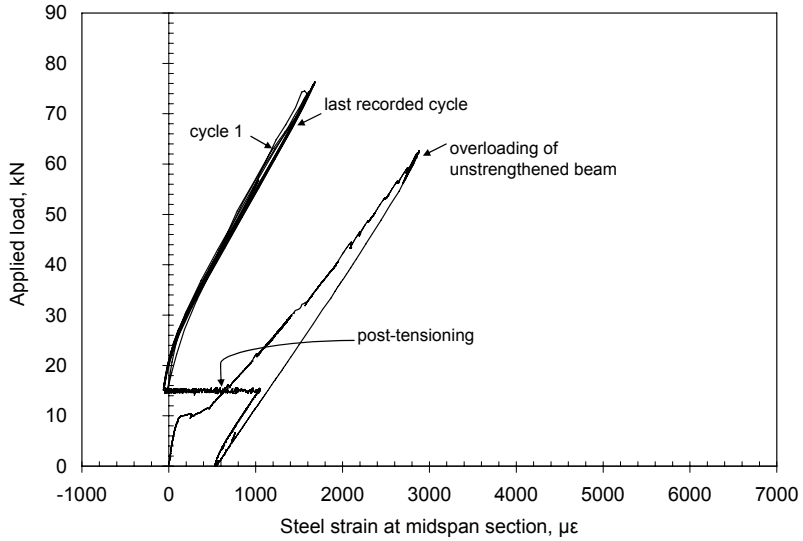

Figure 5.19: Load versus steel strain for the OL15-F76 beam

For most of the beams tested, the steel strains increased at the beginning of the fatigue life (approximately during the first 10% of the fatigue life) and then stabilized. This phenomenon was consistent with the deflection response of the beams under fatigue loading, as previously described. This was more pronounced in the unstrengthened and the in-service strengthened beams than in the overloaded beams. In an overloaded beam, fewer new cracks were developed during this early stage of the life than in the case of an in-service strengthened beam.

Figure 5.20-b shows the change in the range of the measured steel strains with an increasing number of cycles. The range of strains was determined as the difference between the maximum and the minimum strain readings at the peak loads applied to the beam under consideration. In general, the changes in the strain ranges over the life of the beams were not significant as indicated by the overall flat response shown in Figure 5.20.

5.3.3 Changes in the CFRP tendon stresses

The variation of the CFRP tendon stresses under fatigue loading was similar to the deflection and strain responses of the strengthened beams. Figure 5.21 shows the observed relationship between the tendon stress, as a percentage of the tendon capacity, and the number of cycles for all strengthened beams at maximum loads. The stress in the tendons was calculated based on the tendon forces measured by the load cells attached to the ends of the tendons. Only the readings obtained from one load cell are reported. Values of the measured CFRP stress are given in Table 5.5 at three stages of the beam life: at the onset of fatigue cycling, after surviving 50% of the life and at the end (or close to end) of the beam life.

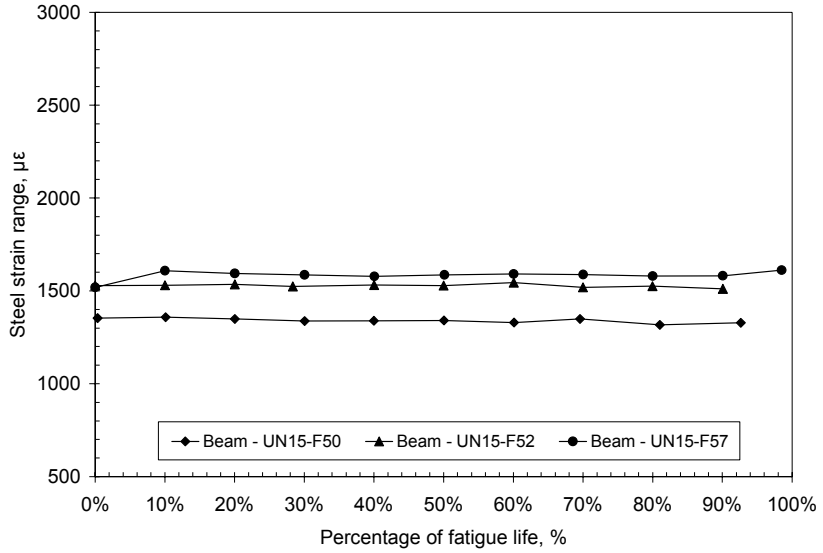

(a)

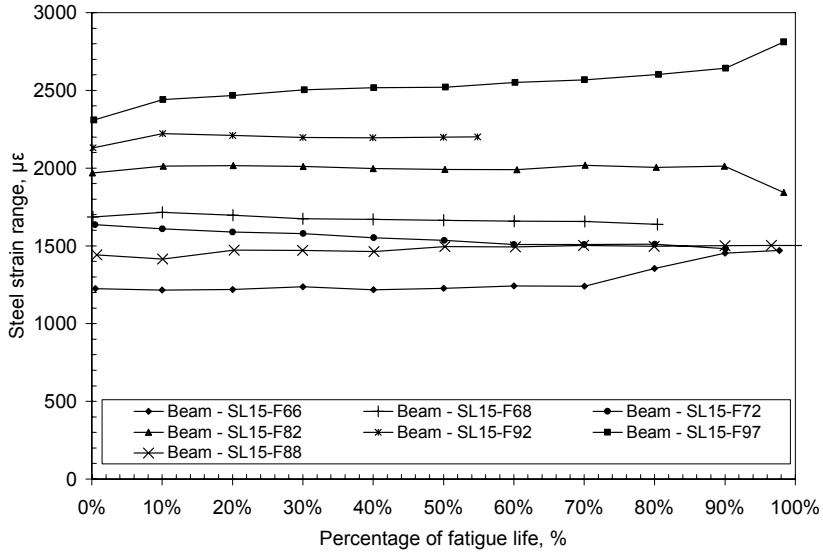

(b)

Figure 5.20: Variation in the steel strain ranges over the beam fatigue life for (a) UN15 beams, (b) SL15 beams, (c) SL20 beams, and (d) OL15 beams

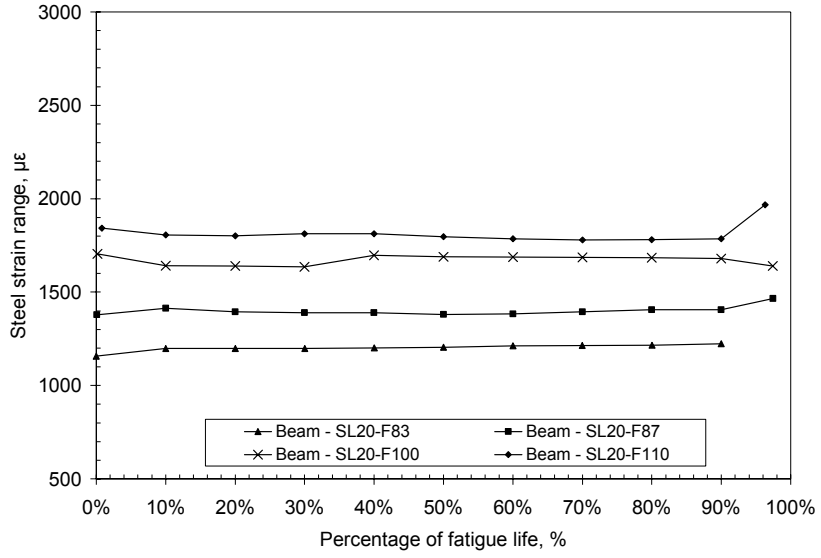

(c)

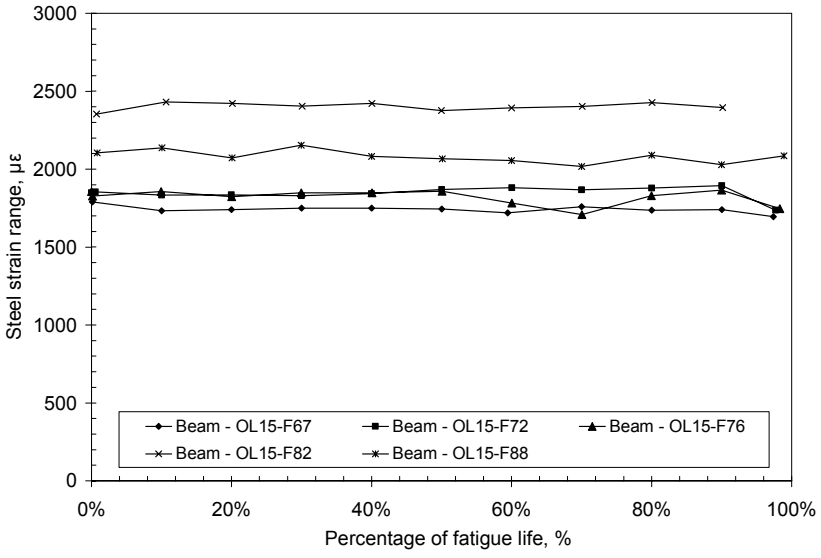

(d)

Figure 5.20 (cont.): Variation in the steel strain ranges over the fatigue life for (a) UN15 beams, (b) SL15 beams, (c) SL20 beams, and (d) OL15 beams

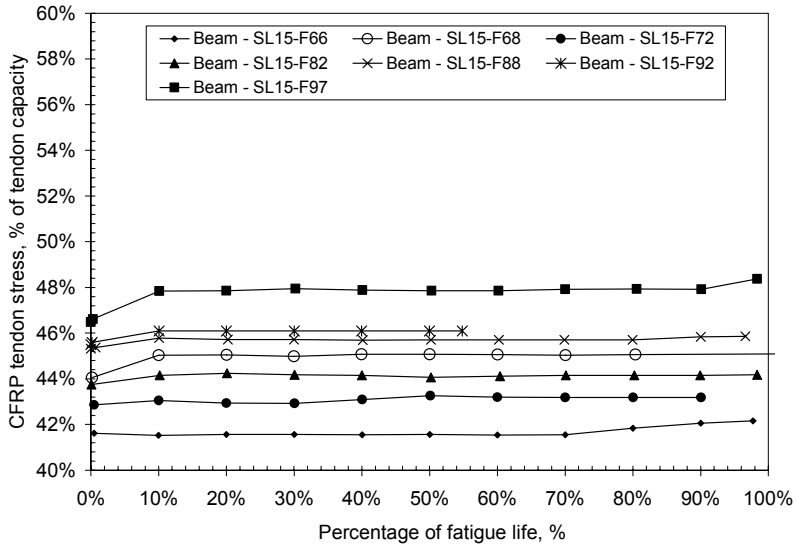

(a)

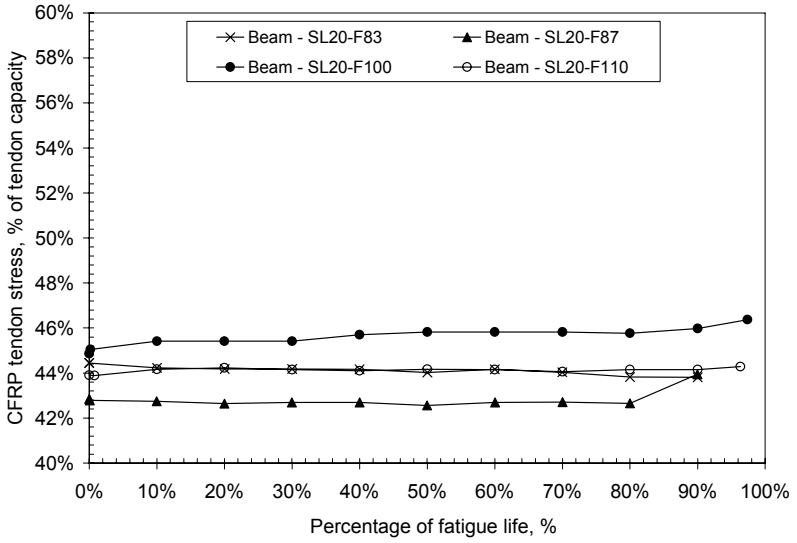

(b)

Figure 5.21: CFRP tendon stress variation over the beam fatigue life at P_{max} for (a) SL15 beams, (b) SL20 beams, and (c) OL15 beams

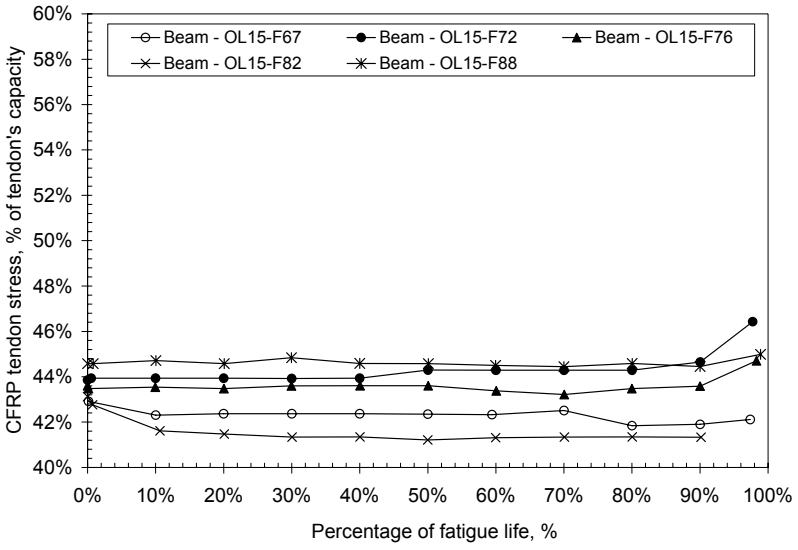

(c)

Figure 5.21 (cont.): CFRP tendon stress variation over the beam fatigue life at P_{max} for (a) SL15 beams, (b) SL20 beams, and (c) OL15 beams

The increase in the maximum tendon stress due to fatigue loading was small and varied between 0.38% and 1.37% of its ultimate strength when the beams reached 50% of their life. Most of the increase in the tendon stress occurred during the early part of the life of the beam. The tendon stress range (between the minimum and maximum loads) was almost constant during the life of the beam until failure. This indicated that no softening occurred in the tendon material due to the repeated loading. It also implied a perfect anchoring of the CFRP tendon, as no slippage was encountered.

There was no indication of distress or deficiency in any of the CFRP external tendons. As a result, the tendons were reused during the fatigue tests of the beams. The load cell readings between the jack and dead ends indicated little or no prestress loss along the tendon length. The

deviated points of the tendon at the saddle locations did not show any evidence of wear or stress concentration that would lead to the fracture of the CFRP tendons.

Table 5.5: Variation of CFRP stresses over the beam fatigue life

Specimen	Peak loads (kN)		Max. stress in CFRP tendons (MPa)		
	Min	Max	Cycle 1	Mid life	End of life
SL15-beams					
SL15-F66	15	66	894	898	911
SL15-F68	15	68	955	974	1030
SL15-F72	15	72	913	935	975
SL15-F82	15	82	940	953	955
SL15-F88	15	88	980	988	991
SL15-F92	15	92	984	996	N.A.
SL15-F97	15	97	1005	1034	1046
SL20-beams					
SL20-F83	21	83	961	952	1018
SL20-F87	21	87	926	920	967
SL20-F100	21	100	970	990	1002
SL20-F110	21	110	950	955	957
OL15-beams					
OL15-F67	15	67	915	915	910
OL15-F72	15	72	948	957	1004
OL15-F76	15	76	943	943	966
OL15-F82	15	82	932	891	893
OL15-F88	15	88	963	963	972

5.3.4 Cyclic strain investigation

As mentioned previously in Section 5.3.2, the measured strains in both the steel and the concrete increased with an increasing number of cycles. At the same time, flexural concrete cracks tended to increase in height and number in the first stages of the fatigue life of the beam before they stabilized. In order to interpret the behaviour of steel and concrete during the cyclic loading of the beam, it was necessary to investigate their behaviour under cyclic loading separately. Therefore, cyclic simulation tests were conducted on steel and concrete specimens, as will be illustrated in the following subsections.

5.3.4.1 Cyclic simulation tests for steel

Cyclic tests were conducted on smooth steel specimens machined from the same reinforcing bars used in the reinforced concrete beams in this study. These tests aimed to interpret the steel strain response encountered during the beam tests, and to quantify the potential amount of creep of the steel material.

Twelve standard fatigue tests specimens were machined from the No. 15 reinforcing bar, as shown in Figure 5.22. The specimens were tested in a MTS, servo-controlled fatigue testing system (Figure 5.23). The strain response of the specimens at different loading stages was recorded using an axial extensometer mounted on the specimen at a gage length of 7.6 mm.

In order to simulate the stress history applied on the steel reinforcing bar in the beam, the machined specimens were subjected to similar loading and unloading scenarios, as explained in section 4.2.2 and 4.2.4 for the in-service (SL15) and the overloaded beams (OL15), respectively. At each stage of loading, the stress applied to the specimens was determined using a monotonic analysis that will be described later in Chapter 6.

Three stress ranges were selected to simulate the fatigue response of the steel embedded in each group of beams. For instance, the beams SL15-F66, SL15-F82, and SL15-F97 were simulated to represent the low, medium, and high stress ranges applied, respectively, within the in-service SL15 group. For the overloaded beams, it was decided to simulate only the beam OL15-F88 as it represented the beam with the highest applied load in the overloaded group of beams.

Figure 5.24 and Figure 5.25 show the variation in the *maximum* steel strain and the *range* of steel strain responses in the early stages of life of the machined specimens, respectively, on a logarithmic scale. As seen from Figure 5.25, the range of the measured steel strains remained unchanged during the applied cyclic stress. This was indicated by the flat response of the recorded data with an increasing number of cycles. These results agreed with the steel strain response when the bars were embedded in the concrete beams, as illustrated previously in Section 5.3.2.2 and shown in Figure 5.20-b. The cyclic simulation test data and the steel strain data from the beam tests, both suggested that steel did not exhibit cyclic creep during its fatigue life. These results were considered in the development of the fatigue model explained later in Chapter 7.

Figure 5.22: (a) Deformed rebar and (b) standard machined fatigue specimen

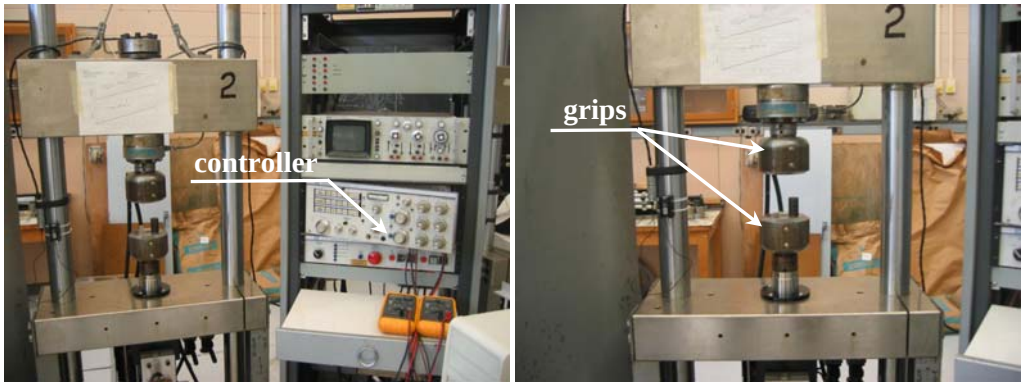

Figure 5.23: Fatigue testing machine for steel specimens

5.3.4.2 Cyclic simulation tests for concrete

A series of uniaxial cyclic compression tests were carried out on standard concrete cylinders 100x254 mm (4x10 in.). The cylinders were cast at the same time as the concrete beams, and had attained the 28-day compressive strength before testing. The cyclic tests were aimed at investigating the response of concrete under fatigue loading when subjected to different ranges of compressive stresses.

Three maximum stress levels representing 41%, 46%, and 53% of the compressive strength of concrete were used. The minimum stress levels were kept constant in all tests at approximately 2% of the concrete compressive strength. Two strain gages were placed vertically on each cylinder in order to measure the strain values induced. All tests were conducted under load control. The applied loads and the corresponding gage readings were recorded automatically at regular intervals of time using a data acquisition system.

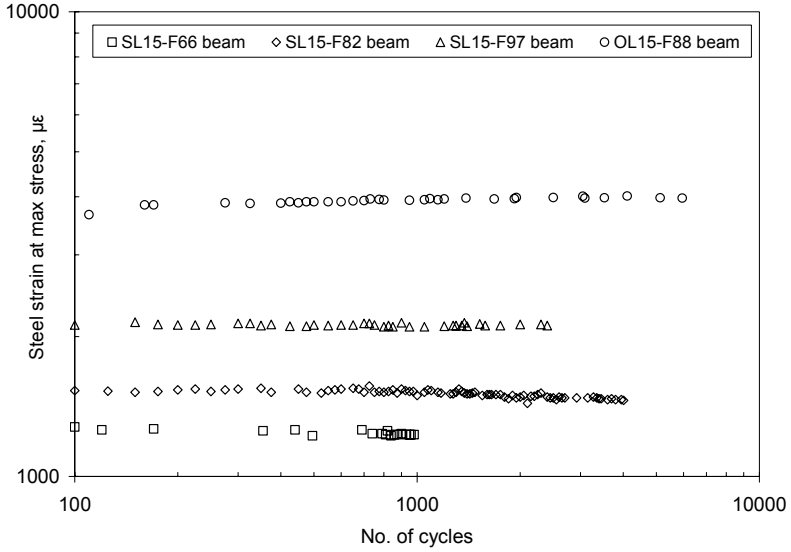

Figure 5.24: Cyclic simulation tests: steel strain response at maximum stress applied

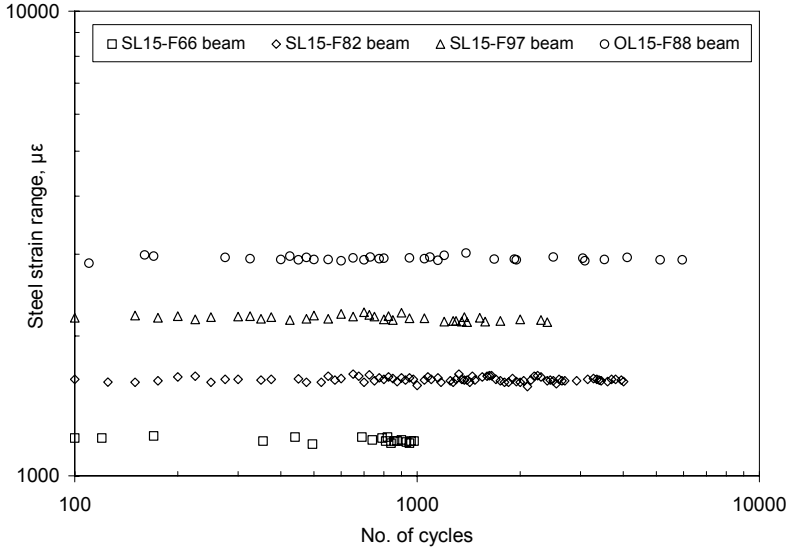

Figure 5.25: Cyclic simulation tests: steel strain range response

Figure 5.26 shows the test setup for the concrete cylinders. Prior to applying the cyclic loads, the cylinder was first loaded to its maximum peak load. The cylinder was then unloaded to the mean load level, defined as the average value of the maximum and the minimum peaks. The load was then cycled between the two peaks until failure occurred or the reading of the strain gages stabilized.

Figure 5.27 shows the variation of the stress-strain relationships of concrete as the number of cycles increased. It was observed that all specimens exhibited cyclic creep as the number of cycles increased. This was indicated by the increase in the measured strain values over the life of the specimen. The recorded strain values increased considerably with an increasing number of cycles until failure occurred.

It was also observed that softening in concrete occurred when high stress range was applied (Figure 5.27-c). Softening was indicated by the change in the slope of the concrete stress-strain curve with an increasing number of cycles. Softening in concrete was more pronounced near the end of the fatigue life. Specimens subjected to low stress range exhibited less softening, as indicated from the similar slopes of the stress-strain curves during the specimen life. These results agreed with the observation reported during the testing of the beam specimens, where no significant change in the range of the recorded concrete strains was obtained (Figure 5.17).

Figure 5.26: Test setup for concrete cylinder cyclic simulation tests

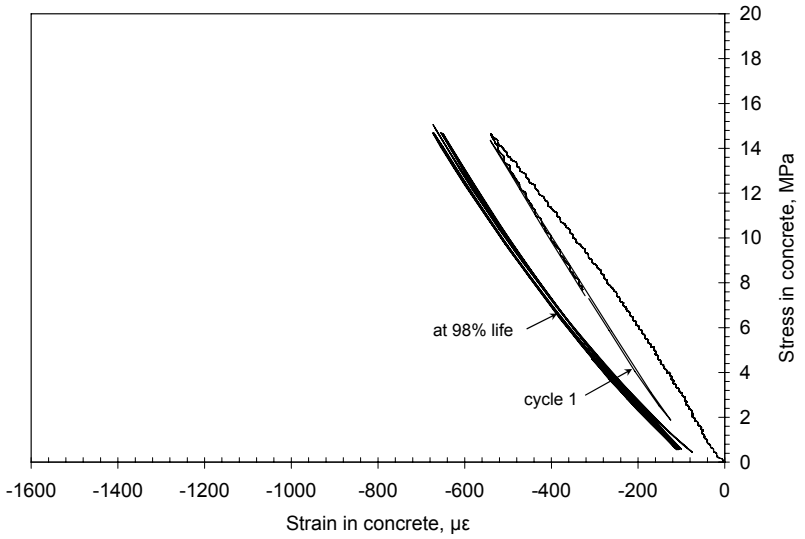

(a)

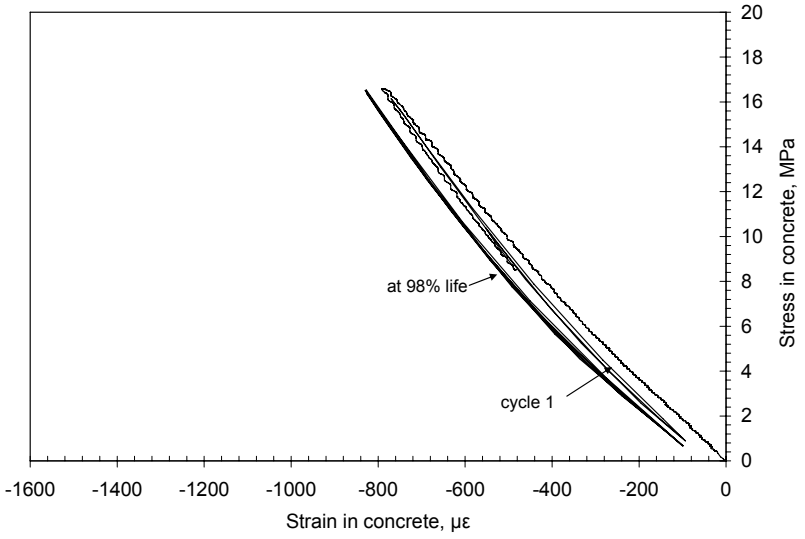

(b)

Figure 5.27: Variation of the concrete stress-strain relationships with number of cycles (a) Low stress range, (b) medium stress range, and (c) high stress range

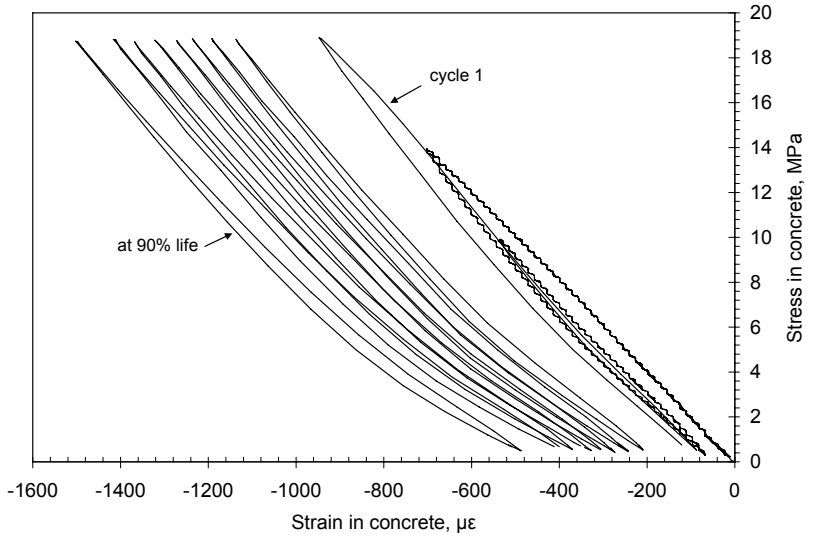

(c)

Figure 5.27 (cont.): Variation of the concrete stress-strain relationships with number of cycles (a) Low stress range, (b) medium stress range, and (c) high stress range

5.3.4.3 Summary of cyclic simulation tests

Simulation tests on steel and concrete specimens were conducted in order to study the behaviour of the constituent materials under cyclic loading. The steel specimens were subjected to stress histories and three stress ranges selected to simulate the fatigue response of the steel reinforcing bars embedded in the beams. Concrete cylinders were also tested under cyclic loading at three stress levels identified as low, medium and high stress ranges.

The test results indicated that the steel specimens showed almost no cyclic creep with an increasing number of cycles. On the other hand, the concrete exhibited an increase in the measured compressive strains as a result of cyclic creep. As such, the increase in the measured strains in the steel reinforcing bars in beam specimens was thus attributed to the cyclic creep behaviour of the concrete. This has previously been reported to increase the curvature of beams

under cyclic loading (Neville and Brooks, 1990). Another factor was also considered; as discussed previously, during the early stages of the fatigue life of the beams, flexural concrete cracks tended to increase in height and number before they stabilized. This crack growth was attributed to a reduction in the modulus of rupture of the concrete due to fatigue loading. This, the cyclic material tests, and the beam fatigue test observations suggested that the increase in the strains in the steel bars was due to a combined effect of the cyclic creep of concrete, and to the fatigue growth of the flexural cracks. However, the available test data was not sufficient to quantify the effect of each phenomenon separately.

5.3.5 Fatigue strength

The fatigue strength of the beams was determined based on two criteria: the total number of cycles survived by the beams and their fatigue failure modes. Table 5.6 provides a summary of the fatigue test results of both the unstrengthened and strengthened beams.

5.3.5.1 Failure Modes

Two characteristic failure modes were observed in the unstrengthened and strengthened beams under the effect of repeated loads: fatigue fracture of the reinforcing steel bars and concrete crushing in the compression zone.

Unstrengthened beams — for almost all of the beams, the typical failure of the unstrengthened beams occurred as a result of the brittle fatigue fracture of one of the tensile steel reinforcing bars. Figure 5.28 shows photographs of the fatigue failure modes of the unstrengthened beams UN15-F50 and UN15-F53. Fracture of the steel bars occurred within the constant moment region at a crack location where high stress concentrations were likely to occur. The fatigue fracture originated at the base of a rib. This was attributed to the presence of discontinuity on the surface

of the steel bar at this location, which caused a significant stress concentration and led to the fracture of the bar. Failure of a bar was followed by a sudden increase in deflection and a significant drop in the beam stiffness.

Beam UN15-F59 failed due to the crushing of the compressed concrete with no indication of fatigue fracture in either steel bar. The beam was subjected to a load close to the yield load. As a result, the steel reinforcing bars yielded during the first loading cycle of the beam fatigue life. This is shown in Figure 5.29. Note that the strain gages were damaged and no further strain readings were recorded. The concrete top surface was subjected to plastic deformations that led to a significant cyclic creep in concrete, as was indicated by the high measured strain values (Figure 5.30). The concrete then completely crushed after surviving 36,388 cycles.

In-service strengthened beams (SL15-group) — the mode of fatigue failure did not vary for the in-service strengthened beams SL15 where brittle facture of one of the steel reinforcing bars occurred, followed by crushing of top fibre concrete. The photos in Figure 5.31 show typical failure modes of the strengthened beams of the SL15 group. In all cases, failure of the beam was observed at a crack location on either side of the tested specimen. This resulted in a deflection excessive enough to trigger the lower limit of the digital controller to stop the test at this point. The rupture of the steel bar always occurred in the vicinity of a stirrup leg at a crack location. Note that all cracks were formed prior to post-tensioning the beam, and were generally controlled by the spacing of the shear stirrups. It was also observed that the fatigue crack in the steel bar initiated at the root of a rib on the deformed surface of the bar, as observed in the case of the unstrengthened beams.

Table 5.6: Summary of beam fatigue parameters and failure modes

Specimen	P_{max} (kN)	Range, R (kN)	R/P_y, (%)	No. of cycles to failure	Mode of failure
Group-A: UN15-beams					
UN15-F50	50	35	56%	431,871	Steel rupture
UN15-F52	51.5	37	59%	353,293	Steel rupture
UN15-F53	53	38	61%	175,600	Steel rupture
UN15-F57	57	42	68%	148,000	Steel rupture
UN15-F59	59	44	71%	36,388	Concrete crushing
Group-B: SL15-beams					
SL15-F61	61	46	43%	>1,000,000	Run-out
SL15-F66	66	51	47%	645,086	Steel rupture
SL15-F68	68	53	49%	356,401	Steel rupture
SL15-F72	72	57	53%	210,844	Steel rupture
SL15-F82	82	67	62%	143,047	Steel rupture
SL15-F88	88	73	68%	117,351	Steel rupture
SL15-F92-a	92	77	71%	2,337	Concrete crushing
SL15-F92-b	92	77	71%	80,318	Steel rupture
SL15-F92-c	92	77	71%	90,831	Steel rupture
SL15-F97	97	82	76%	37,342	Steel rupture
Group-C: SL20-beams					
SL20-F79	79	58	47%	>1,000,000	Run-out
SL20-F83	83	62	50%	707,235	Steel rupture
SL20-F87	87	66	53%	398,788	Steel rupture
SL20-F100	100	79	64%	269,135	Steel rupture
SL20-F110	110	89	72%	138,639	Steel rupture
Group-D: OL15-beams					
OL15-F57	57	42	39%	>1,000,000	Run-out
OL15-F67	67	52	48%	662,911	Steel rupture
OL15-F72-a	72	57	53%	20,916	Concrete crushing
OL15-F72-b	72	57	53%	438,870	Steel rupture
OL15-F76	76	61	56%	138,853	Steel rupture
OL15-F82	82	67	62%	94,931	Steel rupture
OL15-F88	88	73	68%	87,027	Steel rupture

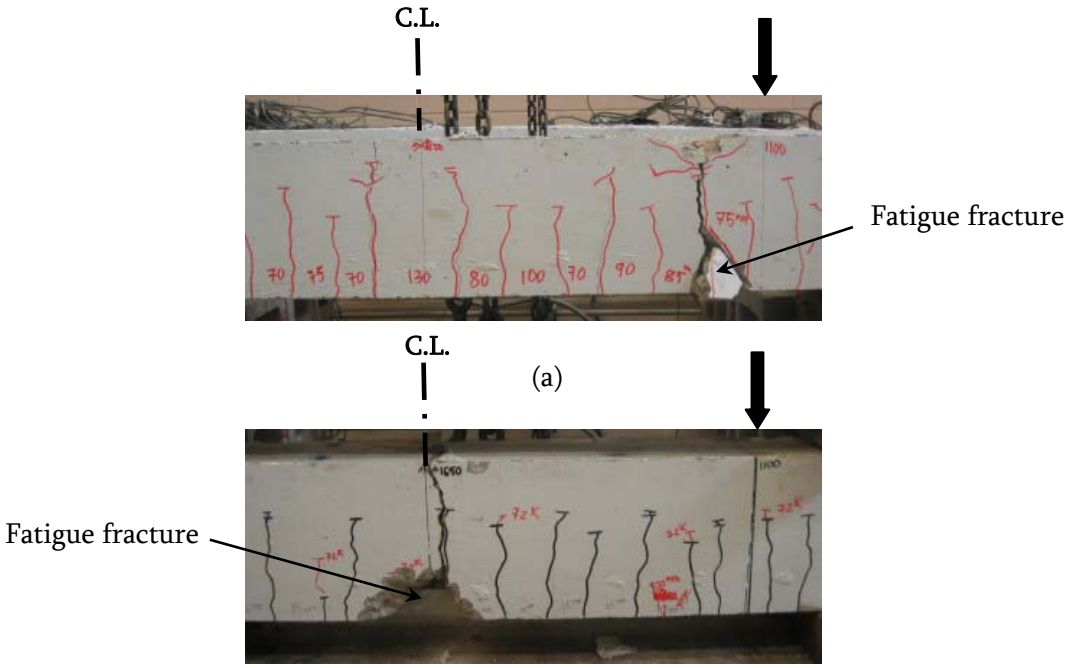

Figure 5.28: Typical failure of the unstrengthened beams (a) UN15-F50 and (b) UN15-F53

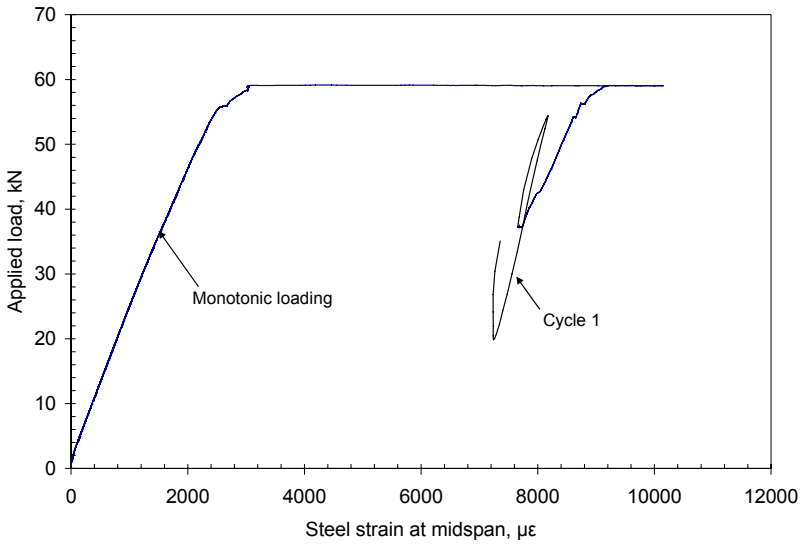

Figure 5.29: Unstrengthened beam UN15-F59: steel strains versus the applied loads

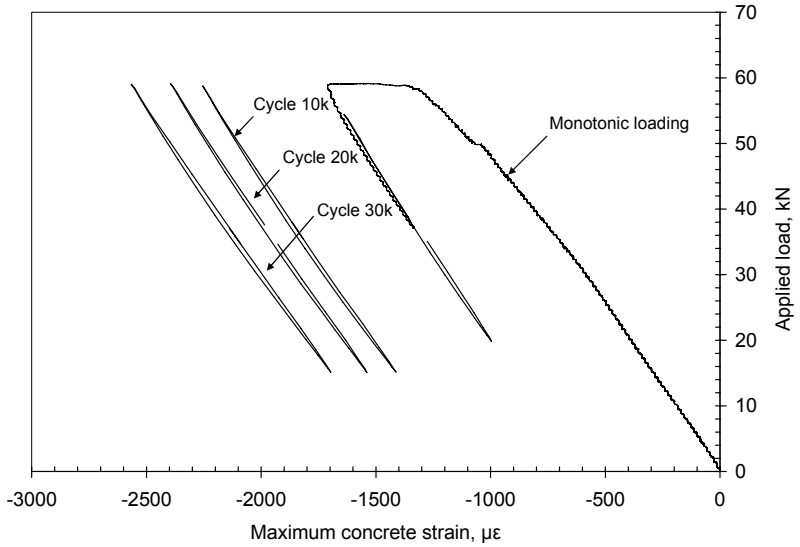

Figure 5.30: Unstrengthened beam UN15-F59: concrete strains versus the applied loads

Rupture of the steel reinforcing bars in the strengthened beams resulted in an increase in the external tendon stress due to the loss of the steel reinforcement and the sudden increase in deflection of the beam. Before the fracture of the bars, the compression force in the concrete was balanced by the tensile force developed in both the steel bars and the CFRP tendons. When the steel bars fractured due to fatigue, this force was balanced only by the CFRP tendons, which resulted in a progressive increase in the tendon stress. This was indicated by the tendon load cell readings. Fatigue failure of the reinforcing bar was accompanied by a sudden extension of the cracks until the upper concrete layers crushed.

A different mode of failure was observed in beam SL15-F92-a (Table 5.6), where the concrete crushed in the vicinity of one of the two point-loads. Local cracks in the top concrete at this location were initiated during the static loading of the strengthened beam at a load of approximately 70 kN (65% of the yielding load). This might have been caused due to an uneven concrete surface finishing under the point-load support, which led to a stress concentration at

this point. During cycling, the crack tended to extend horizontally towards the midspan, as shown in Figure 5.32. As such, an excessive increase in steel strains occurred at mid span with an increase in the number of cycles until the beam failed after 2,337 cycles. The test was thus repeated under the same load range, as reported in Table 5.6 (Beams SL15-F92-b and SL15-F92-c).

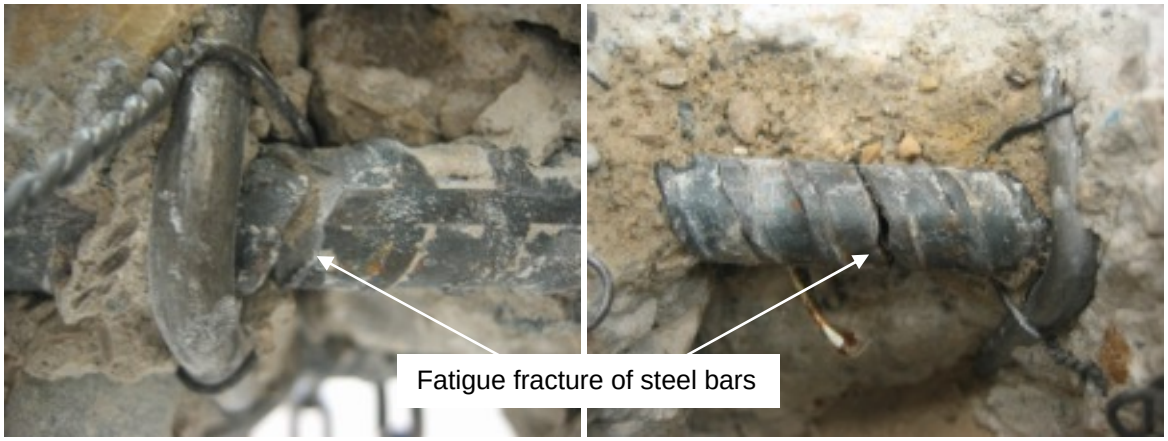

Figure 5.31: Failure of the in-service SL15 beams near the stirrup and at location of lugs

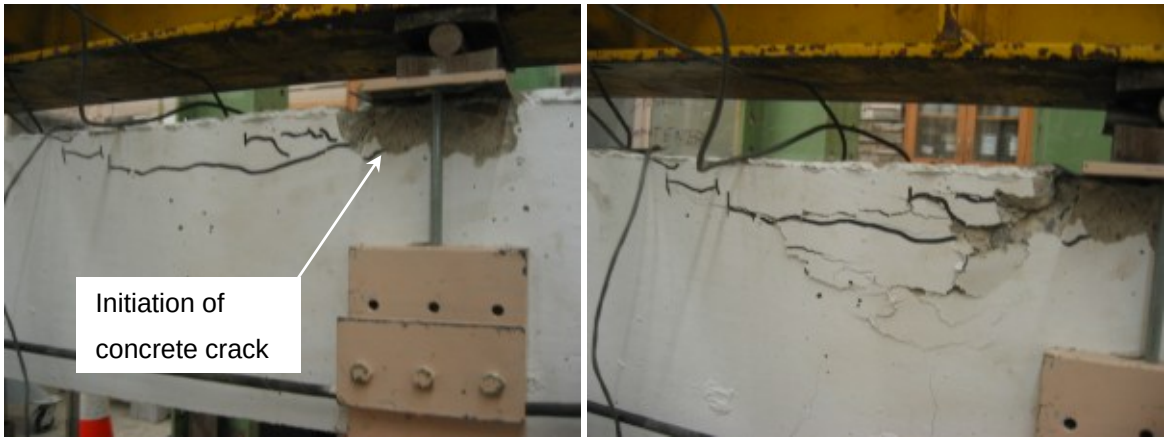

(a) (b)

Figure 5.32: Beam SL15-F92-a: (a) local cracking extending from the loading point and (b) failure due to concrete crushing

In-service strengthened beams (SL20-group) — fatigue fracture of the reinforcing steel bars was the dominant mode of failure of all beams of the SL20-group. Fatigue failure of the beams was characterized by a catastrophic fracture of both steel bars (Figure 5.33-a). Failure usually started with the fracture of one bar under fatigue loading. At that time, the beam was able to continue supporting load cycles until fatigue fracture occurred in the second bar. Then, the deflection of the beam increased sharply and the test was automatically halted. Similar to the unstrengthened and the SL15 beams, failure occurred at the crack location near the stirrups, as shown in Figure 5.33-b.

Overloaded strengthened beams (OL15-group) — A fatigue crack in the steel reinforcing bars of the overloaded beams initiated at the location where the largest flexural crack occurred (location of yielding of the steel reinforcing bar). The beams eventually failed due to a steel rupture at this location. Figure 5.34 shows the failure mode of the beams OL15-F76 and OL15-F88 where the yield crack occurred in the constant moment zone near the applied point-load and near the midspan, respectively. Concrete in the compressive zone crushed immediately after the rupture of the steel bars.

The overloaded beam OL15-F72-a failed by concrete crushing after 20,916 cycles with no fatigue damage observed in the steel reinforcing bars. This was attributed to the extensive plastic deformations in the compressed concrete during the overloading stage as follows: overloading the beams was usually performed under displacement control in order to "fine-tune" the required strain to be applied in the steel bar. The beam OL15-F72-a was loaded under load control rather than displacement control, which caused excessive overloading and a permanent deformation in concrete. Failure of the beam by concrete crushing is shown in Figure 5.35. The test was then repeated under the same load range (beam OL15-F72-b in Table 5.6).

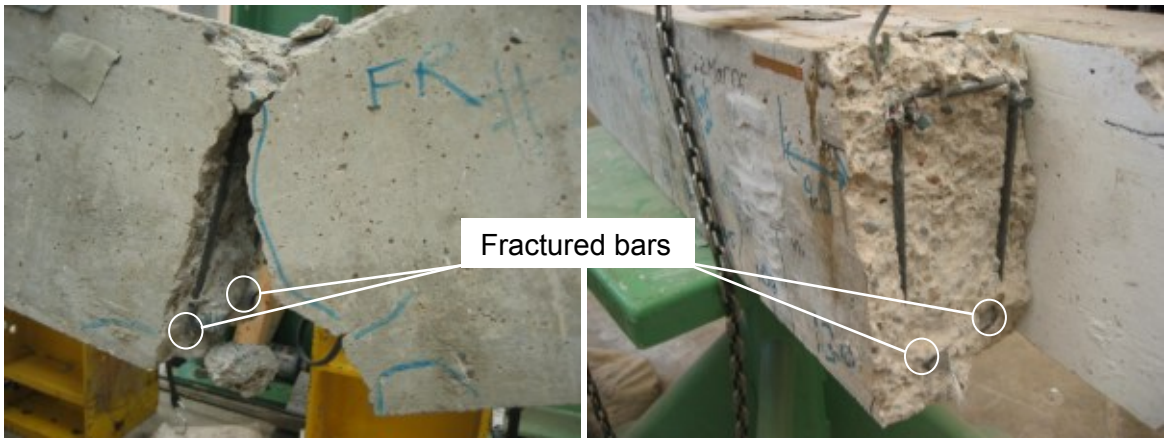

(a) (b)

Figure 5.33: Typical failure of the SL20-group of beams: (a) fatigue fracture of both reinforcing steel bars, (b) failure occurring at the crack location in the vicinity of a stirrup

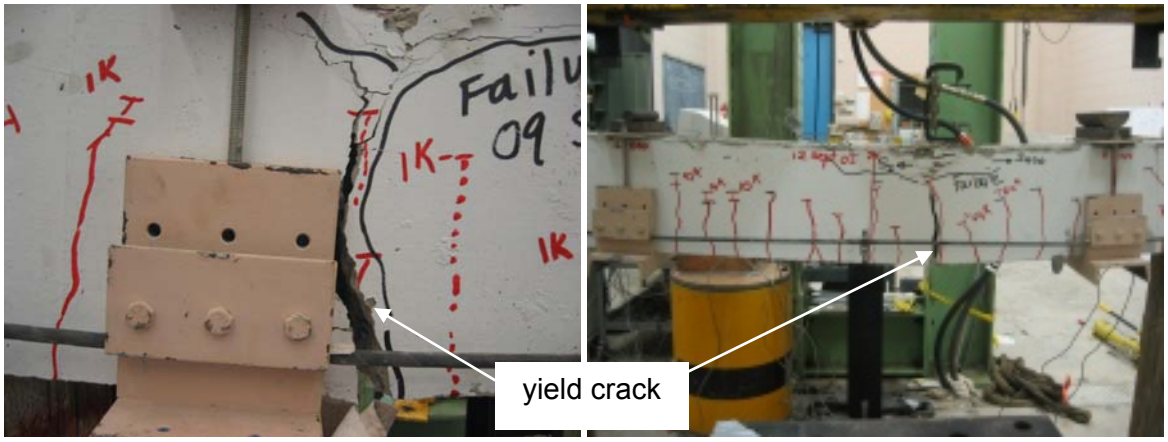

(a) (b)

Figure 5.34: Typical failure of the OL15-group of beams: fatigue fracture at the location of yield crack for the beams (a) OL15-F76, and (b) OL15-F88

It is worth mentioning that, in all in-service and overloaded strengthened beams, the stability of the beams post-failure was ensured by the CFRP tendons. That is, the tendons were able to maintain the beam in the failed position. The CFRP material showed a great flexibility in containing the tremendous impact resulting from the catastrophic fracture of the reinforcing steel bars under fatigue. No failure or distress was encountered in the tendons at that point. No anchorage slip was observed in any of the strengthened beams.

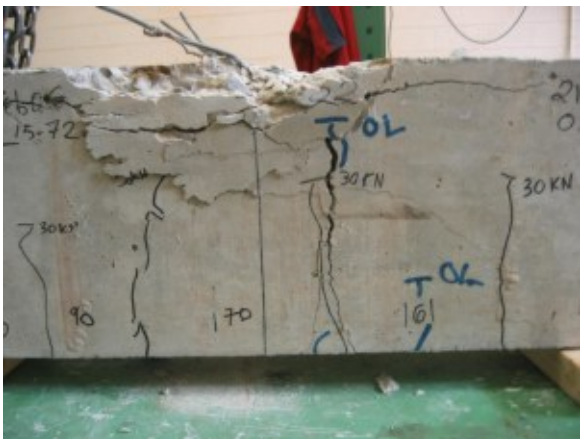

Figure 5.35: Failure of the beam OL15-F72-a by concrete crushing

5.3.5.2 Fatigue life

The fatigue life for the UN15, SL15, SL20, and OL15 groups of beams is presented in terms of the applied load range and the number of cycles to failure in Figure 5.36. A best-fit curve based on a regression analysis of the experimental data is also plotted for each group. Horizontal arrows at the right side of the figure indicate that the specimens did not fail after surviving one million cycles. At this point, the test was halted and the specimens were considered as run-outs. These specimens were then subjected to a higher load range until a finite fatigue life was achieved.

The data for the unstrengthened beam series (UN15) are supplemented by data from tests conducted by Badawi (2006) on five reinforced concrete beams similar to those of group UN15. These beams were tested under fatigue loading having a minimum load of 6 kN, representing 10% of the yielding capacity of the beam. The UN15-group of beams had a minimum peak of 15 kN representing 25% of the yield capacity of the beams. It is worth mentioning that, for a given applied load range, the minimum load has a small effect on the fatigue life of the beam, as reported by ACI-215 (1997).

As expected, the fatigue life of each set of beams decreased with an increase in the applied load range. In addition, for the same load range, the fatigue life of all strengthened beams was considerably longer than the fatigue life of the unstrengthened beams. Comparing the fatigue life curve of the UN15 group with that of the SL15 group, it is observed that the fatigue life of the strengthened beams was approximately 17 times greater than the fatigue life of the unstrengthened beams. For instance, at a load range of 50 kN, the corresponding unstrengthened beam (Badawi, 2006) survived 38,300 cycles, while the post-tensioned beam (SL15-F66) survived 645,086 cycles (Figure 5.36).

Overloading the beams before post-tensioning application had no discernable effect on the fatigue life of the strengthened beams, as shown in Figure 5.36. This is made apparent by a comparison of the best-fit curves for the SL15 and the OL15 groups. This is related to the cyclic behaviour of the steel reinforcing bars under the applied stress range and mean stress, as will be illustrated in Chapter 7.

The influence of the amount of the non-prestressed reinforcement used in the strengthened beams on their fatigue life can be studied by comparing the data of the SL15 and SL20 groups of beams in Figure 5.36. The fatigue life of the SL20 group was on the average of 3 times greater than the fatigue life of the SL15 group. For instance, at an absolute load range of approximately 66 kN, the beam SL15-F82 survived 143,047 cycles, while the beam SL20-F87 survived 398,788

cycles until failure (Table 5.6). Since the post-tensioning force and tendon profile were the same for both groups of beams, the total nominal resistance of the SL20 beams was larger than that of the SL15 beams. Thus, at the same absolute load range, the stress in the steel reinforcing bars in the SL20 beam was considerably less than the stress in the corresponding SL15 beam, which led to a longer fatigue life for the SL20 beam.

Since post-tensioning of beams subjected to fatigue loading is typically used to accommodate an increase in the applied load on the beam, the amount of the additional load range that can be applied to the strengthened beam is important to the designer. Hence, it is useful to express the fatigue performance of the strengthened beams as a ratio of that of the control beam. In Figure 5.37, the load ranges of the UN15, SL15 and OL15 beams were normalized with respect to the yield load of the control unstrengthened UN15 beams. For example, the load range of the beam SL15-F82, which is 67 kN, was divided by the yield load of the control beam as obtained from the tests data (60 kN), giving a normalized load range of 111.7%.

A considerable increase in the load range that could be carried by the beams was obtained after post-tensioning. Referring to the plot shown in Figure 5.37, an average increase of 45% in the normalized load ranges was accommodated by the strengthened beams for the same number of cycles survived by the unstrengthened beams, regardless of the loading history of the beam prior to being strengthened.

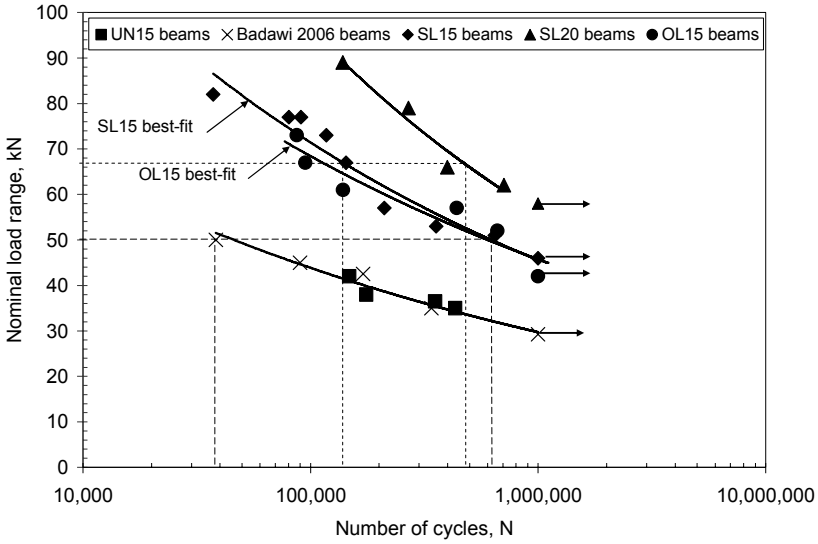

Figure 5.36: Load range versus number of cycles to failure from experimental data

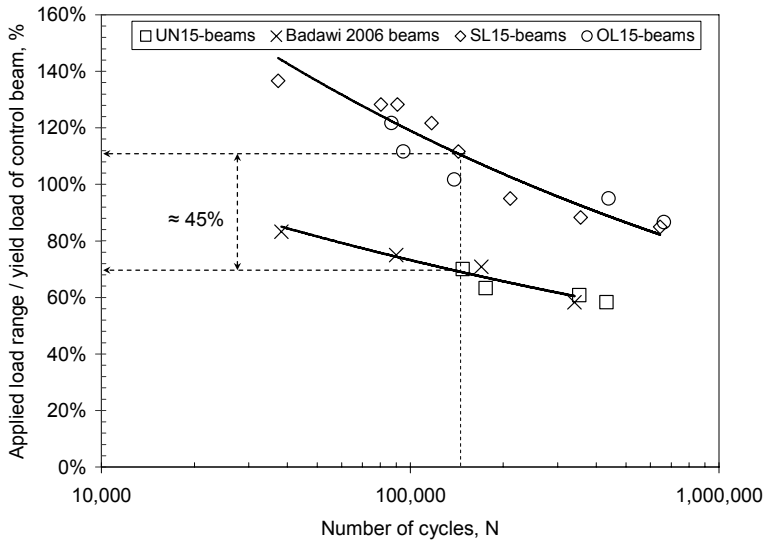

Figure 5.37: Normalized load range for the UN15, SL15, and the OL15 versus number of cycles to failure from experimental data

Since the majority of the unstrengthened and strengthened beams failed due to the fatigue fracture of their reinforcing steel bars, the above results were analyzed by considering the steel stresses induced in the steel bars at midspan section, during the fatigue life of the beam. Figures 5.38 to 5.40 show the relationship between the stress ranges in the steel bars at the midspan sections of the beams and the total number of cycles to failure. Strain data obtained from the fatigue tests were used to determine the steel stresses in the steel bars. Using a regression analysis, the best-fit curves are also plotted. As seen from the plots, increasing the stress range applied to the steel bars significantly decreased the fatigue life of the bar, and thus reduced the life of the beams. This was true for both the unstrengthened and the strengthened beams. For a given steel stress range, the fatigue life of the unstrengthened and strengthened beams fell into a single band (Figures 5.38 and 5.39). This indicates that the main controlling factor for fatigue life of the beam is the stress range in the steel bars.

Some scatter in the fatigue data of the OL15-beams is noticed (Figure 5.40). This was attributed to the fact that the strain gages were not positioned precisely at the location where the flexural yield cracks occurred. As a result, the stress ranges computed from the strain data obtained were not corresponding to the actual stress ranges that led to the failure of the beams.

The mean stress applied to the steel bar also affected its fatigue life. For the same stress range, a tensile mean stress has a detrimental effect on the fatigue life. A compressive mean stress, on the contrary, increases the fatigue life of the bar. This is noticed from the plot shown in Figure 5.40, which compares the fatigue behaviour of the SL15 and the OL15 beams. Taking into consideration the scatter in the fatigue data of the overloaded beams, the increase in the fatigue life of the overloaded beam OL15-F82 compared to that of the SL15-F97 beam is noticeable. Both beams were subjected to approximately the same stress range (about 480 MPa, as obtained from the strain data). However, the overloaded beam OL15-F82 survived 94,931 cycles while the in-service SL15-F97 beam survived only 37,342 cycles. This could be attributed to the magnitude of

the tensile mean stress induced in the overloaded beam during the beam fatigue life. Based on the strain readings, the overloaded beam OL15-F82 was subjected to a tensile mean stress of 38 MPa while the SL15-F97 beam was subjected to a mean stress of 103 MPa (approximately 2.70 times the mean stress of the overloaded beam). The procedure adopted in calculating the stresses induced in the steel bars will be illustrated later in Chapter 7.

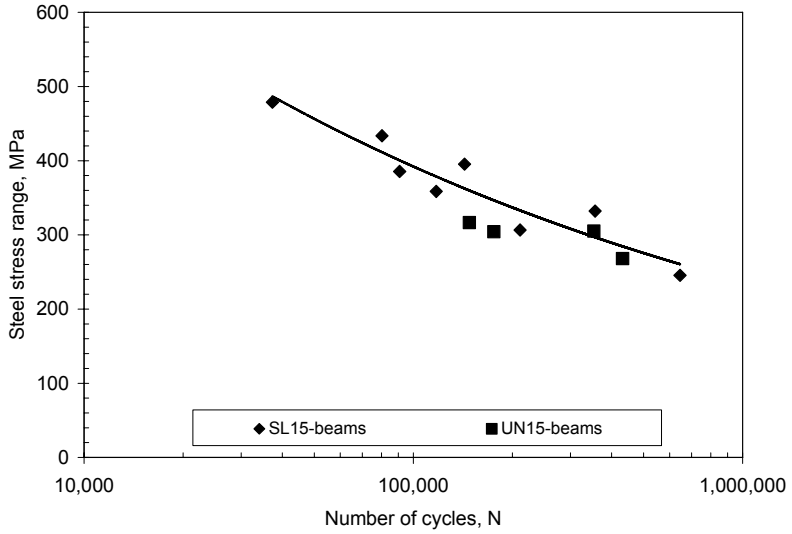

Figure 5.38: Stress range in reinforcing steel versus number of cycles to failure from experimental data: UN15 and SL15 beams

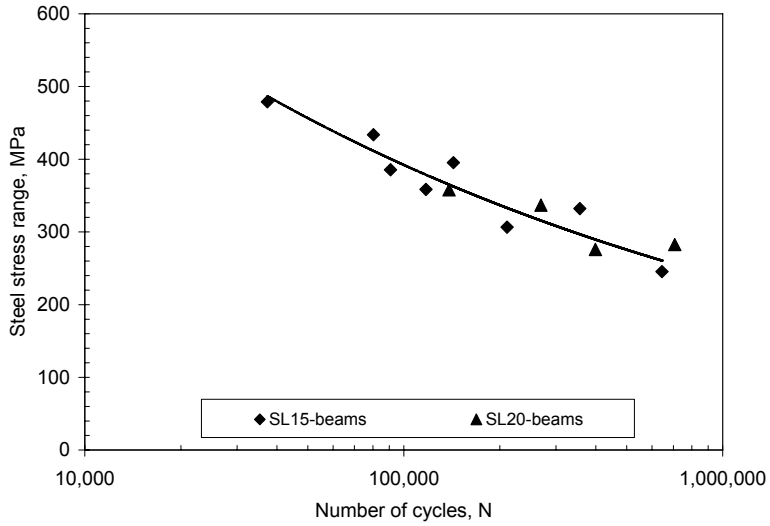

Figure 5.39: Stress range in reinforcing steel versus number of cycles to failure from experimental data: SL15 and SL20 beams

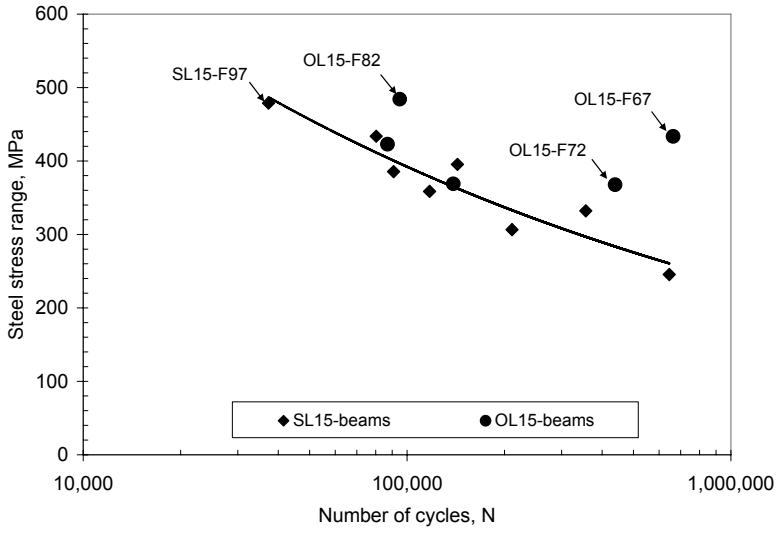

Figure 5.40: Stress range in reinforcing steel versus number of cycles to failure from experimental data: SL15 and OL15 beams

5.4 Summary and conclusions

The results of the monotonic and fatigue tests carried out on the unstrengthened and strengthened reinforced concrete beams were reported. Comparisons between various beam specimens in terms of their structural performance under monotonic and fatigue loadings were presented. The main findings of these tests are summarized in the following subsections.

5.4.1 Monotonic tests

The main findings of the monotonic tests conducted on the beams are as follows:

- The beams post-tensioned with straight tendons behaved similarly to those with double draped tendons at various loading stages up to ultimate stage. Note that guides were used with the straight tendon profile, and these minimized the second-order effect.
- The presence of deviators in both tendon profiles minimized the effect of the change in the tendons eccentricity on the behaviour of the beam. The change in the tendon depth can thus be neglected during the analysis of the in-service and the overloaded beams.
- Post-tensioning the external CFRP tendons at 40% of their ultimate capacity allowed a reasonable strain margin to account for live load applications, with no concern of the premature breakage of the tendon, even if the strengthened element was severely overloaded.
- For the same post-tensioning system, overloading the beam prior to post-tensioning increased the beam deflection and the strains developed in the steel reinforcing bars. Overloading did not have a significant effect on the yield load of the strengthened beam or the mode of failure at ultimate. It also had no discernable effect on the increase in the tendon stress at yielding.

- External post-tensioning with CFRP tendons is an effective technique for strengthening overloaded concrete elements. It also significantly decreased the amount of deflection encountered due to overloading.

5.4.2 Fatigue tests

The main findings of the fatigue tests conducted on the beams are as follows:

- External post-tensioning with CFRP tendons considerably increased the fatigue life of the beam at any applied load range as a result of the stress decrease in the steel reinforcing bars.
- The unstrengthened and strengthened beams exhibited a linear increase in their midspan deflections with an increasing number of cycles. Post-tensioning had a slight effect on reducing the rate of increase in the deflections of the strengthened beams.
- Cyclic tests on the steel specimens indicated that steel showed almost no cyclic creep under fatigue loading. On the other hand, the cyclic tests on the concrete cylinders indicated that the concrete exhibited cyclic creep at all stress ranges with a considerable amount of softening when high stress ranges were applied.
- The increase in the steel strains encountered during the beam tests can be attributed to a combined effect of the cyclic creep of concrete and the fatigue crack growth of the flexural cracks.
- The CFRP external tendons exhibited a stress increase up to 1.37% of its ultimate strength during the fatigue life of the strengthened beams. The tendons are not likely to encounter any softening in their material due to the repeated load.
- The CFRP tendons had an excellent fatigue response with no evidence of wear or stress concentration at the deviated points.

- Failure of the unstrengthened and strengthened beams under fatigue loading occurred due to the fatigue fracture of the steel reinforcing bars. The fatigue rupture occurred at the root of the ribs, which indicated the presence of stress concentration at these locations.
- Overloading the beams prior strengthening had a slight effect on the fatigue life of the strengthened beam. The stress range and the mean stress applied to the steel bar governed the fatigue life of the bar, and hence the fatigue life of the beam.
- At the same load range applied to the beam, increasing the amount of the steel reinforcing bars for the same post-tensioning level decreased the stress range in the bars and significantly increased the fatigue life of the strengthened beams.

Chapter 6

Modeling the Monotonic Flexural Response of Externally Post-Tensioned Beams

6.1 Introduction

In this chapter, a new analytical approach is developed to predict the monotonic flexural response of in-service and overloaded beams post-tensioned with external CFRP tendons. The approach takes into consideration the effect of the loading, unloading, and reloading stages associated with the post-tensioning application. The assumptions used in formulating the model along with the derivations for its main components are presented. The model is validated by the experimental results to measure its applicability and accuracy.

6.2 Analysis approach

The analysis described herein aims to model the monotonic flexural response of the in-service and overloaded strengthened beams tested in this program. The beam tests were carried out in four stages as previously described in Section 4.2, and illustrated in Figure 4.2 (repeated in Figure 6.1 for convenience):

- *The initial loading stage* — for the in-service beam, the virgin beam was initially precracked by loading to 50% of its yield strength (point A in Figure 6.1-a). For the overloaded beam, the virgin beam was overloaded beyond the yield strain of the steel bars. A load producing a steel strain of approximately 4000 microstrain was applied (point A in Figure 6.1-b).
- *The unloading stage* — for the in-service and overloaded beams, the beam was unloaded to 25% of its yield load after being cracked (point B). This load was sustained during the post-tensioning process.
- *The post-tensioning stage* — in this stage, a post-tensioning force of 40% of the ultimate tendon capacity was applied in each tendon (approximately 60 kN in each tendon). Post-tensioning was applied while the beam was subjected to a sustained load of 25% of the yield load of the beam. The end of post-tensioning is represented by point C in Figure 6.1.
- *The reloading stage* — after being post-tensioned, the beam was reloaded until failure occurred under monotonic loading (points D, E, and F in Figure 6.1).

The beam is modeled as a series of longitudinal elements each of length $l_{el\,(j)}$, as shown in Figure 6.2. Each element is assumed to be subjected to a constant flexural moment along its length. The sectional analysis at each element is based on a layer-by-layer evaluation of the section forces. The concrete section is divided into a finite number of discrete horizontal layers, each having a certain height and a width equal to the width of the rectangular section, as shown in Figure 6.3. The implementation of the sectional and longitudinal analyses depends on the stage of loading under consideration. Details about the concrete, steel, and CFRP responses during each stage of loading are given in the following sections.

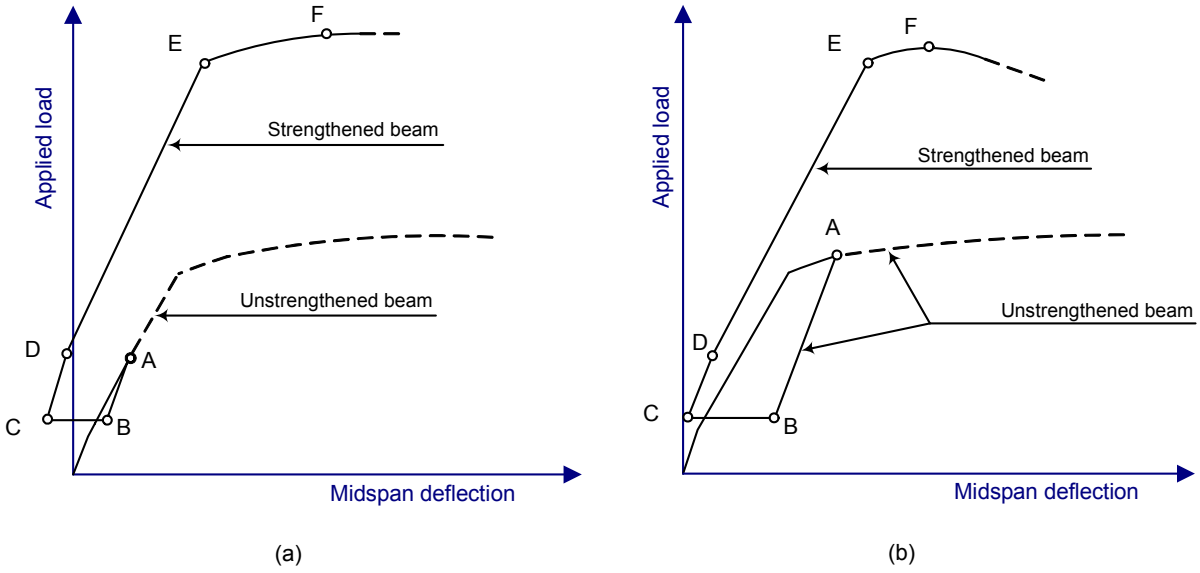

Figure 6.1: Idealization of the stages of monotonic loading of the (a) in-service beam and (b) overloaded beams (D: cracking load, E: yield load, and F: ultimate load)

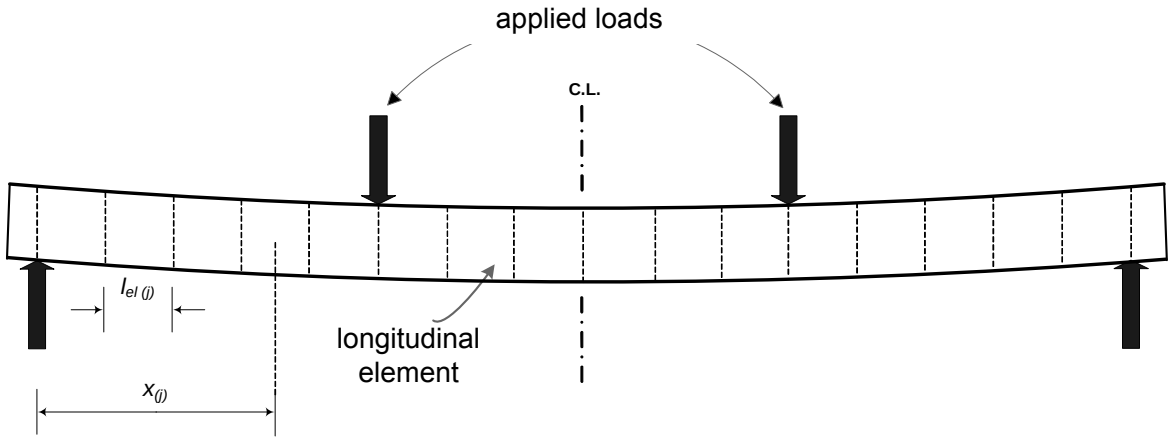

Figure 6.2: Modeling of beam using longitudinal elements

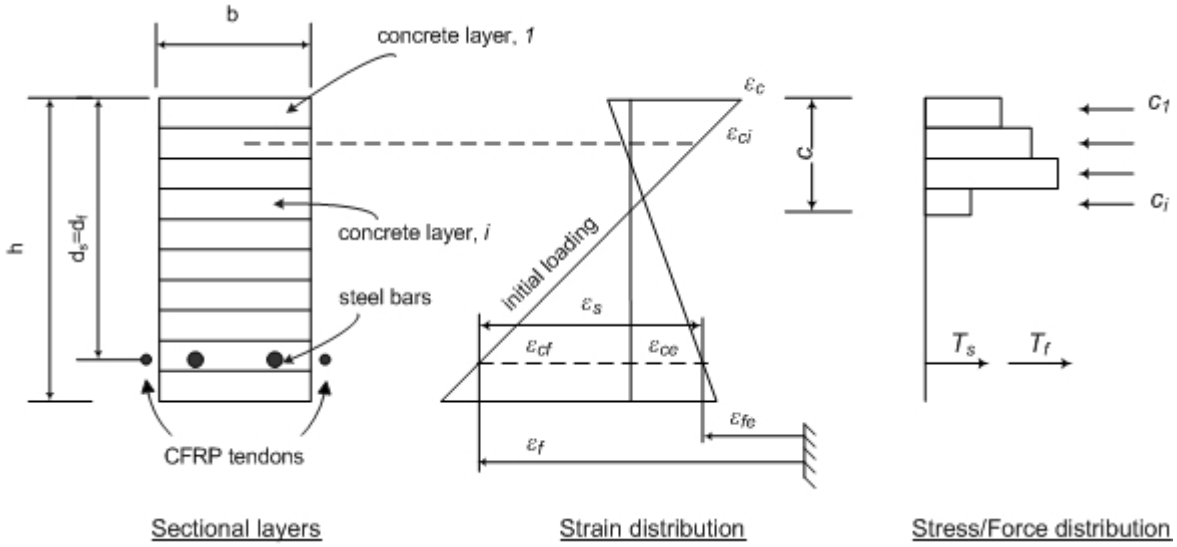

Figure 6.3: Layer-by-layer concrete section analysis

6.3 Materials modeling

6.3.1 Concrete

The assumed stress-strain relationship of concrete is shown in Figure 6.4. A parabolic curve given by Equation 6.1 describes the stress-strain relationship of concrete in compression (Collins and Mitchell, 1991). The concrete strain at crushing, ε_{cu}, is taken as 0.0037.

$$f_c = f_c^{'}\left[\frac{2\varepsilon_c}{\varepsilon_{co}} - \left(\frac{\varepsilon_c}{\varepsilon_{co}}\right)^2\right] \tag{6.1}$$

$$\varepsilon_{co} = \frac{2f_c^{'}}{E_c} \tag{6.2}$$

where:

f'_c = concrete compressive strength in MPa;

ε_{co} = strain corresponding to f'_c, and;

E_c = initial modulus of elasticity of concrete in MPa.

The concrete stress-strain relationship in tension is assumed linear until the rupture strength of concrete, f_r, is reached. The rupture strength of concrete is given by the CSA A23.3-04 (2004) and ACI-318 (2005):

$$f_r = 0.6\sqrt{f_c^{'}} \tag{6.3}$$

When cracks are developed in concrete, tensile stresses still exist within the concrete between successive cracks, due to the bond forces between the steel reinforcing bars and the concrete.

These stresses drop to almost zero at crack locations. Tensile stresses in the concrete between the cracks stiffen the beam and cause a phenomenon termed "tension stiffening" of concrete. To account for the tension stiffening effect on the flexural behaviour of the beams, average, or smeared, stresses and strains are assumed along the concrete elements. This is illustrated in Figure 6.5. The average tensile stress, $f_{c(avg)}$, is generally taken as a percentage of the rupture strength of concrete, as expressed by Equation 6.4 (Tepfers, 1979; Bazant and Oh, 1984; Collins and Mitchell, 1991; Min, 1997; among others).

$$f_{c(avg)} = \beta f_r \tag{6.4}$$

where:

$f_{c(avg)}$ = average tensile stress in concrete beyond its tensile rupture strength, and;

β = tension stiffening bond factor.

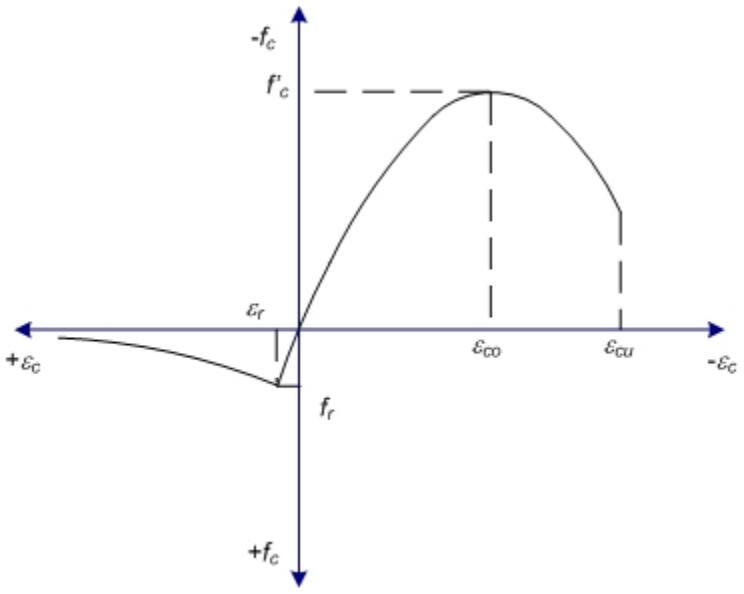

Figure 6.4: Assumed stress-strain relationship of concrete

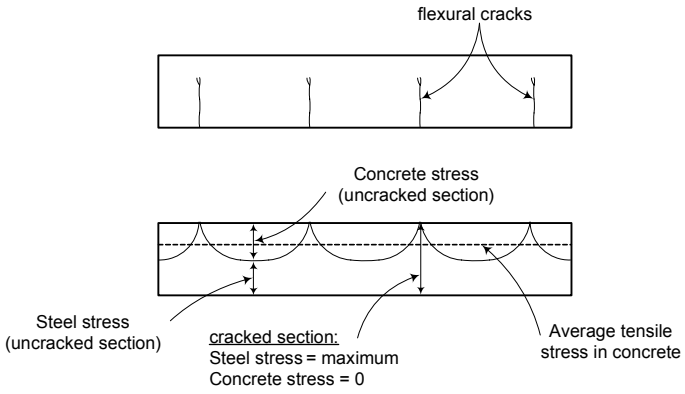

Figure 6.5: Average tensile stress in concrete

Figure 6.6 shows the relationship between the average tensile stress and the average tensile strain in concrete in tension. Various tension-stiffening models estimate the bond factor, β, based on different assumptions. Some models represent the concrete in tension as an elastic-plastic material where the tensile stress after cracking remains constant (Tepfers 1979). This contradicts the fact that, as the applied load increases, the average concrete tensile stress diminishes. The model used in this study is that proposed by Collins and Mitchell (1991) where the bond factor, β, is given by the following relationship:

$$f_{c(avg)} = \frac{\alpha_1 \alpha_2 f_r}{1 + \sqrt{500 \varepsilon_{c(avg)}}} \tag{6.5}$$

where:

$\varepsilon_{c(avg)}$ = average tensile strain in concrete corresponding to the average stress, $f_{c(avg)}$;

α_1 = factor accounting for bond characteristics of reinforcement (1.0, 0.7, 0 for deformed, plain, and unbonded reinforcement, respectively), and;

α_2 = factor accounting for type of loading (1.0 and 0.7 for monotonic and sustained (or repeated) loading, respectively).

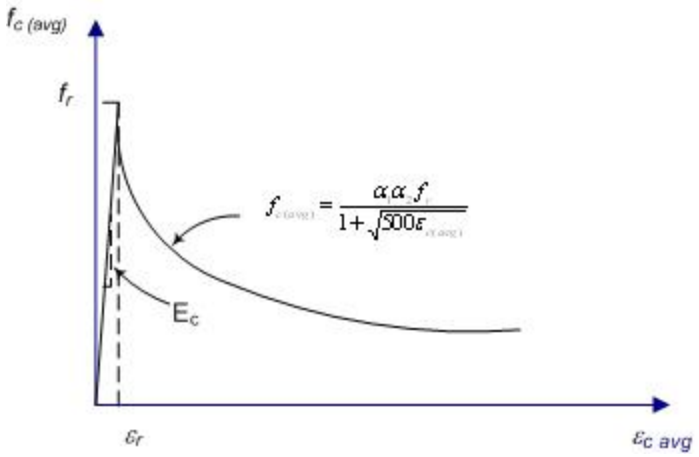

Figure 6.6: Average stress and average strain in concrete beyond cracking (adapted from Collins and Mitchell, 1991)

The tensile stress in concrete between cracks is considered active in a zone of concrete called the effective embedment zone. This zone is determined by the CEB Model Code, 1990 as illustrated in Figure 6.7. Tensile stresses developed in concrete outside the embedment zone are neglected.

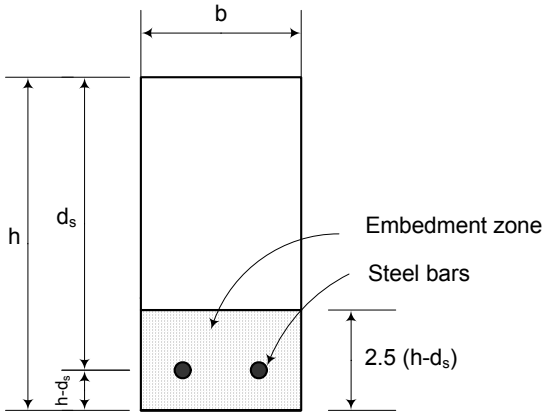

Figure 6.7: Effective embedment zone in cracked section (CEB Model Code, 1990)

6.3.2 Steel reinforcement

The steel reinforcement response is idealized as a linear elastic-perfectly plastic relationship, as shown in Figure 6.8-a. The relationship between the stress and strain in steel at any load level is given by:

$$f_s = \begin{cases} \varepsilon_s E_s & if \quad \varepsilon_s < \varepsilon_{sy} \\ f_{sy} & if \quad \varepsilon_{sy} \le \varepsilon_s \le \varepsilon_{su} \end{cases} \tag{6.6}$$

where:

f_s = the steel stress for a given loading condition;

ε_s = the steel strain corresponding to f_s;

f_{sy} = the yield stress of steel;

ε_{sy} = the yield strain of steel corresponding to f_{sy};

E_s = modulus of elasticity of steel;

ε_{su} = the steel strain at rupture.

The response of the steel reinforcing bar in the overloaded beam will be illustrated in Section 6.5.

6.3.3 CFRP tendon

A linear elastic relationship of the CFRP tendons is used up to failure, as shown in Figure 6.8-b. The stress-strain relationship of the CFRP tendon is given by:

$$f_f = \varepsilon_f E_f \tag{6.7}$$

where:

f_f = the CFRP stress at a given loading condition;

ε_f = the CFRP strain corresponding to f_f;

E_f = the modulus of elasticity of the CFRP material;

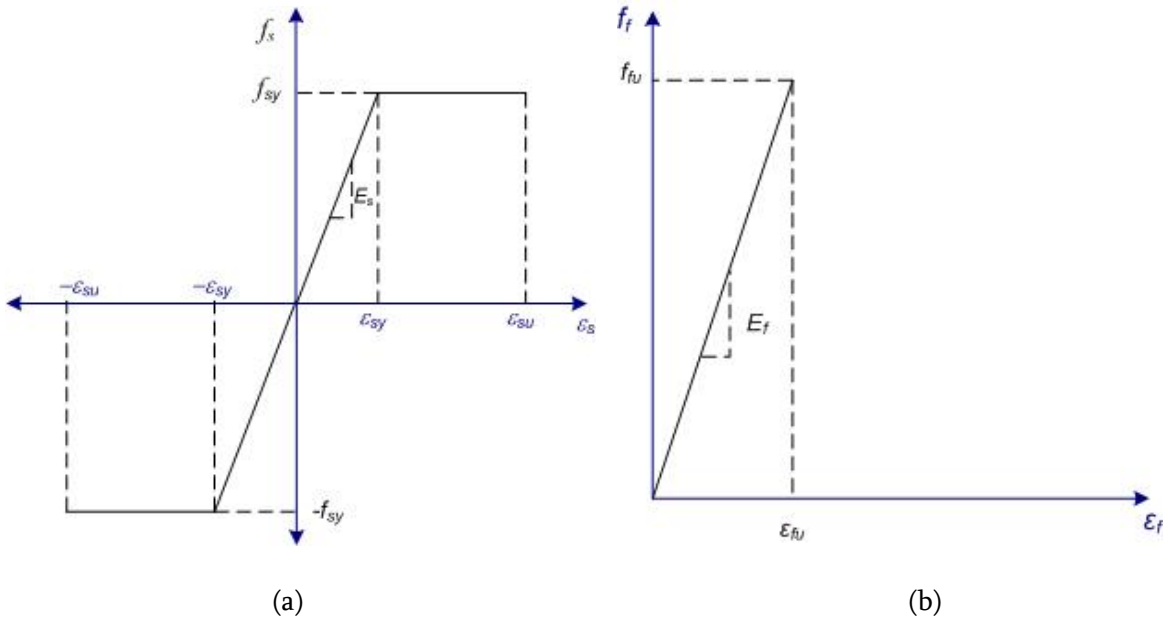

(a) (b)

Figure 6.8: Idealized stress-strain relationship of (a) steel reinforcement and (b) CFRP tendon

6.4 Modeling the monotonic behaviour of the in-service beams

The analysis of the in-service strengthened beams is implemented in a Visual Basic program in successive phases corresponding to the loading scenario described in Section 6.2. Four stages of analysis are adopted as follows.

6.4.1 The initial loading stage: in-service beam

Constant moment region — the monotonic analysis in the initial loading stage is based on the conventional cracked section analysis as recommended by the Canadian Code CSA-A23.3-04 (2004). During this stage of loading, the analysis is implemented by specifying an initial strain in the steel reinforcing bars, ε_s, at midspan section. The maximum compression strain in the concrete, ε_c, is assumed. Using these two strain values to define a linear strain profile for the section, the neutral axis depth, c, is estimated from the strain compatibility between the concrete and steel reinforcement, as given by Equation 6.8. Note that a sign convention of positive for tension and negative for compression is adopted.

$$c = \left(\frac{\varepsilon_c}{\left(\varepsilon_c - \varepsilon_s\right)} \right) d_s \tag{6.8}$$

where d_s is the depth of the steel reinforcement.

As shown in Figure 6.3, the corresponding concrete strain values at the midpoint of each layer are calculated as:

$$\varepsilon_{ci} = \varepsilon_c \left(\frac{c - \sum_{1}^{i-1} h_i - \frac{h_i}{2}}{c} \right) \tag{6.9}$$

where:

ε_{ci} = the strain in concrete at the middle of layer i, and;

h_i = the height of layer i.

The stress in each layer is determined using the stress-strain relationship of concrete shown in Figure 6.4. During this stage of loading, compressive stresses are developed in the upper concrete layers following the parabolic part of the curve, while the tensile stresses are developed in the lower concrete layers until cracking occurs. The cracks initiate when the tensile stress in the bottom layer of concrete reaches its rupture strength, f_r, as shown in Figure 6.4. Tension stiffening of concrete is considered by including the stresses developed in the concrete layers in tension, located within the effective embedment zone, in the section equilibrium equations. The concrete stress in each layer, f_{ci}, is assumed to be constant throughout the layer height. Once all of the stresses have been determined, the corresponding layer forces are computed and equilibrium of the section is checked as follows:

$$\sum C + \sum T = 0 \tag{6.10}$$

where ΣC is the resultant internal compressive force and ΣT is the resultant internal tensile force.

If sectional equilibrium is achieved, the corresponding bending moment and curvature are computed. If equilibrium is not satisfied, a new value of ε_c is assumed and the process is repeated. These steps are replicated for different values of steel strains until the required applied load level is reached (50% of the yield load of the beam).

Elements outside the constant moment region — knowing the applied loading pattern, the moment in each element outside the constant moment region is determined. The elements are analyzed by incrementally increasing the steel strain in the element and iterating for the top fibre

concrete strain required to satisfy sectional equilibrium. The procedure is repeated until the internal moment of the section is equal to the external moment applied, within a reasonable tolerance. The curvature of an element, $\varphi_{(j)}$, is then calculated as follows:

$$\phi_{(j)} = \frac{\varepsilon_{s(j)}}{d_s - c_{(j)}} \tag{6.11}$$

where:

$\varepsilon_{s(j)}$ = the strain in steel at element *j*, and;

$c_{(j)}$ = the depth of the neutral axis of element *j*.

Midspan deflection of the beam — using the symmetry of the beam, the deflection of the beam at mid-span, Δ, is calculated by numerically integrating the curvature of the elements at each load level as follows:

$$\Delta = \sum_{j=1}^{j=n} \phi_{(j)} x_{(j)} l_{el(j)} \tag{6.12}$$

where:

$x_{(j)}$ = the distance from the support to the center of the element *j*;

$l_{el(j)}$ = the length of the element *j*, and;

n = the number of elements within half of the beam span.

6.4.2 The unloading stage: in-service beam

Following the initial loading stage, the beam is unloaded until a specified load level representing 25% of its yield load is reached (the sustained load). A similar procedure of analysis as described in Section 6.4.1 (during the initial loading stage) is adopted to predict the unloading response of the strengthened beams.

During unloading, the stress-strain response of the previously compressed concrete layers (upper layers) is assumed to follow a linear relationship starting from the unloading point A, as shown in Figure 6.9-a. The response of each layer follows a different unloading line depending on its distance from the neutral axis of the section, and on the compressive state of stress/strain previously attained in the initial loading stage. The slope of all unloading curves is assumed to be equal to the initial slope of the parabolic curve at the onset of loading. At the same time, the tensile stresses in the concrete lower layers that have not cracked diminish as the applied load is relieved. The response of these layers will continue on the linear portion of the concrete stress-strain relationship until the sustained load level is attained. Unloading of previously cracked layers follows an average stress-strain relationship represented by the unloading line J-O having a slope E_{un} less than E_c, as shown in Figure 6.9-b.

6.4.3 The post-tensioning stage: in-service beam

Sectional analysis — at the end of post-tensioning, the beam is subjected to a sustained load of 15 kN (25% of the beam yield load), along with an axial eccentric compressive force 120 kN (tendons force). The external moment on the section is thus computed as the sum of the moment resulting from the eccentricity of the tendon forces and the moment obtained from the sustained load. At this stage, the analysis is implemented by incrementally increasing the steel strain at midspan section, and iterating for the top fibre concrete strain until sectional force equilibrium is satisfied.

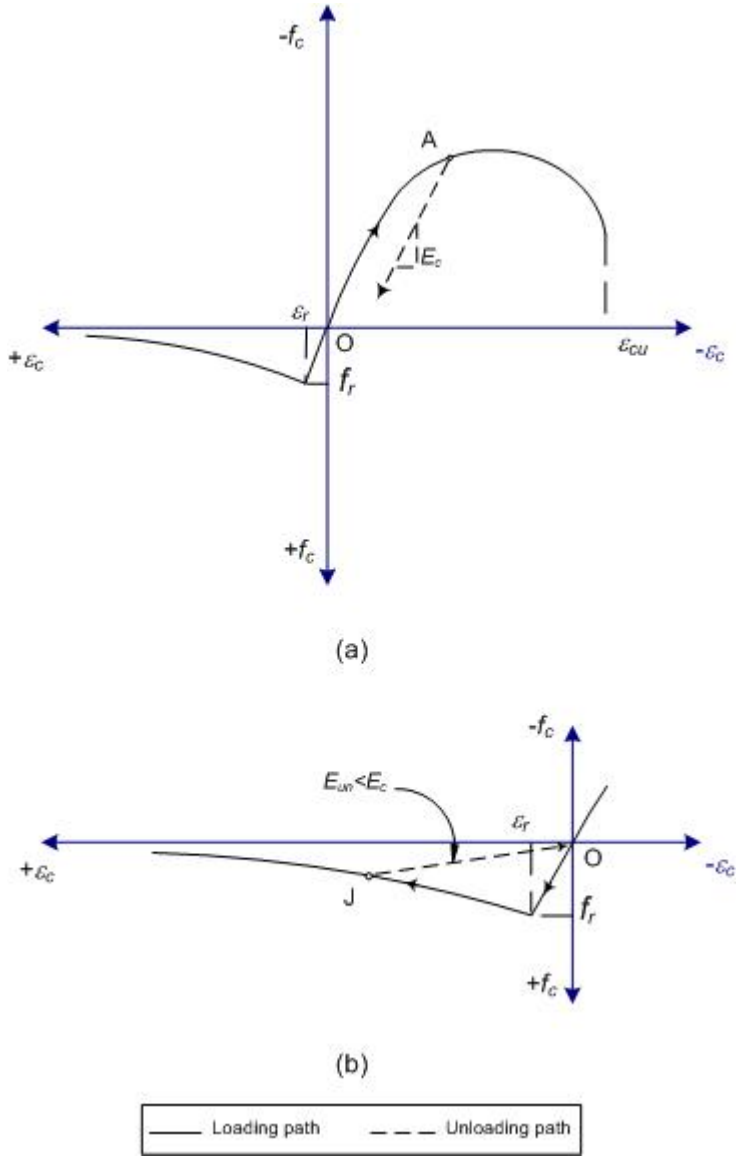

Figure 6.9: Unloading lines of (a) initially compressed and (b) initially cracked concrete layers

At this point, the internal and external moment values are compared. If moment equilibrium is satisfied, the curvature of midspan element, φ, is calculated. Knowing the applied loading pattern, the moment in each element outside the constant moment region is determined, and a similar procedure of analysis takes place to determine the deformation and the strains in both concrete and steel at all other elements. The curvature of an element, $\varphi_{(j)}$, is then calculated as given by Equation 6.11. The deflection of the beam at mid-span, Δ, is calculated by numerically integrating the curvature of the elements as given by Equation 6.12.

It is worth mentioning that the eccentricity of the draped tendons in the shear spans changes gradually along the beam length. The eccentricity of the tendon from the neutral axis for any element distant $x_{(j)}$ from the beam end is computed as follows (Figure 6.10):

$$e_{f(j)} = e_f \frac{x_{(j)}}{\left(\frac{L}{3}\right)} \quad for\ x_{(j)} \le L/3 \tag{6.13}$$

where:

$e_{f(j)}$ = the eccentricity of the tendon at element *j*;

e_f = the eccentricity of the tendon at mid-span, and;

L = the total length of the beam.

Knowing the eccentricity of the tendon at each element *j*, the depth of the tendon, $d_{f(j)}$, is computed as follows (Figure 6.10):

$$d_{f(j)} = e_{f(j)} + \frac{h}{2} \tag{6.14}$$

where h is the total height of the rectangular section.

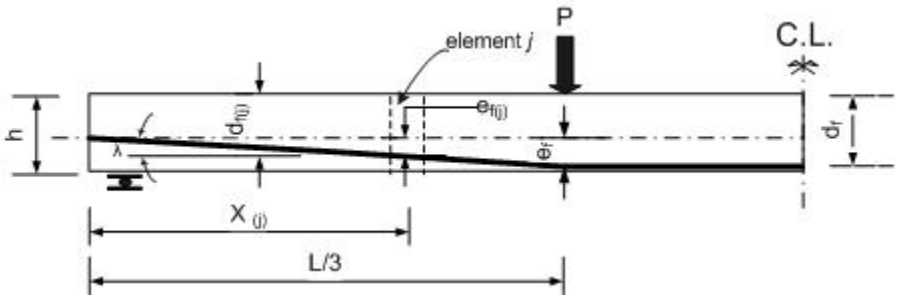

Figure 6.10: Variation of the tendon eccentricity and depth in the shear span

Concrete response — during post-tensioning, the tensile stresses in the cracked lower layers continue to diminish following the unloading linear path J-O (Figure 6.9-b). Compressive stresses will not develop until the previously formed cracks are closed. The cracks are assumed to be closed when the previously developed tensile strains in the concrete layers are completely reduced to zero. At this point, the concrete stresses will follow the parabolic stress-strain relationship, as compressive strains are developed during post-tensioning.

At the same time, the behaviour of the previously compressed upper concrete layers follows the unloading linear relationship A-B in Figure 6.11. The model accounts for the development of any tensile stresses in the upper layers as the applied post-tensioning force increases: if the post-tensioning force is large enough to produce tensile stresses in the upper layers, the unloading line A-B is extended linearly until the concrete reaches its rupture strength, f_r (point C). If cracking occurs, the average tensile stress in the upper layers (represented by the curve C-D) is accounted for, as explained in Section 6.3.1.

Steel response — the tensile stresses in the steel reinforcement diminish during the post-tensioning stage. The stress-strain response of the steel is represented by the sloped linear portion of the curve (Figure 6.8-a). Compressive strains may be developed in the steel depending on the amount of the post-tensioning force applied on the section.

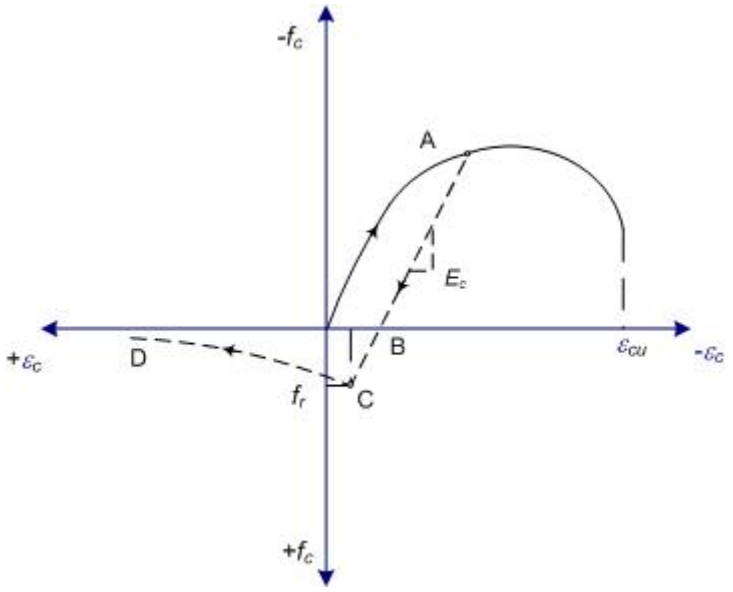

Figure 6.11: Post-tensioning path of the initially compressed upper concrete layers

6.4.4 The reloading stage: in-service beam

After being post-tensioned, the strengthened beam is reloaded gradually until failure occurs by concrete crushing. During this stage of loading, the analysis procedure is similar to that described in Section 6.4.1 (the initial loading stage). The strain in the steel reinforcement, ε_s, and the maximum compression strain in the concrete, ε_c, determined from the previous stage (the post-tensioning stage) are used as starting values for the reloading stage. Assuming a linear strain profile for the section, the neutral axis depth, c, is calculated from the strain compatibility between the concrete and steel reinforcement, as given by Equation 6.8. The corresponding concrete strain values at the midpoint of each layer are then computed, as given by Equation 6.9 (refer to Figure 6.3).

The strain in the CFRP external tendons at midspan section is determined based on the strain-reduction approach developed by Naaman (1990, 2005). The strain in concrete is thus iterated

until sectional equilibrium is satisfied. The internal moment is then determined, and the curvature of midspan section element, φ, is calculated. The analysis of the elements outside the constant moment region is thus carried out as described in Section 6.4.1. Note that the tendon force is considered constant at all beam elements.

CFRP tendons response — due to the lack of bond between the CFRP tendon and the surrounding concrete, the strain in the tendon at any load level during the reloading stage, is given as follows:

$$\varepsilon_f = \varepsilon_{fe} + \Delta\varepsilon_f \tag{6.15}$$

where:

ε_f = the strain in the tendon at any load level during the reloading stage;

ε_{fe} = the effective strain in the tendon due to the initial prestress, and;

$\Delta\varepsilon_f$ = the variation in the tendon strain due to load application.

Based on the strain-reduction approach developed by Naaman (1990, 2005), the strain variation in the unbonded tendon, $\Delta\varepsilon_f$, is determined at the critical section (section of maximum moment) assuming compatibility of strains between the concrete and the unbonded tendons, as if the tendons were bonded (refer to Section 2.5). A reduction factor, Ω, is applied to account for the fact that, for unbonded tendons, no strain compatibility exists between the tendon and the surrounding concrete at the critical section. The strain variation in the unbonded tendon is calculated as follows:

$$\Delta\varepsilon_f = \Omega\left(\varepsilon_{cf} - \varepsilon_{ce}\right) \tag{6.16}$$

where:

ε_{cf} = the strain in the concrete at the tendon level at the load level considered;

ε_{ce} = the strain in concrete at the tendon level due to effective prestress, and;

Ω = the strain reduction factor for unbonded tendons.

The strain-reduction coefficient, Ω, before cracking is taken equal to (5/9) for the draped tendon profile and (2/3) for the straight tendon profile (Naaman, 1990; Alkhairi, 1991; Harajli and Kanj, 1992; Naaman, 2005). Based on the findings of Harajli and Kanj (1992), the cracked coefficient, Ω_{cr}, in the current analysis is taken equal to its uncracked value, Ω (see Section 2.5). Once the average strain in the CFRP tendons is determined, the corresponding stress is obtained from the stress-strain relationship of the tendon material shown in Figure 6.8-b. The post-tensioning force is thus determined at each increment of the applied load.

Concrete response — during the reloading stage, compressive and tensile stresses are re-developed in the upper and lower concrete layers, respectively. If tensile stresses have developed in the upper layers due to post-tensioning, reloading will follow the linear unloading/post-tensioning path C-B-A until the original parabolic curve is rejoined at point A (Figure 6.12). If cracks have occurred in the upper layers, no compressive stresses are developed in these layers until point B is reached (Figure 6.12). In this case, reloading follows the path D-B having a slope $E_{rel(up)}$ that is less than E_c. At this point, the stress-strain relationship will follow the linear path B-A until the original parabolic curve is rejoined at point A (Figure 6.12). Note that the stress in concrete follows the parabolic curve until the limiting strain, ε_{cu}, is reached.

The lower layers that have been initially cracked during the first loading stage behave differently based on their stress-strain state at the end of post-tensioning. This is illustrated in Figure 6.13, where point J represents the end of the initial loading stage and point H represents the end of post-tensioning. If unloading followed by post-tensioning results in a tensile stress in the lower layer (Figure 6.13-a), reloading will commence from point H following the path H-J (having the same unloading slope; $E_{rel(low)} = E_{un}$) before rejoining the average tensile stress-strain

curve J-K at point J. On the other hand, if post-tensioning has produced compressive stress (point H on the parabolic curve in Figure 6.13-b), reloading follows the linear paths H-I and I-J. For each layer during the reloading stage, the path H-I has a slope equal to the initial concrete modulus, E_c, while the path I-J has a smaller slope defined by the points I and J. Beyond that, the average stress-strain curve J-K is rejoined at point J.

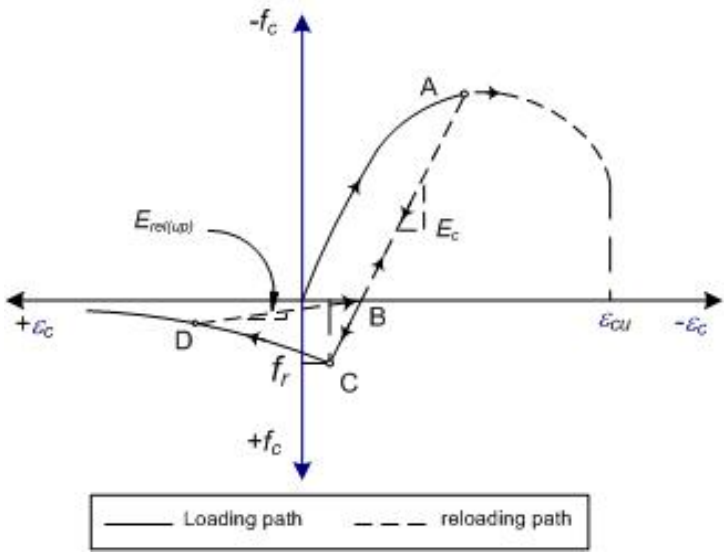

Figure 6.12: Behaviour of the initially compressed upper layers during the reloading stage

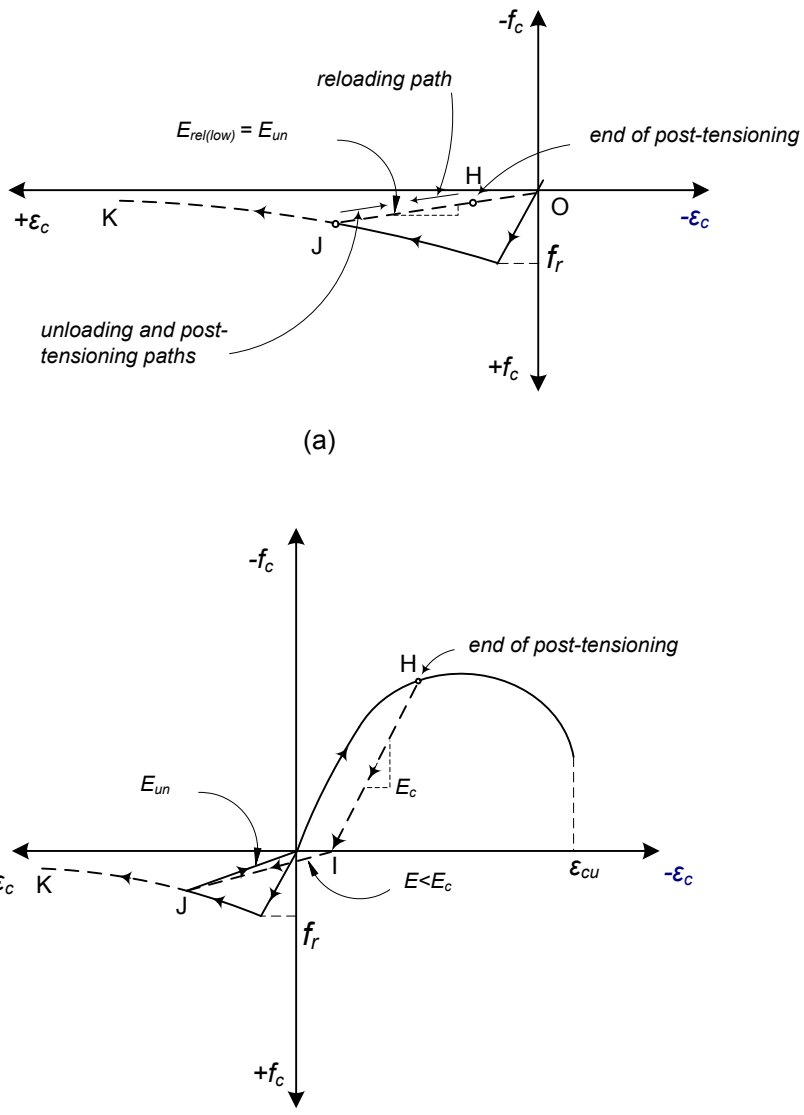

Figure 6.13: Behaviour of the initially cracked lower layers during the reloading stage

6.5 Proposed model for the overloaded beam

The analysis procedure for the in-service strengthened beams was adapted to model the monotonic response of the overloaded specimen. The difference between the two models lies in two main aspects:

1. The steel response during the unloading, post-tensioning, and reloading stages, and;
2. The CFRP tendon response during the reloading stage.

The procedure of analysis is summarized in the following sections. The differences between the analysis approaches of the in-service and overloaded beams are highlighted.

6.5.1 The initial loading stage: overloaded beam

During this stage, the beam is overloaded beyond the yield strain of the internal steel reinforcement. The analysis procedure in this stage does not differ from that described in Section 6.4.1 for the in-service strengthened beams, except that a limiting steel strain value of 4,000 με is set before unloading occurs. The steel response follows the stress-strain relationship previously shown in Figure 6.8-a. The stress-strain relationship of concrete shown in Figure 6.4 defines the concrete response during this stage.

6.5.2 The unloading stage: overloaded beam

The steel response of the overloaded beam conceptually differs from that encountered in the in-service beams. During unloading, the steel reinforcement of the in-service beams follows an inclined linear portion of the stress-strain relationship, as shown in Figure 6.8-a, where the elastic strains are completely recovered. This is not the case in the overloaded beams, where plastic strains exist in the steel reinforcement at midspan section due to overloading. The existence of

plastic strains causes the steel reinforcement to undergo a hysteresis response during the unloading stage, as shown in Figure 6.14. This hysteresis response is modeled using a Ramberg-Osgood function (Figure 6.14) as follows (Park and Paulay, 1975; Dowling, 1999):

$$\Delta\varepsilon_s = \frac{\Delta f_s}{E_s} + 2\left(\frac{\Delta f_s}{2k'}\right)^{\frac{1}{n'}} \tag{6.17}$$

where:

Δf_s = the change in steel stress at a certain level of loading;

$\Delta\varepsilon_s$ = the corresponding change in steel strain;

k' = the strength coefficient of the reinforcing steel material, and;

n' = the strain-hardening exponent of steel.

The coefficients k' and n' are taken as 922.41 and 0.1308, respectively, based on the results of fatigue tests carried out on similar steel samples (Al-Hammoud, 2006), as will be described later in Chapter 7.

The change in steel stress, Δf_s, and the corresponding change in steel strain, $\Delta\varepsilon_s$, are measured from an origin located at the onset of the unloading curve (point A in Figure 6.14). The actual steel stress and strain, f_s and ε_s, for any point K on the unloading portion of the curve (Figure 6.14) are thus computed as follows:

$$f_s = f_{sunl} - \Delta f_s \tag{6.18}$$

$$\varepsilon_s = \varepsilon_{sunl} - \Delta\varepsilon_s \tag{6.19}$$

where f_{sunl} and ε_{sunl} are the steel stress and strain at the onset of the unloading stage, respectively.

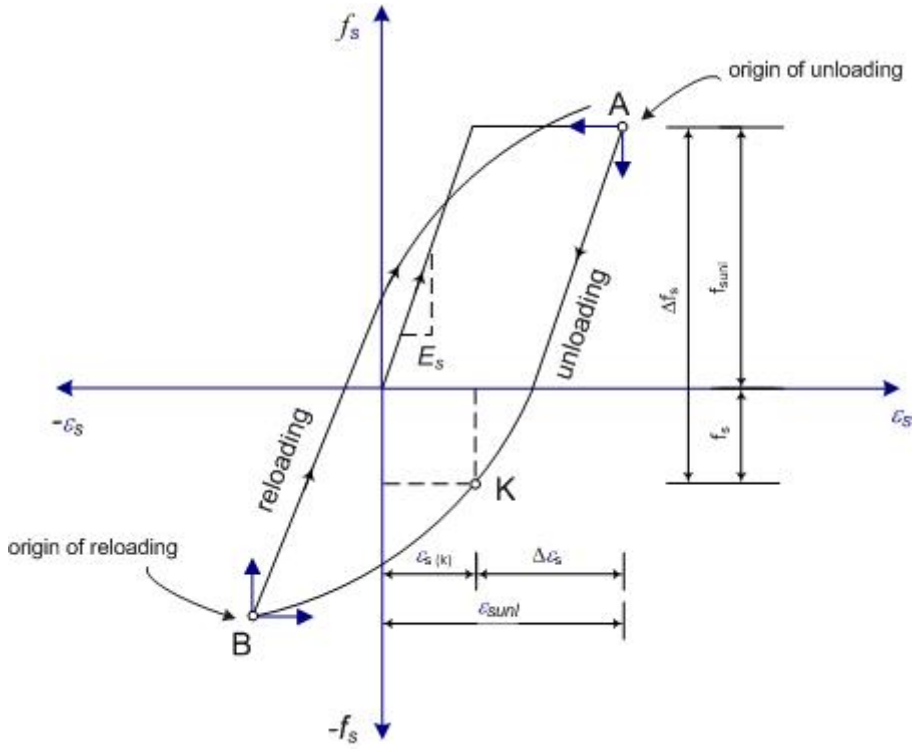

Figure 6.14: Steel response during unloading, post-tensioning, and reloading stages of the overloaded beam

The analysis is implemented by specifying the change in steel stress value, Δf_s, rather than the steel strain as in the case of the in-service beam. The change in the steel strain, $\Delta\varepsilon_s$, is then calculated from Equation 6.17, and the corresponding strain in the concrete top fibre is then iterated until the equilibrium state is satisfied. The analysis is thus carried out in a similar way as described in Section 6.4.2 for the unloading stage of the in-service beam. The concrete layer response during unloading of the overloaded beam is also similar to that described for the in-service beam (Section 6.4.2).

6.5.3 The post-tensioning stage: overloaded beam

During this stage, the steel response continues on the unloading curve A-B as shown in Figure 6.14. At the same time, the steel response in the elements outside the constant moment zone is elastic, and follows the stress-strain relationship shown previously in Figure 6.8-a. The response of the concrete layers during this stage is similar to that described for the in-service beams (Section 6.4.3). A similar method of analysis to that described for the in-service beams during post-tensioning is adopted.

6.5.4 The reloading stage: overloaded beam

Steel and concrete responses — after being post-tensioned, the strengthened beam is reloaded gradually until failure occurs by concrete crushing. During this stage of loading, the steel follows a curve similar to that of the unloading stage (Figure 6.14). The change in steel stress, Δf_s, and the change in strain, $\Delta \varepsilon_s$, given by Equation 6.17, are computed corresponding to a reference point located at point B (Figure 6.14). Point B represents the conclusion of the post-tensioning stage and the onset of reloading. A similar iterative procedure of analysis as described during the initial loading stages is then adopted. The response of concrete during this stage is similar to that described for the in-service beams (Section 6.4.4).

CFRP tendons response — due to overloading, concrete cracks are not completely closed after the post-tensioning force has been applied. Hence, the assumption that the gross moment of inertia of the concrete section is completely effective (as implied by Equation 6.20) is not accurate.

$$\Omega_{cr} \approx \Omega \frac{I_{cr}}{I_g} \tag{6.20}$$

The moment of inertia of the section at the onset of the reloading stage of the overloaded strengthened beam is less than the gross moment of inertia of the virgin beam. Thus, Equation 6.20 would underpredict the strain reduction coefficient, Ω_{cr}, and consequently, will underpredict the strain increase in the CFRP external tendons. Hence, a new moment of inertia, I_{ps}, defined as the moment of inertia of the section at the end of the post-tensioning process, is proposed to replace I_g in Equation 6.20, and is calculated as follows:

$$I_{ps} = \frac{bc_{ps}^{3}}{3} + \Omega_{cr} n_f A_f (d_f - c_{ps})^2 + n_s A_s (d_s - c_{ps})^2 \tag{6.21}$$

$$n_f = \frac{E_f}{E_c} and\, n_s = \frac{E_s}{E_c} \tag{6.22}$$

where:

b = the width of the concrete rectangular section;

c_{ps} = the neutral axis depth of the section at the end of post-tensioning stage;

A_f = the area of the CFRP tendons;

A_s = the area of the steel reinforcing bars;

n_f = the modular ratio for CFRP;

n_s = the modular ratio for steel, and;

d_f = the depth of the CFRP external tendons.

Thus, for the overloaded beam, the strain reduction coefficient Ω_{cr}, is calculated by Equation 6.23:

$$\Omega_{cr} = \Omega \frac{I_{cr}}{I_{ps}} \tag{6.23}$$

It is also noted that the cracked moment of inertia is determined about the neutral axis of the section as follows:

$$I_{cr} = \frac{bc^3}{3} + \Omega_{cr} n_f A_f (d_f - c)^2 + n_s A_s (d_s - c)^2 \tag{6.24}$$

where c is the depth of the neutral axis at any stage of loading beyond the cracking load of the strengthened beam.

Since the moments of inertia, I_{cr} and I_{ps} both depend on the value of Ω_{cr}, another level of iteration is thus adopted to calculate Ω_{cr} for any given values of steel and concrete strains. Starting with Ω_{cr} equal to Ω as an initial approximation, and knowing the neutral axis depth, c, the moments of inertia, I_{cr} and I_{ps}, are calculated. The strain-reduction coefficient, Ω_{cr}, is then calculated using Equation 6.23, and the process is repeated until the values obtained in two successive iterations are equal within a specified degree of tolerance.

6.6 Computer program

The analytical models of the in-service and overloaded strengthened beams were implemented into a computer program called AEPT (Analysis of Externally Post-Tensioned beams). The geometric and material properties used in the models were based on the experimental data reported in Chapter 4. The main algorithm of the program consists of a range of procedures corresponding to the different stages of loading. Each procedure is broken down into two subroutines: one for the programming tasks at the mid span section (critical section), and the other for the calculations at the elements outside the constant moment region. Figures 6.15 to 6.18 show the flowcharts of the main algorithm of the loading, unloading, post-tensioning, and the reloading procedures for the in-service strengthened beams. The algorithms of the overloaded post-tensioned beams are similar to that of the in-service beams (as described in Section 6.5) and hence are not presented. Figure 6.19 shows the algorithm for calculating the strain-reduction coefficient, Ω_{cr}, for the overloaded beams, as explained in Section 6.5.4.

In the AEPT program, the input data consists of the beam geometry, the area of the steel reinforcement, the area of the CFRP tendons, the post-tensioning force, and the material properties of the concrete, steel, and CFRP tendons. The output results are stored in spreadsheet files where the relationships between the applied load and various material straining and deflections are plotted.

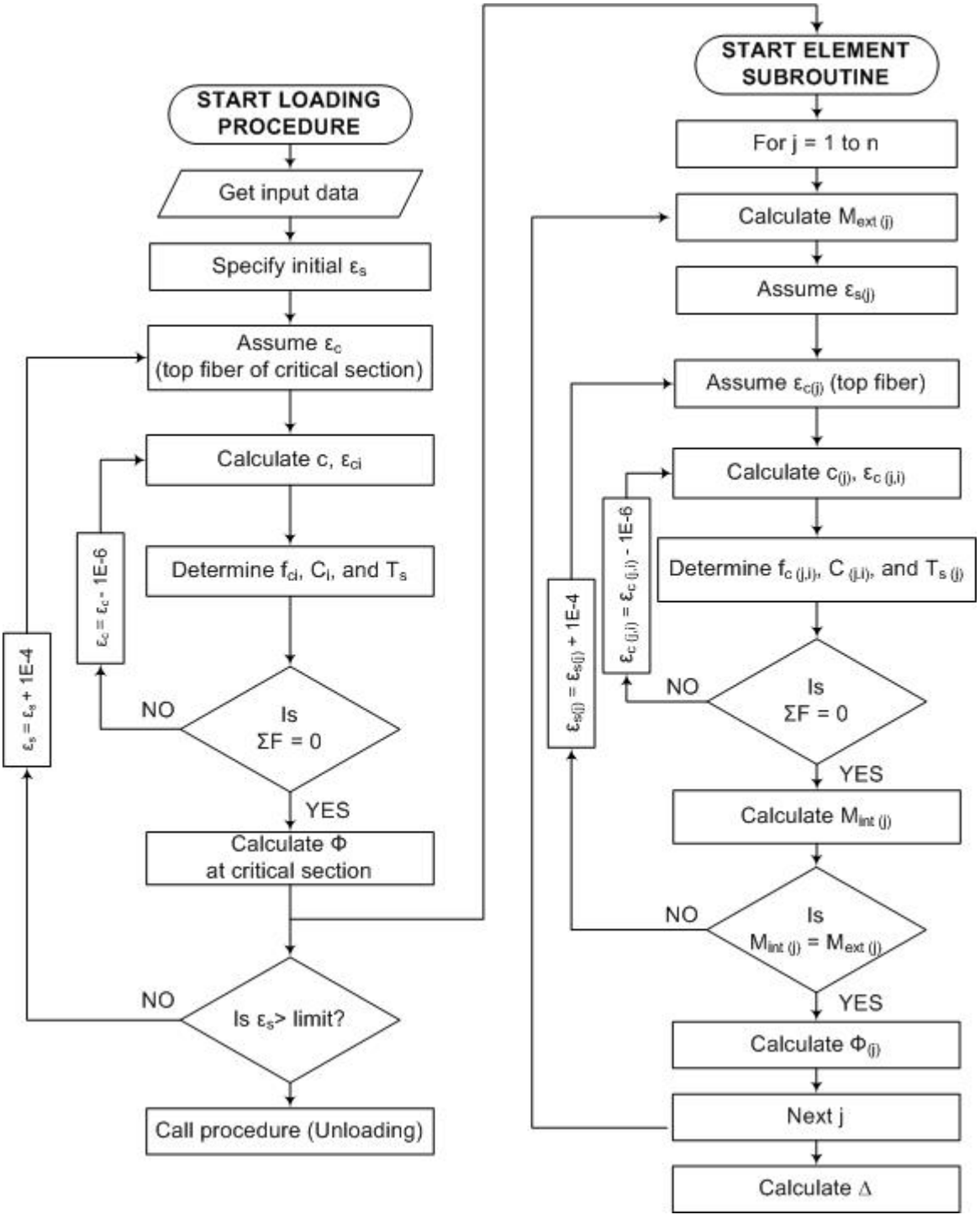

Figure 6.15: Flow chart for the loading procedure (prior to strengthening)

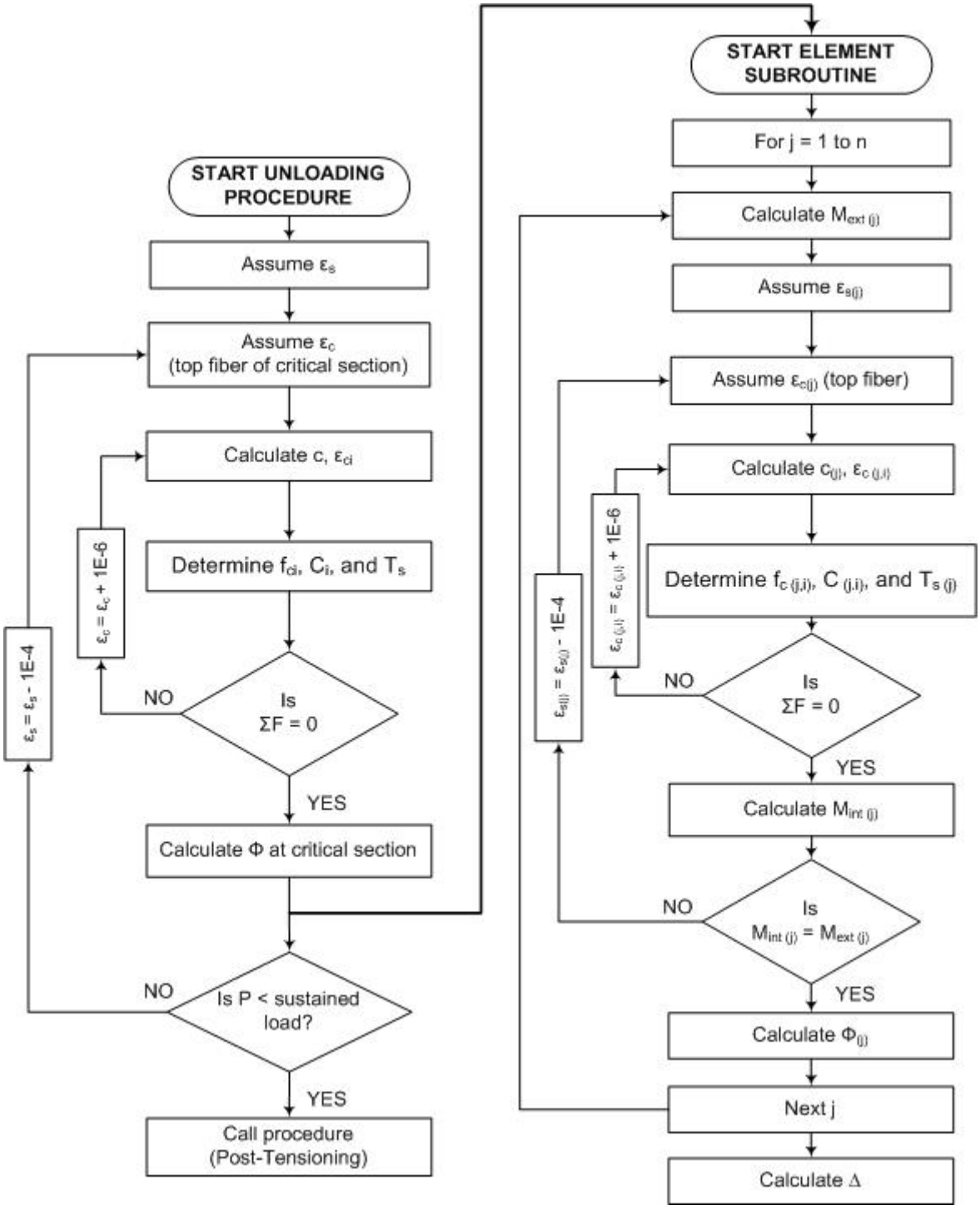

Figure 6.16: Flow chart for the unloading procedure

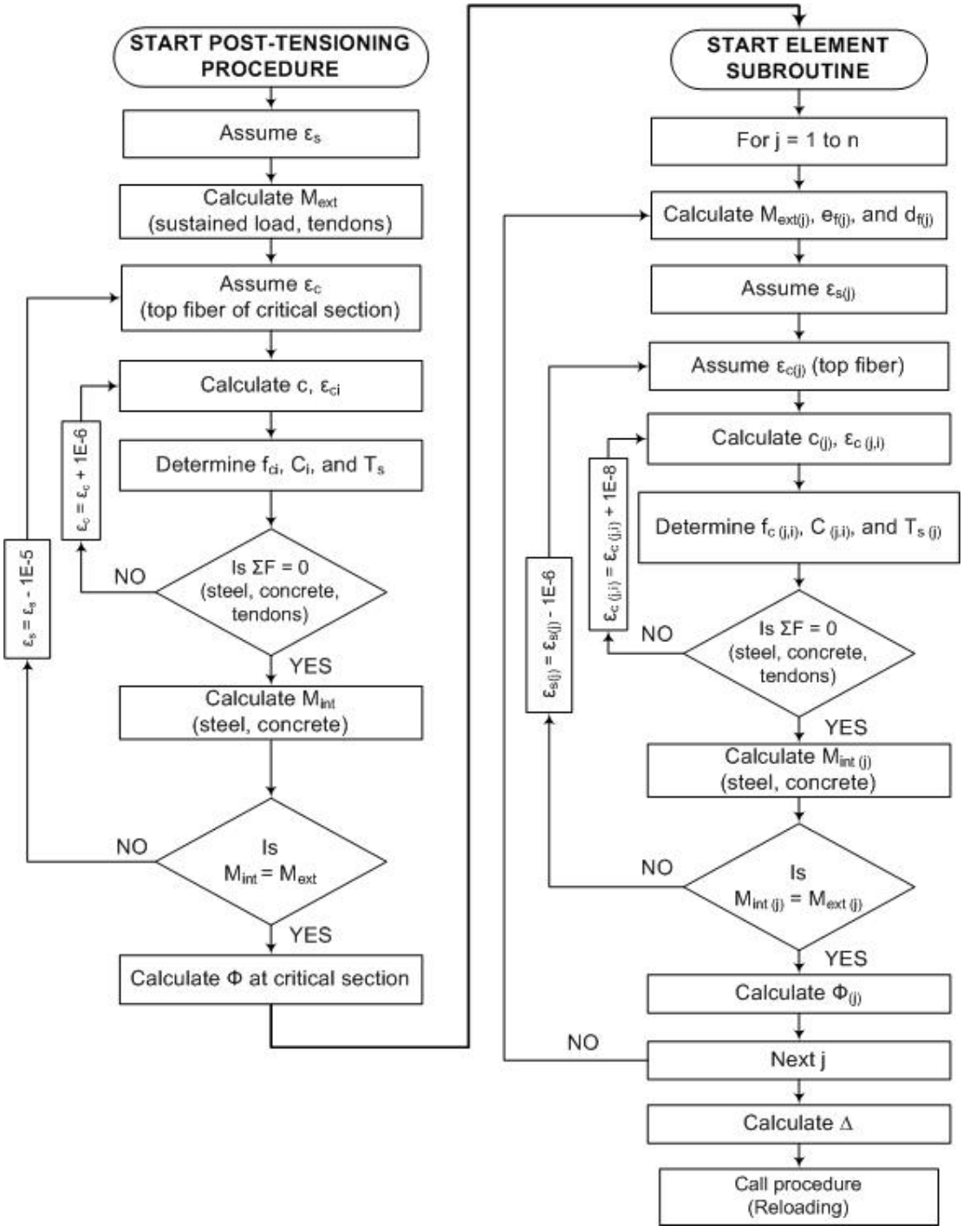

Figure 6.17: Flow chart for the post-tensioning procedure

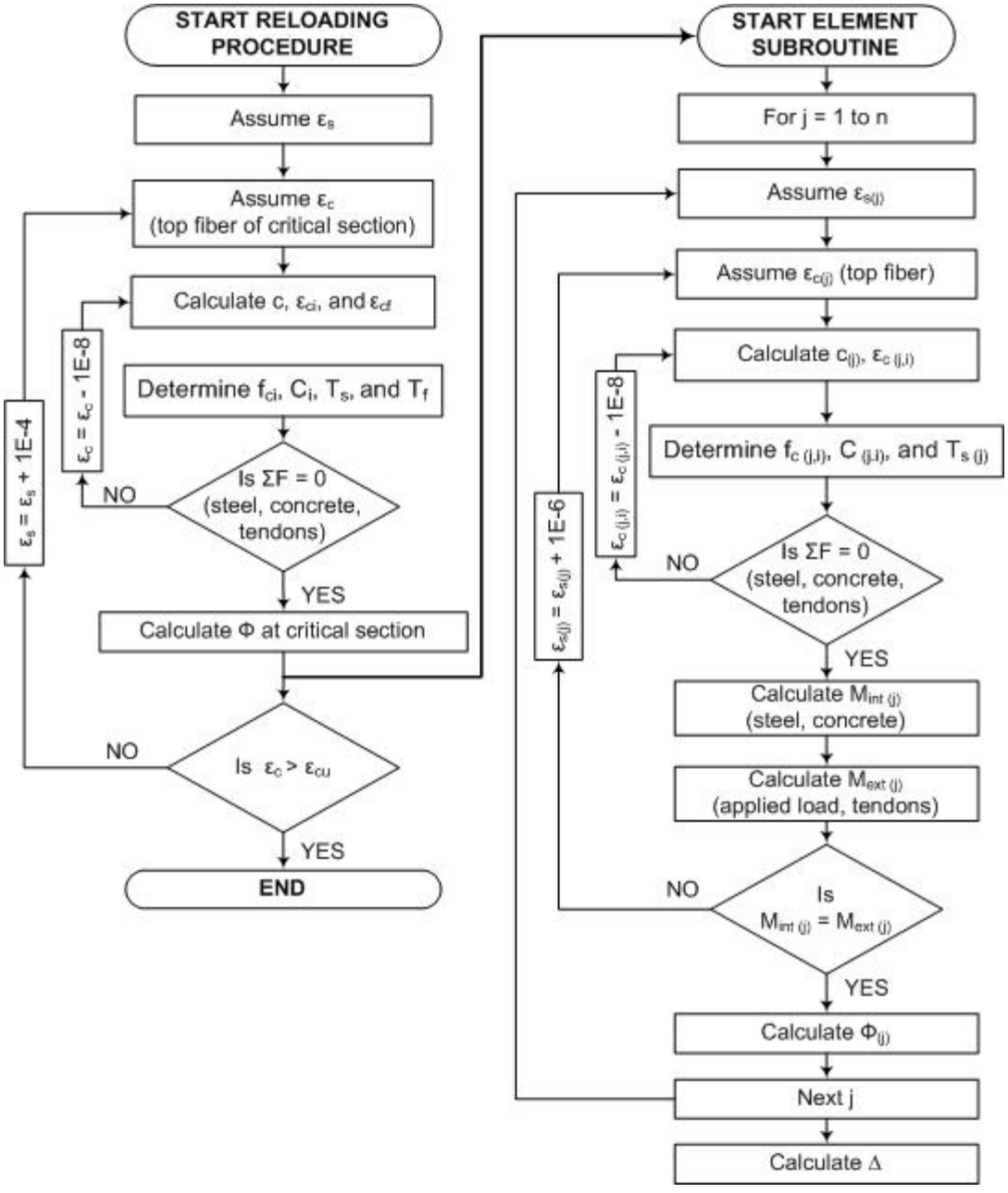

Figure 6.18: Flow chart for the reloading procedure

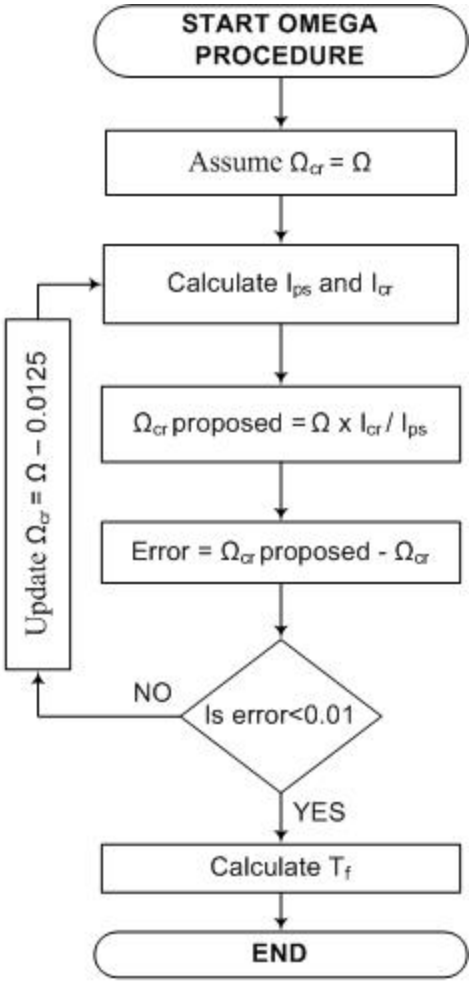

Figure 6.19: Flow chart of the calculation of the cracked strain-reduction coefficient, Ω_{cr}, for overloaded beams

6.7 Analysis results

A comparison between the experimental and analytical results was carried out to examine the accuracy of the model in predicting the flexural response of strengthened beams with two different load histories prior to strengthening. Figure 6.20 shows the relationships between the applied load and the midspan deflections at various stages of loading for the in-service and the overloaded beams. Figure 6.21 compares the experimental and analytical stresses in the CFRP external tendons for the strengthened beams. Average values of stresses in the CFRP tendons were calculated from the readings of the load cells used in the tests. Steel and concrete strains at the mid-section of the beam are also predicted and compared to the strain gage readings in Figure 6.22 and Figure 6.23, respectively.

A good correlation between the experimental and the analytical results is observed in all aspects. Table 6.1 compares the experimental and analytical values of the yield and ultimate loads for the strengthened beams. For the in-service strengthened beam, the model predicted the yield and ultimate loads within +1%, while for the overloaded beam, the predicted values are within +6% to +7% higher than the experimental values.

It is worth mentioning that the variation between the experimental and predicted strains in steel can be attributed to the fact that the gage readings were usually affected by their positions on the steel bars. For instance, a gage bonded to an embedded steel bar would give higher readings if it is located near a rib or a flexural concrete crack, where stress concentrations are likely to occur. A similar situation occurs in case of a gage located on the concrete surface. The readings of the gage are influenced by the presence of any irregularities on the finished concrete surface, the depth of the section at the location of the gage, and its location relative to flexural cracks.

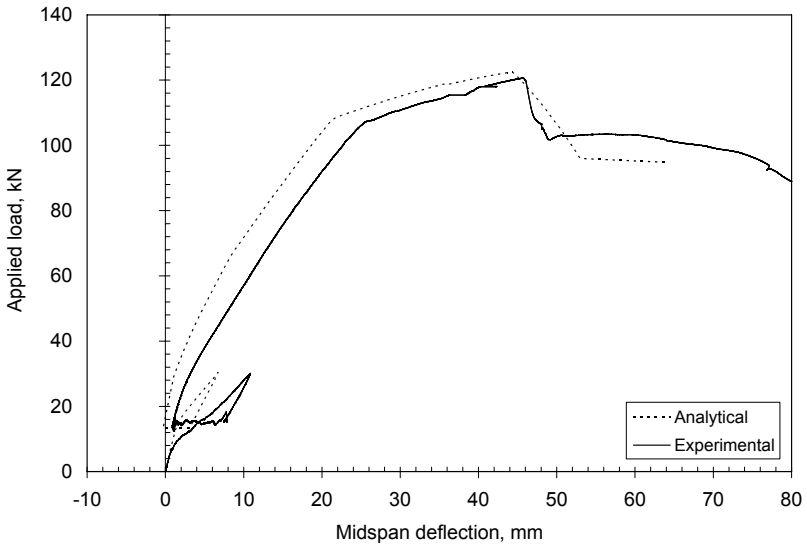

(a)

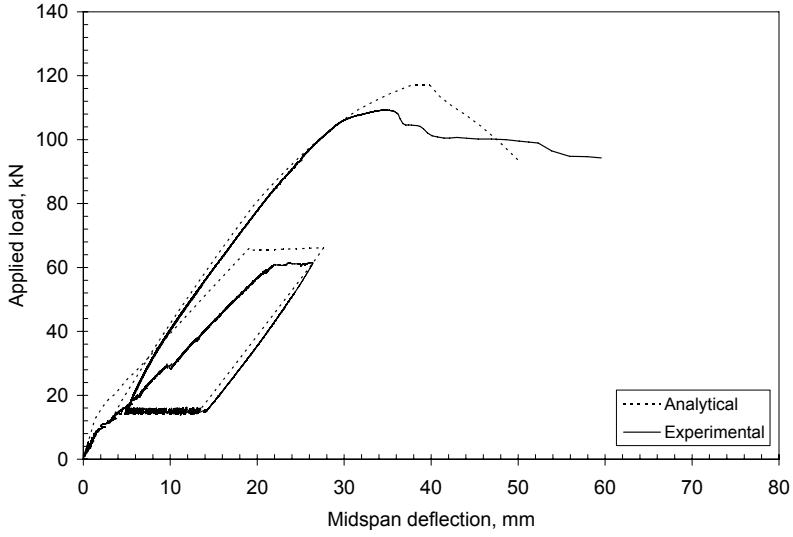

(b)

Figure 6.20: Predicted versus experimental midspan deflection for the (a) in-service strengthened beam and the (b) overloaded beam strengthened beam

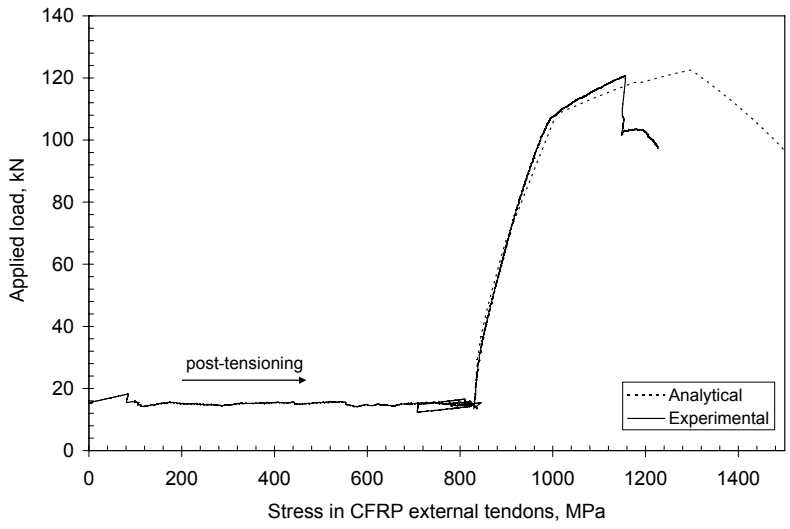

(a)

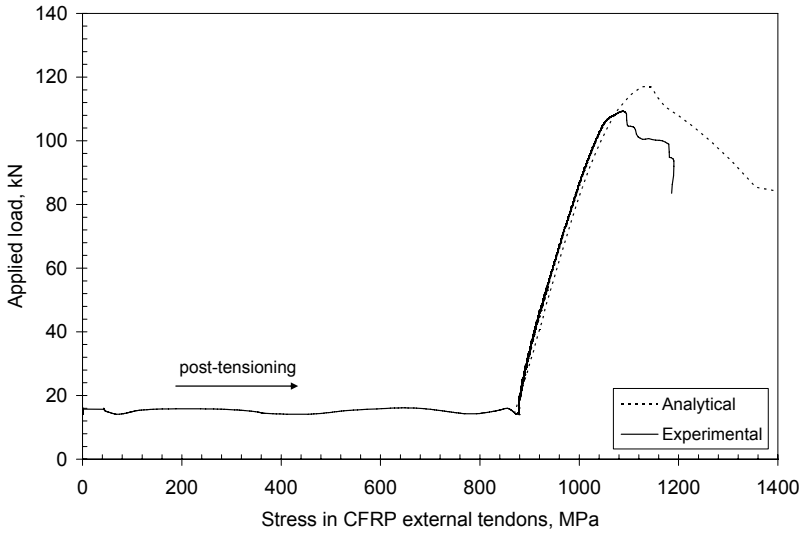

(b)

Figure 6.21: Predicted versus experimental force in the CFRP external tendon for the (a) in-service strengthened beam and the (b) overloaded strengthened beam

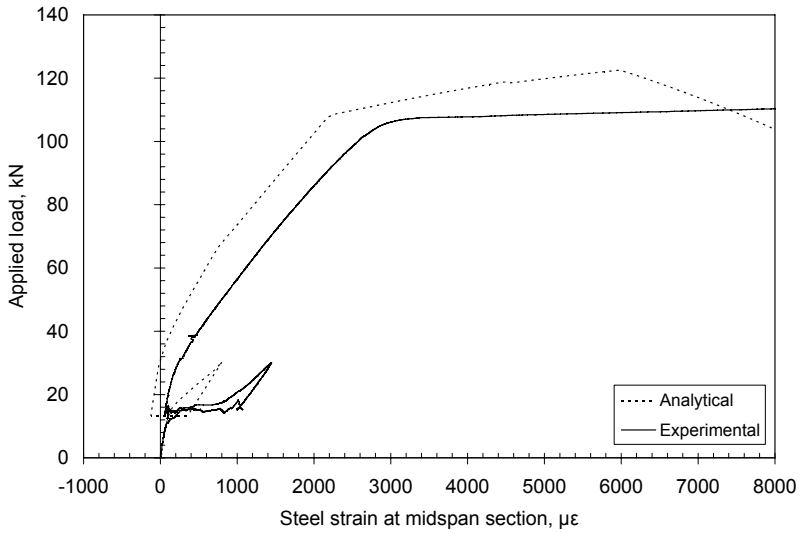

(a)

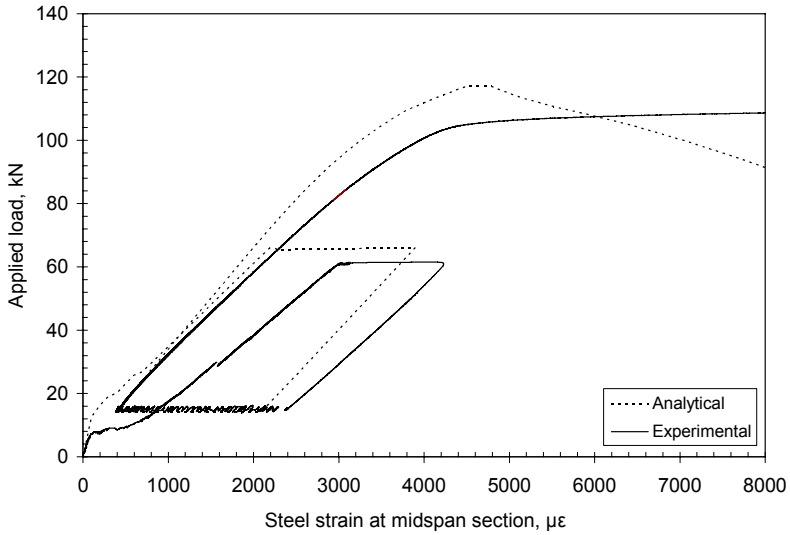

(b)

Figure 6.22: Predicted versus experimental steel strain for the (a) in-service strengthened beam and the (b) overloaded strengthened beam

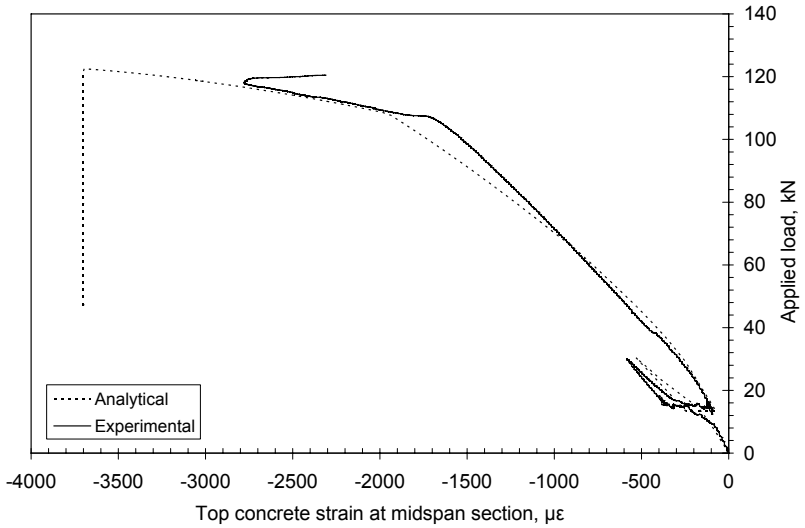

(a)

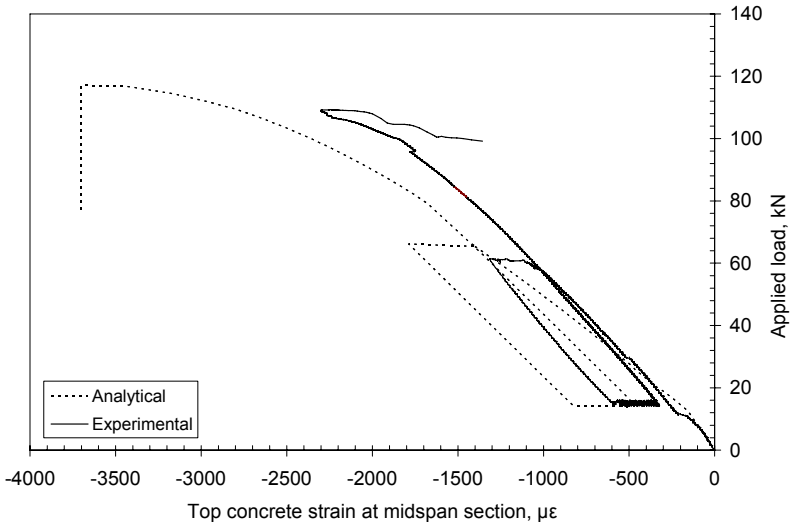

(b)

Figure 6.23: Predicted versus experimental top concrete strain for the (a) in-service strengthened beam and the (b) overloaded strengthened beam

Table 6.1: Predicted versus experimental yield and ultimate loads of the in-service (SL15) and overloaded (OL15) beams

Beam	Yield load (kN)			Ultimate load (kN)		
	Pred.	Exp.	Pred. / Exp.	Pred.	Exp.	Pred. / Exp.
SL15-beam	108.7	108	1.01	122	120	1.01
OL15-beam	116.0	108	1.07	116	109	1.06

Chapter 7

Fatigue Life Prediction for Beams

7.1 General

The fatigue tests carried out on the beam specimens showed that the fatigue life of the majority of the beams was limited by the fatigue fracture of the tensile reinforcing bars. As observed during the tests, the fracture of the bar always occurred at the root of a rib or deformation on the surface of the bars. These ribs acted as stress raisers, and resulted in a significant stress concentration that reduced the fatigue life of the bar. Plastic deformations developed in these localized regions initiated the fatigue crack in the steel. With an increasing number of cycles, the crack grew until the bar fractured. Therefore, a fatigue notch analysis is used herein to quantify the effect of the bar ribs on its fatigue life.

The fatigue model is based on a strain-life approach. The approach takes into consideration the stress-strain history of the reinforcing bar during the fatigue life of the beam, as well as the stress-strain history of the bar prior to strengthening with CFRP external tendons. Plastic deformations that might occur at the root of the ribs are determined. The details of the approach are given in the following sections. A comparison between the experimental and analytical results obtained from the model is presented to evaluate its applicability and accuracy.

7.2 Fatigue model for strengthened beams

The fatigue model for the strengthened beams aims to predict the fatigue life of the beams taking into consideration two aspects:

- The stress increase in the tensile reinforcing steel bars embedded in the concrete at crack locations, and;
- A strain-life approach that accounts for inelastic deformations at the ribs during cycling.

In the following sections, the two components of the fatigue model are described.

7.2.1 Stress increase in the steel at crack locations

Observations of the tested specimens indicated that the fatigue cracks in the steel bars developed at the base of the ribs, near the locations where flexural cracks developed in the beams. Before cracking of the concrete, the bond between the steel bar and the surrounding concrete allowed the transfer of some tensile force from the concrete to the bar. As such, the force applied in the tensile zone was carried by both steel and concrete. When flexural cracks initiated with an increase in the applied load, the tensile force at the crack locations was carried only by the steel bars. Consequently, in the region of constant moment, the stress developed in the steel bars at a cracked section was higher than the stress developed in an adjacent uncracked section (refer to Figure 6.5). Fatigue cracks in the steel bar were thus likely to initiate at these highly stressed locations.

The monotonic analysis described in Chapter 6 takes into account the tension stiffening in the concrete regions between the cracks (Section 6.3). As such, the monotonic analysis evaluates the *average* stress in the steel bar rather than the *peak* stress that occurs at the flexural crack locations. The model is implemented by following the stress-strain relationships of the

constituent materials during the various stages of loading applied, using a layer-by-layer evaluation of the section forces (Sections 6.4 and 6.5).

The monotonic analysis implemented in the proposed fatigue model is conceptually similar to the model described in Chapter 6, except that it accounts for the increased stress in the steel bar at a cracked section. The modified model determines the stress in the steel bar at cracked section locations (peak stress) rather than the average stress in the bar. The model neglects the tension stiffening effect of the concrete between cracks. Concrete in tension is assumed to be effective only before cracking occurs and, after cracking, the tensile stresses in the concrete are neglected.

On the other hand, during cyclic loading of the beam, the concrete surrounding the steel reinforcing bars between the cracks is subjected to tensile fatigue loading. This type of loading causes the concrete to crack at a smaller stress than the static tensile strength (ACI-215, 1997), as given by Equation 6.3, repeated in Equation 7.1. This was indicated by the development of new cracks and the propagation of the existing cracks during the fatigue life of the beams. As such, a lower-bound reduced concrete tensile strength, $f_{r(red)}$, given by AASHTO-A5.5.3.1 (1994) is used in the proposed fatigue model, as given by Equation 7.2:

$$f_r = 0.60\sqrt{f_c'} \tag{7.1}$$

$$f_{r(red)} = 0.25\sqrt{f_c'} \tag{7.2}$$

The reduced concrete tensile strength represents 40% of its static tensile strength and is intended to account for the reduction in tensile strength that occurs under repeated vehicle loads on a bridge. The modified monotonic analysis is then implemented in a strain-based fatigue approach to predict the fatigue life of the reinforcing steel bars. This is explained in the following sections.

7.2.2 Strain-life analysis for the reinforcing steel

The strain-life analysis for the reinforcing steel bars necessitates the following:

- The determination of the cyclic stress-strain curve of the steel;
- The determination of the relationship between the strain amplitude applied to the steel bar and its fatigue life (strain-life curve);
- The determination of the local stress-strain history at the root of the ribs of the steel bar during cycling, and;
- The determination of the fatigue life of the steel taking into account the mean stress applied.

The analysis is as follows:

7.2.2.1 Cyclic stress-strain curve of the steel

The behaviour of the steel reinforcing bar under fatigue loading differs from its behaviour when it is subjected to monotonic loading. Under fatigue loading, the relationship between the stress in the bar and the corresponding strain is defined by the cyclic, rather than the monotonic, stress-strain curve. The cyclic stress-strain curve is a property of steel, usually determined by testing smooth-machined specimens under constant, fully-reversed strain amplitude cycles. The stresses induced in the steel specimens generally change as the number of the cycles increased. This is known as the cycle-dependent softening or cyclic-dependent hardening (Dowling, 1999). These changes usually occur in the early stages of life after which the hysteresis loops stabilize. Typically, the stress and strain data at the half-life of the specimens are recorded, and the points of maximum stress and strain of the stabilized hysteresis loops (known as the loop tips) are connected to form the cyclic curve, as shown in Figure 7.1.

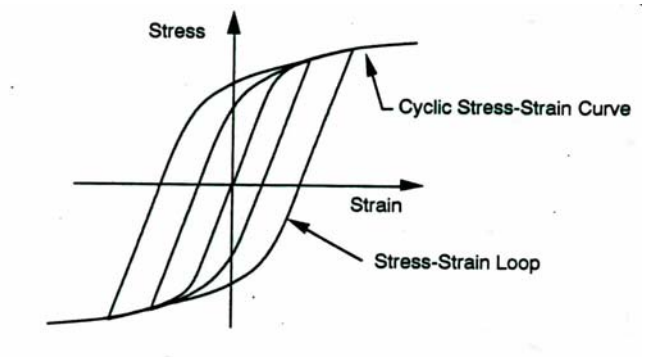

Figure 7.1: Cyclic stress-strain curve obtained by connecting tips of stabilized hysteresis loops (Bannantine et al., 1990)

The cyclic stress-strain curve is described by the Ramberg-Osgood equation as follows:

$$\varepsilon = \frac{\sigma}{E_s} + \left(\frac{\sigma}{k'}\right)^{\frac{1}{n'}} \tag{7.3}$$

where E_s is the modulus of elasticity of steel, k' is the cyclic strength coefficient, and n' is the cyclic strain-hardening exponent. The constants k' and n' are determined by plotting the true cyclic stress versus the true cyclic plastic strain on a logarithmic scale, as shown schematically in Figure 7.2. The slope of the straight line obtained represents n', and the intercept at a strain equal to unity represents k'.

Cyclic tests were carried out at the University of Waterloo on machined steel specimens produced from reinforcing bars similar to those used in this study (Al-Hammoud, 2006). From these tests, the values of k' and n' were reported as 922.41 MPa and 0.1308, respectively (Figure 7.3). Using these data, the cyclic stress-strain curve of steel was obtained.

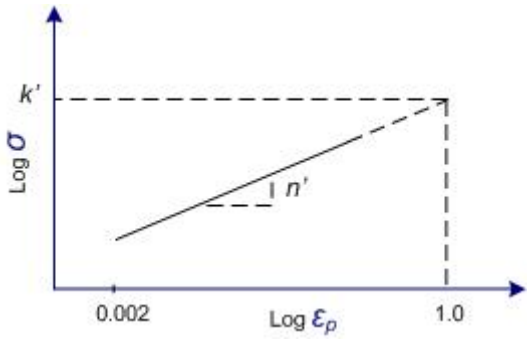

Figure 7.2: True cyclic stress versus true cyclic plastic strain (Bannantine et al., 1990)

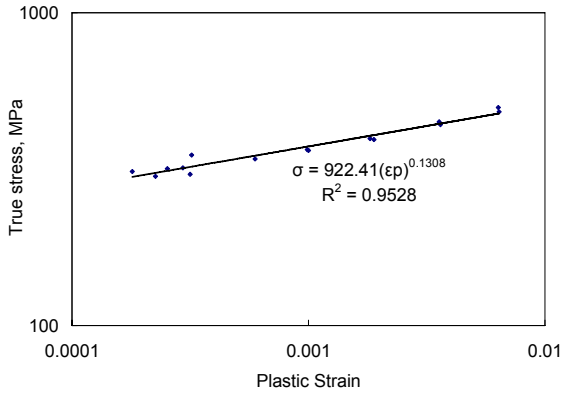

Figure 7.3: True cyclic stress versus true cyclic plastic strain for steel (Al-Hammoud, 2006)

7.2.2.2 Strain-life curve

The strain-life curve is a relationship between the strain amplitude, $\Delta\varepsilon/2$, and the number of cycles to failure, *N*. The curve is determined by testing smooth-machined steel specimens under fully-reversed strain amplitudes. The number of cycles to failure is then recorded for each strain amplitude applied. The data obtained from these tests are then plotted on a logarithmic scale, as shown schematically in Figure 7.4 (total strain curve).

The strain amplitude applied to the steel specimens is divided into elastic and plastic parts, as shown in Figure 7.5. This is expressed in Equation 7.4 (Bannantine et al., 1990):

$$\frac{\Delta\varepsilon}{2} = \frac{\Delta\varepsilon_e}{2} + \frac{\Delta\varepsilon_p}{2} \tag{7.4}$$

where the suffix "e" refers to the elastic strain and the suffix "p" refers to the plastic strain. The elastic part represents the relationship between the elastic stress and strain, in terms of the modulus of elasticity of steel, E_s, as follows:

$$\frac{\Delta\varepsilon_e}{2} = \frac{\Delta\sigma_e}{2E_s} \tag{7.5}$$

The plastic part represents the inelastic part of the hysteresis loop. As shown in Figure 7.5, it represents the width of the loop.

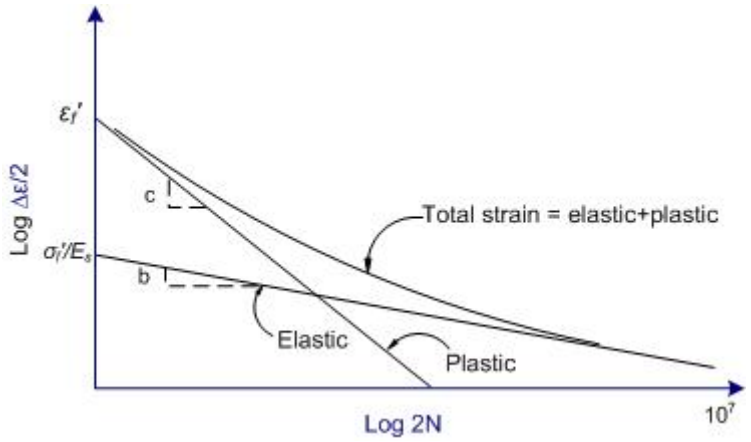

Figure 7.4: Strain-life relationship (adapted from Bannantine et al., 1990)

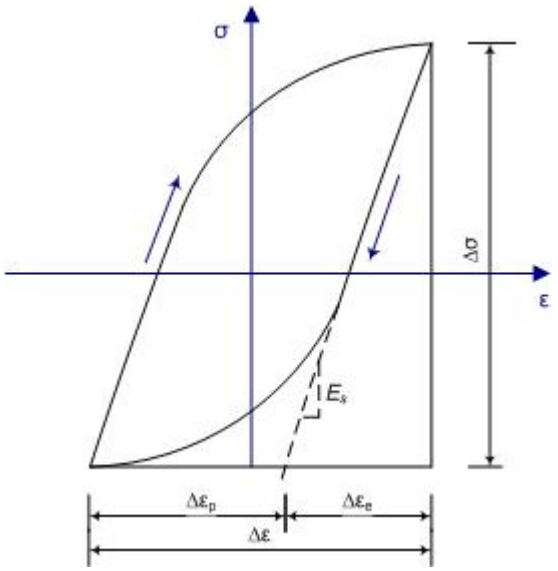

Figure 7.5: Hysteresis loop (adapted from Bannantine et al., 1990)

Linear relationships between the number of cycles to failure and both the elastic and plastic strain amplitudes are usually plotted with the strain-life curve. This is shown schematically in Figure 7.4. The slopes of the lines and their intersections with the strain axis are determined from the test data recorded at half-life of the tested specimens, when the hysteresis loops are stabilized.

These relationships are defined as follows:

$$\frac{\Delta\varepsilon_e}{2} = \frac{\sigma_f^{'}}{E_s}(2N)^b \tag{7.6}$$

$$\frac{\Delta\varepsilon_p}{2} = \varepsilon_f^{'}(2N)^c \tag{7.7}$$

where σ_f' is the fatigue strength coefficient, ε_f' is the fatigue ductility coefficient, b is the fatigue strength exponent, c is the fatigue ductility exponent, and N is the number of cycles to failure (see Figure 7.4).

Equation 7.4 can then be rewritten as:

$$\frac{\Delta\varepsilon}{2} = \frac{\sigma_f^{'}}{E_s}(2N)^b + \varepsilon_f^{'}(2N)^c \tag{7.8}$$

In order to determine the values of the coefficients of Equation 7.8, the fatigue test results reported by Al-Hammoud (2006) are used. A relationship between the applied strain amplitudes and the obtained number of reversals, *2N*, is shown in Figure 7.6. A regression analysis is used to estimate the values of the coefficients of Equation 7.8. These values are given in Table 7.1.

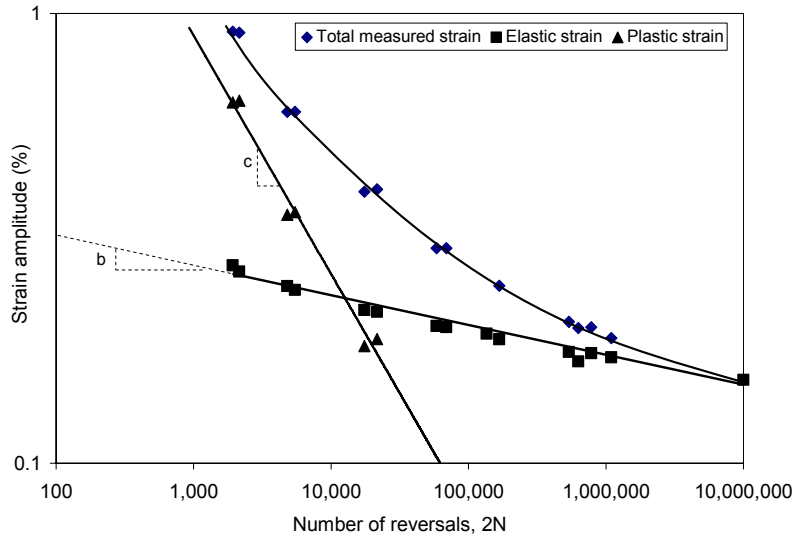

Figure 7.6: Strain-life data for steel as reported by Al-Hammoud (2006)

Table 7.1: Reinforcing steel fatigue properties (Al-Hammoud, 2006)

	Equation (7.8)			
Coefficient	σ'_f(MPa)	ε'_f(με)	b	c
Value	847.87	0.3603	-0.07476	-0.534

7.2.2.3 Local stresses and strains

The nominal stress, S, is the engineering stress applied to the steel bar as obtained from the concrete section analysis. As previously mentioned, stress concentrations occur at the root of the ribs of the steel reinforcing bar. If the applied nominal stress in the bar, S, is elastic, and no yielding occurs at the ribs, the localized stress, σ, and strain, ε, are related to the nominal values by the elastic stress concentration factor, K_t, as given by Equations 7.9 and 7.10, respectively. Note that, in order to be consistent with the notation used in the fatigue literature, the labels S and e will be used throughout this chapter to refer to the *nominal* stress and *nominal* strain in steel instead of f_s and ε_s used in Chapter 6. The labels σ and ε will be used to refer to the *local* stress and the *local* strain in steel.

$$\sigma = K_t S \tag{7.9}$$

$$\varepsilon = K_t \frac{S}{E_s} \tag{7.10}$$

The stress concentration factor depends on the geometry of the rib and the mode of loading applied. If plastic deformations occur at the roots of the ribs, Equations 7.9 and 7.10 are no longer valid. In this case, other methods that relate the local stress and strain at the root of the ribs to the nominal values, such as Neuber's rule, should be used. The procedure used in the analysis is as follows:

Local stress-strain during the initial loading cycle — for the initial loading, the maximum nominal stress, S_{max}, and the corresponding nominal strain, e_{max}, are determined from the modified monotonic analysis, as discussed in Section 7.2.1. Neuber's rule relates the local stress, σ_{max}, and the local strain, ε_{max}, at the root of the ribs, to the maximum nominal stress and nominal

strain, S_{max} and e_{max}, by a hyperbolic relationship, as shown in Figure 7.7. This relationship is expressed as follows (Bannantine et al., 1990):

For elastic nominal behaviour:

$$\sigma_{\max}\varepsilon_{\max} = \frac{\left(K_t S_{\max}\right)^2}{E_s} \tag{7.11}$$

For plastic nominal behaviour:

$$\sigma_{\max}\varepsilon_{\max} = \left(K_t\right)^2 S_{\max} e_{\max} \tag{7.12}$$

Topper et al. (1969) proposed replacing the stress concentration factor, K_t, in Equations 7.11 and 7.12 by the fatigue notch factor, K_f, defined as the ratio of the unnotched fatigue strength to the notched fatigue strength. The fatigue notch factor, K_f, gives smaller fatigue strength reduction than that obtained using the stress concentration factor, K_t, when small radius notches are present, as is the case for the ribs of the reinforcing bars. This agreed well with actual test data, as reported by Dowling (1999). The estimation of the fatigue notch factor from the beam fatigue tests will be explained later in Section 7.3.1.

Once the applied nominal stress-strain state in the steel bar is determined from the monotonic analysis, the product of the local stress and strain is estimated from Equations 7.11 or 7.12. The local stress, σ_{max}, and the local strain, ε_{max}, also satisfy the cyclic stress-strain relationship given by Equation 7.3. Combining Equations 7.3 and 7.12, a closed form solution for the stress and strain at the rib root is expressed as follows (using the fatigue notch factor, K_f):

$$\sigma_{\max}\left[\frac{\sigma_{\max}}{E_s} + \left(\frac{\sigma_{\max}}{k'}\right)^{\frac{1}{n'}}\right] = \left(K_f\right)^2 S_{\max} e_{\max} \tag{7.13}$$

Equation 7.13 represents the intersection of the cyclic stress-strain curve and the Neuber hyperbola, as shown in Figure 7.7. Using a simple iteration procedure, the local stress, σ_{max}, and local strain, ε_{max}, are determined for the corresponding nominal stress and nominal strain applied, S_{max} and e_{max}, respectively.

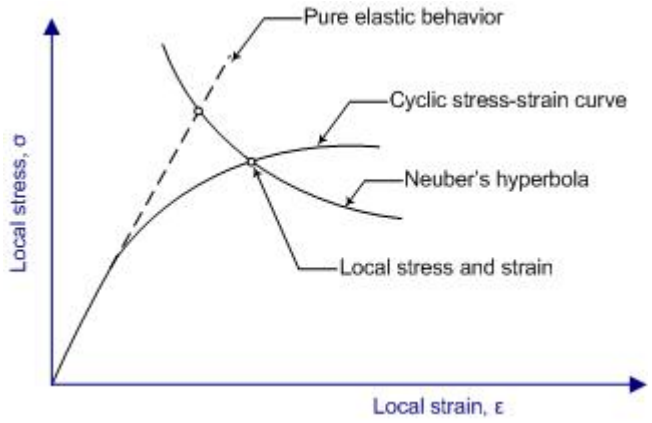

Figure 7.7: Intersection of cyclic stress-strain curve and Neuber's hyperbola (adapted from Bannantine et al. 1990)

Fatigue loading cycles — when the nominal stress applied to the steel bar is reversed due to fatigue loading, a change in the local stress, $\Delta\sigma$, and a corresponding change in the local strain, $\Delta\varepsilon$, at the rib root occurs. These changes satisfy the hysteresis stress-strain curve of the steel. Based on Massing's hypothesis, the hysteresis curve is obtained by doubling the cyclic stress-strain curve using the intersection point P_1 as the new origin (Dowling 1999). This is shown schematically in Figure 7.8.

The hysteresis stress-strain curve is expressed as follows:

$$\Delta\varepsilon = \frac{\Delta\sigma}{E_s} + 2\left(\frac{\Delta\sigma}{2k'}\right)^{\frac{1}{n'}} \tag{7.14}$$

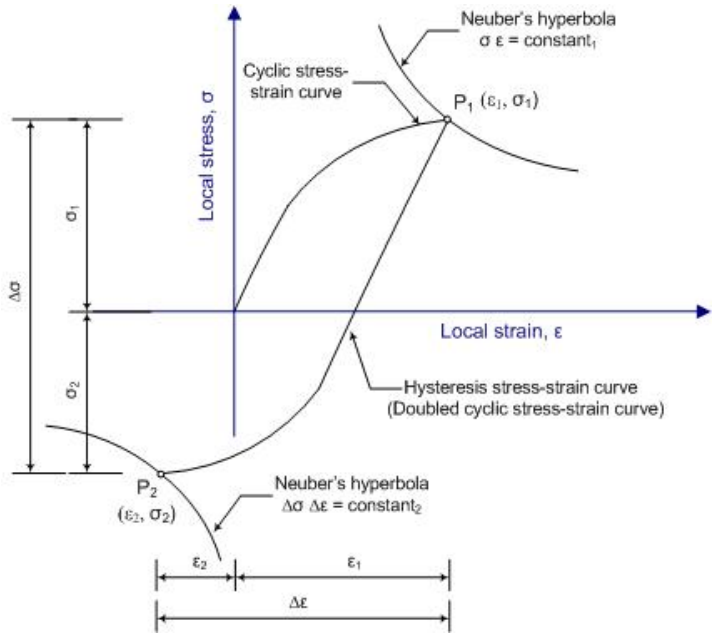

Figure 7.8: Intersection of the hysteresis loop and Neuber's hyperbola (adapted from Bannantine et al., 1990)

At the same time, the change in the local stress, $\Delta\sigma$, and the local strain, $\Delta\varepsilon$, satisfies the reversed Neuber's hyperbola (having the same origin P_1) as follows:

For elastic nominal behaviour:

$$\Delta\sigma\,\Delta\varepsilon = \frac{\left(K_f\,\Delta S\right)^2}{E_s} \tag{7.15}$$

For plastic nominal behaviour:

$$\Delta\sigma\,\Delta\varepsilon = \left(K_f\right)^2\,\Delta S\,\Delta e \tag{7.16}$$

where ΔS is the nominal stress range in the tensile reinforcing bars, calculated as the difference between the maximum and minimum nominal peak stresses, S_{max} and S_{min}, respectively. Equation

7.14, combined with equations 7.15 and 7.16, represents the intersection point P_2 shown in Figure 7.8, and gives a closed form solution for the change in the local stress and strain at the ribs. Once $\Delta\sigma$ and $\Delta\varepsilon$ are determined, the local stress and strain at P_2 are obtained as follows (Figure 7.8):

$$\sigma_2 = \sigma_1 - \Delta\sigma \tag{7.17}$$

$$\varepsilon_2 = \varepsilon_1 - \Delta\varepsilon \tag{7.18}$$

The next loading step starts with point P_2 as the origin. Equations 7.14 to 7.16 are then reapplied to determine the new change in the local stress and strain at the root of the ribs. The procedure is repeated over the fatigue life of the bar each time the nominal stress on the bar is reversed.

7.2.2.4 Fatigue life: accounting for the mean stress

As previously mentioned, the fatigue properties of the machined steel specimens are obtained from tests with completely reversed cycles under strain control having a mean stress of zero. In a concrete structure subjected to fatigue loading, the steel bar experiences a mean stress value depending on the peak stresses attained during its life. Tensile mean stresses are detrimental to the bar and decrease its fatigue life. On the contrary, compressive mean stresses are beneficial and increase the fatigue life of the bar.

Since a mean stress is typically present in fatigue applications, different approaches were developed in order to account for the mean stress in the strain-life expression given by Equation 7.8 (see Appendix C). The following expression proposed by Smith, Watson, and Topper (1970) is used in the current study:

$$\sigma_{\max}\frac{\Delta\varepsilon}{2}=\frac{\left(\sigma_f^{'}\right)^2}{E_s}\left(2N\right)^{2b}+\sigma_f^{'}\varepsilon_f^{'}\left(2N\right)^{b+c} \tag{7.19}$$

Equation 7.19 is used to estimate the fatigue life of the steel bar, *N*. Knowing the maximum local stress, σ_{max} and the local strain amplitude, $\Delta\varepsilon/2$, the fatigue life can be determined by a simple iteration technique.

7.3 Fatigue analysis results

In the following subsections, the results of the fatigue analysis of the unstrengthened and strengthened beams are presented. The geometric and material properties used in the models were based on the experimental data reported in Chapter 4.

7.3.1 Estimation of the fatigue notch factor, K_f

The determination of the local stresses and strains at the root of the ribs requires an estimation of the fatigue notch factor, K_f. Based on the available analytical and experimental investigations, the ACI-215 Committee (1997) recommends a range of K_f between 1.5 and 2.0 (ACI-215R-74 report, Section 2.2.4). Masoud et al. (2005) estimated the fatigue notch factor of steel bars embedded in concrete beams and subjected to fatigue loading to be 1.94. A similar study conducted by Al-Hammoud (2006) reported a value of 1.98 for the fatigue notch factor.

The fatigue notch factor was also estimated based on the current experimental fatigue life data for the unstrengthened control beams. Using the analysis procedure described in Section 7.2.2, the analytical nominal steel strain values obtained from a cracked sectional analysis were used to estimate the fatigue life of the unstrengthened beams. The fatigue notch factor was varied until the experimental and the predicted data trends matched. A fatigue notch factor of 2.0 gave a good correlation between the predicted fatigue life and the experimental data, as shown in Figure 7.9.

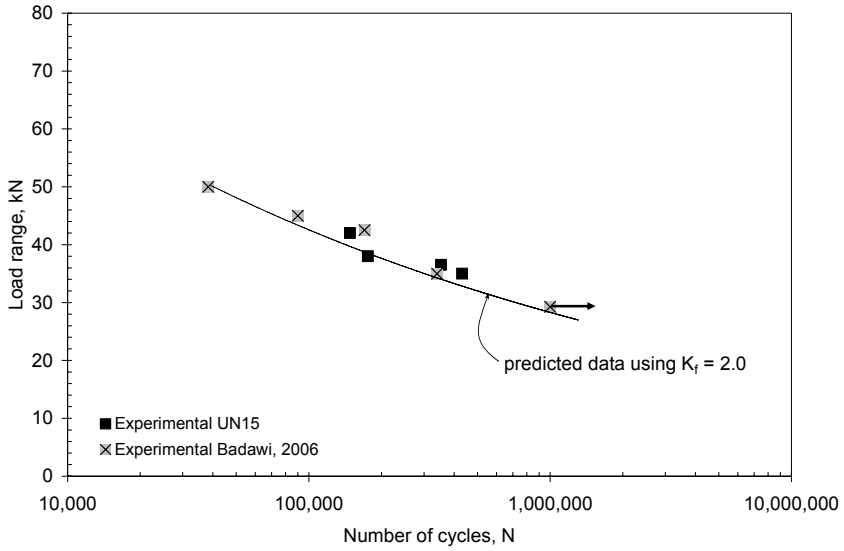

Figure 7.9: Experimental and predicted fatigue life of the unstrengthened beams using K_f= 2.0

7.3.2 Local stresses and strains

The strain-life analysis procedure described in Section 7.2.2 was used to compute the local stresses and strains in the steel bars of all the beam specimens using a fatigue notch factor of 2.0 (Section 7.3.1). The values are given in Table 7.2.

It is worth pointing out that the nominal stress ranges predicted for the OL15 beams were larger than those predicted for the SL15 beams, at given applied load ranges. For instance, the SL15-F72 and the OL15-F72 beams were both subjected to a load range of 57 kN. However, the predicted nominal stresses in the bars of the beams were 292 MPa and 369 MPa, respectively (Table 7.2). The reason for this difference is that all flexural cracks were closed at the end of the post-tensioning operation for the in-service beams, placing the entire concrete section under compression. Consequently, when the beam was reloaded, the whole section was initially effective in resisting the applied loads until the cracks were reopened under loading. This was not the case in the overloaded beams, where not all the cracks were completely closed at the conclusion of post-tensioning. As mentioned previously in Section 5.2.2.1, the yield crack was open due to the plastic deformation of the bar resulting from the overloading process. When the beam was reloaded, the tensile forces resisting the applied moment induced stresses in the steel bars at the locations of these cracks larger than those found when the cracks were closed. As a result, the local stresses computed for the OL15 beams were larger than those computed for the SL15 beams, at a given load range (see Table 7.2). For the same beams, SL15-F72 and OL15-F72, the computed local stress ranges were 562 MPa and 663 MPa, respectively.

The hysteresis loops for the beams are shown in Figures 7.10 to 7.13. The calculated local stresses and strains are given at the peaks of the loops. For the overloaded beams, the local stresses and strains corresponding to each stage of the loading scenario are also shown. The width of the

hysteresis loops indicates the amount of plastic strains induced at the root of the ribs of the steel bars. This can be observed for each group of beams at various levels of the applied loads.

Table 7.2: Analytical nominal stress and local strains and stress values (K_f = 2.0)

Beam	ΔS, MPa	Local strains			Local stresses, MPa			
		ε_{min}	ε_{max}	$\Delta\varepsilon$	σ_{min}	σ_{max}	$\Delta\sigma$	σ_{mean}
Unstrengthened specimens - UN15								
UN15-F50	262	0.00265	0.00533	0.00268	-78	435	513	178
UN15-F52	274	0.00273	0.00555	0.00282	-95	438	533	172
UN15-F53	286	0.00280	0.00576	0.00296	-111	441	552	165
UN15-F57	313	0.00295	0.00627	0.00331	-146	449	594	152
In-service strengthened specimens - SL15								
SL15-F66	249	0.00019	0.00272	0.00253	-122	368	490	123
SL15-F68	263	0.00029	0.00298	0.00269	-137	378	516	120
SL15-F72	292	0.00047	0.00350	0.00304	-167	395	562	114
SL15-F82	366	0.00082	0.00489	0.00407	-233	427	660	97
SL15-F88	409	0.00093	0.00572	0.00480	-264	441	705	88
SL15-F92	438	0.00096	0.00628	0.00533	-282	449	731	84
SL15-F97	468	0.00096	0.00691	0.00594	-299	457	756	79
In-service strengthened specimens - SL20								
SL20-F83	247	0.00028	0.00279	0.00251	-116	371	487	127
SL20-F87	267	0.00041	0.00315	0.00274	-138	384	522	123
SL20-F100	330	0.00078	0.00433	0.00355	-201	416	617	107
SL20-F110	381	0.00097	0.00527	0.00431	-243	434	676	96
Overloaded strengthened specimens - OL								
OL15-F67	336	0.00287	0.00650	0.00363	-350	274	624	-38
OL15-F72	369	0.00287	0.00698	0.00411	-350	313	663	-18
OL15-F76	396	0.00287	0.00744	0.00457	-350	342	692	-4
OL15-F82	436	0.00287	0.00816	0.00529	-350	379	729	15
OL15-F88	476	0.00287	0.00898	0.00611	-350	412	762	31

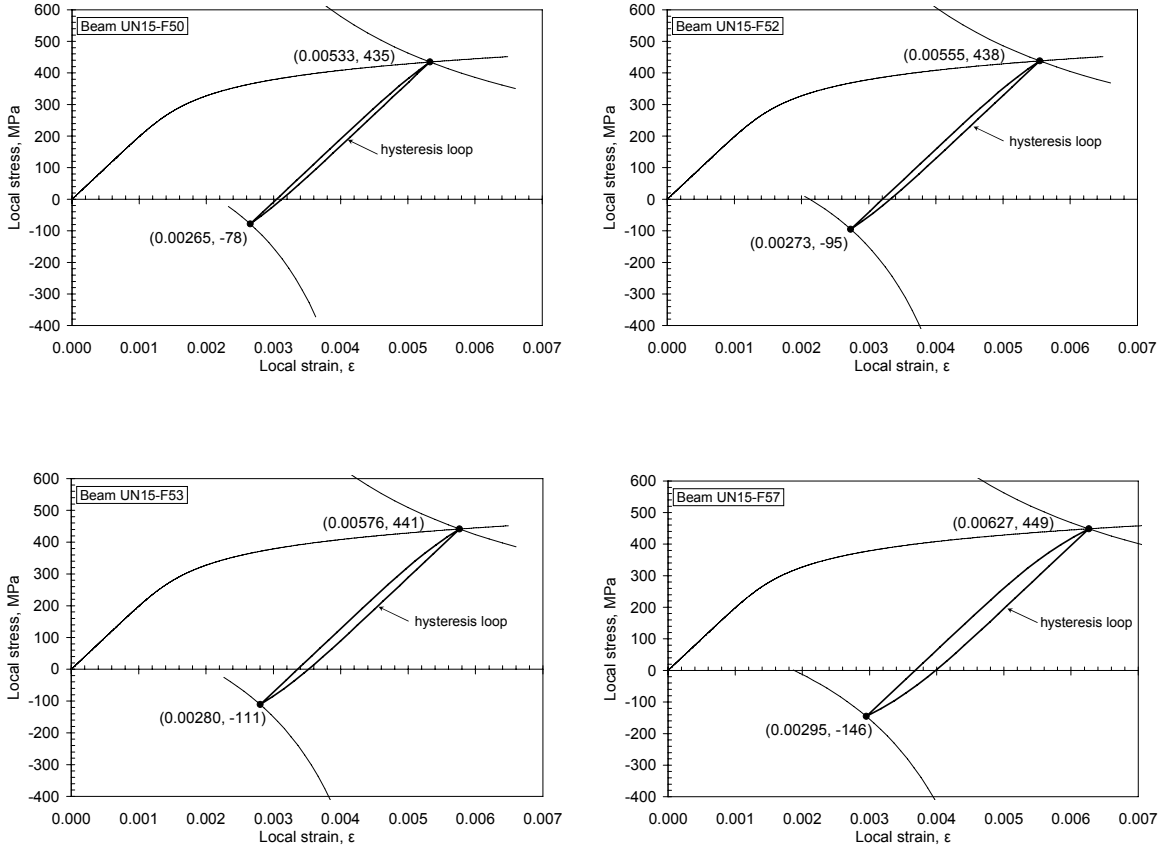

Figure 7.10: Hysteresis loops of the steel of the unstrengthened beams UN15

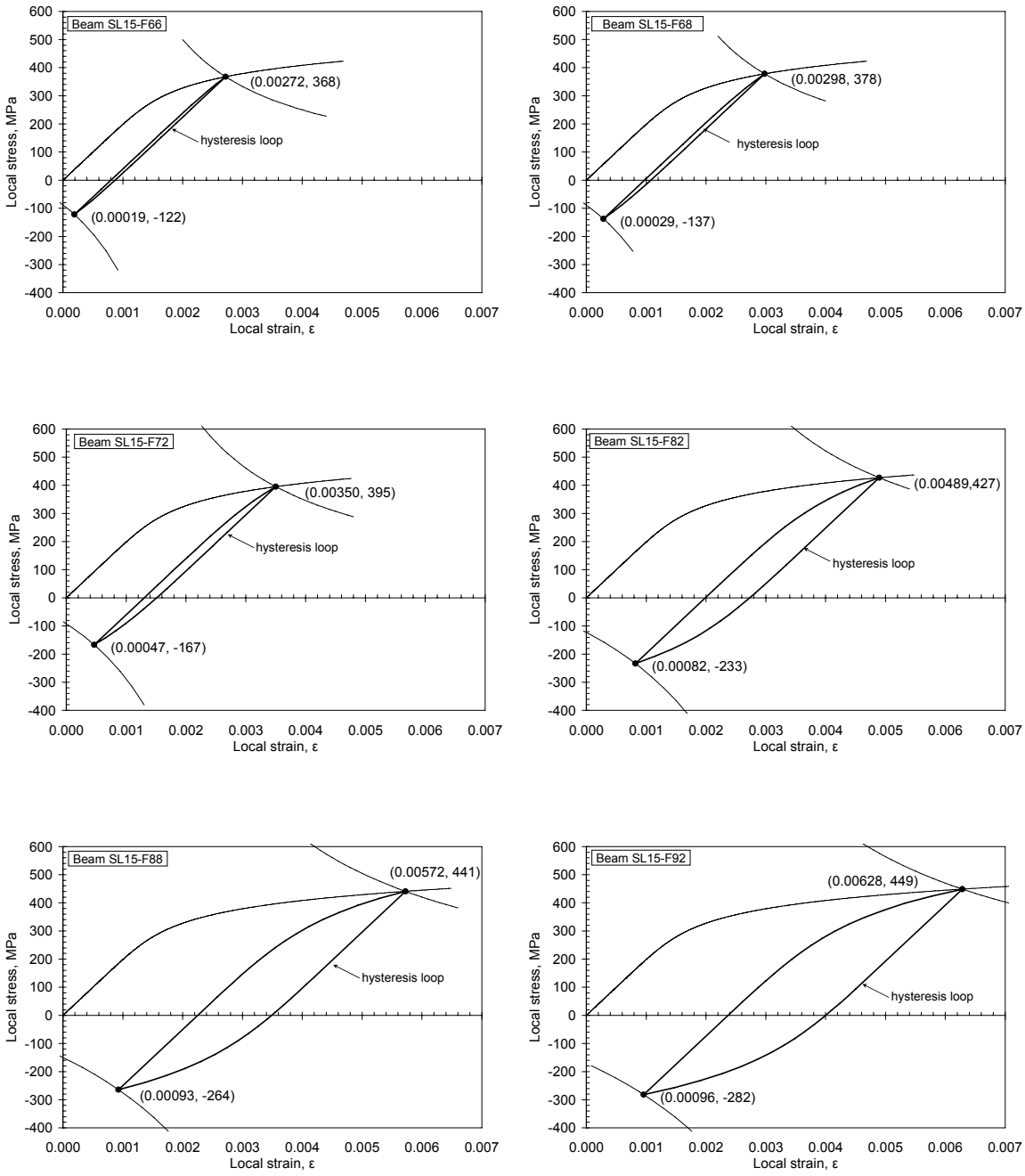

Figure 7.11: Hysteresis loops of the steel of the in-service strengthened beams SL15

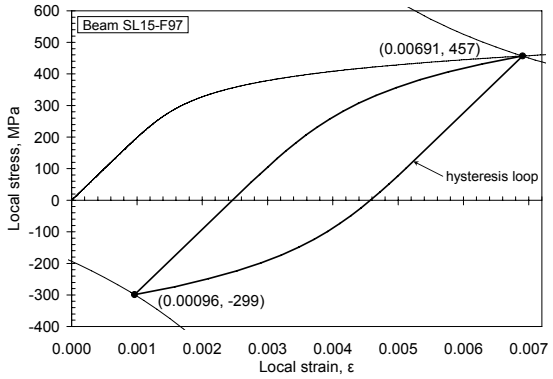

Figure 7.11 (cont.): Hysteresis loops of the steel of the in-service strengthened beams SL15

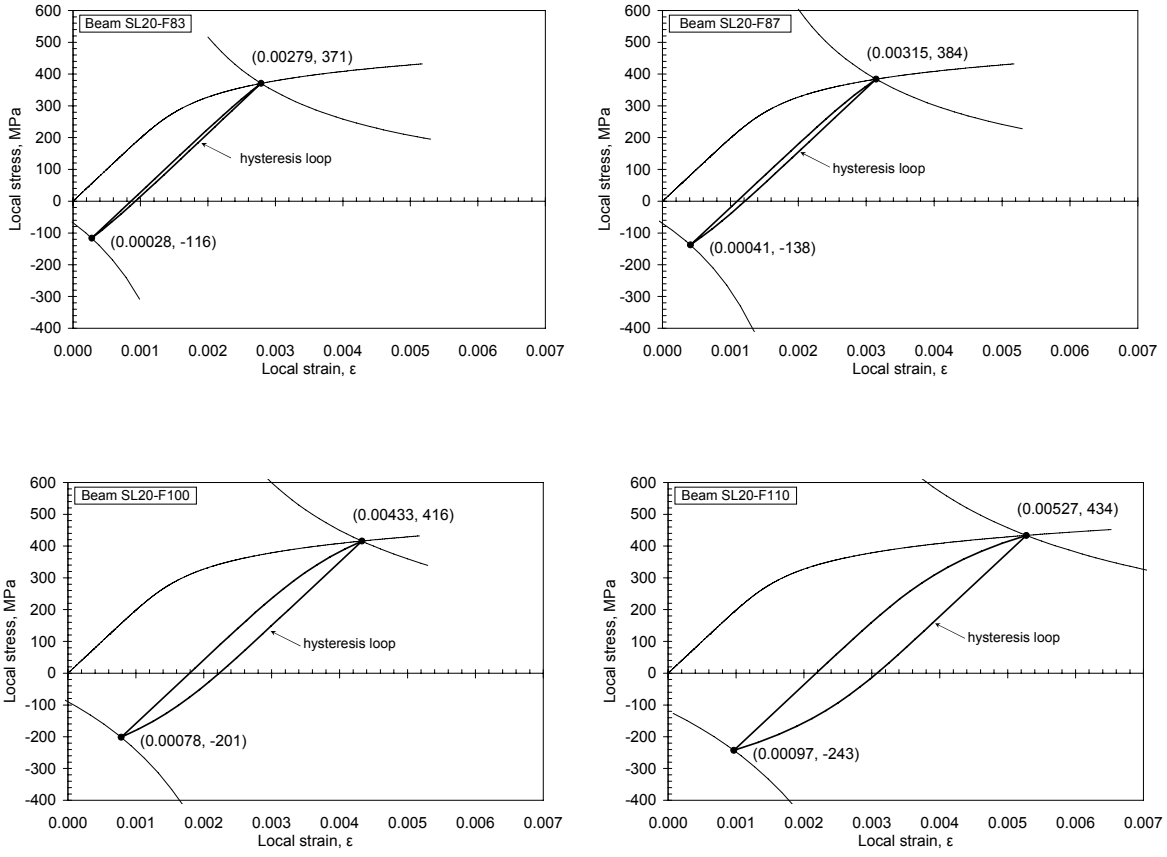

Figure 7.12: Hysteresis loops of the steel of the in-service strengthened beams SL20

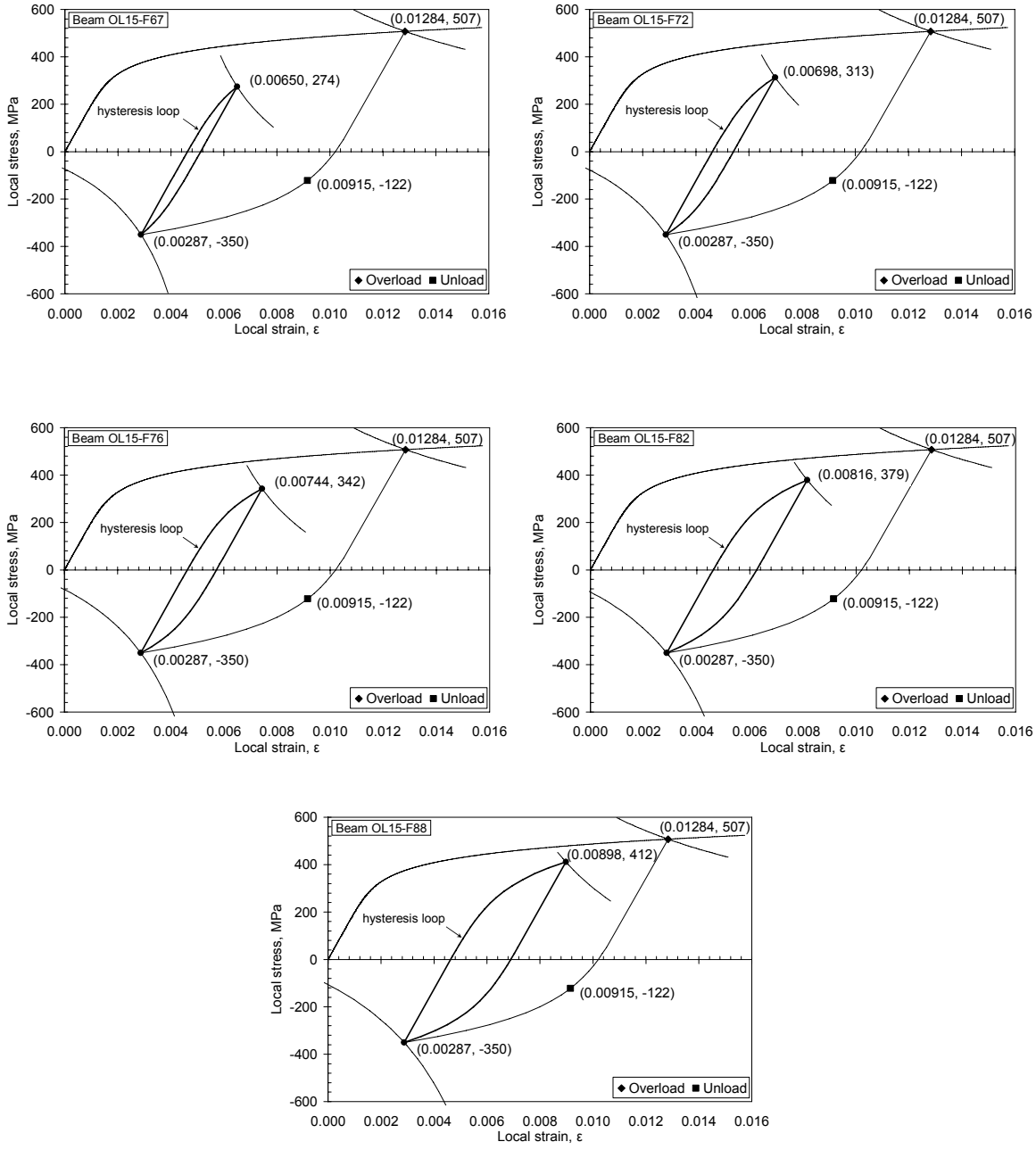

Figure 7.13: Hysteresis loops of the steel of the overloaded strengthened beams OL15

7.3.3 Fatigue life of beams

The relationships between the applied load ranges and the experimental and predicted fatigue life are shown in Figures 7.14 to 7.16 for the in-service and overloaded beams. A value of K_f of 2.0 was used to predict the fatigue life of each beam. The data for the unstrengthened beams are included in the plots for the in-service SL15 and the overloaded OL15 beams for comparison. As shown in the plots, there is a good agreement between the experimental and predicted fatigue life at long lives for all of the beam specimens. At short lives, the fatigue notch factor tends to decrease and, consequently, increases the fatigue life of the bar. This can be explained as follows:

The fatigue life of the steel bar consists of two stages: the crack initiation and the crack propagation stages. During the initiation stage, cyclic loading is used to grow a crack of a certain initiation length, usually taken as 0.1 mm length (Bannantine et al., 1990; Dowling, 1999). If low strain amplitudes are applied, the initiation stage is dominant and most of the fatigue life of the bar is used to grow the crack to its initiation length. On the contrary, if high strain amplitudes are applied, the crack quickly reaches its initiation length and most of the fatigue life is used to propagate the crack beyond that length. Figure 7.17 shows the theoretical stress distribution at a notch root; if most of the life is used to grow the crack to its initiation length, as in the case of low strain amplitudes, the average local stress during the fatigue life of the bar is high, and is close to the value $K_t \, x \, S$, where K_t is the stress concentration factor and S is the nominal stress applied to the bar. On the other hand, if most of the life is used to propagate the crack beyond its initiation length, as in the case of high strain amplitudes, the average local stress is considerably lower, and thus is less than the value $K_t \, x \, S$. This variation in local stress magnitudes is accounted for by using a fatigue notch factor, K_f, that varies depending on the applied strain amplitude.

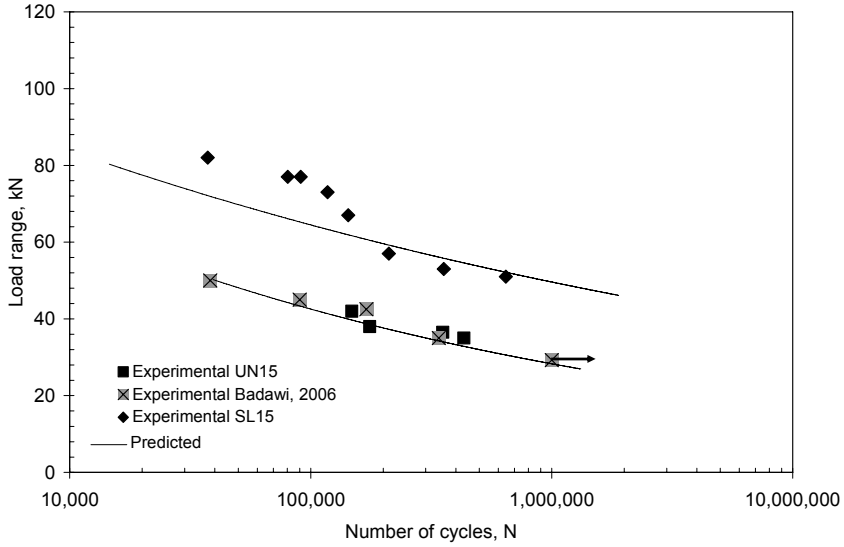

Figure 7.14: Experimental and predicted fatigue life of the in-service SL15 beams versus the load range (K_f= 2.0)

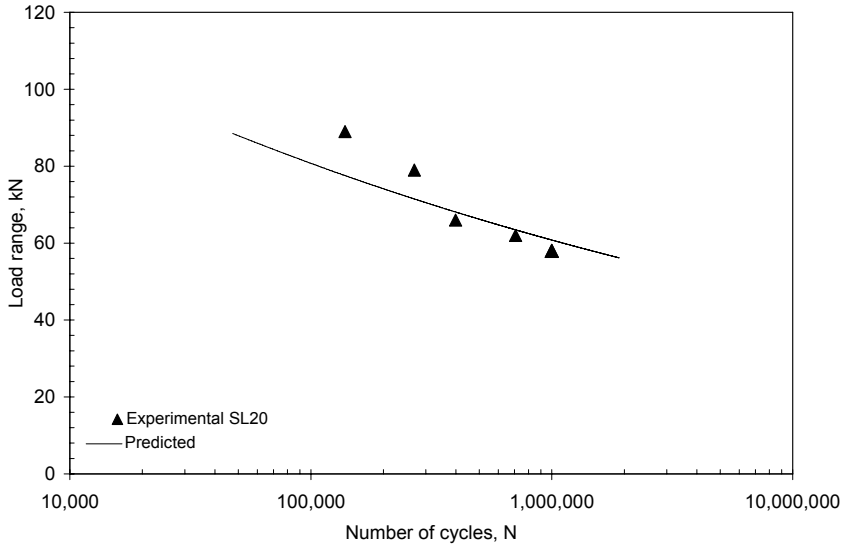

Figure 7.15: Experimental and predicted fatigue life of the in-service SL20 beams versus the load range (K_f= 2.0)

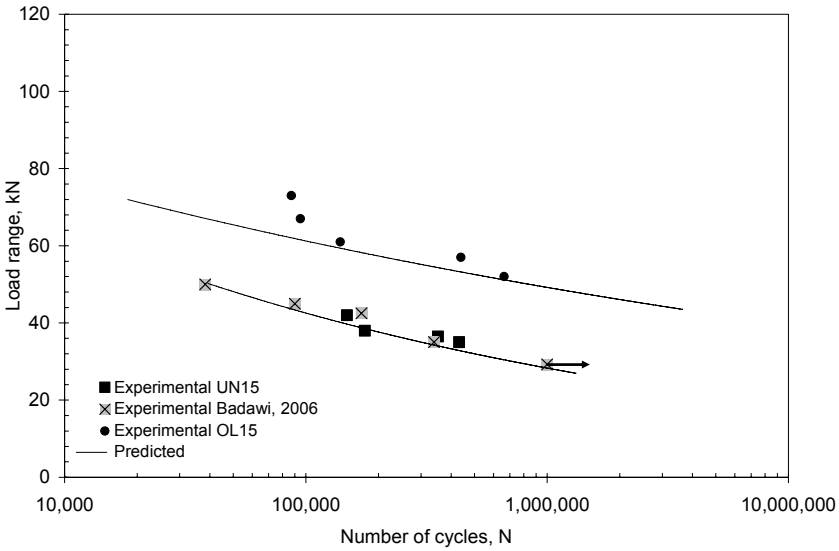

Figure 7.16: Experimental and predicted fatigue life of the in-service OL15 beams versus the load range (K_f= 2.0)

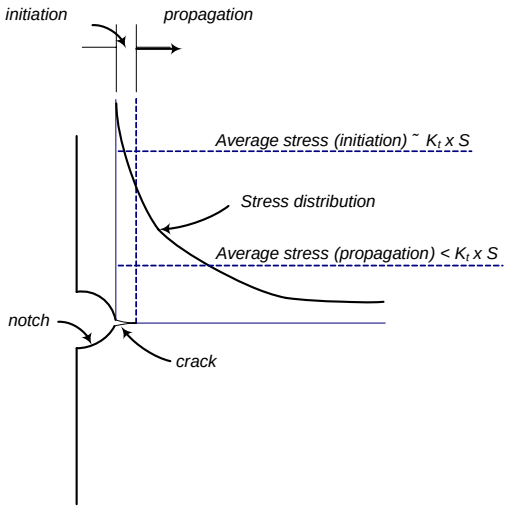

Figure 7.17: Local stress distribution at a notch root (adapted from Masoud, 2002)

7.4 Example of fatigue life calculation

The strain-life fatigue model was used to determine the number of cycles that a strengthened beam can accommodate when the applied load ranges on the beam varied after strengthening. Numerical examples for in-service and overloaded beams are given in Appendix D.

7.5 Existing fatigue design provisions

Most design codes adopt stress-based approaches in the design for the fatigue limit state of steel reinforced concrete beams. The stress-based approach for steel bars is typically based on a statistical analysis of large experimental data obtained from fatigue tests conducted on steel bars at different stress ranges. The relationship between the stress ranges applied to the steel bars and their fatigue life (S-N curves) are determined. The endurance limit of the steel (the stress range below which the steel has an infinite life) together with specified margins of safety can be determined, and is often used to set the limiting stress range for fatigue design.

In the following sections, the fatigue design provisions recommended by the Canadian Highway Bridge Design Code (CHBDC, 2000), the American Concrete Institute (ACI Committee 215, 1997), and the AASHTO-LRFD (2004) are briefly reviewed. A discussion about the fatigue model developed in this study in comparison to the existing fatigue design provisions is presented.

7.5.1 Canadian Highway Bridge Design Code (CHBDC, 2000)

The Canadian Highway Bridge Design Code (CHBDC, 2000) imposes limits on the applied stress range in the steel reinforcing bars embedded in a concrete section for different cases that represent various types of reinforcement, connections, joints, splices, etc. These cases are summarized in Table 7.3. For instance, a permissible stress range of 125 MPa should not be

exceeded in straight reinforcing bars embedded in concrete elements. This is based on the fatigue design provisions for deformed bars reported by Helgason et al. (1976), and expressed as follows:

$$f_{sr} = 145 - 0.33 f_{min} + 55(r/h) \quad (7.20)$$

where:

f_{sr} = the permissible stress range in the bar in MPa;

f_{min} = the minimum stress level in the bar in MPa, and;

r/h = the ratio of base radius to height of rolled-on transverse deformation (taken as 0.3 when actual value is not known).

Table 7.3: Fatigue provisions (adapted from CHBDC, 2000)

	Description	Stress Range (MPa)	Clause
Reinforcing bars	Straight bars	≤ 125	8.5.3.1
	Anchorages, connections and bends	≤ 65	8.5.3.1
	Bars with groove welds	≤ 100	8.5.3.1
	Other types of welds	≤ 65	8.5.3.1
Steel Tendons	Corrugated steel ducts	≤ 125	8.5.3.2
	Pretensioning strands (Radii of curvature< 10 m or more)	≤ 125	8.5.3.2
	Pretensioning strands (Radii of curvature <3.5 m or more)	≤ 70	8.5.3.2
	Corrugated plastic ducts	≤ 125	8.5.3.2
	Deformed high-strength bars	≤ 70	8.5.3.2
	Smooth high-strength bars	≤ 90	8.5.3.2
	Tendons at couplers	≤ 70	8.5.3.2

It is worth mentioning that the expression given by Equation 7.20 considers the possible effect of the stress concentration on the fatigue life of the deformed bar. This is represented by the ratio r/h in the right-hand side of the equation. Increasing the ratio between the radius of the root and

the height of the rib decreases the stress concentration. Note that the implementation of the stress concentration in Equation 7.20 is based on the extensive experimental data carried out by Helgason et al. (1976).

7.5.2 American Concrete Institute (ACI-215 Committee, 1997)

The ACI-215 Committee (1997) reports that the stress range applied to the steel bar is the most critical factor for fatigue. The general fatigue design approach proposed by the Committee is to determine the range of stresses in each of the constituent materials due to fatigue loads, and to check these stresses against the allowable limits. The Committee specifies allowable fatigue stress ranges for the concrete and the reinforcing steel bars, based on the results of fatigue tests carried out on concrete and steel specimens. The criteria used in design are summarized as follows:

- The stress range in concrete should not exceed 40% of its compressive strength, f'_c, when the minimum stress is zero, or a linearly reduced stress range as the minimum stress is increased, so that the permitted stress range is zero when the minimum stress is 0.75 f'_c.
- The stress range in straight deformed reinforcement, f_{sr}, should not exceed the value given by Equation 7.21, where f_{min} is the minimum stress induced during the fatigue loading. For bent bars, the stress range computed from this relation should be reduced by 50 percent.

$$f_{sr} = 161 - 0.33 f_{min} \tag{7.21}$$

For beams prestressed with unbonded steel tendons, the ACI-215 Committee recommends that special attention should be given to the possibility of fatigue in the anchorages. In the absence of test results, the fatigue strength of wire, strand, or bar at the anchorage should not exceed half of the fatigue strength of the prestressing steel tendons.

It is worth mentioning that the equation provided by the ACI Committee 215 resembles that of the CHBDC (Equation 7.20) in expressing the significance of the applied stress range on the fatigue life of the bar. Although the ratio r/h does not appear in the ACI equation, it is implicitly considered by the constant 161 in Equation 7.21. Using the recommended value of the CHBDC (r/h = 0.3) leads to a similar permissible stress range for the same minimum stress level.

7.5.3 AASHTO LRFD specifications (2004)

The fatigue design provisions recommended by the AAHTO-LRFD specifications do not conceptually differ from those provided by the CHBDC (2000) and the ACI-215 Committee (1997). Limits on the applied stress range in the steel reinforcing bars in the concrete are expressed by the following relationship:

$$f_{sr} = 21 - 0.33 f_{min} + 8(r/h) \qquad (7.22)$$

where:

f_{sr} = the permissible stress range in the bar in Ksi;

f_{min} = the minimum stress level in the bar in Ksi, and;

r/h = as previously defined for Equation 7.20.

For prestressing tendons, the specifications also impose a limit of 18 ksi for tendons with radii of curvature in excess of 30 feet, and 10 ksi for tendons with radii of curvatures not exceeding 12 feet. A linear interpolation is then required for tendons with radii between 12 and 30 feet.

7.5.4 Proposed design methodology

The preceding discussion illustrates that the existing fatigue design provisions limit the allowable stress range in the steel reinforcing bars when subjected to fatigue loading. These provisions are typically based on fatigue data obtained from experimental tests on steel bars and reinforced concrete elements. The design equations proposed by these provisions lack an accurate estimation of the local stresses that occur at the roots of the ribs of the steel bars during fatigue. As observed from the fatigue tests presented in this study, fatigue fracture of the reinforcing bars typically occurred at these locations. The equations account for the effect of the discontinuities present on the surface of the steel bars (e.g., the ribs, lugs, or manufacturer marks) in an empirical approach based on the experimental data available.

The fatigue model presented in this chapter deals with the fatigue limit state of concrete beams in a more rational approach. The model allows an accurate estimation of the local stresses induced at the root of the ribs where the fatigue cracks in the bars are likely to initiate due to plastic deformations occurring at these locations. Determining the fatigue properties of the steel bars allows the designer to consider variations that might exist in the mechanical properties of the steel material used and, consequently, the use of different types of steel bars having different characteristics.

The flexibility in design and the possibility of broadening its applications to cover unexpected situations is a significant goal that should also be considered. The proposed fatigue model has the ability to embrace such situations, as in the case of overloading conditions. It is recognized that the stress-based approaches contained in the existing design provisions do not take into account the stress history of the steel bar. This fact makes their applicability questionable in cases such as overloading. Nevertheless, these approaches rely on defining the endurance limits of the steel bar in determining the permissible stresses in the bar during its service in order to prevent fatigue failure. This approach might not be conservative in severe environments, such as corrosive

environments that may cause great variations in the endurance limit values for the steel bars. To address these limitations, the following step-by-step fatigue design approach for CFRP post-tensioned beams is proposed:

1. Using the modified monotonic analysis described in Section 7.2.1, determine the following:
    a. The nominal stresses in the internal steel reinforcing bars, at the section of maximum moment, at the peak values of the fatigue loads;
    b. The nominal stresses in the compressed concrete, at the section of maximum moment, at the peak values of the fatigue loads;
    c. The stress range in the external CFRP tendons at the peaks of the fatigue loads.
2. Determine the cyclic stress-strain relationship and the fatigue properties for the steel reinforcing bars.
3. Conduct a Neuber analysis to determine the local stress-strain state at the root of the ribs of the steel bar based on a conservative value of K_f of 2.1.
4. Calculate the fatigue life of the steel bar taking into account the effect of the applied mean stress. This can be achieved by applying the Equation 7.19 in Section 7.2.2.4.
5. Compare the estimated stress range in the CFRP tendon-anchor assembly in the beam during fatigue with the endurance limit of the assembly, previously obtained as 216 MPa (refer to Chapter 3). If the expected stress range in the assembly is less than its endurance limit, the fatigue life of the post-tensioned beam is unlikely to be governed by the failure of the anchor. If the stress range in the assembly is larger than its endurance limit, estimate the fatigue life of the assembly using Equation 3.1.
6. Determine the fatigue life of the beam based on one of the following two aspects:
    a. The fatigue life of the steel bar, as determined in steps 1 to 4,

b. The fatigue life of the CFRP tendon-anchor assembly, as determined in step 5.

The fatigue life of the beam is thus governed by the lowest life obtained from the above estimates. Varying the design parameters (such as the post-tensioning force, the tendon profile, the tendon eccentricity, or the number and position of the deviators) should vary the calculated life of each beam component. It is thus recommended that different measures of these parameters should be attempted in order to achieve the required fatigue life. It is worth mentioning that the above procedure is based on the assumption that the adequacy of concrete for the designed fatigue loading has been checked following the ACI-215 guidelines (or similar).

Chapter 8

Conclusions and Recommendations

8.1 Introduction

The survey of the previous studies showed that very limited research has been devoted to the fatigue response of externally post-tensioned members, particularly when FRP tendons are used. Little information is available about the enhancement in the fatigue life of the strengthened beams as a result of external post-tensioning. The survey also revealed that, for severely damaged concrete beams (such as overloaded beams), little effort has been devoted to investigating their behaviour under both monotonic and fatigue loading. The fatigue design equations provided by the different codes of practice do not consider such situations.

In this study, the monotonic and fatigue performances of reinforced concrete beams strengthened with external post-tensioned CFRP tendons were investigated experimentally and analytically. Monotonic and fatigue tests were carried out on twenty-eight unstrengthened and strengthened beams. Test parameters included the tendon profile, the initial loading conditions of the beams prior to post-tensioning, the partial prestressing ratio, and the load ranges applied to the beams during their fatigue life. The analytical study included a monotonic model based on a layer-by-layer analysis approach that takes into account the loading history of the beams prior to and after post-tensioning application. The fatigue model was based on a strain-life approach that accounts for local stresses and strains that occur in the deformed steel bars, while considering the different loading conditions prior to strengthening. Finally, a comparison between the

experimental and analytical results was conducted. In the following sections, a summary of the thesis work along with the main conclusions of this study are presented, followed by recommendations for future work.

8.2 Tendon-anchor fatigue tests

Prior to designing the concrete beams, the fatigue behaviour of the newly developed wedge-type anchor used to grip the CFRP external tendons (Waterloo anchor), was investigated under different stress ranges. Due to the absence of a definite acceptance criterion for the FRP tendon-anchor assembly, the Post-Tensioning Institute (PTI, 1997) acceptance criteria for post-tensioning anchors for steel tendons were used. A tensile fatigue setup was fabricated and the CFRP fatigue test specimens were prepared. The following conclusions were drawn from the fatigue tests results:

- The failure of the CFRP tendon-anchor assembly always occurred in the CFRP tendons due to cyclic loading; no premature failure took place in the anchors.
- The fatigue performance of the assembly exceeded the PTI requirements (1997) for anchor systems used in post-tensioned steel tendons.
- Cyclic loading had a minimal effect on the mechanical properties of the CFRP tendon material.
- The fatigue life of the CFRP tendon-anchor assembly was significantly affected by the stress range applied rather than the variation of the minimum stress; the fatigue life of the assembly decreased as the applied stress range increased regardless of the minimum stress applied.
- A log-linear relationship between the fatigue life, N_{anc}, and the stress range, f_{fr}, was proposed in order to predict the fatigue life of the assembly for design purposes.

- The fatigue limit of the CFRP tendon-anchor assembly should be taken as a stress range of 10% of its ultimate capacity (approximately 216 MPa). Below this stress range, the assembly is expected to withstand an infinite fatigue life.

The results of these tests were used in the design of the concrete beams to ensure that the failure of the beams under the fatigue loading would not be governed by the life of the tendon-anchor assembly.

8.3 Monotonic beam tests

The monotonic flexural performance of reinforced concrete beams strengthened with external post-tensioned CFRP tendons was investigated. Variables included straight and double draped tendon profiles, and two post-tensioning conditions: after loading to 50% of the yielding capacity of the beam (in-service beams) or after overloading to approximately twice the steel reinforcement yield strain (overloaded beam). Four beams were tested under monotonic four-point loading: one unstrengthened beam to serve as a control for the strengthened beams, one in-service strengthened beam with straight tendons, one in-service beam with double draped tendons, and one overloaded beam strengthened with double draped tendons. The tendons were post-tensioned to 40% of their ultimate capacity, representing a prestressing level large enough to develop a reasonable strengthening ratio for the post-tensioned beams and to minimize the stress concentration on the CFRP draped tendons at the harped locations.

A new post-tensioning setup, consisting of steel deviators and end-bearing fixtures, was fabricated at the University of Waterloo. Teflon sheets were used at the deviated points to minimize the friction between the steel deviators and the CFRP tendons. The results of the monotonic tests can be summarized as follows:

- The beams post-tensioned with straight tendons behaved similarly to those with double draped tendons at various loading stages up to ultimate when steel deviators were used.

- The presence of deviators minimized the effect of the change in the tendon eccentricity on the behaviour of the beam (the second-order effect). The change in the tendon depth was thus neglected during the analysis of the in-service and the overloaded beams.
- The use of a cushioning material (such as Teflon) between the steel deviators and the CFRP tendon sheets minimized the wear of the tendons at the points of contact. No significant loss in prestress was observed in the tendons at all stages of loading.
- External post-tensioning with CFRP tendons is an efficient technique for strengthening overloaded concrete beams. It significantly decreased the amount of deflection encountered due to overloading.
- Post-tensioning significantly reduced the strains in the steel reinforcing bars for both in-service and overloaded beams. The steel strains attained at the end of post-tensioning depend on the level of prestressing applied and on the magnitude of strains prior to post-tensioning.
- For the same post-tensioning system, overloading the beam prior to post-tensioning increased the beam deflections and the strains developed in the steel reinforcing bars at all stages of loading. Overloading did not have a significant effect on the yield load of the strengthened beam and the mode of failure at ultimate load. It also had no discernable effect on the increase in the tendon stress at yielding.
- Post-tensioning the external CFRP tendons to 40% of their ultimate capacity allowed a reasonable strain margin to account for live load applications without permitting premature breakage of the tendon, even if the strengthened element was severely overloaded.
- Post-tensioning the external CFRP tendons to 40% of their ultimate capacity completely closed the cracks of the in-service beams. However, cracks due to overloading where the steel yielded were not completely closed after post-tensioning application.

- The maximum increase in the CFRP stress at the yield load was approximately 20% of the initial post-tensioning stress, for the in-service and overloaded beams.
- All post-tensioned beams failed by yielding of the steel reinforcing bars followed by concrete crushing in the compression zone. No failure occurred in the CFRP tendons or at the anchors.

8.4 Fatigue beam tests

Twenty-four unstrengthened and strengthened beams were tested under fatigue loading at different load ranges taken as fractions of the yield load of the beams. All beams were strengthened with double draped tendons post-tensioned at 40% of the tendons ultimate capacity. The beams were categorized into four main groups: unstrengthened beams to serve as controls for the post-tensioned beams, in-service post-tensioned beams with a partial prestressing ratio of 0.46, in-service post-tensioned beams with a partial prestressing ratio of 0.36, and overloaded beams with a partial prestressing ratio of 0.46. Different partial prestressing ratios were achieved by changing the amount of the internal non-prestressed reinforcing steel bars. The post-tensioning setup described in the monotonic tests was used in the fatigue tests.

Cyclic tension tests were conducted on smooth steel specimens machined from the reinforcing bars. In addition, a series of cyclic uniaxial compression tests were carried out on standard concrete cylinders. These tests aimed to interpret the steel and concrete fatigue response encountered during the beam tests.

The following conclusions were drawn from the fatigue test results:

- CFRP external draped tendons showed an excellent fatigue response when used in strengthening the concrete beams. The double draped profile represented the most critical shape for FRP tendons in terms of strength, as FRP tendons are known to weaken at the

harped locations. No evidence of wear or stress concentration was observed at the deviated points due to fatigue. As a result, the tendons were reused during the fatigue tests of the beams.

- External post-tensioning with CFRP tendons considerably increased the fatigue life of the beams at all load ranges applied as a result of the stress decrease in the steel reinforcing bars due to post-tensioning.
- The increase in the maximum tendon stress due to fatigue loading varied between 0.38% and 1.37% of its ultimate strength at midlife of the beam. Most of the increase in the tendon stress occurred during the early part of the beam life.
- For the majority of the tested beams, failure was governed by the fracture of the internal steel reinforcing bars at a flexural crack location. The fatigue fracture occurred at the root of the ribs, which indicated the presence of stress concentration at these locations.
- The stress range applied to the steel reinforcing bars was the dominant factor that controls the fatigue life of the unstrengthened and strengthened beams. Increasing the stress range in the steel bars reduced the fatigue life of the beam.
- Overloading the beams prior strengthening had insignificant effect on the fatigue life of the strengthened beam. The stress range and the mean stress applied to the steel bar governed the fatigue life of the bar, and hence the fatigue life of the beam.
- At the same load range applied to the beam, increasing the amount of the steel reinforcing bars for the same post-tensioning level decreased the stress range in the bars and significantly increased the fatigue life of the strengthened beams.
- An average increase of 45% in the normalized load ranges (the applied load range divided by the yield load of the control beam) was accommodated by the strengthened beams, for the same number of cycles survived by similar unstrengthened beams.

- The unstrengthened and strengthened beams exhibited a linear increase in their maximum midspan deflections with an increasing number of cycles. Post-tensioning had a slight effect on reducing the rate of increase in the deflections of the strengthened beams. The increase in the maximum midspan deflections of the overloaded beams was less than the in-service strengthened beams.
- The unstrengthened and strengthened beams exhibited an increase in their concrete and steel strains at midspan sections with an increasing number of cycles. The increase in the concrete and steel strain ranges was minimal.
- Cyclic tests carried out on machined steel specimens indicated that the steel exhibited little or no cyclic creep under fatigue loading. On the other hand, cyclic tests on the concrete cylinders indicated that the concrete exhibited cyclic creep at all stress ranges. Additionally, cyclic softening of the concrete was observed when high stress ranges were applied. Observations from the unstrengthened (UN series) and strengthened (SL series) beam fatigue tests noted the growth of flexural cracks, both in number and height, in the early stages of fatigue life. This crack growth was attributed to a reduction in the modulus of rupture of the concrete due to fatigue loading. Based on the cyclic material test results and beam fatigue test observations, the increase in the maximum concrete and steel strains encountered during the beam fatigue tests was attributed to the combined effect of the cyclic creep and fatigue crack growth of the concrete.

8.5 Modeling of the monotonic response

A new monotonic model that takes into account the loading history of the strengthened beams was developed. The beam was modeled as a series of longitudinal elements each subjected to a constant flexural moment. The sectional analysis at each element was based on a layer-by-layer evaluation of the section forces. At each stage of loading, the state of stress and strain in each

layer was determined based on the position of the layer with respect to the neutral axis, and on the stage of loading under study. The model was implemented into a computer program called AEPT (Analysis of Externally Post-Tensioned beams).

The difference between the algorithm of the in-service beams and the overloaded beams lies in the steel response after the unloading and the post-tensioning stages. During these stages, the steel reinforcement at the section of maximum moment of the in-service beams follows a linear elastic stress-strain relationship. For the overloaded beams, the steel reinforcement response during the unloading, post-tensioning, and the reloading stages follows the hysteresis response given by the Ramborg-Osgood relationship. The strain reduction approach developed by Naaman (1990, 2005) for unbonded tendons was used in predicting the stress increase in the external CFRP tendons.

The following conclusions were drawn from the results obtained from the monotonic model:

- In predicting the monotonic behaviour of the in-service beams, the assumption proposed by Harajli and Kanj (1992) that the strain reduction coefficient after cracking can be taken as its value before cracking showed good agreement between the experimental and predicted results.
- In predicting the monotonic behaviour of the overloaded beams, the assumption that the gross moment of inertia of the concrete section is completely effective is not accurate due to overloading and due to the existence of opened cracks. A new moment of inertia, I_{ps}, defined as the moment of inertia of the section at the end of the post-tensioning process, was proposed to substitute I_g in the equation of the strain reduction coefficient.
- The strain reduction approach proposed by Naaman (1990, 2005) showed a good accuracy in predicting the structural performance of the post-tensioned beams at all stages of loading. A good correlation between the experimental and the analytical results of both beams was observed.

8.6 Modeling of the fatigue response

A fatigue model, based on a strain-life approach, was proposed to predict the fatigue life of the CFRP post-tensioned beams. The fatigue model takes into consideration the stress-strain history at the stress raisers in the steel bars. It accounts for the inelastic deformation at the ribs during cycling and the resulting changes in the local mean stresses.

A modified monotonic model that neglects the tensile stresses in concrete was adopted to account for the stress increase in the steel bars at flexural crack locations. Reduced tensile fatigue strength of concrete was used in order to account for the propagation of the cracks during cyclic loading, as observed during the fatigue tests of the beams. The following conclusions were drawn from the results of the implemented fatigue model:

- The fatigue notch factor, K_f, estimated from the experimental fatigue life data for the unstrengthened beams was equal to 2.0.
- The fatigue model can accurately predict the fatigue life of the in-service and the overloaded beams. A good agreement between the experimental and predicted fatigue life was obtained at long lives for all of the beam specimens, when a fatigue notch factor of 2.0 was used. At short lives, the fatigue notch factor tends to decrease and, consequently, increases the fatigue life of the bar.
- A step-by-step fatigue design approach was proposed for the CFRP externally post-tensioned beams. A conservative value of 2.1 for K_f was proposed for design.

8.7 Recommendations for future studies

Based on the investigations of this study, the following work is recommended for further research:

- Experimental data is needed to investigate the use of straight tendons profile without deviators on the fatigue life of the beams in order to consider the second order effects on the life of the beams.
- Experiments on externally post-tensioned beams under variable amplitude fatigue loading are needed. This type of loading simulates better the loading subjected to the beams in service.
- The effect of increasing the prestressing level in the external tendons on the fatigue life of the in-service and the overloaded beams needs to be investigated. The monotonic and fatigue analytical models presented in the current study can be extended for such an investigation.

Appendix A: Prediction Equations for the Unbonded Tendon Stress at Ultimate

A.1 Introduction

Due to the lack of bond between the concrete and the unbonded tendons, the force in the tendon at any stage of loading is considered uniform at all sections along the post-tensioned element. As the load on the element increases, the stress in the tendon increases beyond its initial post-tensioning value. The general formula for the stress in the tendon at any stage of loading, f_{ps}, is given by the expression shown in Equation A.1:

$$f_{ps} = f_{pse} + \Delta f_{ps} \tag{A.1}$$

where f_{pse} is the effective prestressing force in the tendons at a reference load, and Δf_{ps} is the amount of increase in the tendon stress caused by the increase in load beyond the reference load.

Numerous investigations have been carried out to predict the stress in unbonded steel tendons at ultimate stages of loading. A review of the most commonly used models is given in the following sections. Prediction equations developed by Tao and Du (1985), Harajli (1990), Harajli and Hijazi (1991), Harajli and Kanj (1991), Chakrabarti (1995), Naaman and Alkhairi (1991), and Aravinthan et al. (1997) are provided.

A.2 Models predicting the unbonded tendon stress at ultimate

A.2.1 Tao and Du model (1985)

Tao and Du tested twenty-two beams post-tensioned with unbonded steel tendons under four-point loads. The main parameters considered were the mild and the prestressed steel ratios, the concrete strength, and the effective prestressing level in the unbonded tendons. The span-to-depth ratio for all beams was 19.1. The authors developed the following expression for the calculation of the stress in the unbonded tendons at ultimate, f_{ps}:

$$f_{ps} = f_{pse} + (786 - 1920\omega) \leq f_{psy} \ (MPa) \tag{A.2}$$

where

f_{pse} = the effective prestressing stress in the unbonded reinforcement;

ω = the combined reinforcement index; and

f_{psy} = the yield stress of the unbonded steel tendons.

The authors reported that the initial stress in the unbonded tendons should be limited as follows:

$$0.55 f_{psy} \leq f_{pse} \leq 0.65 f_{psy} \tag{A.3}$$

The combined reinforcement index, ω, was defined as the summation of the prestressing reinforcement index, ω_{ps}, and the non-prestressed reinforcement index, ω_s, as follows:

$$\omega = \omega_{ps} + \omega_s \leq 0.3 \tag{A.4}$$

where

$$\omega_{ps} = \frac{\rho_{ps} f_{psu}}{f_c^{'}} \; and \;\; \omega_s = \frac{\rho_s f_{sy}}{f_c^{'}} \tag{A.5}$$

$$\rho_{ps} = \frac{A_{ps}}{bd_{ps}} \; and \;\; \rho_s = \frac{A_s}{bd_s} \tag{A.6}$$

where

f_{psu} = ultimate strength of the unbonded tendons;

f_{sy} = the yield stress of the bonded reinforcement;

f'_c = the concrete compressive strength;

A_s, A_{ps} = the areas of the bonded and unbonded reinforcement, respectively;

d_s, d_{ps} = the depths of the bonded and unbonded reinforcement, respectively; and

b = the beam width.

A.2.2 Harajli model (1990)

Harajli conducted an analytical investigation to study the effect of the span-to-depth ratio of the unbonded post-tensioned beams and the loading type, on the stress increase in the tendons at ultimate, Δf_{ps}. Harajli concluded that increasing the span-to-depth ratio significantly decreased the predicted increase in stress at ultimate. However, Harajli reported that the change in Δf_{ps} was affected by the geometry of the applied load. The reduction in stress with increasing the span-to-depth ratio is directly related to the length of the plastic region in the member at its ultimate flexural strength. Beams loaded with single concentrated load encountered the highest reduction

in Δf_{ps} with increasing the span-to-depth ratio, in comparison with the 1/3 and 1/6-point concentrated loads. Harajli proposed the following set of equations to predict the stress in the unbonded steel tendons at ultimate (1 psi = 6.895 kPa):

$$f_{ps} = f_{pse} + \left(10{,}000 + \frac{f_c^{'}}{100\rho_{ps}}\right)\left(0.4 + \frac{8}{L/d_{ps}}\right) \leq f_{psy} \ or \ f_{pse} + 60{,}000 \ (psi) \qquad (A.7)$$

where L is the beam span length.

A.2.3 Harajli and Hijazi model (1991)

Harajli and Hijazi (1991) conducted a non-linear analytical investigation on internally unbonded prestressed members. The following equation was proposed to predict the stress in the unbonded steel tendons at ultimate:

$$f_{ps} = f_{pse} + \gamma f_{psu}\left(1.0 - 1.8\frac{c}{d_{ps}}\right) \leq f_{psy} \ psi \qquad (A.8)$$

$$\gamma = \frac{n_o}{n}\left(0.10 + \frac{2.0}{L/d_{ps}}\right) \qquad (A.9)$$

where c is the depth of the neutral axis at ultimate and n_o/n is the ratio of the number of loaded spans to produce maximum moment at the section under consideration to the total number of spans.

A.2.4 Harajli and Kanj model (1991)

Harajli and Kanj (1991) proposed a new model based on the tests carried out on twenty-six beams with various amounts of mild and internally unbonded prestressed steel, and three different span-to-depth ratios of 8, 13, and 20. The authors confirmed the findings of Harajli (1990) that the increase in stress in the unbonded tendons at ultimate, Δf_{ps}, decreased as the span-to-depth ratio of the post-tensioned member increased. However, the authors reported that, contrary to the findings of Harajli (1990), the change in Δf_{ps} was not affected by the geometry of the applied load. The proposed model was similar to that proposed by Harajli and Hijazi (1991) and was based on the following set of equations (1 psi = 6895 MPa):

$$f_{ps} = f_{pse} + \gamma_o f_{psu}(1.0 - 3.0q_o) \leq f_{psy} \quad psi \tag{A.10}$$

where

$$\gamma_o = \frac{n_o}{n}\left(0.12 + \frac{2.5}{L/d_{ps}}\right) \tag{A.11}$$

$$q_o = \frac{A_{ps} f_{pse} + A_s f_{sy}}{b d_{ps} f_c'} \leq 0.23 \tag{A.12}$$

A.2.5 Chakrabarti model (1995)

Chakrabarti (1995) tested thirty-three beams prestressed with unbonded steel tendons up to failure. Parameters included the beams cross sections, concrete strengths, bonded reinforcement,

prestressing steel ratios, and span-to-depth ratios. The author developed an empirical model to predict the stress in the unbonded steel tendons based on the following set of equations.

$$f_{ps} = f_{pse} + k\left[\frac{f_{pse} + 10{,}000 + A}{1 - B} - f_{pse}\right] \leq \begin{cases} f_{pse} + C \\ f_{psy} \end{cases} (psi) \tag{A.13}$$

$$A = \left(\frac{f_c^{'}}{100\rho_s}\right)\left(\frac{d_{ps}}{d_s}\right)\left(\frac{60{,}000}{f_{sy}}\right)\left(1 + \frac{\rho_s}{0.25}\right) \leq 20{,}000\ (psi) \tag{A.14}$$

$$B = r\left(\frac{f_c^{'}}{100\rho_{ps} f_{pse}}\right) \leq 0.25 \tag{A.15}$$

in which:

$$k = 1.00,\ r = 1.0 \text{ and } C = 60{,}000 \text{ for } L/d_e \leq 33 \tag{A.16}$$

$$k = 0.65,\ r = 0.80 \text{ and } C = 40{,}000 \text{ for } L/d_e > 33 \tag{A.17}$$

where d_e is the effective depth from the concrete extreme fiber to the centroidal of the prestressing and mild steel combined.

A.2.6 Naaman and Alkhairi model (1991)

Naaman and Alkhairi (1991) suggested a simplified method to reduce the analysis of the section with unbonded tendons to that of a section with bonded tendons, by applying a reduction coefficient to the strain values of the tendons at ultimate. The authors analyzed previous

experimental results of 143 beams post-tensioned with internally and externally unbonded tendons, and tested under monotonic loading. The span-to-depth ratios of the beams ranged from 7.8 to 45 and the tendons effective prestress was over 50% of their ultimate strength. The best correlation between the experimental and the analytical results led to the following set of equations for the strain reduction coefficient, Ω_u at ultimate:

For one point loading:

$$\Omega_u = \left(\frac{2.6}{L/d_{ps}} \right) \tag{A.18}$$

For third-point or uniform loading:

$$\Omega_u = \left(\frac{5.4}{L/d_{ps}} \right) \tag{A.19}$$

The stress in the unbonded tendons at ultimate is thus obtained as follows:

$$f_{ps} = f_{pse} + \Omega_u E_{ps} \varepsilon_{cu} \left(\frac{d_{ps}}{c} - 1 \right) \leq 0.94 f_{psy} \tag{A.20}$$

where E_{ps} is the modulus of elasticity of the unbonded steel tendons and ε_{cu} is the ultimate concrete compressive strain.

Naaman (2002) claimed that the Equation A.20 could still be valid if unbonded FRP tendons were used. In this case, an upper limit of 0.80 f_{fu} should be used to account for the linear elastic stress-strain response of FRP up to failure, where f_{fu} is the ultimate strength of the FRP tendons. The modulus of elasticity of the steel should then be replaced by that of the FRP tendon.

A.2.7 Aravinthan et al. model (1997)

Aravinthan et al. (1997) modified the model of Naaman and Alkhairi (1991) to account for the change in the tendons eccentricity of the external tendons at ultimate. A reduction coefficient, R_d, was used to reduce the depth of the external steel tendon, depending on the span-to-depth ratio of the beam (L/d_{ps}), the deviator distance-to-span ratio (L_d/L), and the type of loading, where L_d is the distance between the two deviators located along the beam. In this case, the stress in the unbonded steel tendons at ultimate was calculated as follows:

$$f_{ps} = f_{pse} + \Omega_u E_{ps} \varepsilon_{cu} \left(\frac{d_{ps(new)}}{c} - 1 \right) \leq f_{psy} \tag{A.21}$$

$$d_{ps(new)} = R_d d_{ps} \tag{A.22}$$

where $d_{ps(new)}$ is the depth of the external tendons at ultimate after consideration of eccentricity variations. The reduction coefficient, R_d, is calculated as follows:

For one point loading:

$$R_d = 1.14 - 0.005 \left(\frac{L}{d_{ps}} \right) - 0.19 \left(\frac{L_d}{L} \right) \leq 1.0 \tag{A.23}$$

For third-point or uniform loading:

$$R_d = 1.25 - 0.010 \left(\frac{L}{d_{ps}} \right) - 0.38 \left(\frac{L_d}{L} \right) \leq 1.0 \tag{A.24}$$

The authors also proposed different values for the strain reduction coefficient, Ω_u, derived by Naaman and Alkhairi (1991), as follows:

For one point loading:

$$\Omega_u = \frac{0.21}{L/d_{ps}} + 0.04\left(\frac{A_{p(bonded)}}{A_{p(total)}}\right) + 0.04 \tag{A.25}$$

For third-point or uniform loading:

$$\Omega_u = \frac{2.31}{L/d_{ps}} + 0.21\left(\frac{A_{p(bonded)}}{A_{p(total)}}\right) + 0.06 \tag{A.26}$$

where $A_{p(bonded)}$ is the area of the bonded prestressed steel reinforcement and $A_{p(total)}$ is the area of the total (bonded and unbonded) prestressed steel reinforcement.

Appendix B: Load-Deflection Relationships

B.1 General

The relationships between the applied loads and the midspan deflections (recorded by midspan LVDTs) over the life of the unstrengthened and strengthened beams are presented in this appendix. In some cases, when the midspan LVDT showed anomalous readings, the deflections measured under the loading points are given instead.

B.2 Unstrengthened beams: UN15 group

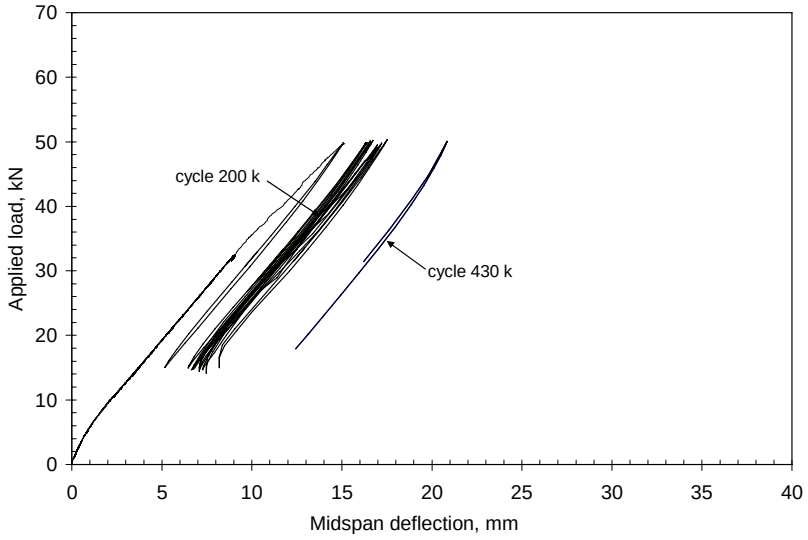

Figure B.1: Beam UN15-F50: load-deflection relationship

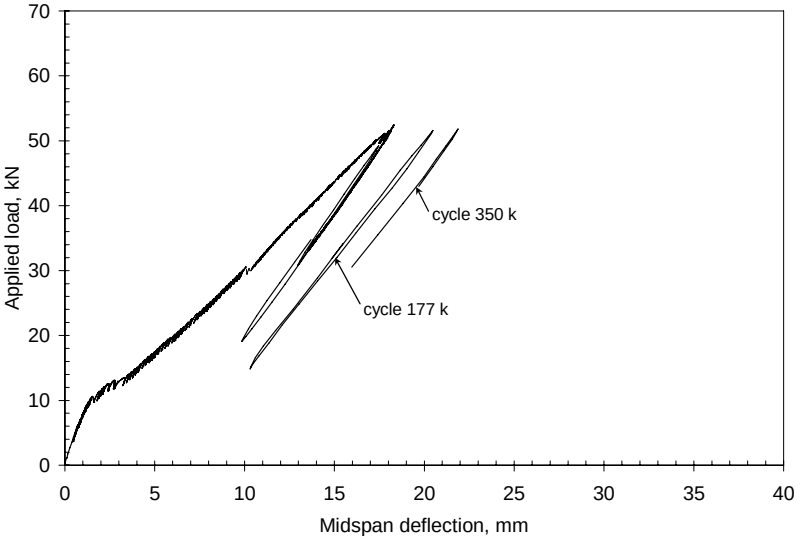

Figure B.2: Beam UN15-F52: load-deflection relationship

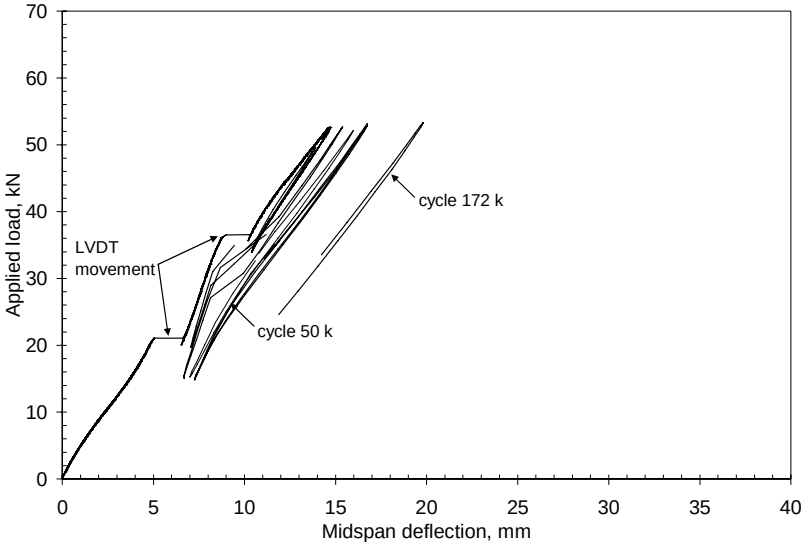

Figure B.3: Beam UN15-F53: load-deflection relationship

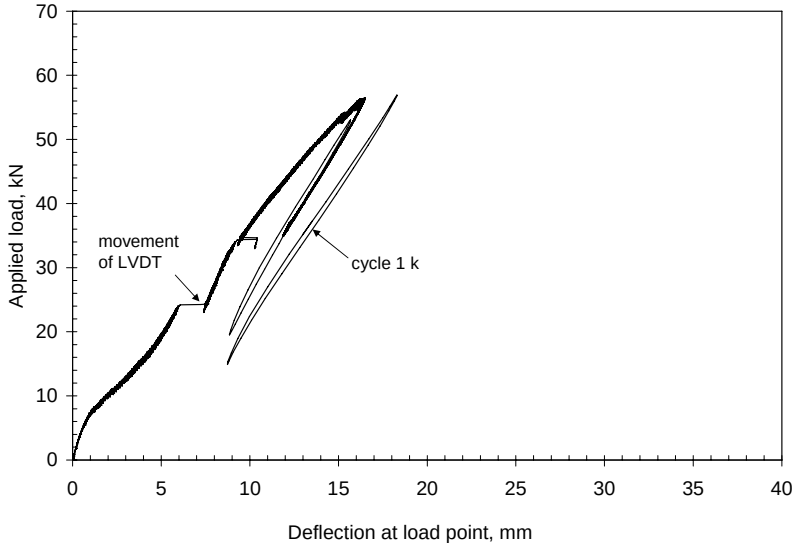

Figure B.4: Beam UN15-F57: load-deflection relationship

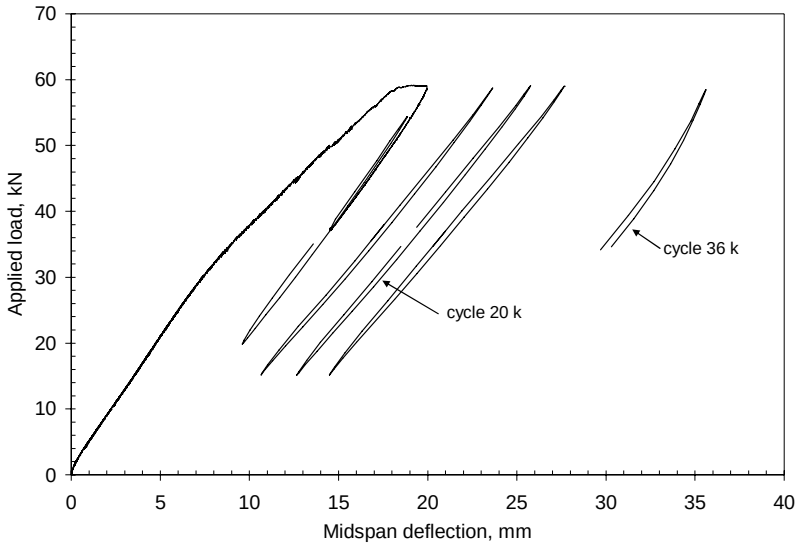

Figure B.5: Beam UN15-F59: load-deflection relationship

B.3 In-service beams: SL15 group

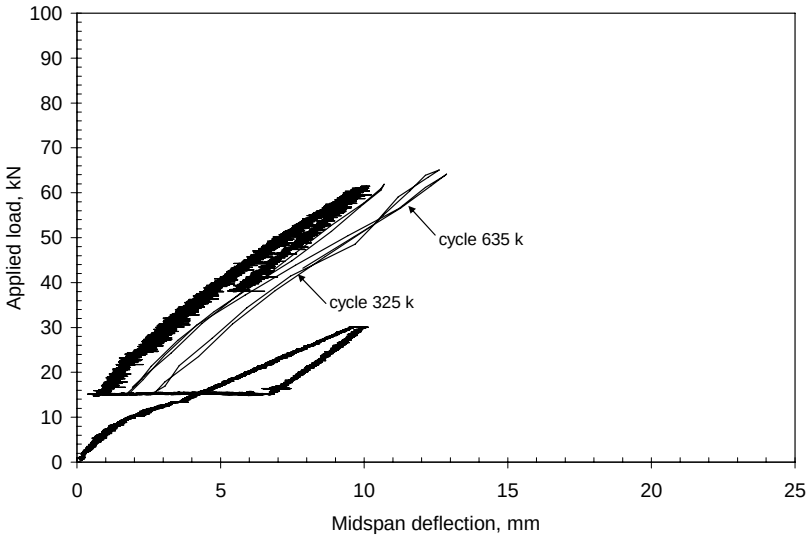

Figure B.6: Beam SL15-F66: load-deflection relationship

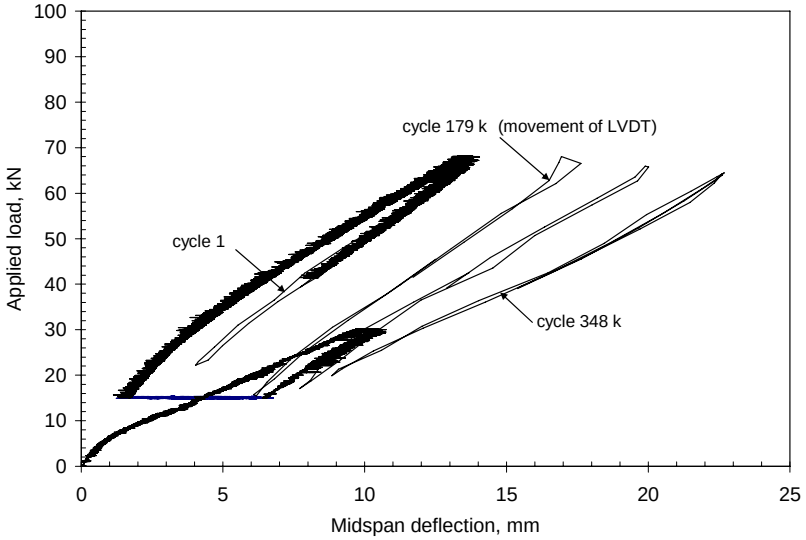

Figure B.7: Beam SL15-F68: load-deflection relationship

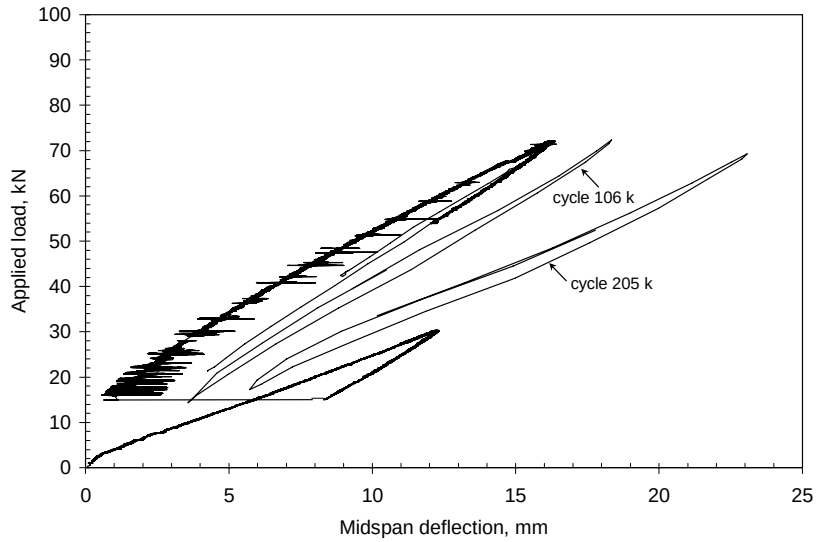

Figure B.8: Beam SL15-F72: load-deflection relationship

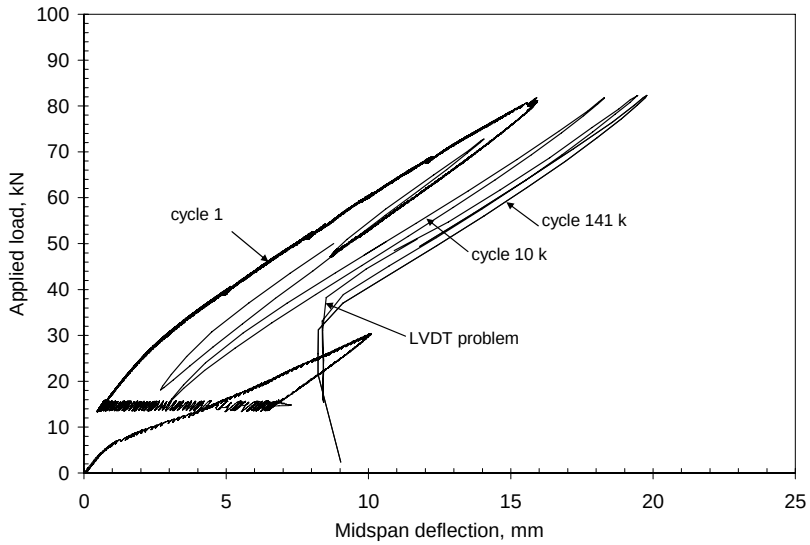

Figure B.9: Beam SL15-F82: load-deflection relationship

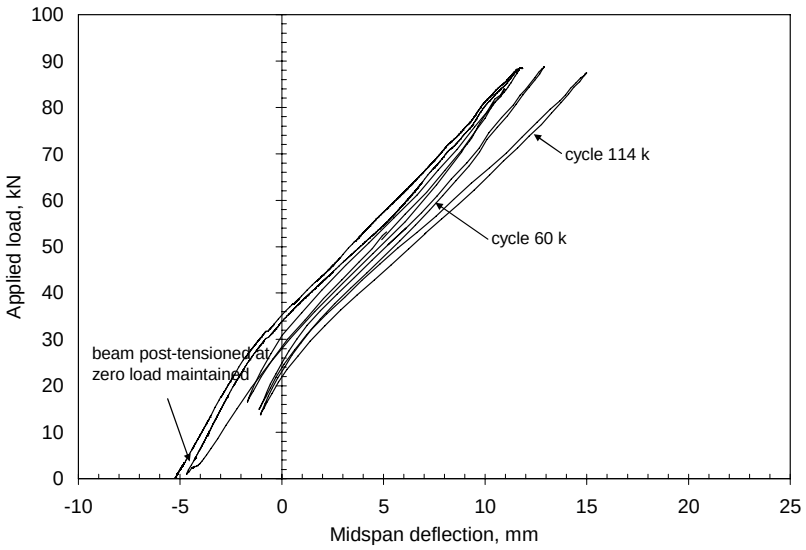

Figure B.10: Beam SL15-F88: load-deflection relationship

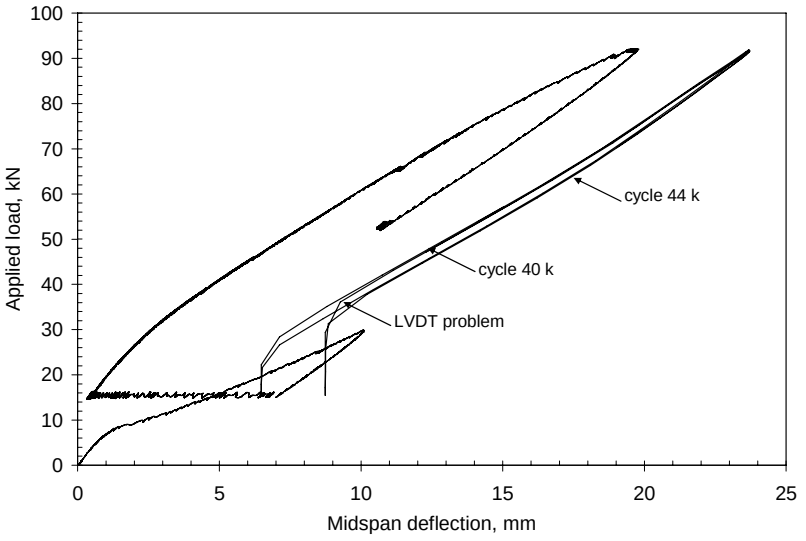

Figure B.11: Beam SL15-F92: load-deflection relationship

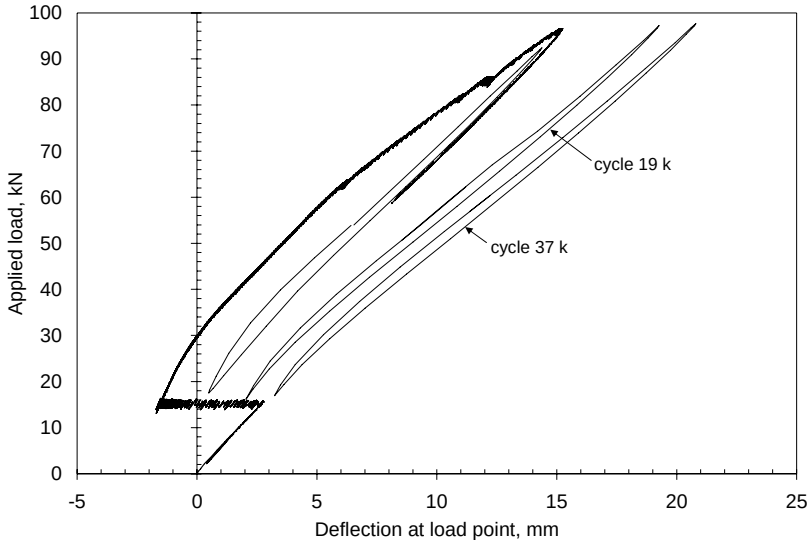

Figure B.12: Beam SL15-F97: load-deflection relationship

B.4 In-service beams: SL20 group

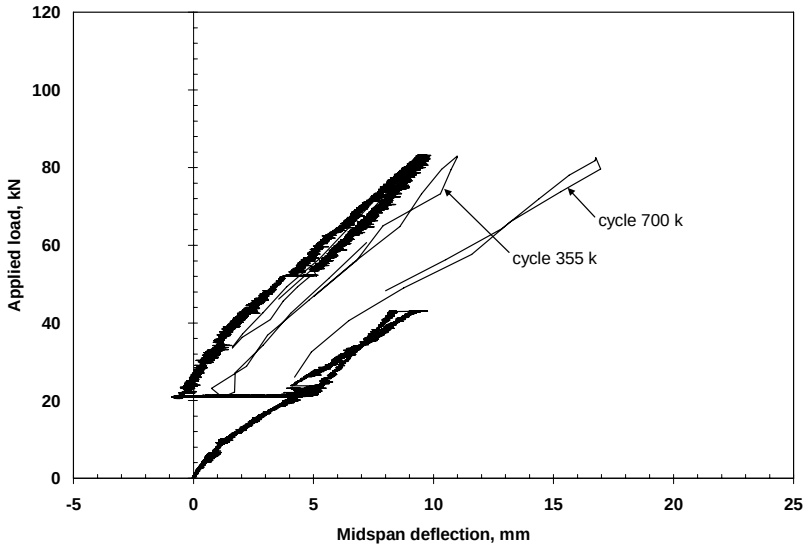

Figure B.13: Beam SL20-F83: load-deflection relationship

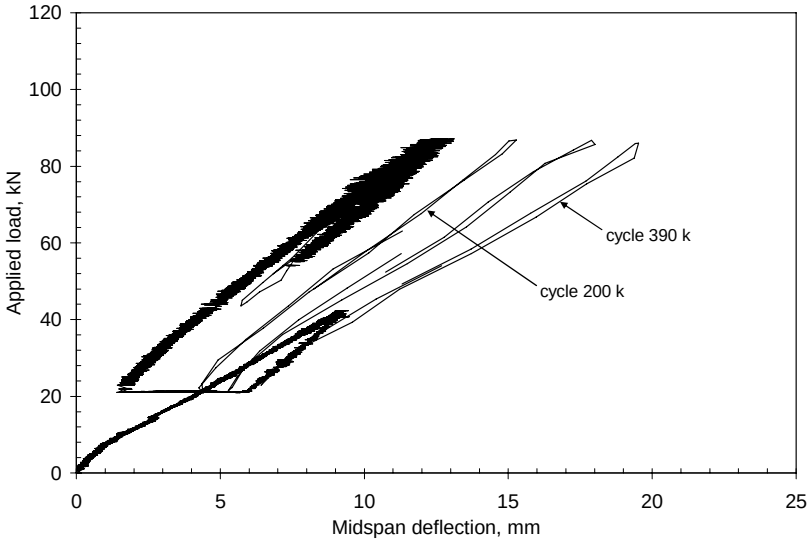

Figure B.14: Beam SL20-F87: load-deflection relationship

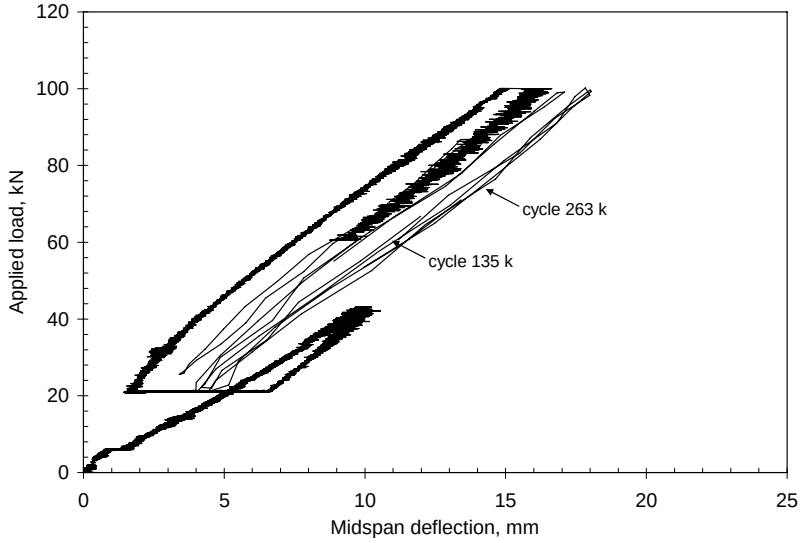

Figure B.15: Beam SL20-F100: load-deflection relationship

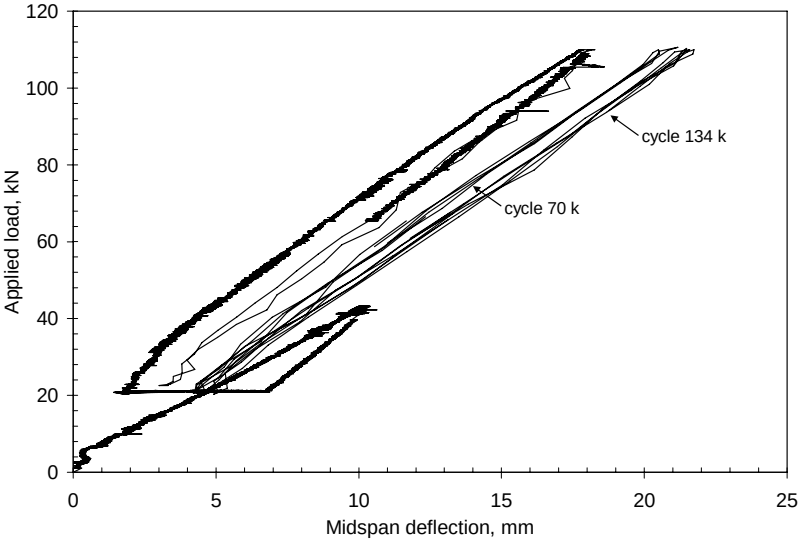

Figure B.16: Beam SL20-F110: load-deflection relationship

B.5 Overloaded beams: OL15 group

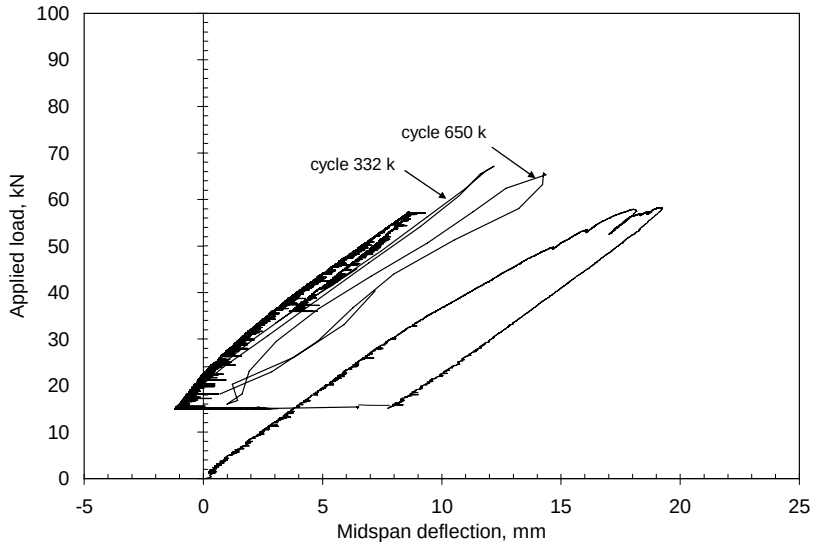

Figure B.17: Beam OL15-F67: load-deflection relationship

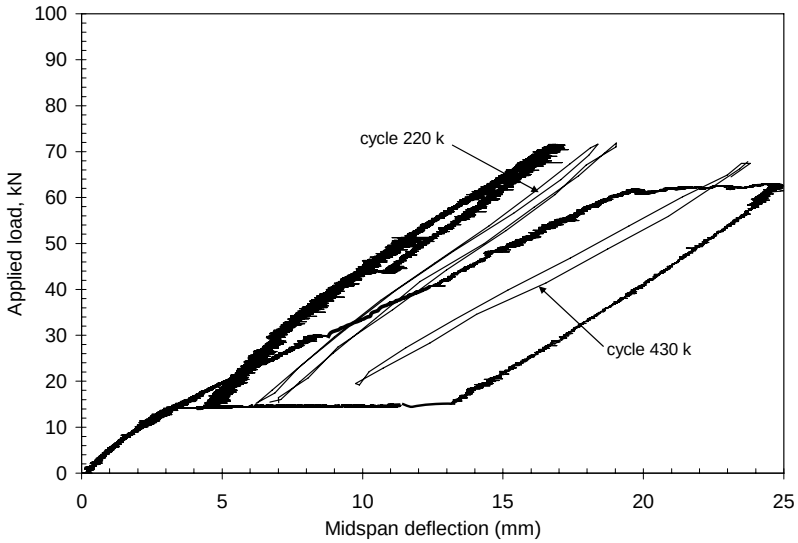

Figure B.18: Beam OL15-F72: load-deflection relationship

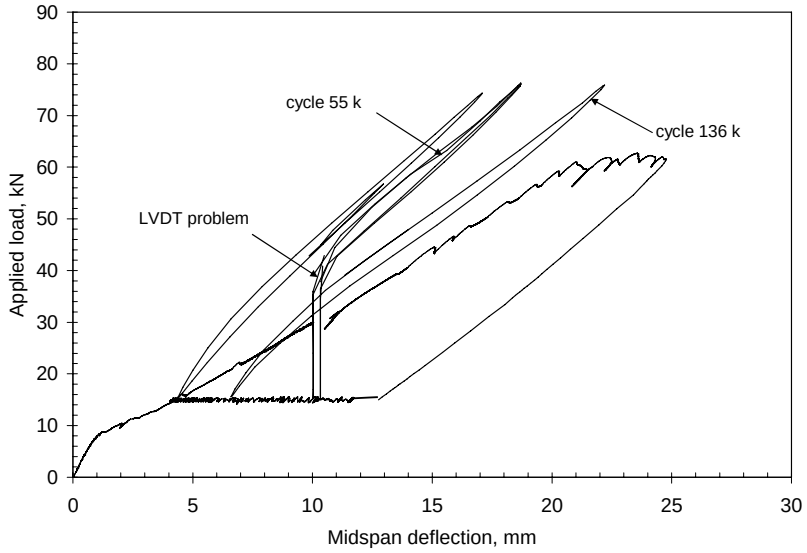

Figure B.19: Beam OL15-F76: load-deflection relationship

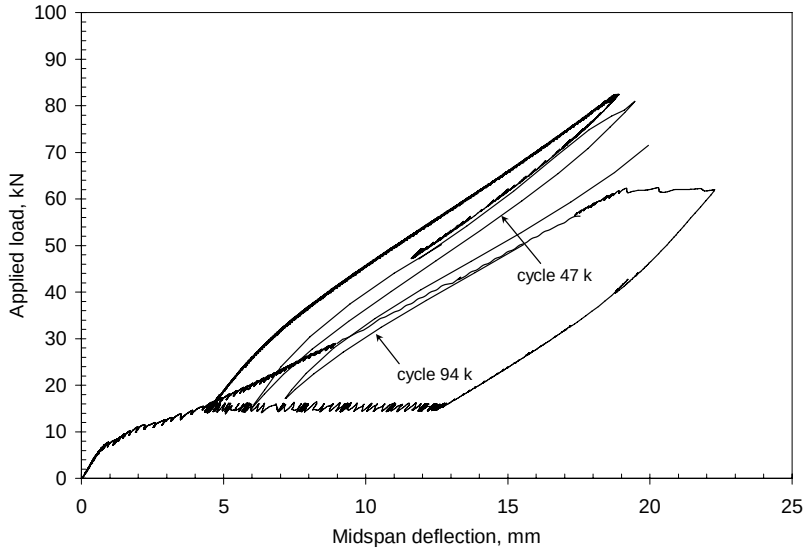

Figure B.20: Beam OL15-F82: load-deflection relationship

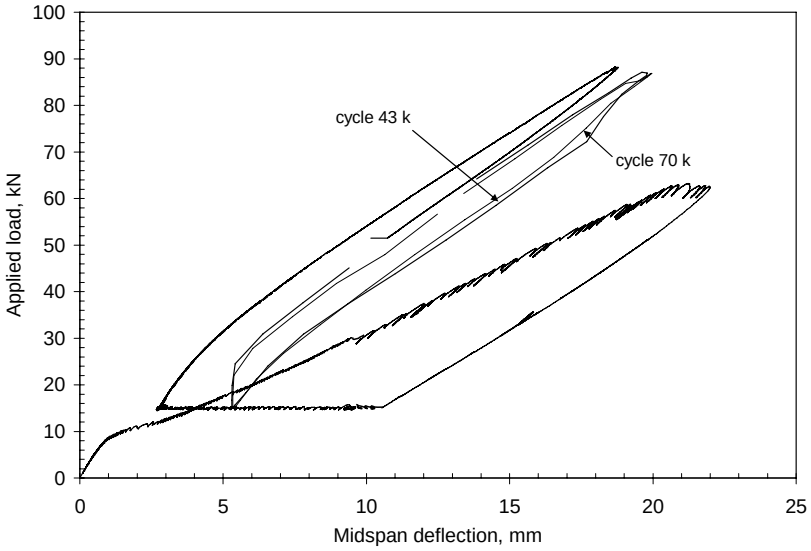

Figure B.21: Beam OL15-F88: load-deflection relationship

Appendix C: Mean Stress Equations

C.1 Introduction

The strain-life relationship is generally expressed as follows:

$$\frac{\Delta\varepsilon}{2} = \frac{\sigma_f'}{E}(2N)^b + \varepsilon_f'(2N)^c \tag{C.1}$$

where $\Delta\varepsilon$ is the strain amplitude, E is the modulus of elasticity of the material, σ_f' is the fatigue strength coefficient, ε_f' is the fatigue ductility coefficient, b is the fatigue strength exponent, c is the fatigue ductility exponent, and N is the number of cycles to failure.

The fatigue coefficients in Equation C.1 are obtained by testing machined specimens under completely reversed strain-controlled cycles at a mean stress of zero. However, typical fatigue applications necessitate the presence of mean stresses, which may have a considerable effect on the fatigue life of the specimen. Tensile mean stresses are detrimental to the specimen and decrease its fatigue life. On the contrary, compressive mean stresses are beneficial and increase the fatigue life of the specimen.

Different approaches were developed in order to account for the mean stress in the strain-life expression given by Equation C.1. The most common approaches were those proposed by Morrow (1968), Smith, Watson, and Topper (1970), and Manson and Halford (1981). The expression proposed by Smith, Watson, and Topper (1970) was used in the current study.

C.2 Morrow's equation (1968)

In order to account for the mean stress effect on the fatigue life, Morrow modified the elastic term in the strain-life equation as follows (Bannantine et al. 1990; Dowling, 1999):

$$\frac{\Delta\varepsilon_e}{2} = \frac{\sigma_f^{'} - \sigma_m}{E}(2N)^b \tag{C.2}$$

where σ_m is the mean stress. Accounting for mean stress, the strain-life equation is thus given as:

$$\frac{\Delta\varepsilon}{2} = \frac{\sigma_f^{'} - \sigma_m}{E}(2N)^b + \varepsilon_f^{'}(2N)^c \tag{C.3}$$

Equation C.3 is consistent with the fact that the mean stress effect on the fatigue life is more pronounced when the elastic strains dominate, i.e., at low values of plastic strains (Bannantine et al., 1990).

C.3 Smith, Watson, and Topper equation (1970)

Smith, Watson, and Topper (1970) proposed another equation to account for mean stress effects. As known, the maximum local stress is given by Equation C.4:

$$\sigma_{\max} = \sigma_f^{'}(2N)^b \tag{C.4}$$

where:

$$\sigma_{\max} = \frac{\Delta\sigma}{2} + \sigma_m \tag{C.5}$$

Multiplying the strain-life equation (Equation C.1) by the maximum stress given in Equation C.4 results in:

$$\sigma_{\max}\frac{\Delta\varepsilon}{2} = \frac{\left(\sigma_f^{'}\right)^2}{E_s}\left(2N\right)^{2b} + \sigma_f^{'}\varepsilon_f^{'}\left(2N\right)^{b+c} \tag{C.6}$$

C.4 Manson and Halford equation (1981)

Manson and Halford (1981) suggested the modification of both elastic and plastic parts of the strain-life equation by the mean stress as follows:

$$\frac{\Delta\varepsilon}{2} = \frac{\sigma_f^{'} - \sigma_m}{E}\left(2N\right)^b + \varepsilon_f^{'}\left(\frac{\sigma_f^{'} - \sigma_m}{\sigma_f^{'}}\right)^{c/b}\left(2N\right)^c \tag{C.7}$$

Since the mean stress effect is applied to both the elastic and plastic parts of the strain-life equation, Equation C.7 tends to overestimate the effect of the mean stress at short lives where plastic strains dominate (Bannantine et al., 1990).

Appendix D: Use of the Fatigue Model in Strengthening Applications

D.1 Introduction

In strengthening applications, designers are typically trying to increase the load ranges that the beam can carry. The following examples demonstrate the use of the proposed fatigue model to calculate the service fatigue life of concrete beams strengthened with externally post-tensioned CFRP tendons. Non-overloaded and overloaded cases are presented.

D.2 Numerical examples

D.2.1 An in-service (non-overloaded) beam

Consider a reinforced concrete beam having the dimensions and material properties of the test specimen used in this study, and designed to resist a service fatigue load that varies between 15 kN and 50 kN. The maximum peak load is to be increased to 66 kN in order to accommodate an increase in the applied live loads. To achieve this new load range, the designer decides to use an externally post-tensioned system similar to that adopted in the current study as follows:

- Double draped CFRP tendons Aslan200™;
- The diameter of the CFRP tendons is 9.4 mm;

– There is a tendon eccentricity of 87 mm at the maximum moment location and zero at the ends of the beam;

– A post-tensioning force of 40% of the ultimate capacity of the tendons (120 kN) is applied;

– The beam will be post-tensioned while under a static load of 15 kN.

In the following, the number of cycles that the strengthened beam can accommodate under the newly applied load range will be determined, assuming that the beam has already experienced 25% of its initially designed fatigue life. The calculations involve the following steps:

a) Calculate the fatigue life of the unstrengthened beam under the initial applied load range;

b) Calculate the stress range in the steel bars after strengthening, using the monotonic analysis described in Section 7.2.1;

c) Calculate the fatigue life of the strengthened beam under this stress range using the fatigue model described in Section 7.2.2;

d) Determine the remaining number of cycles that the strengthened beam can accommodate using Miner's rule.

From the monotonic analysis of the unstrengthened beam, a fatigue load range between 15 kN and 50 kN causes a stress range in the steel bars of 262 MPa. Using a fatigue notch factor, K_f, of 2.0, the fatigue life of the beam is estimated to be 306,800 cycles. Under the new load range applied to the strengthened beam, the monotonic analysis described in Section 7.2.1 shows that the stress range in the steel bars decreases to 249 MPa if a post-tensioning force of 120 kN is used. This stress range corresponds to a fatigue life of 895,900 cycles for the strengthened beam.

In order to determine the number of cycles that the strengthened beam can accommodate under the new stress range, the Miner's linear damage rule is used along with the proposed fatigue model. Miner's rule is expressed by Equation D.1 :

$$1-\frac{n_1}{N_1}=\frac{n_2}{N_2} \tag{D.1}$$

where n_1 is the number of cycles already experienced by the unstrengthened beam (approximately 76,700 cycles in this case representing 25% of its fatigue life), N_1 is the initial fatigue life of the beam before strengthening (306,800 cycles), n_2 is the number of cycles remaining in the life of the strengthened beam, and N_2 is the new design fatigue life after strengthening (895,900 cycles).

Using Miner's rule, the remaining number of cycles that the beam can accommodate under the new stress range is estimated as n_2 = 672,000 cycles.

D.2.2 An overloaded beam

Consider that the same unstrengthened beam has been overloaded during its service and that overloading has caused a strain of 0.004 in the reinforcing steel bars. Assume also that the beam is unloaded to a load level of 15 kN prior to strengthening with external CFRP tendons post-tensioned at 120 kN.

Under the new load range applied to the strengthened beam, the monotonic analysis of the overloaded beam suggests that the stress range in the steel bars is 331 MPa if a post-tensioning force of 120 kN is used. Using a fatigue notch factor of 2.0, the fatigue life of the strengthened beam corresponding to this stress range is estimated to be 636,000 cycles. Using Miner's rule, the remaining number of cycles is estimated as 477,000 cycles.

References

AASHTO (1994). "LRFD Bridge Design Specifications," 1st edition. American Association of State Highway and Transportation Officials, Washington, DC.

ACI Committee 215R-74 (1997). "Considerations for Design of Concrete Structures Subjected to Fatigue Loading," American Concrete Institute (ACI 215R-74), Farmington Hills, MI.

ACI Committee 318 (2005). "Building Code Requirements for Reinforced Concrete," American Concrete Institute (ACI 318-05) and Commentary (ACI 318R-05), Detroit, Michigan.

ACI Committee 440.4R (2004). "Guidelines for Prestressing Concrete Structures With FRP Tendons," American Concrete Institute (ACI 440.4R-04), Farmington Hills, MI.

ACI-ASCE Committee 423.5R (1999). "State-of-the-Art Report on Partially Presressed Concrete," American Concrete Institute, Farmington Hills, MI.

Adachi, Y., Hayashida, M., Sakai, H., Mashima, M., and Miyagawa, T. (1997). "Strengthening of Prestressed Concrete Segmental T-Beam Bridge Using FRP External Prestressing Systems," Proceedings of Non-Metallic (FRP) Reinforcement for Concrete Structures, 1997, pp. 695-702.

Al-Hammoud, R. (2006). "Fatigue Flexural Behaviour of Corroded Reinforced Concrete Beams Repaired With CFRP Sheets," M.Sc. Thesis, University of Waterloo, Waterloo, Ontario, Canada.

Alkhairi, F., (1991). "On the Flexural Behaviour of Concrete Beams Prestressed With Unbonded Internal and External Tendons," Ph.D. Dissertation, University of Michigan.

Al-Mayah, A. (2004). "Interfacial Behaviour of CFRP-Metal Couples for Wedge Anchor Systems," University of Waterloo, Ontario, Canada.

Al-Mayah, A., Soudki, K., and Plumtree, A. (2001). "Experimental and Analytical Investigation of a Stainless Steel Anchorage for CFRP Pretensioning Tendons," PCI Journal, Vol. 46, No. 2, pp. 88-100.

Al-Mayah, A., Soudki, K., and Plumtree, A. (2003). Tension Anchorage. Patent No. PCT/CA03/01469.

An, L., Yamamoto T., Hattori A., and Miyagawa T. (2003). "Comparative Analysis on Stress Calculation Methods for External FRP Cables," Proceedings of the Sixth International Symposium on FRP Reinforcement for Concrete Structures (FRPRCS-6), Tan, K.H. editor, Singapore, pp. 995-1002.

Aravinthan, T., Mutsuyoshi, H, Fujioka, A., and Hishiki, Y. (1997). "Prediction of the Ultimate Flexural Strength of Externally Prestressed PC Beams," Transactions of the Japan Concrete Institute, Vol. 19, 1997, pp. 225-230.

Ariyawardina N. (2000). “Prestressed Concrete with Internal or External Tendons: Behaviour and Analysis”, Ph.D. Dissertation, University of Calgary, Canada.

Badawi, M. (2007). “Monotonic and Fatigue Flexural Behaviour of RC Beams Strengthened with Prestressed NSM CFRP Rods,” Ph.D. Dissertation, University of Waterloo, Ontario, Canada.

Bakis C. E., Bhat B. B., Schokker A. J., and Boothby T. E. (2001). “Flexure of Concrete Beams Prestressed with FRP Tendons,” Proceedings of the Fifth International Conference on Fiber Reinforced Plastics for Reinforced Concrete Structures (FRPRCS-5), Cambridge, UK, Vol. 2, pp. 689-698.

Bannantine, J.A., Comer, J.J., and Handrock, J.L. (1990). “Fundamentals of Metal fatigue Analysis,” Prentice Hall, NJ, USA, First Edition.

Barnes, R.A. and Mays, G.C. (1999). “Fatigue Performance of Concrete Beams Strengthened With CFRP Plates,” Journal of Composites for Construction, ASCE, Vol. 3, No. 2, pp. 63-72.

Bazant, Z., and Oh, B. (1984). “Deformation of Progressively Cracking Reinforced Concrete Beams,” ACI Journal, Vol. 81, No. 3, pp. 268-278.

Benmokrane, B., Zhang, B., and Chennouf, A. (2000). “Tensile Properties and Pullout Behaviour of AFRP and CFRP Rods for Grouted Anchor Applications,” Journal of Construction and Building Materials, Vol. 14, No. 3, pp. 157-170.

Bishara A.G. (1982). “Some Aspects of Dynamic Response of Rectangular Reinforced Concrete Beams,” Fatigue of Concrete Structures, Shah, S.P. editor, ACI SP-75, Detroit, MI, pp. 235-252.

Braimah, A., Green, M. F., and Campbell, T. I. (2006). “Fatigue Behaviour of Concrete Beams Post-Tensioned with Unbonded Carbon Fibre Reinforced Polymer Tendons,” Canadian Journal of Civil Engineering, Vol. 33, No. 9, pp. 1140-1155.

Brena, S.R., Benouaich, M.A., Kreger, M.E., and Wood, S.L. (2005). “Fatigue Tests of Reinforced Concrete Beams Strengthened Using Carbon Fiber-Reinforced Polymer Composites,” ACI Structural Journal, Vol. 102, No. 2, pp. 305-313.

Budelmann, H., Kepp, B., and Rostasy, F. S. (1990). “Fatigue Behaviour of Bond-Anchored Unidirectional Glass-FRPs,” Proceedings of the First Materials Engineering Congress, Serviceability and Durability of Construction Materials, p. 1142-1151.

Burgoyne, C. J. (1993). “Should FRP Be Bonded To Concrete,” International Symposium on Fiber-Reinforced-Plastic Reinforcement for Concrete Structures, Vancouver, Canada, Nanni, A. and Dolan, C. editors, American Concrete Institute, ACI SP-138, pp. 367-380.

Burns, N.H. and Pierce, D.M. (1967). “Strength and Behaviour of Prestressed Concrete Members With Unbonded Tendons,” Journal of Prestressed Concrete Institute, Vol. 12, No. 5, pp. 15-29.

Campbell, T. I. and Chouinard K. L. (1991). “Influence of Non-Prestressed Reinforcement on the Strength of Unbonded Partially Prestressed Concrete Beams,” ACI Structural Journal, Vol. 88, No. 5, pp. 546-551.

Campos C., Guimaraes G., and Burgoyne C. (2001). "Rotation Capacity of Beams Prestressed With Synthetic External Tendons," Proceedings of the Fifth International Conference on Fiber Reinforced Plastics for Reinforced Concrete Structures, FRPRGS-5, Vol. 2, pp. 711-720.

CAN/CSA-S6-00 (2000). Canadian Highway Bridge Design Code.

Canadian Prestressed Concrete Institute-CPCI (1996). "Design Manual of Precast and Prestressed Concrete," 3rd Edition, CPCI, Canada.

Canadian Standards Association (2004). "Design of Concrete Structures," Standard CAN/CSA A23.3-04, Mississauga, Ontario, Canada.

Chakrabarti, P. R. (1995). "Ultimate Stress for Unbonded Prestressed Tendons in Partially Prestressed Beams," ACI structural Journal, Vol. 92, No. 6, pp. 689-697.

Chakrabarti, P. R., Whang T. P., Brown W., Arsad K. M., and Amezeua E., (1994). "Unbonded Prestressed Tendons and Partially Prestressed Beams," ACI Structural Journal, Vol. 91, No. 5, pp. 616-625.

Collins, M. P., and Mitchell, D. (1991). "Prestressed Concrete Structures," Prentice-Hall Inc. Englewood Cliffs, N.J.

Comite Euro-International du Beton (CEB-FIP) (1990). CEB-FIP Model Code, Thomas Telford, London, United Kingdom.

Dolan C., Hamilton, R., Bakis, C., and Nanni, A. (2001). "Design Recommendations for Concrete Structures Prestressed with FRP Tendons," Draft Final Report, University of Wyoming, Report DTFH61-96-C-00019, Laramie Wyoming.

Dolan, C. W. (1993). "FRP Development in the United States," Fiber Reinforced Plastic Reinforcement for Concrete Structures: Properties and Applications, Nanni, A. editor, pp. 129-163.

Dowling, N. E., (1999), Mechanical Behaviour of Materials: Engineering Methods for Deformation, Fracture, and Fatigue. Prentice Hall, NJ, USA, Second Edition.

Eibl J. (1990). "Externally Prestressed Bridges," External Prestressing in Bridges, Naaman, A. and Breen, J. editors, ACI SP-120, Detroit, MI, pp. 375-387.

El Maadawy, T. (2004). "Performance of Corrosion-Damaged Reinforced Concrete Beams Repaired With CFRP Laminates," Ph.D. Thesis, University of Waterloo, Waterloo, Ontario, Canada.

El Refai, A., West, J., and Soudki, K. (2003). "FRP Tendons in Post-Tensioning," PTI Journal, Vol. 1, No. 3, pp. 22-29.

El-Hacha R. (1997). "Strengthening of Concrete Beams with Advanced Composite Materials," M.Sc. Thesis, Concordia University, Montreal, Quebec, Canada.

El-Hacha R. and Elbadry, M. (2001). "Strengthening Concrete Beams With Externally Prestressed Carbon Fiber Composite Cables," Proceedings of the Fifth International Conference on Fiber Reinforced Plastics for Reinforced Concrete Structures (FRPRCS-5), Cambridge, UK, pp. 699-708.

El-Tawil, S., Ogunc, C., Okeil, A., and Shahawy, M. (2001). "Static and Fatigue Analysis of RC Beams Strengthened With CFRP Laminates," Journal of Composites for Construction, ASCE, Vol. 5, No. 4, pp. 258-267.

Ghallab A. and Beeby A. W. (2003). "Deflection of Prestressed Concrete Beams Externally Strengthened Using Parafil Ropes," Magazine of Concrete Research, Vol. 55, No. 1, pp. 1-17.

Ghallab A. and Beeby A. W. (2004). "Calculating Stress of External Prestressing Tendons," Structures and Buildings Journal, Vol. 157, No. 4, pp. 263-278.

Ghallab A. and Beeby A. W. (2005). "Factors Affecting the External Prestressing Stress in Externally Strengthened Prestressed Concrete Beams," Journal of Cement and Concrete Composites, Vol. 27, No. 9-10, pp. 945-957.

Grace N. F. & Abdel-Sayed G. (1998). "Behaviour of Externally Draped CFRP Tendons in Prestressed Concrete Bridges," Journal of Prestressed Concrete International, Vol. 43, No. 5, pp. 88-101.

Harajli M. (1990). "Effect of Span-Depth Ratio on the Ultimate Steel Stress in Unbonded Prestressed Concrete Members," ACI Structural Journal, Vol. 87, No. 3, pp. 305-312.

Harajli M. H. (1993). "Strengthening of Concrete Beams By External Prestressing," PCI Journal, Vol. 38, No. 6, pp. 76-88.

Harajli, M. H. and Kanj, M. Y. (1991). "Ultimate Flexural Strength of Concrete Members Prestressed With Unbonded Tendons," ACI Structural Journal, Vol. 88, No. 6, pp. 663-673.

Harajli, M. H. and Kanj, M. Y. (1992). "Service Load Behaviour of Concrete Members Prestressed With Unbonded Tendons," Journal of Structural Engineering, ASCE, Vol. 118, No. 9, pp. 2569-2589.

Harajli, M., and Hijazi, S. (1991). "Evaluation of the Ultimate Steel Stress in Partially Prestressed Concrete Members," PCI Journal, Vol. 36, No. 1, pp. 62-82.

Harajli, M., Khairallah, N., and Nassif, H. (1999), "Externally Prestressed Members: Evaluation of Second-Order Effects," Journal of Structural Engineering, Vol. 125, No.10, pp. 1151-1161.

Harajli, M.H. (2006). "On the Stress in Unbonded Tendons at Ultimate: Critical Assessment and Proposed Changes," ACI Structural Journal, Vol. 103, No. 6, pp. 803-812.

Heffernan, P.J. (1997). "Fatigue Behaviour of Reinforced Concrete Beams Strengthened with CFRP Laminates," Ph.D. Thesis, Royal Military College of Canada, Ontario, Canada.

Heffernan, P.J., Erki, M., and DuQuesnay, D.L. (2004). "Stress Redistribution in Cyclically Loaded Reinforced Concrete Beams," ACI Structural Journal, Vol. 101, No. 2, pp. 261-268.

Helgason, T., Hanson, J.M., Somes, N.F., Corley, W.G., and Hognestad, E. (1976). "Fatigue Strength of High Yield Reinforcing Bars," NCHRP Report 164, Transportation Research Board.

ISIS Canada Educational Modules (2004), Version 1.0, ISIS Canada Research Network, Winnipeg, MB, Canada.

ISIS Canada, (2003). "Prestressing Concrete Structures with Fiber Reinforced Polymers," Draft Design Manual No. 5, ISIS, Canada.

Jerrett C. V. and Ahmad S. H. (1996). "Behaviour of Prestressed Concrete Beams Strengthened By External FRP Post-Tensioned Tendons", Proceedings of Advanced Composite Materials in Bridges and Structures, pp. 305- 312.

Kato, T., and Hayashida, N. (1993). "Flexural Characteristics of Prestressed Concrete Beams With CFRP Tendons," International Symposium on Fiber-Reinforced-Plastic Reinforcement for Concrete Structures, Vancouver, Canada, Nanni, A. and Dolan, C. editors, American Concrete Institute, ACI SP-138, pp. 419-439.

Keller, T. (2003). "Strengthening of Concrete Bridges with Carbon Cables and Strips," Proceedings of the Sixth International Symposium on FRP Reinforcement for Concrete Structures (FRPRCS-6), Tan, K.H. editor, Singapore, pp. 1331-1340.

Lee, L., Moon, J., and Lim, J. (1999). "Proposed Methodology for Computing of Unbonded Tendon Stress at Flexural Failure," ACI Structural Journal, Vol. 96, No. 6, pp. 1040-1048.

MacGregor, J.G., Jhamb, I.C., and Nuttall, N. (1971). "Fatigue Strength of Hot Rolled Deformed Reinforcing Bars," ACI Journal, Vol. 68, No. 3, pp. 169-179.

Manabe H., Kanaumi S., Inoue S., and Miyagawa T. (1997). "The Ultimate Strength of Prestressed Concrete Segmental T-Girders Using an FRP External Prestressing System," Proceedings of the Third International Symposium on Non-Metallic Reinforcement for Concrete Structures, Sapporo, Japan, pp. 791-798.

Manson, S. S. and Halford, G. R. (1981). "Practical implementation of the Double Linear Damage Rule and Damage Curve Approach for Treating Cumulative Fatigue Damage," International Journal of Fracture, Vol. 17, No. 2, pp. 169-172.

Masoud, S., Soudki, K., and Topper, T. (2005). "Post-Repair Fatigue Performance of FRP-Repaired Corroded RC Beams: Experimental and Analytical Investigation," Journal of Composites for Construction, ASCE, Vol. 9, No.5, pp. 441-449.

Masoud, S.G. (2002). "Behaviour of Corroded Reinforced Concrete Beams Repaired With FRP Sheets under Monotonic and Fatigue Loading," Ph.D. Thesis, University of Waterloo, Waterloo, Ontario, Canada.

Mattock, A. H., Yamazaki, J. and Kattula, B. T., "Comparative Study of Prestressed Concrete Beams, with and without Bond", ACI Journal, No.68-13, Feb. 1971, pp116-125.

Mays, G. C. and Tilly, G. P. (1982). "Long Endurance Fatigue Performance of Bonded Structural Joints," International Journal of Adhesion and Adhesives, Vol. 2, No. 2, pp. 109-114.

Min, C. S. (1997). "Ultimate Behaviour of RC Hyperbolic Paraboloid Saddle Shell," Structural Engineering and Mechanics, Vol. 5, No. 5, pp. 507-521.

Mojtahedi, S. and Gamble, W. (1978). "Ultimate Steel Stresses in Unbonded Prestressed Concrete," Journal of the Structural Division, ASCE, vol. 104, No. 7, pp. 1159-1164.

Mutsuyoshi, H. and Machida, A. (1993). "Behaviour of Prestressed Concrete Beams Using FRP as External Cable," ," International Symposium on Fiber-Reinforced-Plastic Reinforcement for Concrete Structures, Vancouver, Canada, Nanni, A. and Dolan, C. editors, American Concrete Institute, ACI SP-138, pp. 401-417.

Mutsuyoshi, H., Machida, A., and Shiratori, N. (1990). "Application of Carbon fiber Reinforced Cables to Concrete Structures," Symposium of the International Association for Bridge and Structural Engineering, Bruxelles, pp. 623-628.

Naaman A. E., Burns N., French C., Gamble W. L., and Mattock A. H. (2002). "Stresses in Unbonded Prestressing Tendons at Ultimate: Recommendation," ACI Structural Journal, Vol. 99, No. 4, pp. 518-529.

Naaman, A. and Siriaksorn, A. (1979). "Serviceability Based Design of Partially Prestressed Beams," PCI Journal, Vol. 24, No. 2, pp. 64-89.

Naaman, A. E. (1990). "A New Methodology For The Analysis of Beams Prestressed With External or Unbonded Tendons," External Prestressing in Bridges, Naaman, A. and Breen, J. editors, ACI SP-120, Detroit, MI, pp. 339-354.

Naaman, A. E. (2005). "PC Beams With Unbonded Tendons: Analysis in Cracked, Uncracked, and Ultimate State," Historic Innovations in Prestressed Concrete, ACI SP-231, Bruce Russell and Shawn Gross editors, pp. 105-127.

Naaman, A., and Alkhairi, F. (1991). "Stress at Ultimate in Unbonded Post-Tensioning Tendons; Part 2 - Proposed Methodology," ACI Structural Journal, Vol. 88, No. 6, pp. 683-692.

Nanni, A., Bakis, C., O'Neil, E., and Dixon, T. (1996). "Performance of FRP Tendon-Anchor Systems for Prestressed Concrete Structures," PCI Journal 1996, Vol. 41, No. 1, pp. 34-44.

Neville, A. M. and Brooks, J.J. (1990). "Concrete Technology: Properties of Concrete," John Wiley and Sons, Inc., NJ, USA.

Ng, C. K. (2003). "Tendon Stress and Flexural Strength of Externally Prestressed Beams," ACI Structural Journal, Vol. 100, No. 5, pp. 644-653.

Odagiri, T., Matsumoto, K., and Nakai, H. (1997). "Fatigue and Relaxation Characteristics of Continuous Aramid Fiber Reinforced Plastic Rods," Proceedings of the Third International Symposium on Non-Metallic Reinforcement for Concrete Structures, Sapporo, Japan, pp. 227-234.

Park, R., and Paulay, T. (1975). "Reinforced Concrete Structures," John Wiley & Sons, Inc., USA.

Post-Tensioning Institute – PTI (1997). Post-Tensioning Manual: Fifth Edition. Phoenix, AZ.

Quayle, T. (2005). "Tensile-flexural Behaviour of Carbon-Fiber Reinforced Polymer (CFRP) Prestressing Tendons Subjected to Harped Profiles," M.Sc. thesis, University of Waterloo, Ontario, Canada.

Rao, S. and Mathew, G. (1996). "Behaviour of Externally Prestressed Concrete Beams With Multiple Deviators", ACI Structural Journal, Vol. 93, No. 44, pp. 387-396.

Rosenboom, O. and Rizkalla, S. (2006). "Behaviour of Prestressed Concrete Strengthened With Various CFRP Systems Subjected to Fatigue Loading," Journal of Composites for Construction, ASCE, Vol. 10, No. 6, pp. 492-502.

Saadatmanesh, H. and Tannous, F. E. (1999). "Relaxation, Creep, and Fatigue Behaviour of Carbon Fiber Reinforced Plastic Tendons," ACI Materials Journal, Vol. 96, No. 2, pp. 143-153.

Saeki, N., T. Horiguchi, K., Inomata, M., Hata, S., and Ikeda, T. (1993). "Strengthening of Damaged Concrete Beams By External Prestressing of Aramid Fiber Cable", International Symposium on Fiber-Reinforced-Plastic Reinforcement for Concrete Structures, Vancouver, Canada, Nanni, A. and Dolan, C. editors, American Concrete Institute, ACI SP-138, pp. 913-932.

Santoh, N. (1993). "CFCC: Carbon Fiber Composite Cable," FRP Reinforcement for Concrete Structures: Properties and Applications, Nanni, A. Editor, Elsevier Science Publishers B.V. Amsterdam, pp. 223-248.

Sayed-Ahmed, E., and Shrive, N. (1998). "A New Steel Anchorage System for Post-Tensioned Applications Using Carbon Fiber Reinforced Plastic Tendons," Canadian Journal of Civil Engineering, Vol. 25, No. 1, pp. 113-127.

Schmidt, R. J., Dolan, C.W., and Holte, L. E. (1994). "Anchorage of Non-Metallic Prestressing Tendons," Proceedings of the Structures Congress XII, Atlanta, GA, USA, pp. 1415-1420.

Shahrooz B. M., Boy S., and Baseheart T. M. (2002). "Flexural Strengthening of Four 76-Year-Old T-Beams With Various FRP Systems: Testing and Analysis", ACI Structural Journal, Vol. 99, No. 5, pp. 681-691.

Smith, K.N., Watson, P., and Topper, T.H. (1970). "A Stress-Strain Function for the Fatigue of Metals," Journal of Materials, Vol. 5, No. 4, pp. 767-778.

Taha, M. R. and Shrive, N. G. (2003). "New Concrete Anchors for Carbon Fiber-Reinforced Polymer Post-Tensioning Tendons - Part 1: State-of-the-art review/design," ACI Structural Journal, Vol. 100, No. 1, pp. 96-104.

Taha, M. R. and Shrive, N. G. (2003). "New Concrete Anchors for Carbon Fiber-Reinforced Polymer Post-Tensioning Tendons - Part 2: Development/Experimental Investigation," ACI Structural Journal, Vol. 100, No. 1, pp. 96-104.

Tan, K. and Ng, C. (1997). "Effects of Deviators and Tendon Configuration On Behaviour of Externally Prestressed Beams", ACI Structural Journal, Vol. 94, No. 1, pp. 13-22.

Tan, K., Al Farooq, M. A., and Ng, C. (2001). "Behaviour of Simple-Span Reinforced Concrete Beams Locally Strengthened With External Tendons," ACI Structural Journal, Vol. 98, No. 2, pp. 174-183.

Taniguchi, H., Mutsuyoshi, H., Kita, T., and Machida, A. (1997). "Flexural Behaviour of Externally Prestressed Concrete Beams Using CFRP and Aramid Rope Under Static and Dynamic Loading," Proceedings of the Fifth International Conference on Fiber Reinforced Plastics for Reinforced Concrete Structures (FRPRCS-5), Cambridge, UK, Vol. 2, pp. 783-790.

Tao X., and Du G. (1985). "Ultimate Stress of Unbonded Tendons in Partially Prestressed Concrete Beams," PCI Journal, Vol. 30, No. 6, pp. 72-91.

Tepfers, R. (1979). "Cracking of Concrete Cover along Anchored Deformed Reinforcing Bars," Magazine of Concrete Research, Vol. 31, No. 106, pp. 3-12.

Tilly, G. P. (1979). "Fatigue of Steel Reinforcement Bars in Concrete: A Review," Fatigue of Engineering Materials and Structures, Vol. 2, No. 3, pp. 251-278.

Tjandra R. A. and Tan K. H. (2001). "Strengthening of RC Continuous Beans With External CFRP Tendons", Proceedings of the Fifth International Conference on Fiber Reinforced Plastics for Reinforced Concrete Structures (FRPRCS-5), Cambridge, UK, Vol. 2, pp. 661-669.

Tjandra, R., and Tan K. (2003). "Strengthening of RC Beams With External FRP Tendons: Tendon Stress at Ultimate", Proceedings of the Sixth International Symposium on FRP Reinforcement for Concrete Structures (FRPRCS-6), Tan, K.H. editor, Singapore, pp. 985-994.

Uomoto, T., Nishimura, T., and Ohga, H. (1995). "Static and Fatigue Strength of FRP Rods for Concrete Reinforcement," Non-Metallic Reinforcement for Concrete Structures, L. Taerwe editor, London, pp. 100-107.

Walton, M. and Yeung, Y. (1986). "The Fatigue Performance of Structural Strands of Pultruded Composite Rods," Journal of the Institute of Mechanical Engineers (C286/86), London, England, pp. 315-320.

Whaley, C.P. and Neville, A.M. (1973). "Non-elastic deformation of concrete under cyclic compression," Magazine of Concrete Research, Vol. 25, No. 84, pp. 145-154.

Wight, R.G. and Erki, M.A. (2003). "Prestressed CFRP Sheets For Strengthening Concrete Slabs in Fatigue," Advances in Structural Engineering Journal, Vol. 6, No. 3, pp. 175-182.

Wu, Xiao-Han and Lu, Xilin (2003). "Tendon Model for Nonlinear Analysis of Externally Prestressed Concrete Structures," Journal of Structural Engineering, Vol. 129, No. 1, pp. 96-104.